# DESIGN, SYNTHESIS, AND EVALUATION OF FLUORESCENT SENSORS FOR INTRACELLULAR IMAGING OF MONOVALENT COPPER

A Thesis
Presented to
The Academic Faculty

by

Liuchun Yang

In Partial Fulfillment
of the Requirements for the Degree
Doctor of Philosophy
in the
School of Chemistry and Biochemistry

Georgia Institute of Technology
August 2005

**DESIGN, SYNTHESIS, AND EVALUATION OF FLUORESCENT SENSORS FOR INTRACELLULAR IMAGING OF MONOVALENT COPPER**

Approved by:


Dr. Christoph J. Fahrni, Advisor
School of Chemistry and Biochemistry
*Georgia Institute of Technology*

Dr. Donald F. Doyle
School of Chemistry and Biochemistry
*Georgia Institute of Technology*

Dr. Angus P. Wilkinson
School of Chemistry and Biochemistry
*Georgia Institute of Technology*

Dr. Z. John Zhang
Chemistry and Biochemistry
*Georgia Institute of Technology*

Dr. Harish Radhakrishna
School of Biology
*Georgia Institute of Technology*


Date Approved: July 14, 2005

*Dedicated to my husband*

# ACKNOWLEDGEMENTS

I would like to acknowledge Prof. Christoph J. Fahrni for his guidance, support and encouragement during my graduate career. I appreciate the contribution of Reagan McRae and John Cody to this thesis. I thank Dr. Maged M. Henary for his support, and all the members of the research group; it has been a pleasure to work with them. I would like to acknowledge the members of Prof. Janata's research group for their assistance with electrochemical measurements. I would also like to express my gratitude to all my friends who have provided assistance and support in the past years.

I grateful acknowledge the financial support of Georgia Institute of Technology and National Institutes of Health (Grants R01GM067169 and R01DK68096). I appreciate the support of the Argonne National Laboratory; the use of the Advanced Photon Source was supported by the U. S. Department of Energy, Office of Science, Office of Basic Energy Sciences, under Contract No. W-31-109-Eng-38. I would also like to express my appreciation to the members of my thesis committee.

# TABLE OF CONTENTS

# LIST OF TABLES

# LIST OF FIGURES

# LIST OF SYMBOLS AND ABREVIATIONS

| | |
|---|---|
| Å | Angstrom |
| [15]aneNS$_4$ | 1,4,7,10-Tetrathia-13-aza-cyclopentadecane |
| ATPase | Adenosine triphosphatase |
| Atx1 | Antioxidant 1 |
| b | Broad signal |
| BODIPY | Boron-dipyrromethene |
| C | Celsius |
| Ccc2 | Cross-complements the $Ca^{2+}$-sensitive phenotype of *csg1* mutant 2 |
| CT | Charge transfer |
| CcsP | Copper chaperone for SOD protein |
| Cox17p | Cytochrome c oxidase assembly protein |
| CTAP-1 | Copper-responsive triarylpyrazoline |
| Ctr1p | Copper transport protein |
| d | Doublet |
| DMEM | Dulbecco's modified Eagle's medium |
| DNMR | Dynamic NMR |
| Dns | Dimethylamino naphthalene-1-sulfonamide |
| EI | Electron ionization |
| ESI | Electron spray ionization |
| ET | Electron transfer |

| | |
|---|---|
| eV | Electron volt |
| FALS | Familial amyotrophic lateral sclerosis |
| FEF | Fluorescence enhancement factors |
| GHK | Glycly-histiday-lysine |
| GSH | Glutathione |
| HAH1 | Human antioxidant 1 homologue 1 |
| hCox17p | Human Cox17p analogous |
| HEPES | 4-(2-Hydroxyethyl)-1-piperazineethanesulfonic acid |
| HOMO | Highest occupied molecular orbital |
| HPLC | High performance liquid chromatography |
| HRMS | High resolution mass spectrometry |
| Hz | Hertz |
| ICT | Intramolecular charge transfer |
| K | Kelvin |
| λ | Wavelength |
| LDA | Lithium diisopropylamide |
| LE | Local-excited state |
| LUMO | Lowest unoccupied molecular orbital |
| m | Multiplet |
| Mhz | Megahertz |
| micro-XANES | Microprobe X-ray absorption near-edge spectroscopy |
| MNK | Menkes' protein |
| MS | Mass spectroscopy |

| | |
|---|---|
| MT | Metallothionein |
| NMR | Nuclear magnetic resonance |
| ORTEP | Oak ridge thermal ellipsoid plot |
| PBS | Phosphate-buffered saline |
| PET | Photoinduced electron transfer |
| PIPES | Piperazine diethanesulfonic acid |
| q | Quartet |
| s | Singlet |
| SOD | Superoxide dismutase |
| SXRF | Synchrotron X-ray fluorescence |
| t | Triplet |
| TD-DFT | Time-dependent density functional theory |
| TEMEA | Tris-(2-ethylsulfanyl-ethyl)-amine |
| TGN | Trans-Golgi network |
| TPEN | Tetrakis-(2-pyridylmethyl)ethylenediamine |
| TSQ | 6-Methoxy-8-p-toluenesulphonamido-quinoline |
| XANES | X-ray absorption near-edge spectroscopy |
| WND | Wilson's protein |

# SUMMARY

Copper is an essential micronutrient that is important for a broad range of biological processes. Over the past decade it became increasingly apparent that a number of diseases such as Wilson's disease, Menkes syndrome, and Alzheimer's disease are due to impaired copper transport and regulation. While there is compelling evidence that the intracellular milieu does not contain any free copper ions, the rapid kinetics of copper uptake and release suggests the presence of a labile intracellular copper pool that might play a critical role in copper homeostasis. The main theme of this thesis is to develop a copper(I)-selective fluorescent sensor for the elucidation of the subcellular localization of this labile copper pool. The design of the copper sensors is based on 1,3,5-triaryl-2-pyrazolines as fluorophore platform which is combined with various copper-selective polythioether receptors. Copper binding to the receptor moiety is translated into a fluorescence increase by means of a photoinduced electron transfer (PET) switching mechanism.

Chapter I introduces the biological background as well as recent developments of fluorescent sensors for metal detection in a cellular environment.

In chapter II, a series of donor-substituted 1,3,5-triaryl-2-pyrazoline fluorophores are structurally characterized by X-ray diffraction and the photophysical properties are described by steady-state absorption and emission spectroscopy. The photoinduced electron transfer thermodynamics of the fluorophores was investigated based on spectroscopic and electrochemical data. It was found that the aryl substituents on 1- and 3-position of the pyrazoline ring influence the photophysical properties of the

fluorophore in distinctly different ways. The excited-state equilibrium energy $\Delta E_{00}$ is primarily influenced by changes of the substituents in the 1-position, whereas the reduction potential of the fluorophore is determined by the 3-aryl group. Quantum chemical calculations agree well with the experimental data and provided further insights regarding the unique electronic structure of the pyraoline fluorophore platform. A water-soluble pyrazoline derivative (**2-2c**) was evaluated *in vivo* as a potential intracellular pH sensor. The sensor exhibits membrane permeability, low toxicity and high quantum yield.

A pyrazoline fluorophore library with varying numbers of fluorine substituents was synthesized. The photophysical and electrochemical properties of these fluorophores are described in chapter III. The compounds cover a broad range of excited state energies and reduction potentials, and allow for selective and differential tuning of these two parameters.

Chapter IV investigates copper receptors. A series of thiazacrownethers and tripodal aniline copper(I) receptors were synthesized and their copper binding stoichiometries and stability constants were studied by proton NMR titrations. Dynamic NMR techniques were utilized to investigate the exchange kinetics of copper between free ligand and complex. The measured exchange activation parameters revealed for all studied ligands a negative activation entropy, suggesting a predominant associative exchange mechanism. All the copper receptors exhibit high binding affinity and fast exchange rates. All of the synthesized copper receptors **4-1** to **4-6** exhibit high binding affinities ($\log K > 10^7$) and fast copper(I)-self-exchange rates with average lifetimes ranging between 15 μs to 208 μs at 283K.

With detailed knowledge of the photophysical and thermodynamic properties of the pyrazoline fluorophore platform and various copper receptors, a series of copper-selective fluorescent sensors were synthesized and characterized. The lead compound showing the best fluorescence emission enhancement was characterized both *in vitro* and *in vivo*. This sensor (**CTAP-1**) undergoes a 4.6-fold emission enhancement and reaches a quantum yield of 14% in pH 7.20 PIPES buffer solution upon saturation with Cu(I). The sensor exhibits excellent selectivity towards Cu(I), and its emission response is not compromised by the presence of millimolar concentrations of Ca(II) or Mg(II) ions. Mouse fibroblast cells (3T3) incubated with the sensor produced a copper-dependent perinuclear staining pattern, which colocalizes with the subcellular locations of the mitochondria and the Golgi apparatus. To evaluate and confirm the sensor's copper-selectivity, the subcellular topography of copper is illustrated by synchrotron-based x-ray fluorescence (SXRF) microscopy. Furthermore, microprobe x-ray absorption measurements at various subcellular locations showed a near-edge feature that is characteristic for low-coordinate monovalent copper. The data provide a coherent picture with strong evidence for a kinetically labile copper pool, which is predominantly localized in the mitochondria and the Golgi apparatus.

# CHAPTER I

# BACKGROUND

## 1.1. The Role of Copper in Biology

Copper is an essential trace element that is required for many biochemical and physiological functions. As a cofactor for many enzymes, copper participates in critical biological processes, such as respiration, antioxidant defense, and iron metabolism.[1] However, free copper ions are toxic since they catalyze the generation of highly reactive hydroxyl radicals, which cause cellular damage.[2] In order to maintain the copper balance between essentiality and toxicity, cells must store copper and distribute it to cellular compartments and proteins while at the same time preventing its toxic effects. Recent studies have shown that defects in copper transport and the associated regulatory processes cause fatal diseases, including Wilson's disease and Menkes' syndrome.[3-8] Certain neurodegenerative diseases, such as familial amyotropic lateral sclerosis (FALS) and Alzheimer's disease, are presumably also related to disorders of copper metabolism.[3,9]

A detailed knowledge of the molecular mechanism of copper uptake, intracellular trafficking, and regulation is critical for the understanding of diseases caused by copper imbalance. Recent research revealed significant details of the molecular mechanism of cellular copper transport and regulation in yeast. As shown in Figure 1-1, extracellular copper ions are reduced to monovalent copper and transported across the membrane by the high affininity membrane protein Ctr1p.[10,11] Then, copper is transported in its monovalent oxidation state by specialized chaperone proteins to secretory vesicles, mitochondria, or cytosolic metalloproteins. At present three major pathways of copper

transport have been elucidated. Ccsp transfers copper to superoxide dismutase (SOD),[12] which is a homodimeric enzyme containing zinc and copper in its active site. By utilizing the redox-activity of the copper cofactor, SOD catalyzes the disproportionation of superoxide ($O_{2}^{\cdot -}$) to hydrogen peroxide ($H_2O_2$) and $O_2$,[13] and plays therefore a critical role in the defense against oxidative stress. Cox17p shuttles copper to the mitochondria, where it is incorporated into cytochrome c oxidase, the terminal oxidase of the respiratory chain.[14] The metallochaperone Atx1p transfers copper to post-Golgi vesicles by specifically coordinating with the Ccc2p copper-transporting P-type adenosine triphosphatase (ATPase).[4,15-18] Then Ccc2p pumps copper inside the vesicle to metallate the copper-dependent ferroxidase Fet3p, which is involved in the iron uptake system.[15,16] An analogous set of proteins has been recently identified for copper trafficking in human cells. For example, human Cox17p (hCox17p) is homologous to Cox17p of yeast and is likely to function in delivery of copper to mitochondria.[19] HAH1p, the human homologue of Atx1p functions as antioxidance defense and for the delivery of copper to ATP-dependent membrane transporters.[16,20,21] The human homologues of Cccc2p are the Menkes' (MNK) and Wilson's protein (WND), both of which are members of the P-type ATPase cation transporter family and are present in the membranes of secretory vesicles and the Golgi apparatus.[22,23] Defects in the genetic coding of these ATPase are presumably the cause of the Wilson's and Menkes' diseases, both of which lead to disorders of the cellular copper homeostasis.

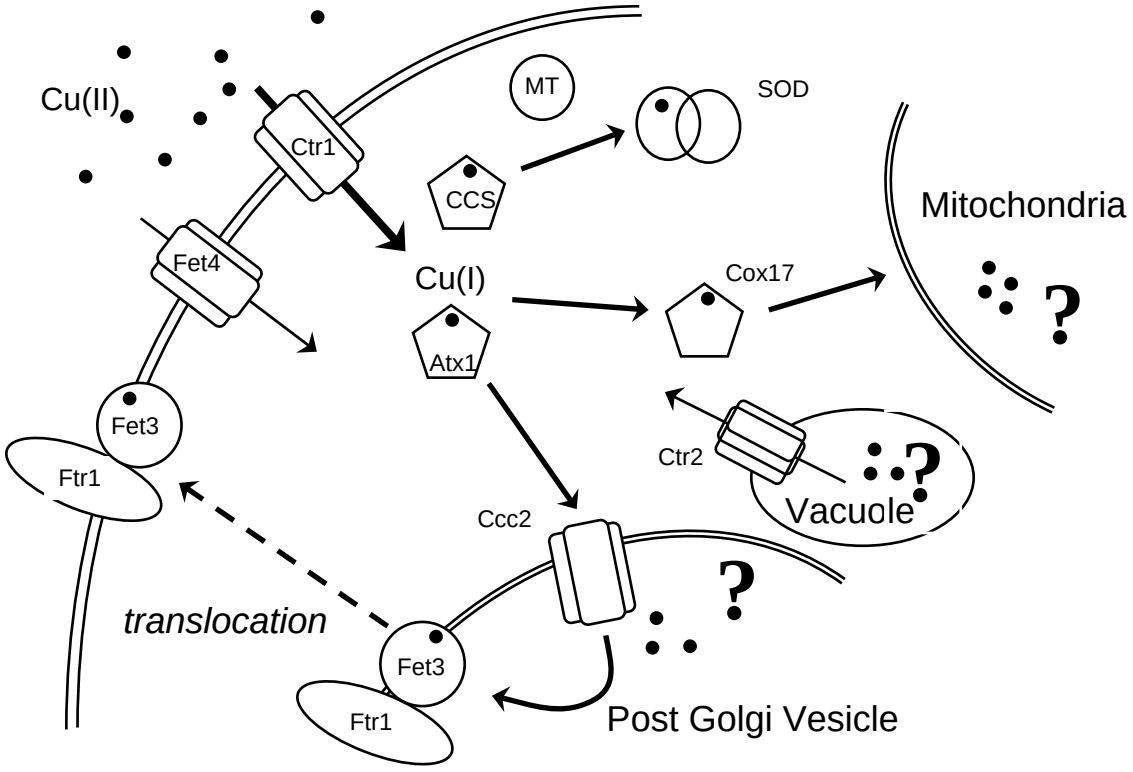


**Figure 1-1.** Copper trafficking pathways in yeast.

Since SOD and the chaperone transport systems have both a high copper affinity, free (hydrated) copper ions are not likely to be present in the cytoplasm. Recent studies have indicated that the cytosolic concentration of free copper ions is less than a single atom per cell and that all cytoplasmic copper must be tightly bound to cytoplasmic proteins, in particular superoxide dismutase (SOD) and metallothionein (MT).[24] At the same time, cellular copper uptake and release occurs with a surprisingly rapid kinetics,[25] an observation that would support the presence of a *kinetically* labile copper pool, which might play a critical role in copper homeostasis. For example, incubation experiments with radioactive $^{64}$Cu(II) demonstrated that the amount of accumulated intracellular copper is proportional to the concentration of copper in the extracellular medium.[26,27] The copper uptake process is very fast at the beginning, further proceeds at a slower rate, and finally approaches a steady state level after 40-60 minutes. The release of copper to the extracellular space occurs with similar rapid kinetics (within one hour) when cells are washed with copper depleted medium.[25] Metallothionein (MT) might principally serve as cytoplasmic buffer ligand; however, its high copper affinity (logK = 17-19)[28] implies a slow dissociation off-rate that clearly contradicts the fast efflux kinetics. As illustrated by Figure 1-2a), even with a diffusion-controlled on-rate, the dissociation of a metal-ligand complex with high thermodynamic stability involves a large activation barrier. However, if copper is associatively exchanged between two ligands $L_1$ and $L_2$ with similar copper affinities, the activation energies $E_a^f$ and $E_a^b$ for the forward and back reactions, respectively, are typically much smaller (Figure 1-2b). Consequently, the exchange kinetics can be very fast inspite of the high thermodynamic stabilities of $ML_1$ and $ML_2$. This has been demonstrated for intermolecular exchange of zinc in metallothionein.[29]

Similarly, the kinetics of copper release from MT to the extracellular medium could be greatly accelerated, if the exchange would follow an associative mechanism involving a second endogenous ligand, such as a copper chaperone protein.[17,30]

Kinetically labile copper might be also present in specific intracellular vesicles, compartments, or organelles. The lipid bilayer membrane of these structures would spatially separate the copper ions from the cytoplasm, thus preventing potentially damaging redox reactions. Since the copper concentration in these vesicles is higher compared to the cytoplasm, the copper transfer across the membrane must occur against a concentration gradient. The Menkes protein, located in post-Golgi secretory vesicles, is an ATP-dependent transporter that is responsible for copper incorporation into ceruloplasmin.[31,32] In addition to this function, it is conceivable that it might participate in copper regulatory processes where the post-Golgi vesicles would serve as transient copper storage sites, or as cargo containers for copper release via the secretory system.[31] This hypothesis is strongly supported by recent studies of copper-dependent trafficking of the Menkes and Wilson's disease proteins:[33-35] At low copper ion concentration, the MNK containing vesicles are located in the trans-Golgi network (TGN), while under elevated copper conditions rapid trafficking of MNK from the Golgi to the plasma membrane occurs.[33,36,37]

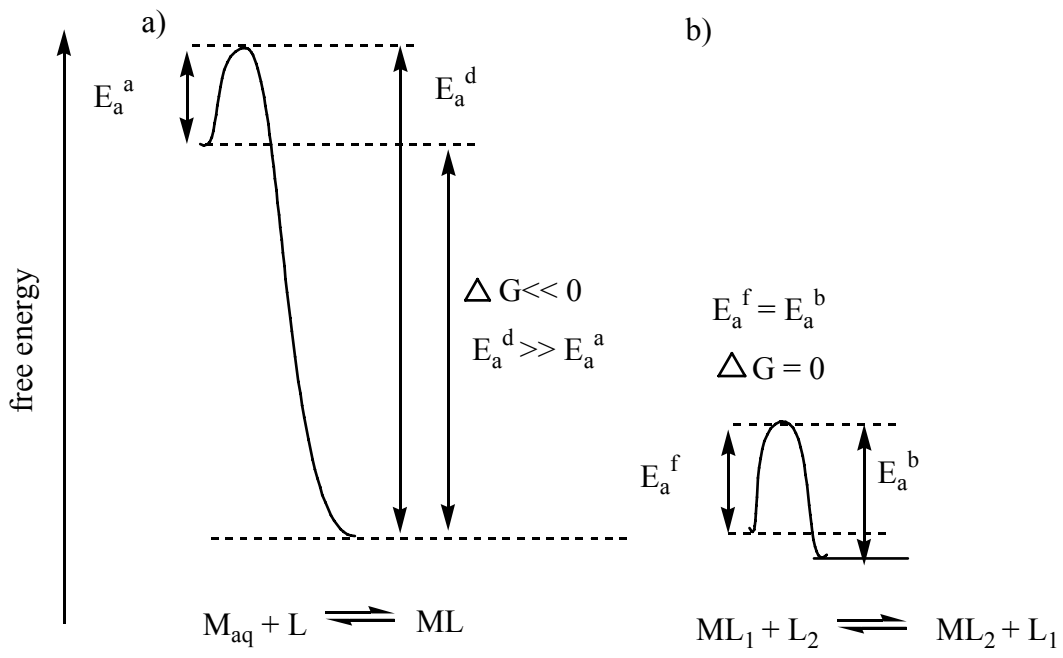


**Figure 1-2.** Free energy reaction pathways for metal coordination equilibrium in aqueous solution: a) Coordination of a hydrated metal cation $M_{aq}$ with a high-affinity ligand L, $E_a^a$: activation barrier of binding ligand, $E_a^d$: activation barrier of releasing ligand. b) Metal exchange equilibrium between two high-affinity ligands $L_1$ and $L_2$ via an associative mechanism, $E_a^f$: activation barrier of forward reaction, $E_a^b$: activation barrier of backward reaction.

The structure of the metal binding sites of the copper chaperones Ccsp[38] and Atx1p[39] has been characterized. Both proteins use CXXC binding motif (single-letter amino code where C is cysteine and X is any amino acid), bidentate ligand coordinating Cu(I) in linear coordination geometry.[40] These structural data provide evidence that copper is transported in its monovalent oxidation state.

## 1.2. Fluorescent Sensors for the Visualization of Labile Metal Pools

Although traditional methods for copper quantification such as atomic absorption spectroscopy,[41] inductively coupled plasma atomic emission spectroscopy,[42,43] can be used to determine the intracellular copper concentration, these techniques are only suitable for the measurement of bulk samples and result in destruction of the cells. Laser ablation inductively coupled plasma mass spectrometry,[44] Synchrotron X-ray fluorescence microprobe[45,46] and radiolabelling[47] (such as Positron Emission Tomography[48]) have been used for the detection copper. However, these techniques require special instruments or reagent (such as radiolabelling copper). In contrast, membrane permeant fluorescent sensors have been demonstrated to be powerful tools for the non-invasive visualization of intracellular metal cation distribution in single cells.[49] Dynamic changes of intracellular metal concentrations can be monitored in live cells in real time or by means of time-lapse imaging microscopy.[50,51] Currently, a plethora of fluorescent sensors are available that are selective for a wide range of biologically relevant cations, including calcium,[49,52-54] magnesium,[55,56] sodium and potassium,[57-59] or zinc.[60-63] For example, Fura-2 and Indo-1 have provided information of calcium neurophysiology.[53] Mag-fura-2 is also commercially available magnesium selective probe.[55] (molecular structures of these probes are shown in Figure 1-3).

### *1.2.1. Fluorescent Sensors for Zn(II)*

Over the past decades several different fluorophore platforms have been developed for the *in vivo* measurement of zinc, starting with the widely used quinoline-based derivatives TSQ (6-methoxy-8-p-toluenesulphonamido-quinoline),[64,65] Zinquin,[66,67] TFLZn,[68] and Danquin,[69] to the greatly improved fluorescein sensors. Representative

fluorescein sensors include the DPA(di-2-picolylamine)-based ZPs (Zinpyr family)[62,70-72] and ZnAFs[73,74], shown in Figure 1-4. Combining DPA to the xanthenone of the fluorescein (Figure 1-5 and Figure 1-6) provides Zinpyr sensor family, which includes Zinpyr-1 (ZP1),[71] Zinpyr-2 (ZP2),[62] Zinpyr-4 (ZP-4).[72] ZnAFs, including ZnAF-1 and ZnAF-2, have also been reported.[73,74]

These fluorescent probes have used for the intracellular $Zn^{2+}$ imaging.[68,75] For example, kinetically labile pools of Zn(II) have been visualized in live mouse fibroblasts using Zinquin.[50,67,76] Zinpyr-1 also revealed a similar perinuclear staining pattern in Cos-7 cells, suggesting that the observed zinc-rich vesicles act as storage sites.[51,71] ZnAF derivatives were used for the measurement of zinc intracellular changes both in the cultured macrophages and hippocampal slices.[74] The secretion of zinc from pancreatic β-cells has been recently visualized in real-time using Fluozin-3.[77-79]

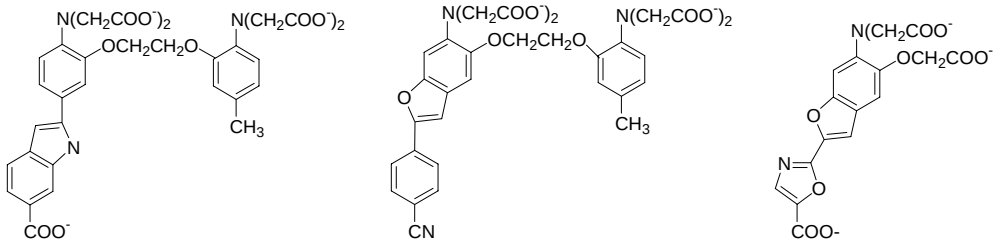


Indo-1 **1-1** | Fura-2 **1-2** | Mag-fura-2 **1-3**

**Figure 1-3.** Molecular structures of probes for $Na^+$, $K^+$ and $Mg^{2+}$.

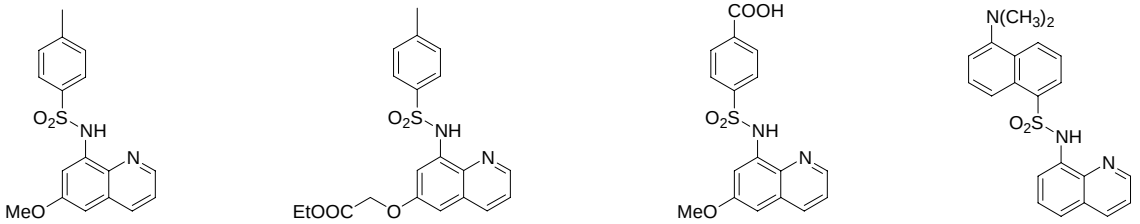


TSQ **1-4** | Zinquin **1-5** | TFLZn **1-6** | Danquin **1-7**

**Figure 1-4.** Structures of quinoline-based sensors.

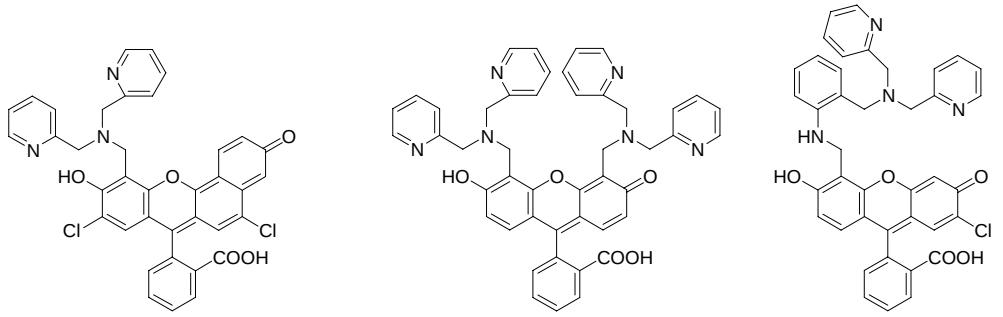


Zinpyr-1 (ZP1) **1-8** | Zinpyr-2 (ZP2) **1-9** | Zinpyr-4 (ZP-4) **1-10**

**Figure 1-5.** Structures of the Zinpyr family sensors.

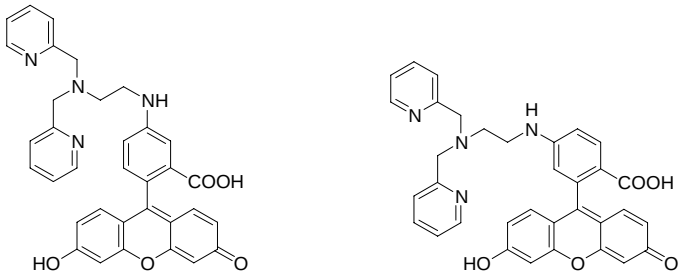


ZnAF-1 **1-11** | ZnAF-2 **1-12**

**Figure 1-6.** Structures of the ZnAF family sensors.

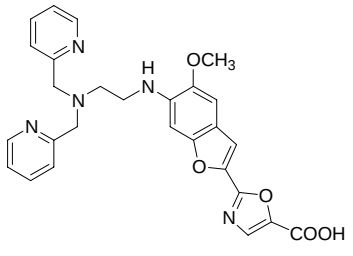


ZnAF-R2

**1-13**

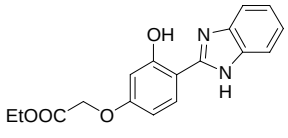


**1-14**

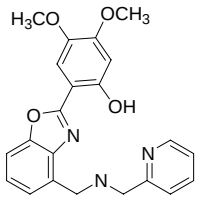


Zinbo-5

**1-15**

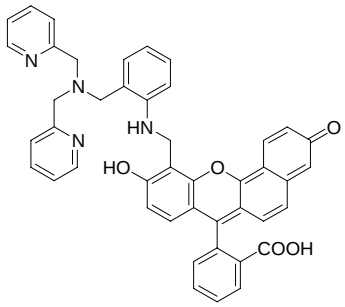


ZNP1

**1-16**

**Figure 1-7.** Ratiometric sensors for $Zn^{2+}$.

Besides these fluorescent sensors based on the change of emission intensity upon $Zn^{2+}$ binding, ratiometric sensors have been developed for $Zn^{2+}$ imaging (Figure 1-7). Ratiometric sensors, which shift excitation or emission wavelength upon $Zn^{2+}$ complexation, allow accurate and quantitative measurement of intracellular $Zn^{2+}$. Nagano and his coworkers designed ZnAF-R1 and ZnAF-R2 (**1-13**) derivatives based on benzofuran fluorophore, which can be utilized for ratiometric imaging of intracellular $Zn^{2+}$ in cultured macrophages.[80] Benzoxazole fluorophores have been reported for

ratiometric sensing of intracellular $Zn^{2+}$ (**1-14**, **1-15**).[81,82] Lippard and his coworkers reported Zin-naphthopyr 1(ZNP1).[83]

### *1.2.2. Copper-Selective Fluorescent Sensors*

A number of copper-selective fluorescent sensors have been developed over the past few years. However, for most of the reported $Cu^{2+}$ fluorescent sensors, structures shown in Figure 1-8, the binding of the metal ion caused fluorescence emission quenching. For example, bathocuproine disulfonate (BCS), the bidentate nitrogen donor ligand, was been used as copper selective sensors.[84] The commercially available phenanthroline-based indicator Phen Green FL (**1-18**) has been suggested as a general-purpose heavy metal sensor capable of detecting a broad range of metal ions, including Cu(II) and Cu(I).[85-87] The fluorophore 5-(dimethylamino)naphthalene-1-sulfonamide (Dns) has been utilized in conjunction with various Cu(II)-binding ligand such as polypeptides (**1-19**)[87] and pyrazine derivatives[88,89] for the design of copper sensors. Czarnik and co-workers developed an anthracene-based chemosensor that responded to Hg(II) and Cu(II) in aqueous solution by quenching the fluorescence.[90-92] Anthracene tethered metal receptor moieties, such as 14-membered tetrathia crown (**1-20**), tripeptide glycly-histiday-lysine (GHK) (**1-21**) and triamino-cyclohexane, yielded chemosensors, which are selective for Cu(II).[93] Interaction of Cu(II) with the lanthanide complex Eu(III)-cyclen-phen (**1-22**) results in quenching of the Eu(III)-centered luminescence.[94] However, all of these sensing approaches result in a reduction of the emission intensity upon binding of copper ions, a characteristics that is not suitable for microscopy imaging applications. The weak or completely quenched emission of the copper-bound sensor would be completely covered by the strong fluorescence background of the free sensor.

Therefore, it would be impossible to discern small subcellular structures, e.g. vesicles or mitochondria that might serve as intracellular storage places of copper. Fluorescence quenching of above fluorophore systems is either due to the "heavy metal effect", resulting in rapid intersystem crossing through enhanced spin-orbit coupling,[95] or due to electron transfer or energy transfer pathways initiated by the redox acitivity of Cu(I), or by the open d-shell electronic structure of Cu(II), respectively.[96,97,98] Hence, for imaging microscopy copper binding must not result in fluorescence quenching, but a bright enhancement of the sensor's emission intensity.

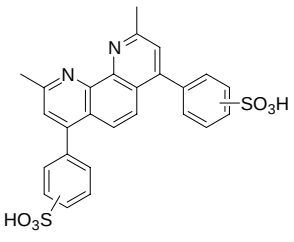

BCS

**1-17**

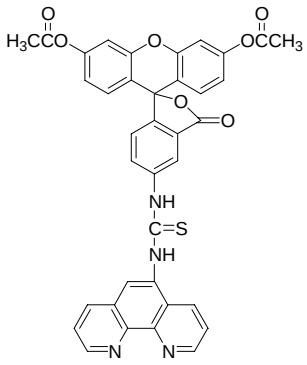

Phen Green FL

**1-18**

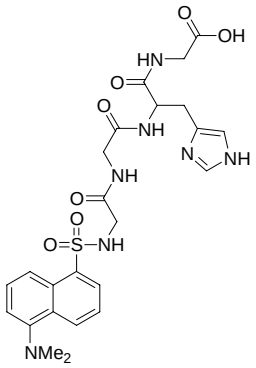

dansyl-gly-gly-his-gly

**1-19**

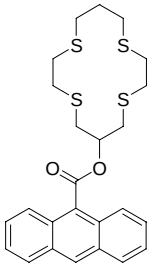

**1-20**

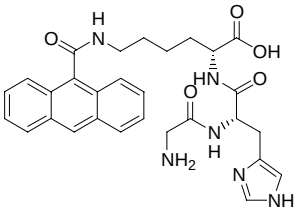

**1-21**

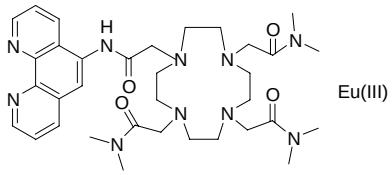

**1-22**

**Figure 1-8.** Molecular structures of previously published copper-selective fluorescent sensors (see text for details).

There are also a few sensors which exhibit fluorescence emission enhancement upon binding to $Cu^{2+}$ ions. Trifluorophore cryptand system was reported that fluorescence do not quench with transition metals.[99,100] Ramachandaram and Samanta have reported fluorescene enhancement of fluorophores **1-23** and **1-24** upon complexation with transition metal ions such as Cu(II), Cr(II), Co(II).[101,102] Anthracence- and anthraquinone-based chemosensor **1-25** and **1-26** enhances the fluorescence emission at the presence of $Cu^{2+}$.[103] Czarnik and his coworks reported rhodamine B hydrazide **1-27** as a "chemodosimeter". $Cu^{2+}$ cleaves the N,O bond and releases the fluorescent rhodamine.[104] (molecular structures of these probes are shown in Figure 1-9).

A few of ratiometric fluorescent sensors for Cu(II) have also been reported. Canary and his coworkers utilized two commercially available fluorogenic ligands: calcein blue (**1-28**), fluozin-1 (**1-29**) and one equimolar quantity of Cd(II) as a sensor system.[105] Naphthalimde derivative (**1-30**) showed 50 nm blue shift of fluorescence emission since binding of $Cu^{2+}$ reduced the electron-donating ability of two amino groups conjugated to the naphthalene ring. Therefore, charge transfer (CT) character emission shifted to high energy.[106] The other example is naphthalimide fluorophore **1-31**. Binding to $Cu^{2+}$ caused the deprotonation of two secondary amines conjugated to naphthalimide and lead to a red-shift of the UV-vis and fluorescence spectra.[97-100,107] (molecular structures of these probes are shown in Figure 1-10).

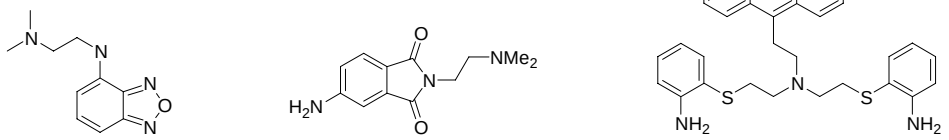

**1-23** **1-24** **1-25**

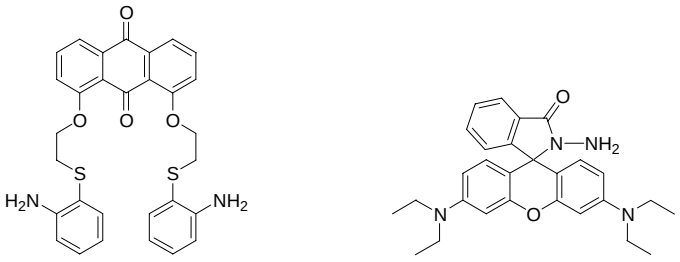

**1-26** **1-27**

**Figure 1-9.** Molecular structures of previously published copper-selective fluorescent sensors, which increase fluorescence intensity with copper(II).

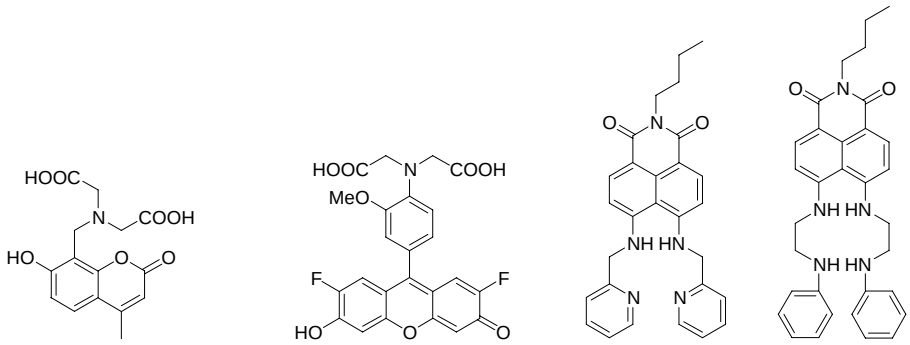

Calcein blue fluozin-1

**1-28** **1-29** **1-30** **1-31**

**Figure 1-10.** Ratiometric fluorescent sensors for copper(II).

However, all these Cu(II) sensors reported are not suitable for intracellular monovalent copper detection. Firstly, they are all sensitive to Cu(II), not Cu(I). Most of these sensors are not water soluble, such as trifluorophore cryptand system and nitrobenzoxadiazole.[102] Some sensors require specific condition, such as Canary's two fluorophores and Cd(II) system, which can not be accomplished in cellular environment. Some sensors are not responding specific to copper, for example, anthracene-based sensor is pH sensitive;[31] rhodamine B hydrazide can hydrolysis by enzyme.

### *1.2.3. Requirements of a Copper-Selective Probe for Biological Microscopy*

Because the reducing environment of the cytosol is expected to stabilize monovalent copper,[108] the sensor must be specifically designed for this oxidation state. However, a Cu(I)-selective probe that would undergo bright fluorescence enhancement is still lacking, indicating the considerable challenges in the design of such a system. Beside the fluorescence enhancement, a number of additional requirements are important specifically for biological imaging applications:

#### *1) Solubility and Membrane Permeability*

Ideally, the fluorescent probe should be sufficiently hydrophobic to passively diffuse across the plasma membrane, although microinjection could principally serve as an alternative tool to manually load a non-permeant dye into individual cells.[109] At the same time, the probe should be sufficiently water soluble, typically at a concentration between 1 to 10 μM. In addition, the lipid layer facing the extracellular space is negatively charged; therefore, molecules with a net negative charge are typically not

membrane permeable. Hence, the molecular structure of the probe must therefore encompass the right balance between hydrophobicity and water solubility.

***2) Stabilization of Monovalent Copper***

Because at higher than nanomolar concentrations monovalent copper readily undergoes a disproportionation reaction to yield Cu(II) and Cu(0), the cation receptor moiety of the sensor must be able to stabilize Cu(I). Likewise, kinetically labile intracellular Cu(I) must be coordinated to an endogenous ligand, which can sufficiently stabilize Cu(I) towards disproportionation while at the same time still providing sufficient kinetic lability for associative exchange as part of intracellular copper transport. The presence of this yet unknown endogenous ligand also implies, that the sensor must have a stronger copper affinity and engage in a competitive metal exchange reaction, preferably in a 1:1 metal-to-ligand binding stoichiometry. *In this context it is very important to realize, that the sensor will not provide information about intracellular copper concentrations, but rather serve as a tool to visualize the subcellular distribution and localization of kinetically labile copper pools.*

***3) Cation Selectivity***

The intracellular environment contains a number of other metal cations that might potentially interfere with the sensor repsonse. Notably, the sensor should be insensitive towards Ca(II) and Mg(II), both of which are found in micro- to millimolar concentrations in the cytoplasm. According to recent studies, certain intracellular vesicles might contain up to millimolar concentrations of zinc. Furthermore, it has been suggested

that eukaryotic cells contain a labile iron pool, who's identity is still the subject of controversy.[62,74,77] In the human body, the total amount of copper is by about 20 fold lower than zinc and 40 fold lower than iron in the human body. Given their fundamental differences in coordination properties, it should be straight forward to discriminate binding of Cu(I) over Ca(II) and Mg(II); however, Zn(II) and Fe(II) exhibit rather similar coordination chemistries compared to Cu(I) and deserve therefore special attention in probe design and evaluation.

***4) Kinetics***

In order to dynamically measure changes of the intracellular copper distribution, the probe should provide a fast metal exchange kinetics with the endogenous copper pool. Because the reaction rate is determined by the activation barrier of the metal exchange reaction, a high binding affinity is not necessarily in contradiction with fast exchange kinetics. As discussed above (see Figure 1-2), even a complex with very high thermodynamic stability can undergo fast metal exchange by means of an associative mechanism.

***5) Photophysical Properties***

As mentioned previously, the probe must exhibit emission enhancement upon binding to copper. Furthermore, the peak excitation wavelength of the probe should be in the visible range or at least above 350 nm, corresponding to the UV-transmission cutoff of standard fluorescence microscope lenses. For live cell imaging applications, UV excitation can be damaging to cells, and causes also interfering background fluorescence

through endogenous fluorophores such as tryptophane, NADH, or nucleic acids. Nevertheless, if the fluorophore exhibits a peak emission of 480 nm or higher, interfering background autofluorescence can be readily removed by means of a suitable band-pass emission filter, even if excitation below 400 nm is required. To guarantee sufficient optical sensitivity, the molar extinction coefficient of the fluorophore should be greater than 5000 $M^{-1}cm^{-1}$ and the quantum yield should exceed at least 5%. Finally, the probe should be photochemically stable and not be subject to excessive photobleaching under long time exposure.

***6) Structural Flexibility***

The synthesis of many widely used fluorophore platforms, e.g. fluorescein, rhodaime, or BODIPY dyes, involves tedious multi-step steps syntheses accompanied by often unsatisfactory yields.[110] To effectively tune the thermodynamic and photophysical properties of the sensor, a synthetically modular platform would be desirable, allowing for independent structural changes of the cation receptor moiety and fluorophore.

***7) Toxicity***

The probe should exhibit low toxicity under the given experimental conditions, which typically require incubation at micromolar concentrations and exposure times up to several hours.

***8) Subcellular Distribution and Staining Artifacts***

Since the probe is used in a cellular environment, it is important to carefully evaluate the probe for potential artifacts caused by the complex biological milieu. Copper binding is possibly not the only reason for fluorescence emission enhancement. If changes in pH alter the fluorescence intensity, the probe might stain acidic vesicles or organelles. To test if the staining pattern is due to copper binding or pH changes, intracellular pH gradients can be neutralized by incubation with certain drugs, such as nigericin or monensin.[111] Because the fluorescence quenching thermodynamics of PET-based probes depends on the polarity of the environment, partitioning of the probe into vesicular membranes might also cause fluorescence enhancements and thus producing staining artifacts.[112,113] Furthermore, if the probe carries a net positive charge, it might accumulate in the negatively charged lumen of the mitochondria.[107,114-116] Golgi vesicles are mildly acidic and have a pH around 6.5, which could be sufficient to trap mildly basic fluorophores. Cation-selective fluorescent probes usually utilize weakly basic metal receptor and might therefore potentially lead to such artifacts. Therefore, the nature of the staining pattern must be carefully investigated as a function of copper concentration as well as changes in intracellular pH to avoid possible artifacts.

## 1.3. Thesis Objective

The goal of this thesis is to develop a copper-selective fluorescent probe, which allows for visualization of the subcellular distribution and localization of kinetically labile copper pools. In the future, the probe is expected to provide critical insights into details of cellular copper homeostasis, and thus advancing the understanding of copper-related disorders and diseases.

## 1.4. References


1. Tapiero, H.; Townsend, D.; Tew, K., *Biomed. Pharmacother.* **2003,** 57, (9), 386.

2. Halliwell, B.; Gutteridge, J., *Biochem. J.* **1984,** 219, (1), 1.

3. Waggoner, D.; Bartnikas, T.; Gitlin, J., *Neurobiol. Dis.* **1999,** 6, (4), 221.

4. Huffman, D.; O'Halloran, T., *Annu. Rev. Biochem.* **2001,** 70, 677.

5. Daniel, K.; Harbach, R.; Guida, W.; Dou, Q., *Front Biosci.* **2004,** 9, 2652.

6. Fatemi, N.; Sarkar, B., *J. Bioenegrg. Biomembr.* **2002,** 34, (5), 339.

7. Fatemi, N.; Sarkar, B., *Inorg. Chim. Acta* **2002,** 339, 179.

8. Sarkar, B., *Chem. Rev.* **1999,** 99, (9), 2535.

9. Strausak, D.; Mercer, J.; Dieter, H.; Stremmel, W.; Multhaup, G., *Brain Res. Bull.* **2001,** 55, (2), 175.

10. Dancis, A.; Haile, D.; Yuan, D.; Klausner, R., *J. Biol. Chem.* **1994,** 269, (41), 25660.

11. Dancis, A.; Yuan, D.; Haile, D.; Askwith, C.; Eide, D.; Moehle, C.; Kaplan, J.; Klausner, R., *Cell* **1994,** 76, (2), 393.

12. Culotta, V.; Klomp, L.; Strain, J.; Casareno, R.; Krems, B.; Gitlin, J., *J. Biol. Chem.* **1997,** 272, (38), 23469.

13. Mccord, J.; Fridovic.I, *J. Biol. Chem.* **1969,** 244, (22), 6049.

14. Glerum, D.; Shtanko, A.; Tzagoloff, A., *J. Biol. Chem.* **1996,** 271, (24), 14504.

15. Pufahl, R.; Singer, C.; Peariso, K.; Lin, S.; Schmidt, P.; Fahrni, C.; Culotta, V.; Pennerhahn, J.; O'Halloran, T., *Science* **1997,** 278, (5339), 853.

16. Lin, S.; Pufahl, R.; Dancis, A.; O'Halloran, T.; Culotta, V., *J. Biol. Chem.* **1997,** 272, (14), 9215.

17. Huffman, D.; O'Halloran, T., *J. Biol. Chem.* **2000,** 275, (25), 18611.

18. Portnoy, M.; Rosenzweig, A.; Rae, T.; Huffman, D.; O'Halloran, T.; Culotta, V., *J. Biol. Chem.* **1999,** 274, (21), 15041.

19. Amaravadi, R.; Glerum, D.; Tzagoloff, A., *Hum. Genet.* **1997,** 99, (3), 329.

20. Lin, S.; Culotta, V., *Proc. Natl. Acad. Sci. U.S.A.* **1995,** 92, (9), 3784.

21. Klomp, L.; Lin, S.; Yuan, D.; Klausner, R.; Culotta, V.; Gitlin, J., *J. Biol. Chem.* **1997,** 272, (14), 9221.

22. Koch, K.; Pena, M.; Thiele, D., *Chem. Biol.* **1997,** 4, (8), 549.

23. Lutsenko, S.; Petris, N., *J. Membr. Biol.* **2003,** 191, (1), 1.

24. Rae, T.; Schmidt, P.; Pufahl, R.; Culotta, V.; O'Halloran, T., *Science* **1999,** 284, (5415), 805.

25. Herd, S.; Camakaris, J.; Christofferson, R.; Wookey, P.; Danks, D., *Biochem. J.* **1987,** 247, (2), 341.

26. Voskoboinik, I.; Strausak, D.; Greenough, M.; Brooks, H.; Petris, M.; Smith, S.; Mercer, J.; Camakaris, J., *J. Biol. Chem.* **1999,** 274, (50), 36030.

27. Eisses, J.; Chi, Y.; Kaplan, J., *J. Biol. Chem.* **2005,** 280, (10), 9635.

28. Hamer, D., *Annu. Rev. Biochem.* **1986,** 55, 913.

29. Maret, W.; Larsen, K.; Vallee, B., *Proc. Natl. Acad. Sci. U.S.A.* **1997,** 94, (6), 2233.

30. Wernimont, A.; Yatsunyk, L.; Rosenzweig, A., *J. Biol. Chem.* **2004,** 279, (13), 12269.

31. Puig, S.; Thiele, D., *Curr. Opin. Chem. Biol.* **2002,** 6, (2), 171.

32. Hellman, N.; Kono, S.; Mancini, G.; Hoogeboom, A.; De Jong, G.; Gitlin, J., *J. Biol. Chem.* **2002,** 277, (48), 46632.

33. Petris, M.; Mercer, J.; Culvenor, J.; Lockhart, P.; Gleeson, P.; Camakaris, J., *EMBO. J.* **1996,** 15, (22), 6084.

34. Petris, M.; Voskoboinik, I.; Cater, M.; Smith, K.; Kim, B.; Llanos, R.; Strausak, D.; Camakaris, J.; Mercer, J., *J. Biol. Chem.* **2002,** 277, (48), 46736.

35. Petris, M.; Camakaris, J.; Greenough, M.; Lafontaine, S.; Mercer, J., *Hum. Mol. Genet.* **1998,** 7, (13), 2063.

36. Hamza, I.; Prohaska, J.; Gitlin, J., *Proc. Natl. Acad. Sci. U.S.A.* **2003,** 100, (3), 1215.

37. Pase, L.; Voskoboinik, I.; Greenough, M.; Camakaris, J., *Biochem. J.* **2004,** 378, 1031.

38. Banci, L.; Bertini, I.; Ciofi-Baffoni, S.; Huffman, D.; O'Halloran, T., *J. Biol. Chem.* **2001,** 276, (11), 8415.

39. Arnesano, F.; Banci, L.; Bertini, I.; Huffman, D.; O'Halloran, T., *Biochemistry* **2001,** 40, (6), 1528.

40. Rosenzweig, A., *Chem. Biol.* **2002,** 9, (6), 673.

41. Ghazy, S.; Kabil, M., *Bull. Chem. Soc. Jpn.* **1994,** 67, (8), 2098.

42. Silva, P.; Dorea, J.; Boaventura, G., *Bio. Trace Elem. Res.* **1997,** 59, (1-3), 57.

43. Chew, L.; Bradley, D.; Mohd, A.; Jamil, M., *Appl. Radiat. Isot.* **2000,** 53, (4-5), 633.

44. Becker, J.; Zoriy, M.; Pickhardt, C.; Palomero-Gallagher, N.; Zilles, K., *Anal. Chem.* **2005,** 77, (10), 3208.

45. Twining, B.; Baines, S.; Fisher, N.; Maser, J.; Vogt, S.; Jacobsen, C.; Tovar-Sanchez, A.; Sanudo-Wilhelmy, S., *Anal. Chem.* **2003,** 75, (15), 3806.

46. Twining, B.; Baines, S.; Fisher, N.; Jacobsen, C.; Maser, J., *J. Phys. IV* **2003,** 104, 435.

47. Camakaris, J.; Petris, M.; Bailey, L.; Shen, P.; Lockhart, P.; Glover, T.; Barcroft, C.; Patton, J.; Mercer, J., *Hum. Mol. Genet.* **1995,** 4, (11), 2117.

48. Smith, S., *J. Inorg. Biochem.* **2004,** 98, (11), 1874.

49. Tsien, R., *Chem. Eng. News* **1994,** 72, (29), 34.

50. Zalewski, P.; Millard, S.; Forbes, I.; Kapaniris, O.; Slavotinek, A.; Betts, W.; Ward, A.; Lincoln, S.; Mahadevan, I., *J. Histochem. Cytochem.* **1994,** 42, (7), 877.

51. Fahrni, C.; Simon, K.; Suhy, D.; Nasir, M.; Dwivedi, R.; O'Halloran, T., *J. Inorg. Biochem.* **1999,** 74, (1-4), 125.

52. Tsien, R., *Biochemistry* **1980,** 19, (11), 2396.

53. Grynkiewicz, G.; Poenie, M.; Tsien, R., *J. Biol. Chem.* **1985,** 260, (6), 3440.

54. Minta, A.; Kao, J.; Tsien, R., *J. Biol. Chem.* **1989,** 264, (14), 8171.

55. London, R., *Annu. Rev. Physiol.* **1991,** 53, 241.

56. Cielen, E.; Stobiecka, A.; Tahri, A.; Hoornaert, G.; De Schryver, F.; Gallay, J.; Vincent, M.; Boens, N., *J. Chem. Soc. Perkin. Trans. 2* **2002**, (6), 1197.

57. Minta, A.; Tsien, R., *J. Biol. Chem.* **1989,** 264, (32), 19449.

58. Crossley, R.; Goolamali, Z.; Sammes, P., *J. Chem. Soc. Perkin. Trans. 2* **1994**, (7), 1615.

59. Xu, X.; Xu, H.; Ji, H., *Chem. Commun.* **2001**, (20), 2092.

60. Jiang, P.; Guo, Z., *Coordin. Chem. Rev.* **2004,** 248, (1-2), 205.

61. Kikuchi, K.; Komatsu, K.; Nagano, T., *Curr. Opin. Chem. Biol.* **2004,** 8, (2), 182.

62. Burdette, S.; Walkup, G.; Spingler, B.; Tsien, R.; Lippard, S., *J. Am. Chem. Soc.* **2001,** 123, (32), 7831.

63. Lim, N.; Yao, L.; Freake, H.; Bruckner, C., *Bioorg. Med. Chem. Lett.* **2003,** 13, (14), 2251.

64. Frederickson, C.; Kasarskis, E.; Ringo, D.; Frederickson, R., *J. Neurosci. Meth.* **1987,** 20, (2), 91.

65. Andrews, J.; Nolan, J.; Hammerstedt, R.; Bavister, B., *Cytometry.* **1995,** 21, (2), 153.

66. Zalewski, P.; Forbes, I.; Betts, W., *Biochem. J.* **1993,** 296, 403.

67. Mahadevan, I.; Kimber, M.; Lincoln, S.; Tiekink, E.; Ward, A.; Betts, W.; Forbes, I.; Zalewski, P., *Aust. J. Chem.* **1996,** 49, (5), 561.

68. Budde, T.; Minta, A.; White, J.; Kay, A., *Neuroscience* **1997,** 79, (2), 347.

69. Jiang, P.; Chen, L.; Lin, J.; Liu, Q.; Ding, J.; Gao, X.; Guo, Z., *Chem. Commun.* **2002**, (13), 1424.

70. Sjoback, R.; Nygren, J.; Kubista, M., *Spectrochim. Acta, part A* **1995,** 51, (6), L7.

71. Walkup, G.; Burdette, S.; Lippard, S.; Tsien, R., *J. Am. Chem. Soc.* **2000,** 122, (23), 5644.

72. Burdette, S.; Frederickson, C.; Bu, W.; Lippard, S., *J. Am. Chem. Soc.* **2003,** 125, (7), 1778.

73. Hirano, T.; Kikuchi, K.; Urano, Y.; Higuchi, T.; Nagano, T., *Angew. Chem., Int. Ed. Engl.* **2000,** 39, (6), 1052.

74. Hirano, T.; Kikuchi, K.; Urano, Y.; Nagano, T., *J. Am. Chem. Soc.* **2002,** 124, (23), 6555.

75. Nasir, M.; Fahrni, C.; Suhy, D.; Kolodsick, K.; Singer, C.; O'Halloran, T., *J. Biol. Inorg. Chem.* **1999,** 4, (6), 775.

76. Fahrni, C.; O'Halloran, T., *J. Am. Chem. Soc.* **1999,** 121, (49), 11448.

77. Gee, K.; Zhou, Z.; Qian, W.; Kennedy, R., *J. Am. Chem. Soc.* **2002,** 124, (5), 776.

78. Gee, K.; Zhou, Z.; Ton-That, D.; Sensi, S.; Weiss, J., *Measuring zinc in living cells. A new generation of sensitive and selective fluorescent probes*, **2002**; Vol. 31, 245.

79. Qian, W.; Gee, K.; Kennedy, R., *Anal. Chem.* **2003,** 75, (14), 3468.

80. Maruyama, S.; Kikuchi, K.; Hirano, T.; Urano, Y.; Nagano, T., *J. Am. Chem. Soc.* **2002,** 124, (36), 10650.

81. Henary, M.; Fahrni, C., *J. Phys. Chem. A* **2002,** 106, (21), 5210.

82. Taki, M.; Wolford, J.; O'Halloran, T., *J. Am. Chem. Soc.* **2004,** 126, (3), 712.

83. Chang, C.; Jaworski, J.; Nolan, E.; Sheng, M.; Lippard, S., *Proc. Natl. Acad. Sci. U.S.A.* **2004,** 101, (5), 1129.

84. Rapisarda, V.; Volentini, S.; Farias, R.; Massa, E., *Anal. Biochem.* **2002,** 307, (1), 105.

85. Chavez-Crooker, P.; Garrido, N.; Ahearn, G., *J. Exp. Biol.* **2001,** 204, (8), 1433.

86. Torrado, A.; Walkup, G.; Imperiali, B., *J. Am. Chem. Soc.* **1998,** 120, (3), 609.

87. Zheng, Y.; Gattas-Asfura, K.; Konka, V.; Leblanc, R., *Chem. Commun.* **2002**, (20), 2350.

88. Singh, A.; Yao, Q.; Tong, L.; Still, W.; Sames, D., *Tetrahedron Lett.* **2000,** 41, (49), 9601.

89. Yoon, J. Y.; Ohler, N. E.; Vance, D. H.; Aumiller, W. D.; Czarnik, A. W., *Tetrahedron Lett.* **1997,** 38, (22), 3845.

90. Zheng, Y.; Huo, Q.; Kele, P.; Andreopoulos, F.; Pham, S.; Leblanc, R., *Org. Lett.* **2001,** 3, (21), 3277.

91. Desantis, G.; Fabbrizzi, L.; Licchelli, M.; Mangano, C.; Sacchi, D.; Sardone, N., *Inorg. Chim. Acta* **1997,** 257, (1), 69.

92. Beltramello, M.; Gatos, M.; Mancin, F.; Tecilla, P.; Tonellato, U., *Tetrahedron Lett.* **2001,** 42, (52), 9143.

93. Gunnlaugsson, T.; Leonard, J.; Senechal, K.; Harte, A., *Chem. Commun.* **2004**, (7), 782.

94. McClure, D. S., *J. Chem. Phys.* **1952,** 20, (4), 682.

95. Varnes, A. W.; Wehry, E. L.; Dodson, R. B., *J. Am. Chem. Soc.* **1972,** 94, (3), 946.

96. de Silva, A.; Gunaratne, H.; Gunnlaugsson, T.; Huxley, A.; Mccoy, C.; Rademacher, J.; Rice, T., *Chem. Rev.* **1997,** 97, (5), 1515.

97. Ghosh, P.; Bharadwaj, P.; Mandal, S.; Ghosh, S., *J. Am. Chem. Soc.* **1996,** 118, (6), 1553.

98. Banthia, S.; Samanta, A., *J. Phys. Chem. B* **2002,** 106, (21), 5572.

99. Ramachandram, B.; Samanta, A., *Chem. Commun.* **1997**, (11), 1037.

100. Ramachandram, B.; Samanta, A., *J. Phys. Chem. A* **1998,** 102, (52), 10579.

101. Kaur, S.; Kumar, S., *Chem. Commun.* **2002**, (23), 2840.

102. Kumar, S.; Pramila; Kaur, S., *Tetrahedron Lett.* **2002,** 43, (6), 1097.

103. Dujols, V.; Ford, F.; Czarnik, A., *J. Am. Chem. Soc.* **1997,** 119, (31), 7386.

104. Royzen, M.; Dai, Z.; Canary, J., *J. Am. Chem. Soc.* **2005,** 127, (6), 1612.

105. Xu, Z.; Xiao, Y.; Qian, X.; Cui, J.; Cui, D., *Org. Lett.* **2005,** 7, (5), 889.

106. Xu, Z.; Qian, X.; Cui, J., *Org. Lett.* **2005**.

107. Seksek, O.; Biwersi, J.; Verkman, A., *J. Biol. Chem.* **1995,** 270, (10), 4967.

108. Ainger, K.; Avossa, D.; Morgan, F.; Hill, S.; Barry, C.; Barbarese, E.; Carson, J., *J. Cell. Biol.* **1993,** 123, (2), 431.

109. Kakhlon, O.; Cabantchik, Z., *Free Radical Bio. Med.* **2002,** 33, (8), 1037.

110. Millot, C.; Millot, J.; Morjani, H.; Desplaces, A.; Manfait, M., *J. Histochem. Cytochem.* **1997,** 45, (9), 1255.

111. Fahrni, C.; Yang, L.; Vanderveer, D., *J. Am. Chem. Soc.* **2003,** 125, (13), 3799.

112. Kandela, I.; Bartlett, J.; Indig, G., *Photochem. Photobiol. Sci.* **2002,** 1, (5), 309.

113. Trapp S., R. W. H., *European Biophysics Journal with Biophysics Letters* **2005**.

114. Mellman, I.; Fuchs, R.; Helenius, A., *Annu. Rev. Biochem.* **1986,** 55, 663.

115. Nelson, N., *Curr. Opin. Cell Biol.* **1992,** 4, 654.

116. Mellman, I., *J. Exp. Biol.* **1992,** 172, 39.

# CHAPTER II

# ELECTRON TRANSFER MODEL STUDIES

## 2.1. Background and Introduction

### *2.1.1. Photophysical Background*

On basis of their molecular architecture, fluorescence sensors can be divided into two different classes: intrinsic fluorescence sensors and receptor-spacer-fluorophore sensors (Figure 2-1). The signal transduction is either based on a charge transfer (CT) process or photoinduced electron transfer process (PET). In both types, an electron-rich receptor moiety acting as Lewis base for metal coordination typically serves as electron-donor and is combined with a fluorophore as electron-acceptor.

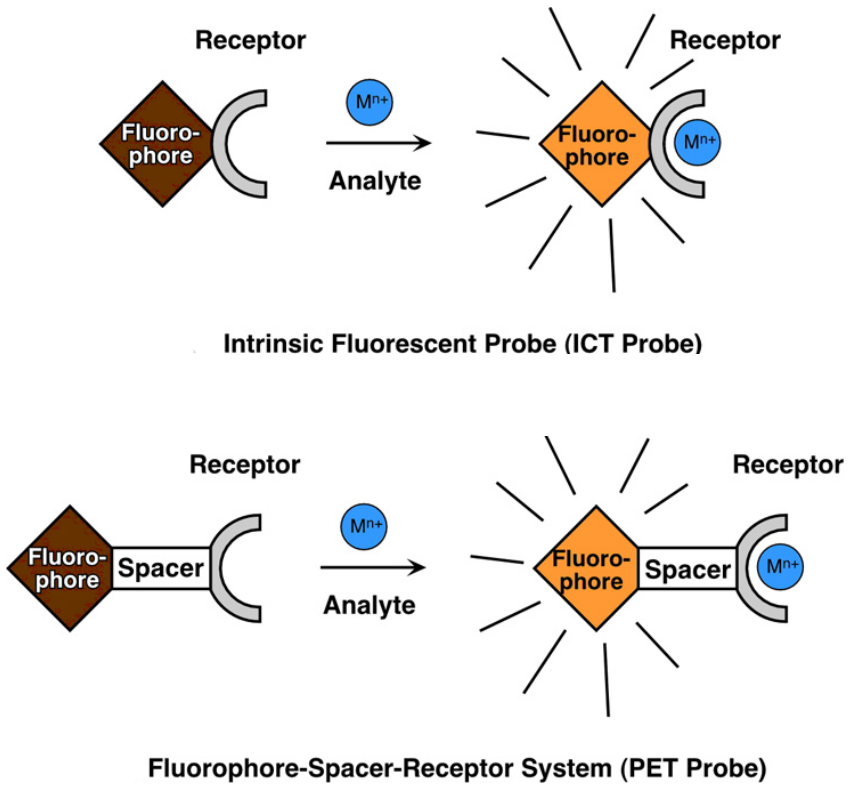


**Figure 2-1.** Molecular architectures for the most common types of fluorescence probes.

In intrinsic fluorescence sensors, the receptor is directly linked to the fluorophore and therefore is part of the fluorophore π–electron system. Because this probe usually uses intramolecular charge transfer as signal transduction mechanism, it is also termed ICT probe. Binding of a cation to the receptor not only changes the fluorescence intensity and lifetime, but typically induces a spectral shift of the absorption and emission bands. In general, such probes have two relevant excited singlet states: a local-excited state (LE) and a charge transfer state (CT) formed indirectly upon excitation. Binding of the electron-donating receptor to the analyte increases the energy of both states. As a result, the fluorescence emission shifts to higher energy (blue shift) as shown in Figure 2-2. Since the excited CT state is highly polarized, the fluorescence emission is strongly Stokes-shifted and the shifting behavior of ICT probes is strongly solvent dependent. Furthermore, when intrinsic fluorescence sensors are used for the detection of transition or heavy metals, the fluorescence emission is typically quenched, either due to the presence of low-lying, metal-centered d-d states, or through increased intersystem crossing due to enhanced spin-orbit coupling.[1-3] For example, the fluorescence emission of 1,10-phenanthroline is effectively quenched upon coordination of Cu(I) to the nitrogen donor atoms, rendering this fluorophore a selective probe for Cu(I).[4,5] In general, intrinsic fluorescence sensors that are design for the detection of open d-shell or heavy metal cations, exhibit typically fluorescence quenching upon binding of the analyte. However, because microscopy applications require a fluorescence enhancement rather than quenching, the ICT architecture is not suitable for the design of a copper-selective sensor for cellular imaging.

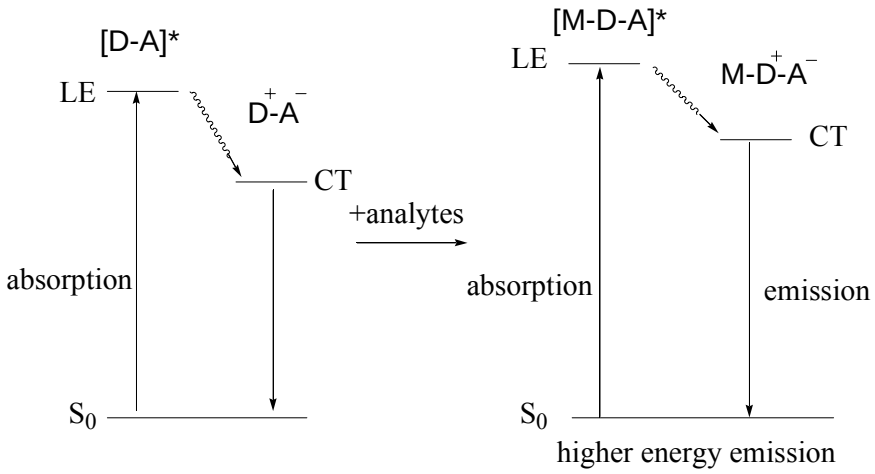


**Figure 2-2.** Simplified Jablonski diagram for ICT probe ($S_0$, singlet ground state; LE, local-excited state (Franc-Condon state); CT, charge transfer state). Upon binding of the analyte to the probe, the CT energy increases, and fluorescence undergoes a blue shift.

In contrast, the receptor-spacer-fluorophore architecture of PET sensors utilizes a short alkyl spacer to electronically decouple the cation-binding unit from the fluorophore system, a concept that has been successfully used for sensing of open d-shell cations and heavy metals.[6,7] Signal transduction between the receptor and fluorophore unit is typically modulated by means of a photoinduced excited state electron transfer (PET) mechanism. The fluorescence on or off switching depends on the energy ordering of the non-emissive, charge separated electron transfer state ET and the emissive local-excited state LE. As illustrated in Figure 2-3, prior to binding of the metal cation, the non-emissive ET state is at lower energy compared to the emissive LE state. When the fluorophore is excited, the fluorescence is quenched through photoinduced electron transfer ($\Delta G_{ET} < 0$). Binding of the cation to the receptor reduces its donor strength and therefore increases the ET state energy level. The PET process is inhibited ($\Delta G_{ET} > 0$), which results in an increase of the fluorescence emission signal. Since the receptor and

fluorophore are electronically decoupled, direct ground-state interactions between the analyte and the fluorophore are effectively inhibited. Therefore, it is principally possible to achieve fluorescence enhancements even with heavy or open d-shell transition metal cations. Hence, the receptor-spacer-fluorophore architecture is a promising approach for the design of heavy and transition metal cation sensors.

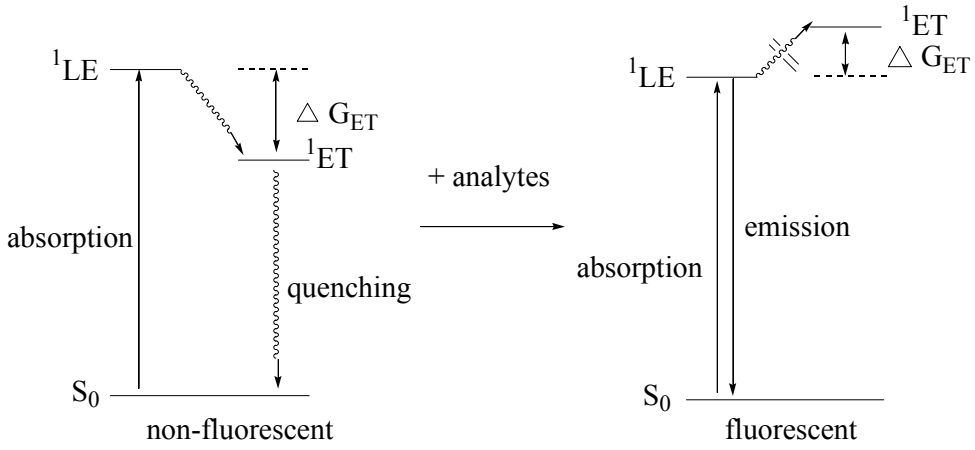


**Figure 2-3.** Simplified Jablonski diagram for PET probes ($S_0$, singlet ground state; $^1$LE, emissive locally excited singlet state; $^1$ET, electron-transfer state). Analyte binding to the receptor inhibits fluorescence quenching through ET.

### *2.1.2. Fluorescence Sensors for Paramagnetic and Heavy Metal Cations*

As previously described, the design of probes for paramagnetic and heavy metal cations is challenging since many of these cations quench the fluorescence by means of spin-orbit coupling (e.g. Hg(II)),[1] energy, or electron transfer (e.g. Cu(I) or Cu(II)).[3] To effectively prevent from fluorescence quenching, electronic decoupling of the cation

receptor and fluorophore unit through a rigid molecular architecture is pivotal. Recently, several fluorophores containing electronically decoupled systems have been used as chemosensors that exhibit a fluorescence *enhancement* upon binding of heavy or transition metals. For example, boron-dipyrromethene (BODIPY) dyes,[6] and 1,3,5-triaryl-pyrazoline[7] have been reported to give a magnificent fluorescence enhancement upon binding to transition and heavy metals.

#### *2.1.2.1.BODIPY Fluorophores*

Boron-dipyrromethene (BODIPY) dyes are very attractive as sensor fluorophore platforms because they exhibit high photostability, high molar absorption coefficients ($\varepsilon > 50{,}000\ M^{-1}cm^{-1}$), combined with a high fluorescence quantum yields ($\Phi_f > 0.5$),[8] and can be excited at relatively long wavelengths (> 480 nm). As shown in Figure 2-4, by attaching methyl groups in the 3-position of each pyrrol ring, the aryl substituent twists into a nearly orthogonal position (dihedral angle > $75^o$), thus effectively decoupling the receptor unit (electron donor) from the dipyrromethene fluorophore. For example, fluorophore **2-7** has been reported to undergo 2500- and 5900-fold fluorescence enhancements in acetonitrile upon binding of Cu(II) and Hg(II), respectively.[6]

In general, BODIPY dyes exhibit dual emission in polar solvents, with a higher energy emission originating from the locally excited state (LE), and a second, weaker emission at lower energy, presumably from a highly delocalized charge transfer state (CT). Upon binding of the cation, the CT state rises above the LE level, resulting in an enhanced emission from the LE state. Interestingly, this characteristic fluorescence switching is often not observed in aqueous solution. Because the CT state has intrinsically a large dipole moment, its energy is strongly depended on the solvent

polarity. In aqueous solution or highly polar organic solvents, this state is effectively stabilized due to strong dipole-dipole solute-solvent interactions. Therefore, the CT state lies at a significantly lower energy compared to the LE state, such that the CT state typically does not rise above LE upon metal coordination to the donor site. Hence, application of the BODIPY molecular architecture is less suitable for the design of fluorescence probes for sensing cation in aqueous solution.

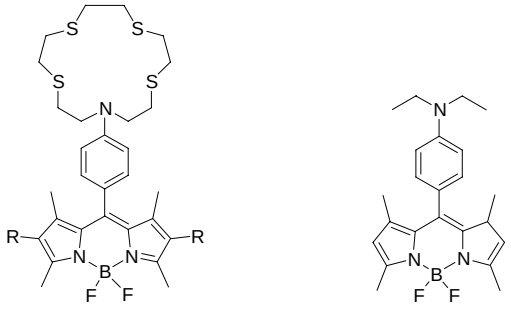

R = H, **2-7**

R = $CH_2CH_2COOEt$, **2-8**

**2-9**

**Figure 2-4.** Structures of selected BODIPY-based fluorescence sensors. Left: Cu(II) and Hg(II)-selective sensor. Right: pH-sensitive fluorescent probe.

Preliminary experiments on using **2-7** and **2-8** as Cu(I) selective cellular sensors provided a set of interesting data.[9] While binding of Cu(II) to **2-7** enhanced the fluorescence intensity by more than 2500 fold in acetonitrile as previously reported by Rurack et al.,[6] no intensity changes were observed in buffered aqueous solution under simulated physiological conditions (pH 7.2, 0.1 M ionic strength). Furthermore, addition

of Cu(I) to a solution of **2-7** did not affect the emission intensity, neither in acetonitrile nor in aqueous solution. Literature data indicate that the tetrathiaza crownether receptor of **2-7** has femtomolar affinity towards Cu(I) in aqueous solution,[10,11] however, Cu(I) is strongly solvated in acetonitrile, which significantly reduces the Cu(I) binding affinity of the crownether ligand through competitive binding. Interestingly, in dichloromethane, which does not appreciably coordinate to Cu(I), the fluorescence intensity increased indeed by a factor of 170 with a quantum yield of 50% upon saturation with Cu(I). In contrast, although water is not expected to effectively compete for coordination to Cu(I), no increase in fluorescence was observed at equimolar concentrations of Cu(I) and **2-8** at neutral pH.[9] Therefore, the emission enhancement or absence thereof cannot be simply ascribed to differences in the solvent-dependent Cu(I) binding affinities. It is more likely, that the emission enhancement is primarily governed by a different degree of stabilization of the highly polar CT state as described above.

When HeLa cells were incubated with **2-8** in PBS buffer solution for 50 minutes, an intriguing vesicular staining pattern was observed. The staining pattern was not affected by treatment with TPEN or bathocuproin, both of which are effective transition metal chelators. Furthermore, control experiments with fluorophore **2-9**, which lacks the Cu(I) binding moiety, revealed a similar staining pattern. These results suggest that the observed staining pattern is most likely not due to binding of copper ions to the fluorophore. Because the fluorescence intensity of BODIPY dyes depends strongly on the solvent polarity, the observed staining pattern might be due to partitioning of the fluorophore into the low polarity environment of vesicular membranes. In such an environment, the charge transfer state (CT) might rise above the locally excited state (LE)

and therefore switch on the fluorescence. This hypothesis was tested by titration of the fluorophore with Cu(I) in the presence of negatively charged or neutral liposomes. The emission intensity of the locally excited state centered around 512 nm indeed increased in the sole presence of liposomes, and further increased upon addition of Cu(I).

In conclusion, the strong dependence of the fluorescence emission on the solvent renders boron-dipyrromethene (BODIPY) dyes not suitable as fluorophore platform for the detection of Cu(I) in a cellular environment. In addition, the preliminary data unequivocally demonstrated that it is very important to carefully test the properties of a fluorophore under various conditions in order to avoid staining artifacts and false interpretation of intracellular staining patterns.

#### *2.1.2.2.Pyrazolines*

Triaryl-$\Delta^2$–pyrazolines are known for their structural flexibility, bright fluorescence emission, and rigid molecular structure that can provide effective electronic decoupling. The synthesis of 1,3,5-triaryl-substituted pyrazolines is readily accomplished in two condensation reactions as outlined in Figure 2-9. Despite these favorable aspects, surprisingly few cation- or pH-selective probes have been described that utilize pyrazolines as fluorophore platform. De Silva and coworkers designed a series of pyrazoline-based probes for pH measurements and selective sensing of Na(I), Ca(II), and Mg(II).[12-15] For example, fluorophore **2-10** undergoes a 92-fold fluorescence enhancement upon saturation with Ca(II) in aqueous solution.[16] Furthermore, Rurack *et al*. recently demonstrated that thiazacrownether-functionalized pyrazolines yield fluorescence enhancement factors (FEF) of up to 15-fold for Hg(II) in acetonitrile, despite the fact that Hg(II) is a potent fluorescence quencher.[17] Given the combination of

favorable photophysical properties and structural flexibility, 1,3,5-triaryl-$\Delta^2$–pyrazolines are promising fluorophores for the development of Cu(I)-selective fluorescence sensors.

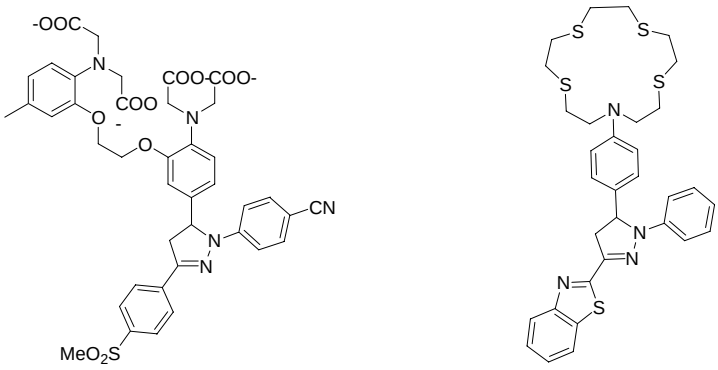


**2-10** **2-11**

**Figure 2-5.** Pyrazoline-based fluorescence sensors for Ca(II) (**2-10**) and Hg(II) (**2-11**).

### *2.1.2.3.Other Examples of Fluorophores with Decoupled Receptors*

Over the pass few years, other electronically decoupled fluorophore-receptor systems have been used as fluorescence probes. Czarnik and co-workers developed an anthracene-based chemosensor **2-12**, which responds to Hg(II) and Cu(II) in aqueous solution by quenching the fluorescence.[18] Although the receptor is electronic decoupled from the anthracene fluorophore, both spacer and receptor are too flexible to prevent electronic interaction between metal ion and fluorophore. In contrast, 8-hydroxyquinoline derivative (**2-13**) was reported to enhance the fluorescence upon binding to Hg(II) in aqueous media.[19] In this system, the fluorescence properties are influenced by the protonation state. Binding to the metal cation affects the p$K_a$ values of the quinoline

nitrogen and the phenolic group, and changes in turn the UV absorption as well as the fluorescence emission intensity.[19] Ramachandaram and Samanta have reported fluorescence enhancements with nitrobenzoxadiazole (compound **1-23**) upon complexation with transition metal ions, including Cu(II), Cr(II), or Co(II).[20] Although the complex between the metal cation and fluorophore is principally redox active, the electron-deficient fluorophore is apparently able to minimize oxidative quenching by means of a photoinduced electron transfer process.

In summary, the key factor for the successful design of a sensor for open d-shell transition metals and heavy metal cations lies in a rigid molecular framework that provides effective electronic decoupling between the cation receptor and fluorophore system.

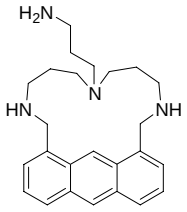


**2-12**

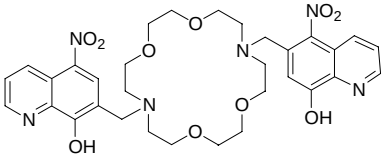


**2-13**

**Figure 2-6.** Examples for electronically decoupled fluorescence probes for transition metals.

### *2.1.3. Exploring the Excited-State Electron Transfer Thermodynamics*

#### *2.1.3.1.Rehm-Weller Formalism*

A key determinant of the photophysical properties of fluorescence sensors based

on photoinduced electron transfer (PET) is provided by the thermodynamics of the excited state electron transfer. The free energy change of an excited state electron transfer process can be estimated on basis of the Rehm-Weller equation:[21]

$$\Delta G_{ET} = nF[E^0(D/D^+) - E^0(A/A^-)] - \Delta G_{00} - \Delta G_{IPS} \quad (2.1)$$

$$\Delta G_{00} = \frac{1}{2}(h\nu_{abs} + h\nu_{em}) \quad (2.2)$$

where F stands for the Faraday constant, $\Delta G_{00}$ refers to the energy difference between the thermally equilibrated excited and ground-state, $E^0$ ($D/D^+$) and $E^0$ ($A/A^-$) are the ground-state oxidation potentials of the donor and reduction potential of the fluorophore, respectively, and $\Delta G_{IPS}$ refers to the stabilization energy provided by formation of the excited state ion pair in a polar solvent. Assuming reasonably harmonic potential surfaces for the ground and excited states, the excited state equilibrium energy $\Delta G_{00}$ can be estimated according to equation 2.2 based on the peak absorption and emission energies $h\nu_{abs}$ and $h\nu_{em}$, respectively (Figure 2-7).

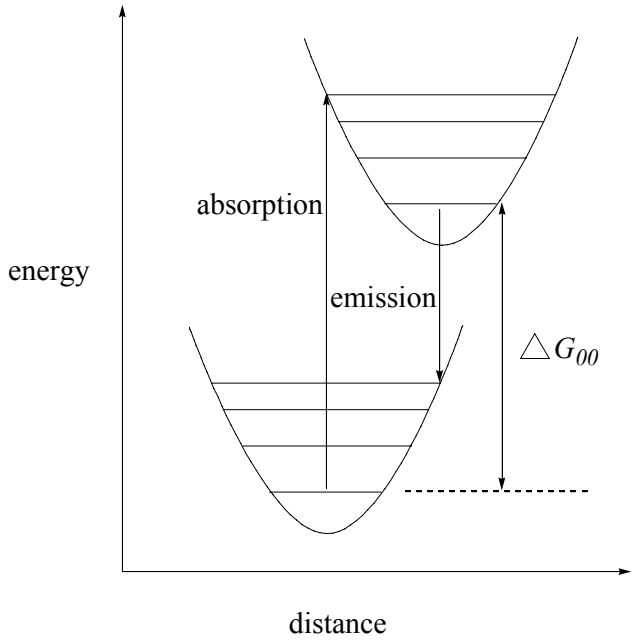


**Figure 2-7.** Estimation of $\Delta G_{00}$ based on the absorption and emission energy maxima.

The PET quenching efficiency is determined by the relative rates of radiative deactivation vs electron transfer. According to Marcus' theory the electron transfer rate directly correlates with the driving force $-\Delta G_{ET}$ of the PET process. On basis of the Rehm-Weller formalism, the driving force $-\Delta G_{ET}$ for formation of the PET state can be readily estimated with knowledge of the excited-state equilibrium energy $\Delta G_{00}$, the oxidation potential $E^0(D/D^+)$ of the receptor, and reduction potential $E^0(A/A^-)$ of the fluorophore. Before binding to the metal cation, the large driving force $-\Delta G_{ET}$ leads to fast electron transfer and thus efficient fluorescent quenching. Upon coordination of the metal cation, the oxidation potential of the donor increases and both $-\Delta G_{ET}$ and the ET rate decrease. As a result radiative deactivation is kinetically favored and the fluorescence intensity increases. In order to switch on/off the fluorescence, the free

energy change of the excited state electron transfer process $\Delta G_{ET}$ must be carefully tuned. With the appropriate $\Delta G_{ET}$, the ET state energy will reside below the LE state ($\Delta G_{ET} < 0$) in absence of the cation, thus inducing efficient fluorescense quenching, whereas upon coordination of the cation to the electron donor D the PET levels will rise above the LE level ($\Delta G_{ET} > 0$) to yield a bright fluorescence enhancement.

#### *2.1.3.2.Potential Window for Copper Sensing*

For most non-redox active cations, such as alkaline and alkaline-earth metal ions or transition metals with a full d-shell, metal binding to the receptor increases $\Delta G_{ET}$ dramatically and therefore raises the ET energy level sufficiently above the LE level. Because Cu(I) is readily oxidized itself, it can act as an additional source of electrons to quench the fluorescence. As a consequence, depending on the degree of stabilization of Cu(I) through binding to the receptor moiety, the overall change of $\Delta G_{ET}$ upon binding to Cu(I) is expected to be rather small. Adjusting $\Delta G_{ET}$ is becoming therefore particularly important for sensing of Cu(I): the ET energy must be below the LE level to quench the fluorescence in absence of the metal, but must sufficiently increase above the LE to switch on the fluorescence after binding to Cu(I). Hence, a synthetically flexible molecular structure is therefore critical to effectively tune the electron transfer driving force.

### *2.1.4. Experimental Design*

We chose triaryl-substituted–pyrazoline fluorophores as platform because of their favorable photophysical properties and structural flexibility. As shown in Figure 2-8, the fluorophore π-system is composed of two aryl substituents attached to 1- and 3-position of the pyrazoline ring as well as the bridging p-orbitals provided by N1-N2-C3. The

remaining two carbon atoms (C4 and C5) of the pyrazoline ring system are $sp^3$ hybridized and are therefore not in conjugation with the fluorophore π-system. The receptor moiety is attached through the aryl substituent on C5, therefore effectively preventing electronic interactions in the ground state.

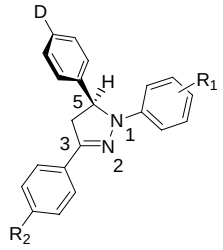


**Figure 2-8.** Molecular structure of 1,3,5-triaryl-substituted pyrazoline fluorophore.

As previously shown by Rurack et al.,[7] the photophysical properties of substituted pyrazolines are determined by the relative energy ordering of the excited state localized on the fluorophore ($^1$LE) and an electron transfer state ($^1$ET) formed by means of an ultrafast electron transfer between the donor (D) and the fluorophore upon photoexcitation. Emission from the locally excited state ($^1$LE) is very bright, while the electron transfer state ($^1$ET) is typically non-emissive. As outlined in Section 2.1.3.1 radiative deactivation of the locally excited state ($^1$LE) is competing with the rate of phontoinduced electron transfer to form $^1$ET. Ideally, the energy of $^1$ET lies below the energy of $^1$LE before cation binding, and rises above upon metal complexation to the receptor. As described in Section 2.1.3.1, the driving force of the excited state electron transfer process is determined by the excited state equilibrium energy, the oxidation

potential of the donor, and the reduction potential of the fluorophore. Because the aryl substituents in the 1- and 3-position are expected to influence not only the excited equilibrium energy, but also the redox properties of the fluorophore, it should be possible to effectively tune the ET thermodynamics by choosing the appropriate substituents $R_1$ and $R_2$ on the pyrazoline ring system. To systematically explore how the two substituents $R_1$ and $R_2$ alter the driving force of the electron transfer process, we synthesized and characterized an extended set of substituted 1,3,5-triaryl-$\Delta^2$–pyrazoline derivatives.

## 2.2. Synthesis

As summarized in Table 2-1, a series of 12 pyrazoline derivatives with various electron donating or withdrawing substituents $R_1$ and $R_2$ were synthesized and subsequently studied. To simplify the overall synthesis, a diethylamino group was selected as the electron donor instead of the thiazacrownether cation receptor unit. Modulation of the electron transfer process can then be simply studied as a function of the protonation state of the diethyl amino group, which should have a p$K_a$ around 6.5.

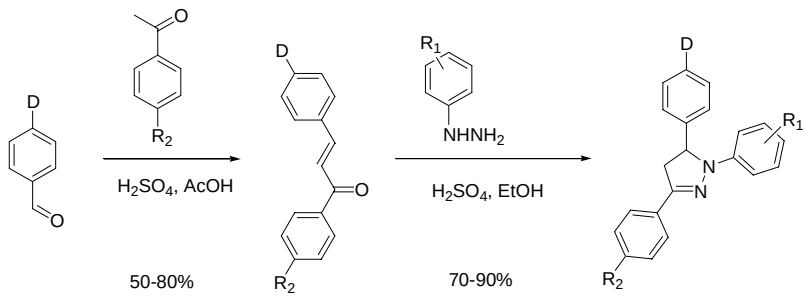


**2-14** D = $NEt_2$, $R_2$ = COOEt

**2-15** D = $NEt_2$, $R_2$ = H

**2-16** D = $NEt_2$, $R_2$ = CN

**2-17** D = $NEt_2$, $R_2$ = OMe

**2-18** D = H, $R_2$ = COOEt

**Figure 2-9.** General scheme for the synthesis of pyrazoline derivatives.

**Table 2-1.** Substituent Key for the Synthesized Pyrazoline Derivatives.

| compd | $R_1$ | $R_2$ | D |
|---|---|---|---|
| **2-1a** | H | H | $NEt_2$ |
| **2-1b** | | CN | |
| **2-1c** | | COOEt | |
| **2-2a** | 4-CN | H | $NEt_2$ |
| **2-2b** | | CN | |
| **2-2c** | | COOEt | |
| **2-2d** | | OMe | |
| **2-2e** | | COOH | |
| **2-3a** | 2,3,4,5,6-$F_5$ | H | $NEt_2$ |
| **2-3b** | | COOEt | |
| **2-4a** | 4-OMe | CN | $NEt_2$ |
| **2-4b** | | COOEt | |
| **2-5** | 4-F | COOEt | $NEt_2$ |
| **2-6** | 4-CN | COOEt | H |

As shown in Figure 2-9, the syntheses of racemic pyrazoline derivatives **2-1** to **2-6** was accomplished in two steps, starting with an aldol condensation followed by cyclization with the corresponding phenyl hydrazine derivatives. Initial attempts to conduct the aldol condensation under standard base-catalyzed conditions proved to be unsuccessful. The electron-donating diethylamino group presumably decreases the electrophilicity of the aldehyde, resulting in unsatisfactory reactivity even in the presence of strong bases such as LDA, potassium *tert*-butoxide, or sodium hydroxide. In contrast, the yields were increased to 60%-70% under acidic conditions, presumably due to protonation of the diethylamino group and thus effective activation of the aldehyde. The orange chalcone intermediates were precipitated from the reaction mixture, and coupled with the corresponding phenylhydrazine derivatives with 60%-80% yield using sulfuric acid as catalyst. The crude products were typically purified by gradient flash chromatography followed by reversed-phase HPLC. All chemical structures were confirmed by $^{1}$H NMR, MS, and high-resolution mass spectrometry (HRMS). Detailed descriptions of all syntheses and analytical data are provided in the experimental section.

## 2.3. Structural Studies

X-ray quality crystals for derivatives **2-1b**, **2-2a-d** and **2-3b** were obtained by slow evaporation from acetonitrile-water solutions over several days. The ORTEP plots and atomic numbering schemes of each structure are shown in Figures 2-10 to Figure 2-15, and selected structural parameters are compiled in Table 2-2. A comprehensive list of all relevant X-ray structural data is given in the Appendix, Section A. The structural parameters, notably bond lengths and bond angles, obtained for the central pyrazoline ring-system are in good agreement with the structural data of related 1,3,5-triaryl-$\Delta^2$-

pyrazolines recently reported by Rurack and coworkers.[7] Despite the rigidity of the overall molecular framework, the dihedral angle $\theta_1$ shows substantial variations ranging from $-34^o$ to $-63^o$, suggesting that the phenyl ring attached to the 5-position of the pyrazoline ring is conformationally rather flexible. Consistent with this observation, quantum chemical calculations of the potential energy curve for rotation around the C5-C18 bond axis revealed a relatively shallow minimum with a low activation barrier of 28.3 $kJmol^{-1}$ (see Appendix, Section B). The nitrogen atom of the diethylamino group is planar in all structures, indicating significant interactions of the lone pair electrons with the $\pi$-system of the neighboring phenyl ring. The average bond length of N24-C21 is $1.376 \pm 0.002$ Å, which is shorter compared to the N24-C25 single bond (average $1.460 \pm 0.015$ Å), and further supports the partial double bond character due to delocalization of electron density from the nitrogen to the aromatic ring. As shown in Figure 2-10 to Figure 2-15, the ethyl group on N24 shows a number of different orientations in each structure, indicating a rather high degree of conformational flexibility.

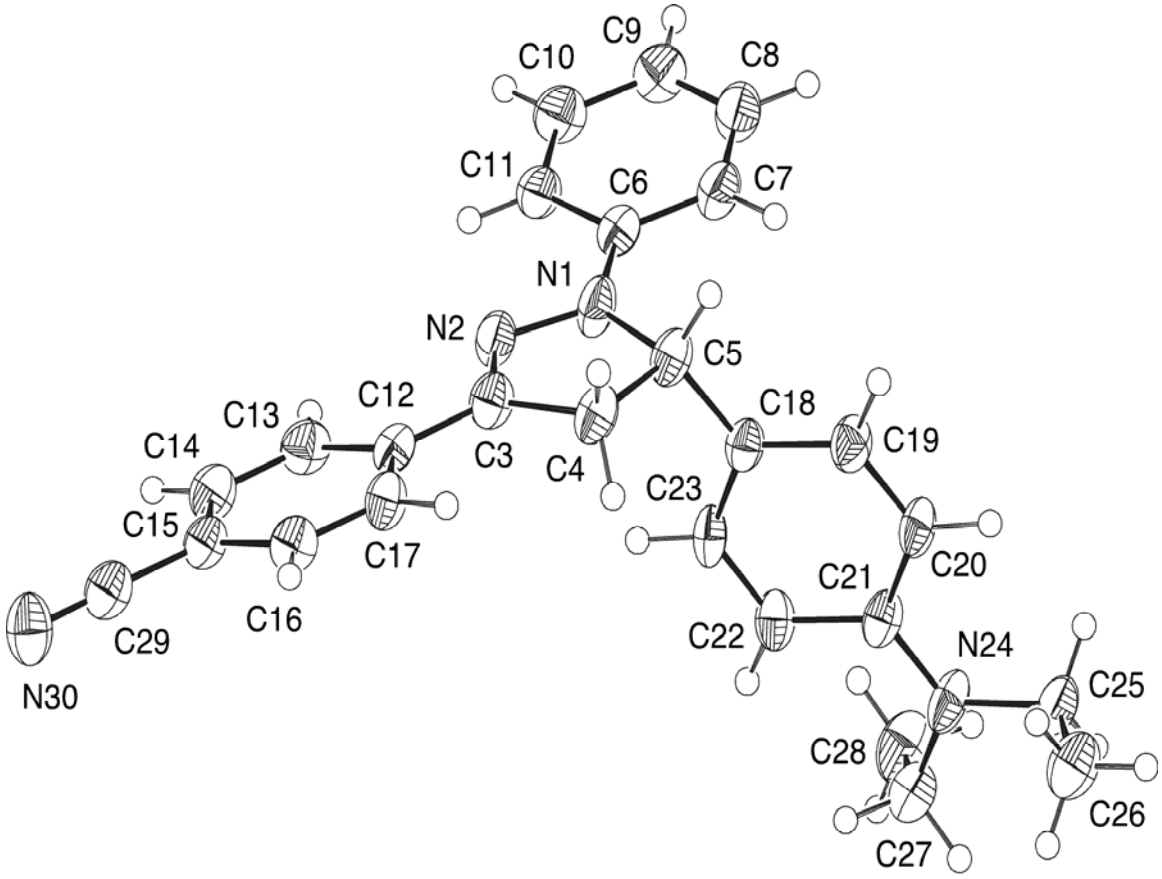


**Figure 2-10.** ORTEP representation and numbering scheme for **2-1b**. Thermal ellipsoids are drawn at the 50% probability level.

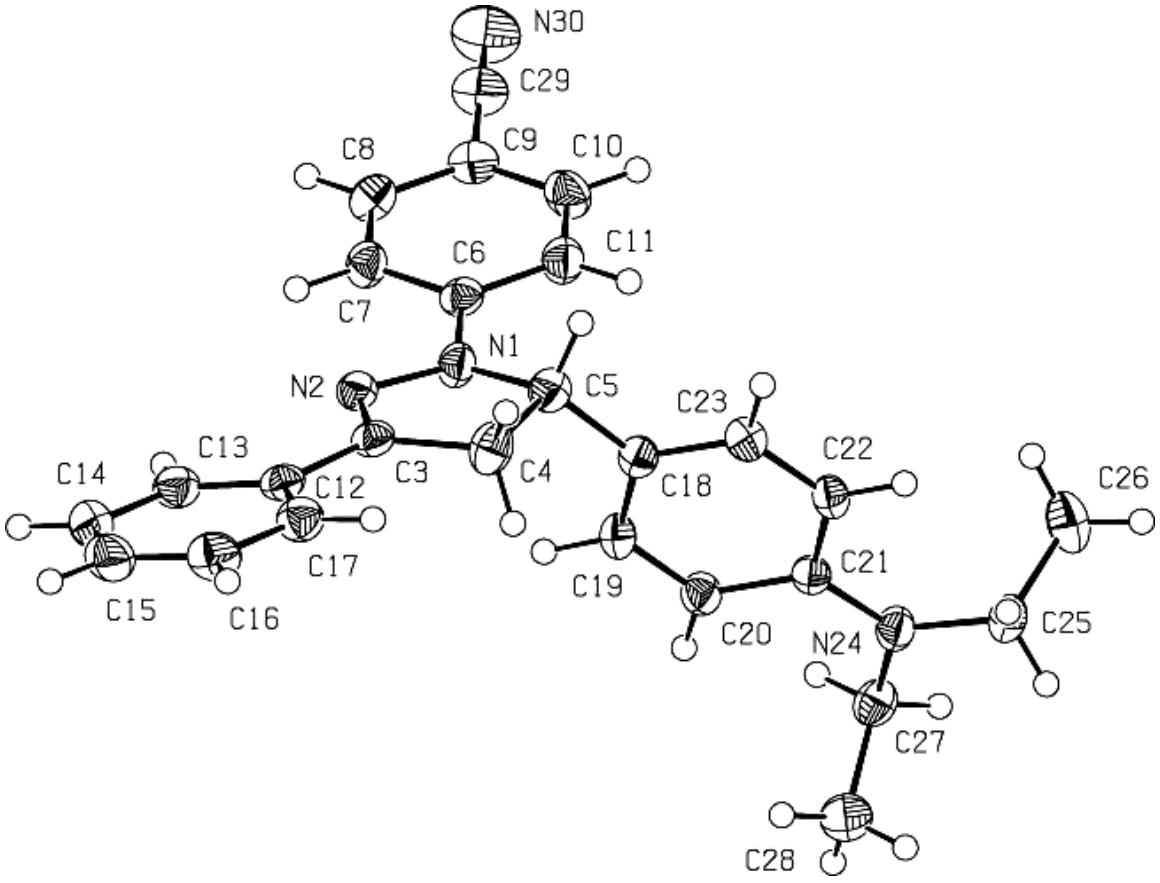


**Figure 2-11.** ORTEP representation and numbering scheme for **2-2a**.

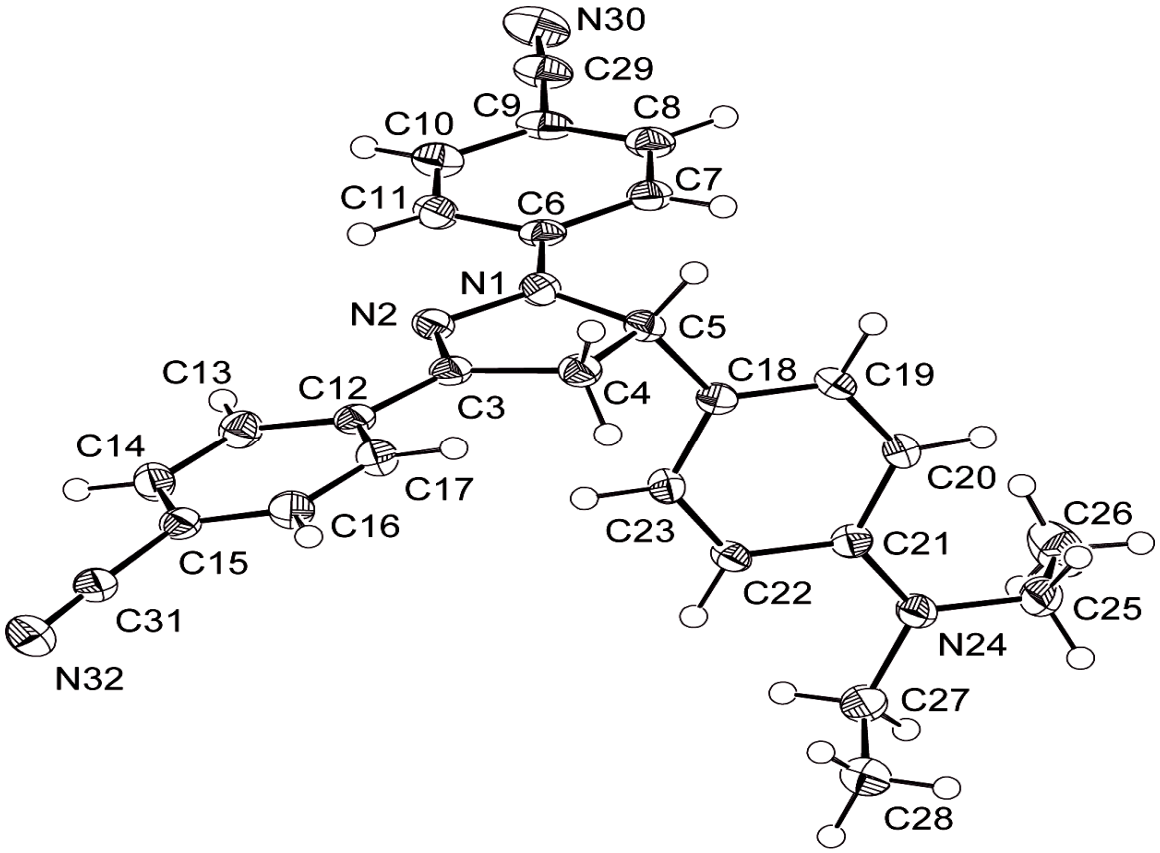


**Figure 2-12.** ORTEP representation and numbering scheme for **2-2b**.

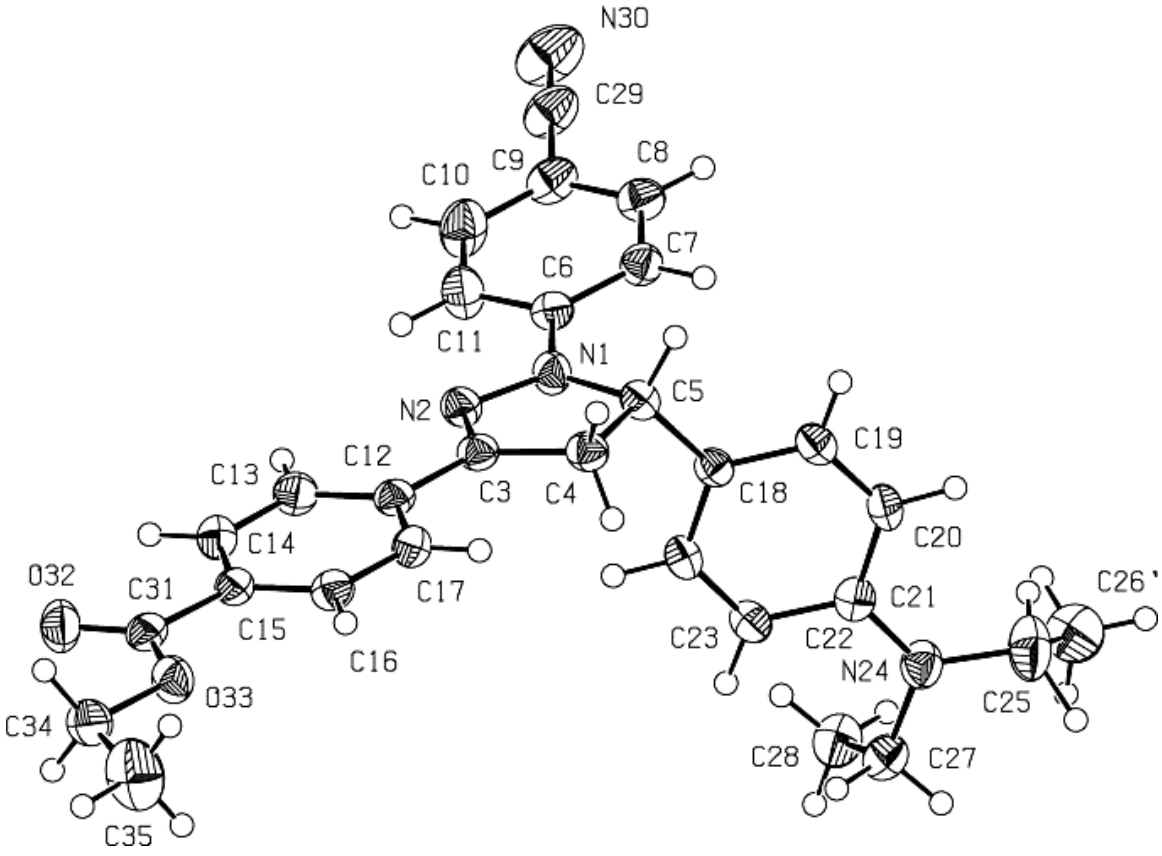


**Figure 2-13.** ORTEP representation and numbering scheme for **2-2c**.

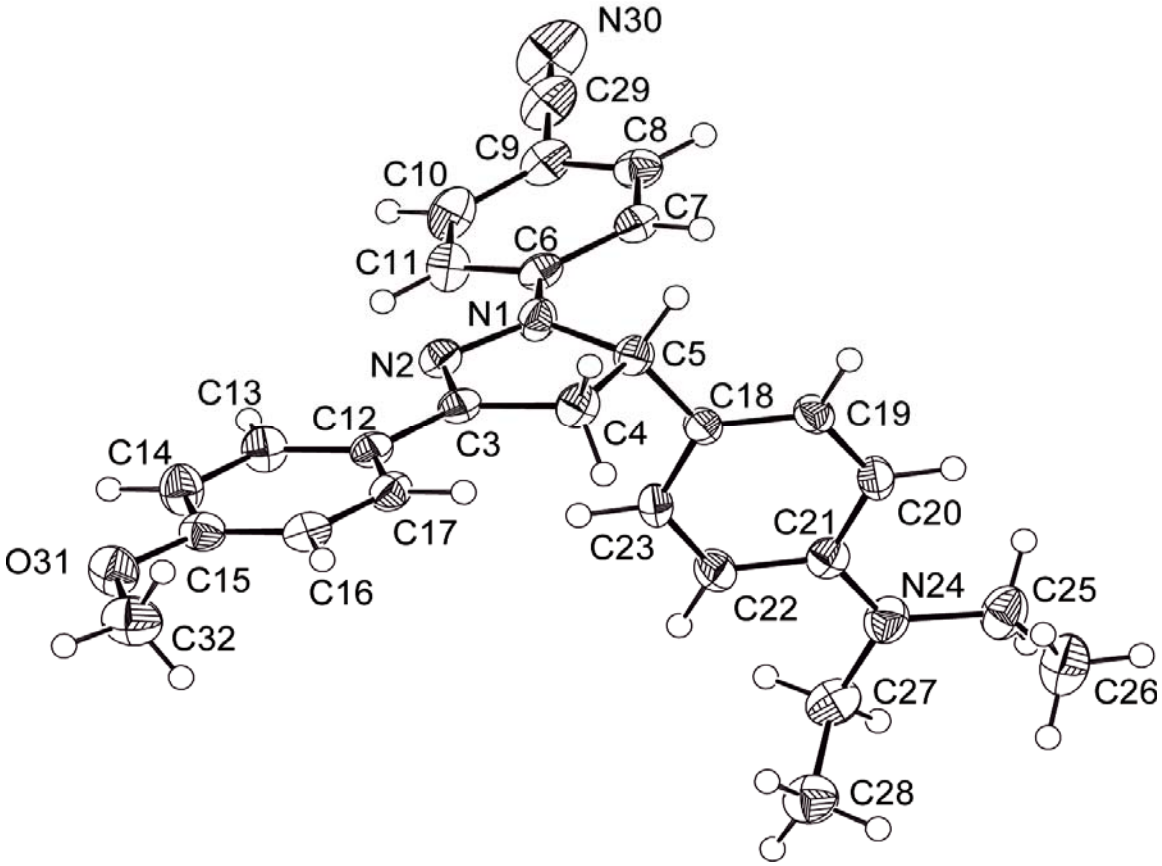


**Figure 2-14.** ORTEP representation and numbering scheme for **2-2d**.

A)

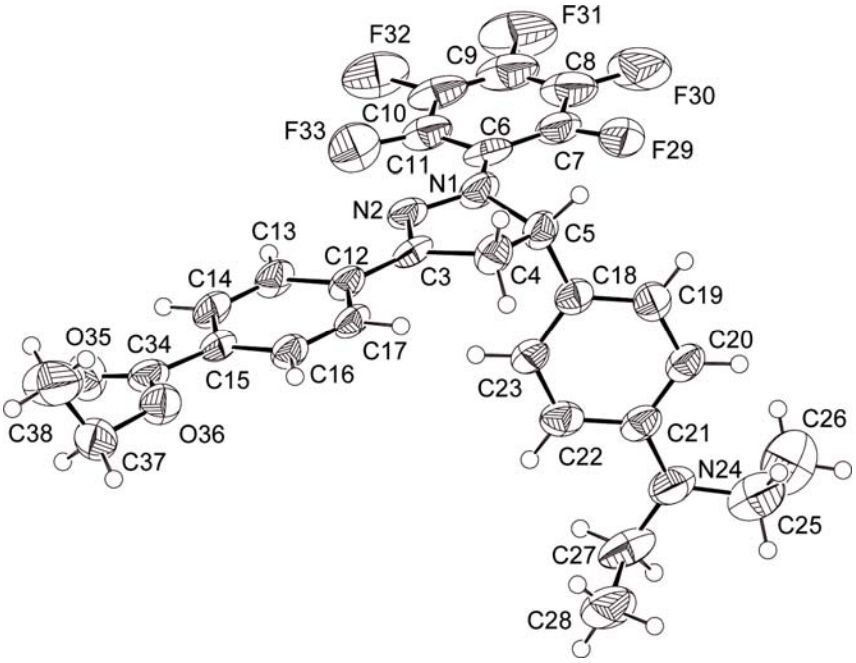


B)

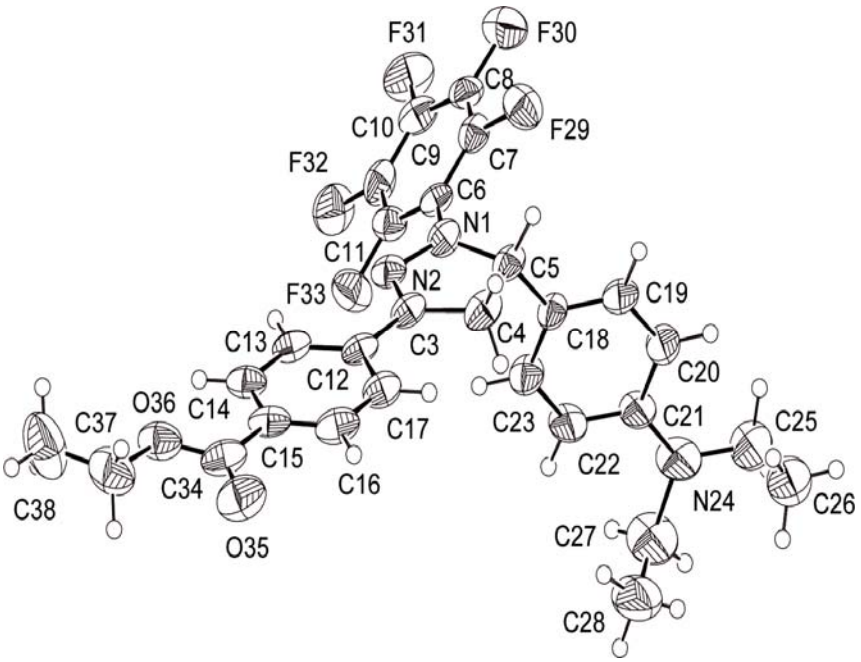


**Figure 2-15.** X-ray structure and numbering schemes for pyrazoline derivative **2-3b**. The two conformations (A and B) are crystallographically unique. For better comparison, both (*S*) isomers are depicted. Thermal ellipsoids are drawn at the 50% probability level.

The 1,3-diarly-$\Delta^2$-pyrazoline chromophore is nearly planar, which is best reflected by the fact that the sums of the bond angles at N(1) and C(3) are all close to 360°. Interestingly, the pentafluorophenyl-substituted derivative **2-3b** crystallized in two crystallographically unique conformations within the same unit cell. In conformation **A** the pentafluorophenyl substituent and the pyrazoline ring are essentially coplanar with a dihedral angle of –2.4°, while in the other conformation the pentafluorophenyl ring is twisted along the N1-C6 bond axis ($\theta_2$ = –32.8°). For all other derivatives, the dihedral angles $\theta_2$ and $\theta_3$ deviate only by a few degrees (< 10°) from an ideal coplanar orientation between the phenyl ring and the pyrazoline π-system.

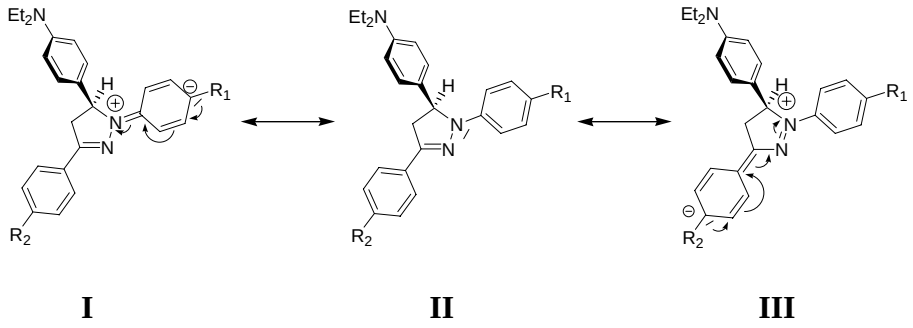


**Figure 2-16.** Electronic delocalization of the electron lone pair on N-1 illustrated by Lewis structures.

Consistent with a pronounced electronic interaction, the distances of the carbon atoms that connect the aryl and the pyrazoline ring systems are significantly shorter as would be expected for a single bond. For example, the average bond length of N1-C6 is 1.377 ± 0.010 Å, which is significantly shorter compared to the N24-C25 single bond

distance (average 1.460 ± 0.015 Å). Likewise, the C3-C12 bond length is with 1.454 ± 0.009 Å substantially shorter compared to the C27-C28 Å single bond distance (average 1.516 ± 0.010 Å). More subtle variations of bond lengths within the pyrazoline π-system reflect differences in the degree of charge delocalization, as illustrated by the Lewis structures in Figure 2-16. The two aryl substituents are electronically separated and communicate only indirectly via the lone pair electrons located on nitrogen N1. This lone pair can be localized toward either the aryl ring in the 1-position (structure **I**, Figure 2-16) or the aryl substituent in the 3-position (structure **III**, Figure 2-16). The degree of delocalization is expected to vary as a function of the electron-donating or -withdrawing character of the substituents $R_1$ and $R_2$, respectively. For example, **2-2b** has a more electron withdrawing substituent $R_1$ compared to **2-1b**, shortening the bond distance N1-C6 from 1.384 Å to 1.379 Å. Analogously, the C3-C12 bond length decreases with increasing electron withdrawing character of the substituent $R_2$. For example, the C3-C12 bond is 1.463 Å for **2-2a**, while with a cyano substituent as in **2-2b** the bond shortens to 1.458 Å. The C3-C12 bond of **2-1b** is even shorter because the substituent $R_1$ allows for more charge delocalization towards to $R_2$.

In summary, the X-ray studies revealed a concise picture of the molecular framework of triaryl pyraoline, which is strongly governed by electron delocalization within the fluorophore structure.

**Table 2-2:** Selected Structural Data for Pyrazoline Derivatives **2-1b**, **2-2a**, **2-2b**, **2-2c**, **2-2d**, **and 2-3b**.

| parameter[a] | **2-1b** | **2-2a** | **2-2b** | **2-2c** | **2-2d** | **2-3b** (A) | **2-3b** (B)[e] |
|---|---|---|---|---|---|---|---|
| N(1)-N(2) (Å) | 1.376(4) | 1.379(2) | 1.373(2) | 1.374(2) | 1.379(2) | 1.377(8) | 1.380(8) |
| N(1)-C(5) (Å) | 1.493(4) | 1.482(2) | 1.496(2) | 1.483(2) | 1.490(2) | 1.515(9) | 1.496(9) |
| N(1)-C(6) (Å) | 1.384(5) | 1.380(2) | 1.379(2) | 1.377(2) | 1.373(2) | 1.382(10) | 1.373(9) |
| N(2)-C(3) (Å) | 1.291(5) | 1.291(2) | 1.296(2) | 1.292(2) | 1.297(2) | 1.300(10) | 1.287(9) |
| C(3)-C(12) (Å) | 1.449(5) | 1.463(2) | 1.458(3) | 1.462(3) | 1.459(2) | 1.431(9) | 1.456(9) |
| C(3)-C(4) (Å) | 1.512(5) | 1.499(2) | 1.515(2) | 1.504(3) | 1.501(2) | 1.509(10) | 1.502(10) |
| N(2)-C(3)-C(12) (deg) | 120.9(3) | 121.58(13) | 122.13(16) | 120.52(16) | 121.20(15) | 121.5(6) | 120.6(6) |
| C(6)-N(1)-N(2) (deg) | 119.9(3) | 119.74(11) | 119.42(14) | 119.56(15) | 120.34(13) | 119.8(6) | 119.2(5) |
| N(1)-C(5)-C(18) (deg) | 112.7(3) | 113.40(14) | 112.44(13) | 112.21(15) | 110.96(13) | 111.2(5) | 112.5(5) |
| N(l)-C(5)-C(18)-C(23) ($\theta_1$)[b] (deg) | -48.6(4) | -34.63(13) | -63.6(2) | -54.2(2) | -46.9(2) | -58.5(9) | -47.0(8)[f] |
| N(2)-N(1)-C(6)-C(11) ($\theta_2$)[b] (deg) | -3.6(6) | 8.1(2) | 0.6(2) | -7.8(3) | -4.2(2) | -2.4(8) | -32.8(10)[f] |
| N(2)-C(3)-C(12)-C(13) ($\theta_3$)[b] (deg) | 10.9(6) | -8.5(2) | 8.8(2) | 0.5(3) | 4.0(2) | 4.7(8) | -0.5(10)[f] |
| $\Sigma_1$ at N(l)[c] (deg) | 359.9 | 357.86 | 359.73 | 359.65 | 358.56 | 357.9 | 358.8 |
| $\Sigma_2$ at C(3)[d] (deg) | 360.0 | 359.94 | 359.98 | 360.0 | 359.98 | 359.9 | 359.9 |

[a]Numbering scheme given in the corresponding ORTEP plots. [b] Dihedral angles refer to the (*S*) stereoisomer.[c] Sum of bond angles N2-N1-C6, N2-N1-C5, and C5-N1-C6.[d] Sum of bond angles N2-C3-C12, C4-C3-C12, and N2-C3-C4.[e] Crystallographically independent conformations with opposite chirality.[f] (*S*) isomer.

## 2.4. Photophysics

### *2.4.2. Steady State Absorption Spectra*

The absorption maxima and molar absorptivity values for all derivatives are shown in the Table 2-3. All UV-vis absorption spectra show featureless, strong bands centered around 24,000 $cm^{-1}$ to 28,000 $cm^{-1}$ in all solvents investigated, with molar absorption coefficients varying between 8,000 and 30,000 $M^{-1}cm^{-1}$, The lowest energy absorption can be assigned to an allowed $\pi \rightarrow \pi^*$ transition localized on the pyrazoline ring system, corresponding to excitation into the $^1$LE state. Because this electronic transition involves intramolecular charge transfer from the aromatic ring attached to N1 (including N1) towards the N2-C3-aryl π-system, the transition energy is strongly influenced by the nature of the substituents in the 1- and 3-position of the pyrazoline ring. For the same $R_2$, the peak absorption energy increases slightly with increasing electron-withdrawing character of $R_1$. Among all of the studied derivatives, **2-3a** and **2-3b** have the strongest electron withdrawing group $R_1$ (pentafluoro-aryl) and therefore show the highest energy absorptions at 31,560 $cm^{-1}$ and 28,820 $cm^{-1}$, respectively. Figure 2-17 illustrates the trend for a set of fluorophores, **2-1b**, **2-2b** and **2-4a,** that contain the same *p*-cyanophenyl group $R_2$, but differ in $R_1$. With increasing electron-withdrawing character of the substituent $R_1$, the absorption energy increases gradually: the *p*-methoxyphenyl derivative **2-4a** exhibits an absorption maximum of 24,100 $cm^{-1}$, while the phenyl (**2-1b**) and *p*-cyanophenyl (**2-2b**) derivatives are peak at 24,880 $cm^{-1}$ and 25,640 $cm^{-1}$, respectively. In contrast, the substituent $R_2$ has the exact opposite influence on the absorption energy. The absorption band shifts to lower energy with increasing electron-withdrawing character of substituent $R_2$. For example, *p*-cyano derivative **2-2b** and *p*-

ethylcarboxylate derivative **2-2c** show lower energy absorptions compared to **2-2a,** shown in Figure 2-18. Interestingly, the strongly electron-donating methoxy group in **2-2d** does not further shift the absorption maximum to higher energy. In general, the influence of the substituent $R_2$ on the absorption spectra is greater compared to substituent $R_1$.

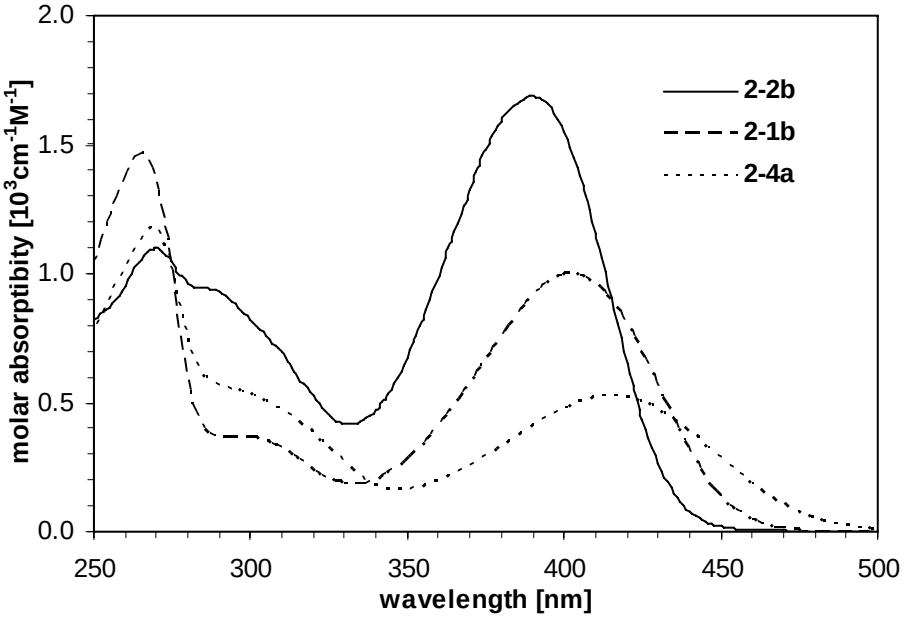


**Figure 2-17.** UV absorption spectra of **2-1b, 2-2b** and **2-4a** in methanol at room temperature. **2-1b**, **2-2b** and **2-4a** have all a *p*-CN group for $R_2$; the $R_1$ subtituents are H, *p*-CN and *p*-OMe, respectively.

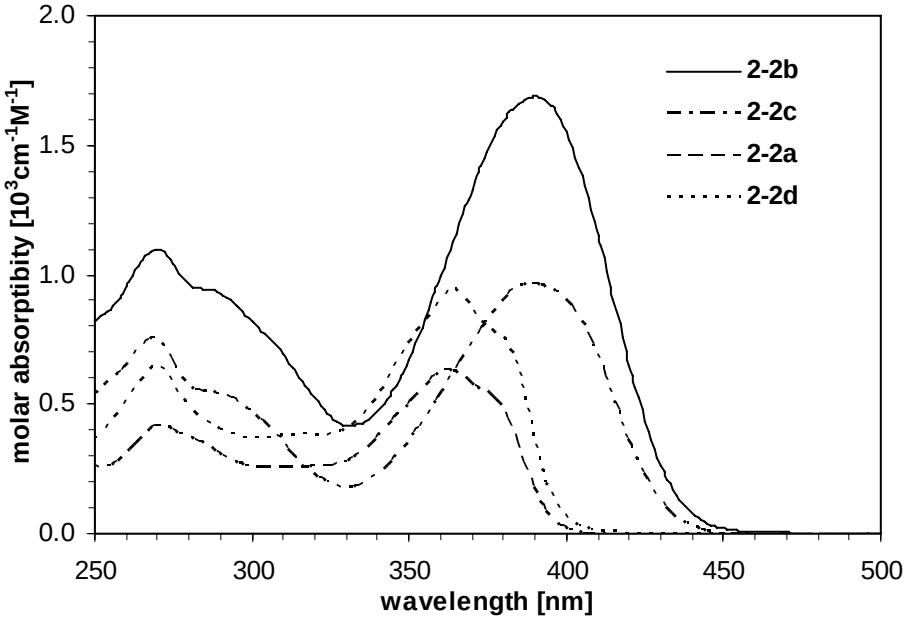


**Figure 2-18.** UV absorption spectra of **2-2a**, **2-2b, 2-2c** and **2-2d** in methanol at room temperature. **2-2a**, **2-2b, 2-2c** and **2-2d** have all a *p*-CN group for $R_1$; the $R_2$ substituents are H, *p*-CN, *p*-COOEt, and *p*-OMe, respectively.

**Table 2-3.** Room Temperature Photophysical Data of Pyrazolines **2-1** to **2-6** in Various Solvents.

| comp | solvent | $\nu_{abs}$ ($10^3 cm^{-1}$) | $\varepsilon$ ($10^3 M^{-1}cm^{-1}$) | $\nu_{em}$ ($10^3 cm^{-1}$) | $\nu_{abs} - \nu_{em}$ ($cm^{-1}$) |
|---|---|---|---|---|---|
| **2-1a** | MeOH | 28.00 | 18.54 | 21.13 | 6867 |
| | MeCN | 28.00 | 20.39 | 21.91 | 5872 |
| | EtOAc | 27.70 | 19.20 | 22.51 | 5348 |
| | $Et_2O$ | 27.77 | 19.49 | 22.83 | 4939 |
| | Hexane | 27.54 | 19.37 | 23.30 | 4236 |
| **2-1b** | MeOH | 24.88 | 29.24 | 19.65 | 5229 |
| | MeCN | 24.94 | 18.48 | 19.57 | 5374 |
| | EtOAc | 24.88 | 16.60 | 20.58 | 4299 |
| | $Et_2O$ | 24.94 | 30.60 | 20.70 | 4239 |
| | Hexane | 24.75 | 27.73 | 22.03 | 2726 |
| **2-1c** | MeOH | 25.20 | 24.91 | 19.08 | 6111 |
| | MeCN | 25.31 | 22.58 | 19.57 | 5741 |
| | EtOAc | 25.20 | 23.66 | 20.53 | 4661 |
| | $Et_2O$ | 25.31 | 21.45 | 20.92 | 4390 |
| | Hexane | 25.20 | 25.46 | 21.60 | 3597 |
| **2-2a** | MeOH | 27.62 | 15.60 | 24.00 | 3626 |
| | MeCN | 27.54 | 29.24 | 23.54 | 4000 |
| | EtOAc | 27.54 | 32.28 | 23.85 | 3691 |
| | $Et_2O$ | 27.63 | 21.62 | 24.14 | 3495 |
| | Hexane | 27.47 | 22.87 | 24.95 | 2522 |
| **2-2b** | MeOH | 25.64 | 34.71 | 21.39 | 4251 |
| | MeCN | 25.70 | 18.80 | 21.31 | 4387 |
| | EtOAc | 25.57 | 34.99 | 21.65 | 3919 |
| | $Et_2O$ | 25.70 | 24.53 | 21.97 | 3805 |
| | Hexane | 25.77 | 40.02 | 23.07 | 2627 |
| **2-2c** | MeOH | 25.70 | 58.68 | 20.96 | 4736 |
| | MeCN | 25.70 | 34.07 | 21.28 | 4424 |
| | EtOAc | 25.70 | 33.70 | 21.74 | 3961 |
| | $Et_2O$ | 25.91 | 34.83 | 22.22 | 3685 |
| | Hexane | 25.83 | 28.67 | 23.53 | 2304 |

**Table 2-3. (**continued).

| comp | solvent | $\nu_{abs}$ ($10^3 cm^{-1}$) | $\varepsilon$ ($10^3 M^{-1}cm^{-1}$) | $\nu_{em}$ ($10^3 cm^{-1}$) | $\nu_{abs} - \nu_{em}$ ($cm^{-1}$) |
|---|---|---|---|---|---|
| **2-2d** | MeOH | 27.47 | 22.44 | 23.92 | 3549 |
| | MeCN | 27.40 | 31.07 | 23.85 | 3548 |
| | EtOAc | 27.47 | 33.16 | 24.00 | 3417 |
| | $Et_2O$ | 27.55 | 34.37 | 24.06 | 3492 |
| | Hexane | 27.47 | 20.30 | 24.07 | 3405 |
| **2-3a** | MeOH | 31.56 | 19.57 | 28.33 | 3227 |
| | MeCN | 31.65 | 17.76 | 29.76 | 1884 |
| | EtOAc | 31.05 | 18.71 | 25.77 | 5273 |
| | $Et_2O$ | 31.05 | 20.27 | 25.58 | 5471 |
| | Hexane | 30.86 | 20.63 | 25.91 | 4957 |
| **2-3b** | MeOH | 28.82 | 21.66 | 22.08 | 6734 |
| | MeCN | 29.24 | 22.61 | 22.42 | 6818 |
| | EtOAc | 28.74 | 24.73 | 17.95 | 5379 |
| | $Et_2O$ | 28.65 | 21.70 | 20.62 | 8077 |
| | Hexane | 28.48 | 24.79 | 22.03 | 6455 |
| **2-4a** | MeOH | 24.10 | 16.54 | 17.48 | 6614 |
| | MeCN | 24.15 | 14.54 | 17.51 | 6641 |
| | EtOAc | 24.04 | 15.68 | 18.45 | 5588 |
| | $Et_2O$ | 24.10 | 10.33 | 18.87 | 5228 |
| | Hexane | 23.92 | 8.43 | 19.84 | 4076 |
| **2-4b** | MeOH | 24.45 | 15.83 | 17.09 | 7356 |
| | MeCN | 24.51 | 19.10 | 17.61 | 6904 |
| | EtOAc | 24.45 | 15.83 | 17.76 | 6688 |
| | $Et_2O$ | 24.51 | 17.05 | 19.01 | 5498 |
| | Hexane | 24.45 | 14.65 | 20.24 | 4207 |
| **2-5** | MeOH | 25.38 | 13.62 | 19.27 | 6113 |
| | MeCN | 25.51 | 16.25 | 19.42 | 6093 |
| | EtOAc | 25.44 | 16.19 | 20.53 | 4905 |
| | $Et_2O$ | 25.57 | 17.49 | 20.92 | 4648 |
| | Hexane | 25.38 | 14.56 | 21.60 | 3782 |
| **2-6** | MeOH | 26.05 | 20.29 | 20.88 | 5172 |
| | MeCN | 26.05 | 27.37 | 21.14 | 4907 |
| | EtOAc | 26.05 | 23.72 | 21.98 | 4070 |
| | $Et_2O$ | 26.18 | 24.39 | 22.52 | 3662 |
| | Hexane | 26.18 | 18.73 | 22.68 | 3509 |

### *2.4.3. Steady State Fluorescence Emission Spectra*

#### *2.4.3.1.Influence of Substituents*

Compared to the absorption spectra, the emission spectra are much more sensitive towards the nature of substituents $R_1$ and $R_2$. Changes of the substituents vary the emission maxima by more than 7000 $cm^{-1}$. The influence of the substituents $R_1$ and $R_2$ on the emission maxima is similar to the influence on the absorption spectra, as previously described in Section 2.4.1. For a given substituent $R_2$, the emission maxima shift to higher energy with increasing electron-withdrawing character of substituent $R_1$. Presumably, with increasing electron-withdrawing character of substituent $R_1$, the lone pair electrons on N1 are more delocalized towards the phenyl ring attached to the 1-position of the pyrazoline system, thus reducing the degree of charge-transfer towards C3 and shifting the emissive state towards higher energy. This effect can be observed for all derivatives. For example, the cyano-substituted pyrazolines **2-2b**, **2-1b** and **2-4a** show emission shifts from 21,390 $cm^{-1}$ to 19,650 $cm^{-1}$ and 17,480 $cm^{-1}$ with decreasing electron-withdrawing character of the substituent on the 1-phenyl ring, as shown in Figure 2-19. The Stokes' shifts reveal a similar trend. **2-2b**, **2-1b** and **2-4a** show a gradually increasing Stokes' shift going from 4,200 $cm^{-1}$ to 5,200 $cm^{-1}$ and 6,600 $cm^{-1}$ with decreasing electron-withdrawing character of substituents $R_1$. Derivative **2-2d** with a *p*-methoxyphenyl substituent in the 3-position exhibits Stokes' shift of only 3,500 $cm^{-1}$. This trend is further illustrated by a comparison of the phenyl-substituted pyrazolines **2-1a**, **2-2a** and **2-3a**, which show emission maxima shifts from 21,130 $cm^{-1}$ to 24,000 $cm^{-1}$ and 28,330 $cm^{-1}$ with increasing electron-withdrawing character of the substituent attached to the 1-aryl ring The pyrazoline series **2-4b**, **2-1c**, **2-5**, **2-2c** and **2-3b** containing a *p*-ethyl ester substitutent for $R_2$ exhibit the analogous trend. The derivatives cover a

rather large range of emission energies spanning approximately 5000 $cm^{-1}$, starting with the strongly electron-donating methoxy group and ending with the electron-withdrawing fluoro-, cyano-, and pentafluoro-aryl substituents, showing (shown in Figure 2-20).

As already observed for the UV-vis absorption spectra, the effect of $R_2$ on the emission energies is essentially opposite of $R_1$. For a given substituent $R_1$, the emission maxima shift to lower energy with increasing electron-withdrawing character of substituent $R_2$, as shown in Figure 2-21. For example, derivatives **2-2a** and **2-2b** exhibit emission maxima at 24,000 and 21,390 $cm^{-1}$, respectively.

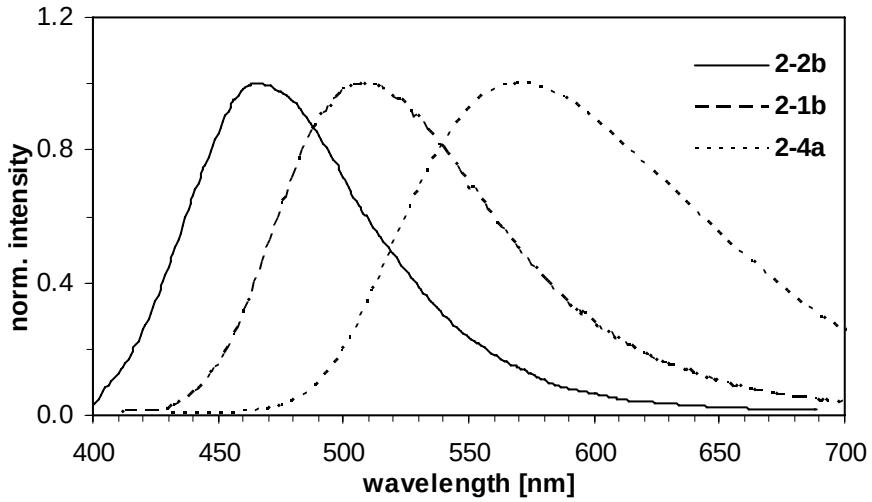


**Figure 2-19.** Normalized emission spectra of pyrazolines **2-1b**, **2-2b** and **2-4a** in methanol at room temperature. **2-1b**, **2-2b** and **2-4a** have all a *p*-CN group for $R_2$; the $R_1$ substituents are H, *p*-CN, and *p*-OMe, respectively.

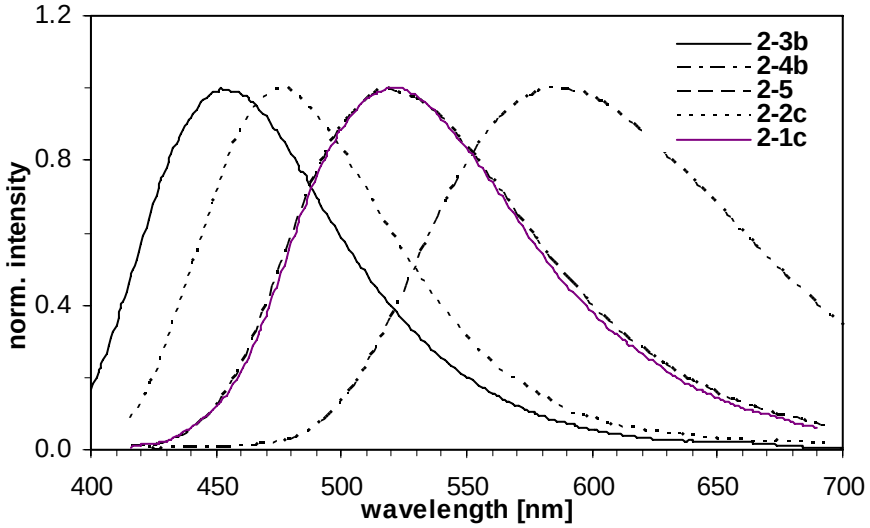


**Figure 2-20.** Normalized emission spectra of pyrazolines **2-4b**, **2-1c**, **2-5**, **2-2c** and **2-3b** in methanol at room temperature. The spectra of **2-1c** and **2-5** are almost identical.

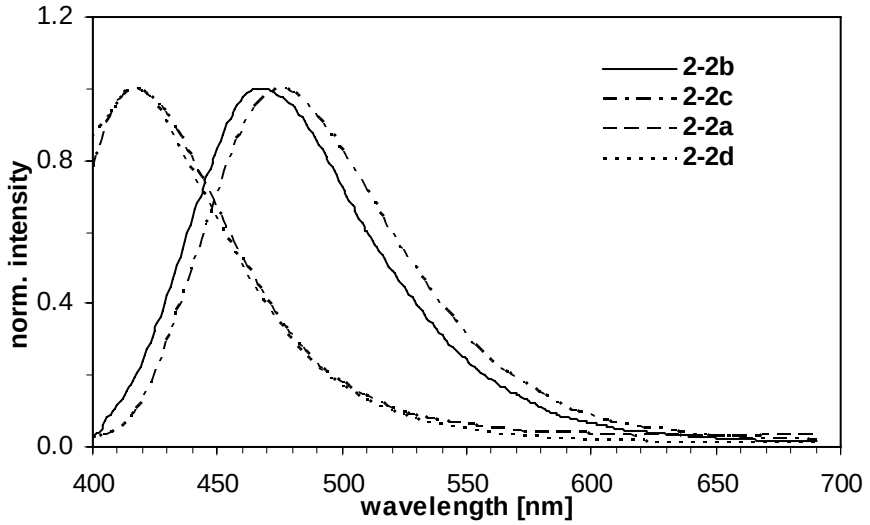


**Figure 2-21.** Normalized emission spectra of pyrazolines **2-2a**, **2-2b, 2-2c** and **2-2d** in methanol at room temperature. **2-2a**, **2-2b, 2-2c** and **2-2d** have all a *p*-CN group for $R_1$; the $R_2$ substituents are -H, *p*-CN, *p*-COOEt, and *p*-OMe, respectively.

In summary, the synthesized set of 1,3,5-triaryl-substited pyrazoline fluorophores show great flexibility in terms of their tunability of both, the absorption and emission energies, and the measured data are consistent with the spectroscopic trends of previously characterized 1,3- and 1,3,5-aryl-substituted pyrazolines.[22,23]

#### *2.4.3.2.Quantum Yields*

The quantum yields of all derivatives under neutral and acidic conditions in methanol are listed in Table 2-4 and graphically illustrated in Figure 2-22. Protonation of the diethylamino group, which is acting as the electron-donor moiety in the excited-state electron transfer process, is expected to increase the donor oxidation potential and should therefore strongly influence the quenching pathway. As outlined in Section 2.1.1, the fluorescence enhancement is determined by the relative energy ordering of the emissive $^1$LE and nonemissive $^1$ET levels. Protonation of the diethylamino group does not necessarily guarantee a significant change of the emission quantum yield. Only if the $^1$ET level rises significantly above $^1$LE, a large fluorescence enhancement is observed. The aryl-substituents in the 1- and 3-position not only influence the absorption and emission energy of the molecule, but also determine the redox properties of the fluorophore, and therefore influence the thermodynamics of the excited state electron-transfer quenching process.

The fluorescence quantum yield for most of the pyrazoline derivatives **2-1** and **2-5** increases significantly in the presence of 0.1% trifluoroacetic acid and reaches an average value of 0.5. The *p*-methoxy-substituted derivatives **2-4a** and **2-4b** show a quantum yield of 0.1 in neutral methanol and remain unchanged upon protonation. The methoxy group increases the charge transfer character of the fluorophore core and therefore decreases the

excited-state equilibrium energy, which in turn increases the free energy of the excited-state electron-transfer process according to the Rehm-Weller formalism. At neutral conditions, the energy of the ET state is presumably in proximity to the LE state, and therefore radiative deactivation from LE competes successfully with the electron transfer quenching process. For the pentafluorophenyl substituted derivatives **2-3a** and **2-3b**, the quantum yield is essentially identical under neutral conditions, while only **2-3b** gives fluorescence enhance factor of 160 upon addition of acid. For **2-3a**, the strong electron-withdrawing pentafluoro group increases the excited-state equilibrium energy, and therefore the energy level of the ET state is significantly lower and does apparently not rise above LE upon protonation of the diethylamino group. However, the electron-withdrawing ester group in **2-3b** increases the degree of charge transfer character of the LE state, thus lowering its energy sufficiently such that the ET level rises above LE upon protonation. As a consequence, a large fluorescence enhancement is observed. This explanation is further supported by the quantum chemical calculation of the energy differences between the ET and LE states (see Section 2.5.2). Furthermore, the control compound **2-6,** which is lacking the electron-donating diethylamino group, exhibits a high quantum yield in neat methanol that is not affected by addition of acid.

**Table 2-4.** The Emission Quantum Yields in Neutral and Acidic Methanol Containing 0.1% Trifluoroacetic Acid.

| compd | neutral[a] | acidic[a] | ef[b] |
|---|---|---|---|
| **2-1a** | 0.11 | 0.24 | 2 |
| **2-1b** | 0.04 | 0.89 | 20 |
| **2-1c** | 0.01 | 0.51 | 37 |
| **2-2a** | 0.012 | 0.58 | 50 |
| **2-2b** | 0.011 | 0.43 | 40 |
| **2-2c** | 0.011 | 0.59 | 55 |
| **2-2d** | 0.032 | 0.20 | 6 |
| **2-3a** | 0.004 | 0.004 | 1 |
| **2-3b** | 0.004 | 0.66 | 160 |
| **2-4a** | 0.12 | 0.12 | 1 |
| **2-4b** | 0.10 | 0.11 | 1 |
| **2-5** | 0.028 | 0.40 | 14 |
| **2-6** | 0.63 | 0.62 | 1 |

[a]Quantum yield; determined with quinine sulfate in 1.0 N $H_2SO_4$ as reference. [b]Fluorescence enhancement factor between neutral and acidic solution (based on quantum yield).

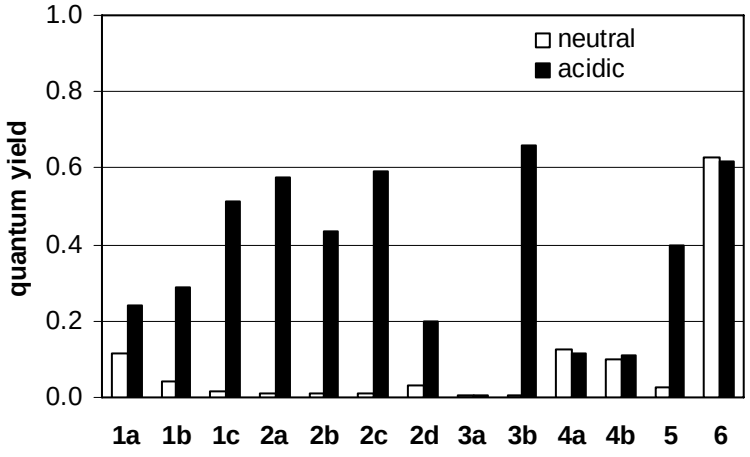


**Figure 2-22.** Comparison of the emission quantum yields in neutral and acidic methanol containing 0.1% trifluoroacetic acid.

#### *2.4.3.3.Solvatochromic Shifts*

To perform a solvatochromic shift analysis, the absorption and emission spectra of all derivatives were measured in five solvents covering a large polarity range (cyclohexane, diethyl ether, ethyl acetate, acetonitrile and methanol). The corresponding absorption and emission maxima are compiled in Table 2-3. In all solvents, emission occurs from the local-excited state having considerable charge-transfer character; therefore, the emission energy is strongly influenced by the polarity of the solvent. In a polar solvent such as methanol, the charge-transfer state is stabilized by dipole-dipole interaction with the solvent, and therefore the emission is shifted to lower energy compared to non-polar or low polarity solvents. For most of the derivatives, the Stokes' shifts increase with increasing solvent polarity. To illustrate this trend Figure 2-23 displays the emission spectra of derivative **2-2c** in various solvents. While in *n*-hexane a vibrationally structured emission spectrum is observed, all other solvents exhibit a featureless broad emission band presumably due to extensive excited-state solvent interactions. With decreasing solvent polarity the fluorescence maximum shifts gradually to higher energy, starting at 21,000 $cm^{-1}$ in methanol and going to 23,500 $cm^{-1}$ in hexane. The positive solvatochromic shift indicates an increased molecular dipole moment in the excited state compared to the vibrationally non-relaxed ground state. Similarly, the overall Stokes' shift increases with increasing solvent polarity, indicating a higher dipole moment in the vibrationally cooled excited state $S_1$ compared to the ground state $S_0$, as shown illustrated by the values compiled in Table 2-7.

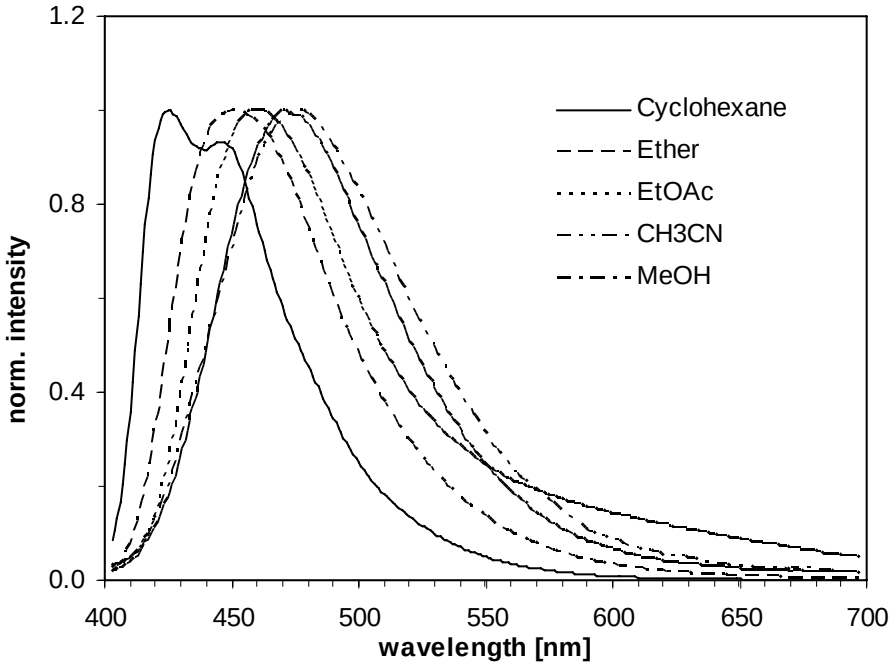


**Figure 2-23.** Normalized emission spectra of **2-2c** in various solvents at room temperature.

According to the Lippert-Magaga formalism,[24-26] the difference between the excited-state and ground state dipole moments ($\mu_e$-$\mu_g$) can be determined from a plot of the Stokes' shift $\Delta\nu_{(abs\text{-}em)}$ versus the solvent polarity function $\Delta f = f(\in_s)$- $f$(n):

$$\Delta\nu = \nu_{abs} - \nu_{em} = \Delta\nu_0 + \frac{2}{hc}\frac{(\mu_e - \mu_g)}{a_0^{\,3}}\Delta f \tag{2.3}$$

with

$$\Delta f = f(\in_s) - f(n) = \frac{\in_s -1}{2\in_s +1} - \frac{n^2 -1}{2n^2 +1} \tag{2.4}$$

where $a_0$ is the Onsager cavity radius,[27] $\in_s$ and $n$ are the relative permittivity and refractive index of the corresponding solvent, respectively, and $\Delta\nu_0$ is the extrapolated Stokes' shift in a vacuum.

The X-ray data of compounds **2-1b**, **2-2a-d** and **2-3b** allowed for determination of the molecular volume using the unit cell dimensions, cell occupancy and molecular weight. The cavity radius for each of the remaining compounds was estimated based on the corresponding geometry-optimized structure and Monte-Carlo integration of the volume inside a contour of 0.001 electrons/bohr$^3$ density (B3LYP/6-31G*//B3LYP/6-31G*).[28] The computationally determined radii matched the experimentally derived values within 0.05 Å, and therefore represented reliable estimates for the compounds for which no X-ray data were available.

**Tabel 2-5.** Polarity Function $\Delta f$ for Selected Solvents According to Equation 2.4.

| solvent | $\Delta f$ |
|---|---|
| cyclohexane | -0.00131 |
| $Et_2O$ | 0.16690 |
| EtOAc | 0.20022 |
| MeCN | 0.30457 |
| MeOH | 0.30856 |

Plots of the Stokes' shifts as a function of the solvent polarity parameter $\Delta f$ are shown in Figure 2-24 to Figure 2-26 for selected derivatives, and the corresponding numerical values of the Stokes' shifts in various solvents are listed in Table 2-6. Because the solvent polarity parameter of methanol is very similar compared to acetonitrile, it was not included in the Lippert-Mataga plots. In order to analyze differences in effects of the substituents $R_1$ and $R_2$, the plots were arranged according to identical substituents $R_1$ with varying $R_2$, as well as identical substituents $R_2$ with varying $R_1$.

Interestingly, the substituents $R_1$ and $R_2$ influence the solvatochromic plots in substantially different ways. For a given substituent $R_1$, such as the *p*-cyano-substituted derivatives **2-2d**, **2-2a**, **2-2b** and **2-2c**, the slope of the solvatochromic plots is gradually increasing from 452 to 4981, 5866, and 8024 $cm^{-1}$, as shown in the Figure 2-24. In contrast, the linear regression lines for the derivatives with identical substituents $R_2$ and varying substituents $R_1$ are almost parallel and exhibit similar slopes, as illustrated by Figures 2-25 and 2-26. Apparently, changes in the electron-withdrawing character of $R_1$ have no significant effect on the slope; however, the intercept $\Delta\nu_{0,}$ which corresponds to the extrapolated Stokes' shift in vacuum, is substantially affected. For example, the

unsubstituted derivatives **2-1a** and **2-2a** reveal very similar slopes of 5099 and 4981 $cm^{-1}$, respectively. Likewise, the slopes for the ester-substituted derivatives **2-1c**, **2-2c**, **2-3b**, **2-4b** are 8,864, 8,024, 8,673 and 8,803 $cm^{-1}$, which are identical within experimental error, but substantially different compared to the unsubstituted group **2-1a** and **2-2a**.

**Table 2-6.** Solvent Polarity Function $\Delta f$ and Stokes' Shifts $\Delta\nu_{(abs\text{-}em)}$ for Selected Pyrazoline Fluorophores.

| | $\nu_{abs}$-$\nu_{em}$ of selective pyrazoline derivatives | | | | | | | | | | |
|---|---|---|---|---|---|---|---|---|---|---|---|
| solvent | **2-1a** | **2-1b** | **2-1c** | **2-2a** | **2-2b** | **2-2c** | **2-2d** | **2-3a** | **2-3b** | **2-4a** | **2-4b** |
| cyclohexane | 4236 | 2726 | 3597 | 2522 | 2627 | 2304 | 3405 | 4957 | 6455 | 4076 | 4207 |
| $Et_2O$ | 4939 | 4239 | 4390 | 3495 | 3805 | 3685 | 3492 | 5471 | 8077 | 5228 | 5498 |
| EtOAc | 5348 | 4299 | 4661 | 3626 | 3919 | 3961 | 3417 | 5273 | 5379 | 5588 | 6688 |
| MeCN | 5872 | 5229 | 5741 | 3691 | 4251 | 4424 | 3548 | 1884 | 6818 | 6641 | 6904 |
| MeOH | 6867 | 5374 | 6111 | 4000 | 4387 | 4736 | 3549 | 3227 | 6734 | 6614 | 7356 |

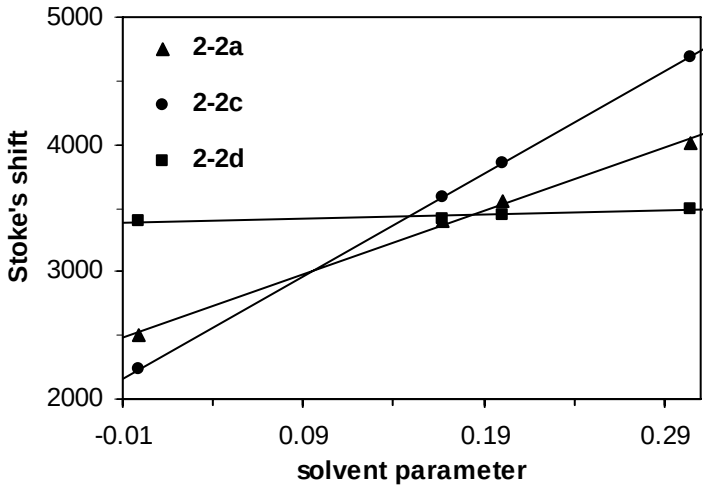


**Figure 2-24.** Solvatochromic shifts as a function of the solvent polarity parameter $\Delta f$ according to the Lippert-Mataga formalism (equation 2.3).

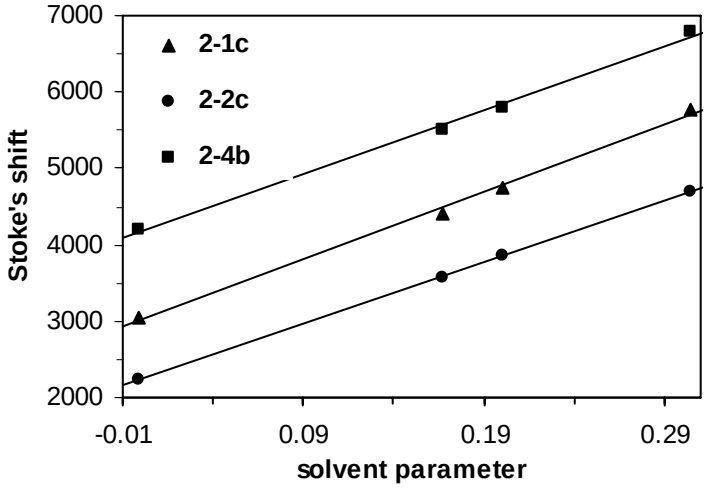


**Figure 2-25.** Solvatochromic shifts as a function of the solvent polarity parameter $\Delta f$ according to the Lippert-Mataga formalism (equation 2.3).

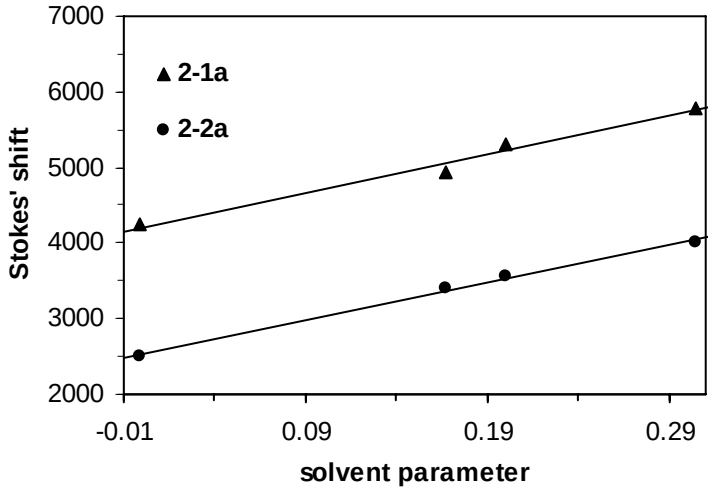


**Figure 2-26.** Solvatochromic shifts as a function of the solvent polarity parameter $\Delta f$ according to the Lippert-Mataga formalism (equation 2.3).

Finally, linear regression analysis of the Lippert-Mataga plots provided estimates for the difference between the excited-state and the ground dipole moment, indicating the extent of the charge-transfer process in the excited state. Estimates for the excited state dipole moments were obtained on basis of computed ground state dipole moment at the B3LYP/6-31G*//B3LYP/6-31G* level of theory. The corresponding slopes of the solvatochromic plots and estimated dipole moments are compiled in the Table 2-7.

**Tabel 2-7.** Solvatochromic Data and Estimated Dipole Moments According to the Lippert-Mataga Model.

| comp | $2(\mu_e - \mu_g)^2/a_0^{3\,a}$ [$cm^{-1}$] | $a_0^{3\,b}$ [Å] | $\mu_g$[D] (DFT)[c] | $\mu_e - \mu_g$ [D] | $\mu_e$ [D] | d[e] [Å] |
|---|---|---|---|---|---|---|
| **2-1a** | 5099 | 5.51 | 4.4 | 9.2 | 13.6 | 2.8 |
| **2-1b** | 8581 | 5.67 | 8.5 | 12.5 | 20.9 | 4.4 |
| **2-1c** | 8864 | 5.73 | 6.4 | 12.9 | 19.3 | 4 |
| **2-2a** | 4981 | 5.56 | 9.3 | 9.2 | 18.5 | 4.5 |
| **2-2b** | 5866 | 5.66 | 9.0 | 10.3 | 19.3 | 3.8 |
| **2-2c** | 8024 | 5.72 | 10.4 | 12.2 | 22.6 | 4.7 |
| **2-2d** | 452 | 5.69 | 10.9 | 2.9 | 13.8 | 2.9 |
| **2-3a** | 2744 | 5.39 | 5.0 | 6.5 | 11.5 | 2.4 |
| **2-3b** | 8673 | 5.81 | 7.0 | 12.9 | 20 | 4.2 |
| **2-4a** | 8309 | 5.52 | 8.2 | 11.8 | 19.9 | 4.1 |
| **2-4b** | 8803 | 5.69 | 5.3 | 12.7 | 17.9 | 3.7 |
| **2-5** | 7327 | 5.83 | 7.0 | 12 | 19 | 3.9 |
| **2-6** | 8136 | 5.49 | 9.2 | 11.6 | 20.7 | 4.3 |

[a] Slope of solvatochromic plot (from equation 2.3).[b] Onsager cavity radii $a_0$ were calculated from the molecular volumes based on X-ray data or geometry-optimized structures and increased by 0.5 Å to account for the first solvation shell (see Supporting Information for details).[c] Computed ground-state dipole moment (B3LYP/6-31G*//B3LYP/6-31G*).[d] Calculated based on computed $\mu_g$.[e] Charge separation (4.8 D is one electron separated by 1 Å).

With the exception of **2-2d** all pyrazoline derivatives exhibit a considerably larger dipole moment in the excited state compared to the ground-state. As previously concluded from the absorption and emission data acquired in methanol the charge-transfer character increases with increasing electron-withdrawing ability of the substituent $R_2$. For example, within the series of the *p*-cyanophenyl substituted derivatives **2-2d**, **2-2a**, **2-2b**, and **2-2c** the estimated excited-state dipole moments increase accordingly from 13.8 to 18.5, 19.3 and 22.6 D, respectively. Evidently, the strong electron-withdrawing ester-group in **2-2c** results in an excited-state with the greatest charge-transfer character and the largest dipole moment of 22.6 D. In a polar solvent such as methanol or water, the excited state of this derivative is more effectively stabilized compared to the other compounds within the series, and therefore also yields the lowest emission energy.

In summary, the two substituents $R_1$ and $R_2$ influence the charge-transfer process in the excited state in two distinctly different ways. The change of dipole moment between ground- and excited state is primarily determined by $R_2$, which is therefore the major determinant for the magnitude of the solvatochromic shifts.

### *2.4.4. Electron Transfer Thermodynamics*

#### *2.4.4.1.Cyclic Voltammetry*

To analyze quantitatively the electron transfer thermodynamics according to the Rehm-Weller equation (equation 2.1) the redox potentials of all pyrazoline derivatives **2-1** to **2-6** were acquired in acetonitrile. The corresponding half-wave potentials are listed in Table 2-8.

**Tabel 2-8.** Redox Potentials for Pyrazolines **2-1** to **2-6** in Acetonitrile/0.1M $Bu_4NPF_6$ vs $Fc/Fc^+$.

| compd | $E_{1/2}$(ox) [V] | | | $E_{1/2}$(red) [V] | |
|---|---|---|---|---|---|
| **2-1a** | 0.37 | 0.51 | | -2.82[a] | |
| **2-1b** | 0.41 | 0.6 | | -2.27[b] | -2.57 |
| **2-1c** | 0.4 | 0.56 | | -2.3 | -2.68 |
| **2-2a** | 0.42 | 0.77 | | -2.63 | |
| **2-2b** | 0.44 | 0.87 | | -2.14 | -2.56 |
| **2-2c** | 0.43 | 0.84 | | -2.19 | -2.56 |
| **2-2d** | 0.43 | 0.54[b] | 1.03 | -2.8 | |
| **2-3a** | 0.42[b] | 0.92[b] | | -2.7 | |
| **2-3b** | 0.43[b] | 0.99[b] | | -2.24 | -2.78[a] |
| **2-4a** | 0.29 | 0.54[a] | 0.98 | -2.28 | -2.53 |
| **2-4b** | 0.24 | 0.53 | 1.02[a] | -2.3 | -2.84 |
| **2-5** | 0.41 | 0.61[b] | | -2.29 | -2.49 |
| **2-6** | | 0.78 | | -2.17 | -2.41 |

[a] Not resolved.[b] Reversible.

With the exception of **2-4a** and **2-4b**, all derivatives are oxidized irreversibly within a range of 0.37 to 0.43 V. This first oxidation potential is not influenced by the substituents $R_1$ and $R_2$ and can be assigned to the removal of an electron from the 5-aryl diethylamino group. Accordingly, this peak is absent in compound **2-6**, which is lacking the diethylamino group. The two derivatives **2-4a** and **2-4b** containing the electron rich *p*-methoxy substituents in $R_1$ exhibit a substantially lower potential of 0.29 and 0.24 V, respectively, and a third oxidation potential was observed around 1 V. Furthermore, compound **2-2d** with a methoxy-substituent in $R_2$ also shows a third oxidation potential at 1 V. Presumably, in case of **2-4a** and **2-4b**, the first potential can be attributed to the removal of an electron from the electron-rich methoxyphenyl group rather than the diethylamino group. The second oxidation potential is similar for both derivatives (about 0.53 V), and corresponds presumably to removal of an electron from the diethylamino group. In contrast, **2-2d** with a methoxy group attached to the 3-aryl substituent exhibits the expected oxidation potential at 0.43 V. Apparently, the methoxy group attached to the 3-aryl position is not as easily oxidized compared to the 1-aryl position.

The first reduction potential is distributed over a large range (–2.1 to –2.8 V) and clearly varies as a function of the aryl substituent $R_1$ and $R_2$. This first reduction step can be attributed to the addition of an electron to the 1,3-diaryl-pyrazoline moiety, forming the corresponding radical anion of the fluorophore. The compounds **2-6** and **2-2c** have the same 1,3-diaryl-pyrazoline moiety and therefore exhibit similar reduction potentials (–2.19 versus –2.17 V). As expected, the diethylamino group attached to the 5-aryl ring does not significantly influence the reduction potential of the fluorophore. Interestingly, for a given substituent $R_2$, the first reduction potential varies insignificantly with different

substituents $R_1$. For example, the derivatives with a *p*-cyano substituent $R_2$, **2-1b**, **2-2b** and **2-4a** show a reduction potential at –2.27, –2.14 and –2.28 V, respectively, while all the ethyl carboxylate derivatives **2-1c**, **2-2c**, **2-3b**, **2-2-4b** and **2-5** are reduced around –2.25 V, regardless of the nature of $R_1$ ( Figure 2-27). In contrast, the reduction potential is strongly influenced by the nature of substituent $R_2$. For example, the *p*-cyano-substituted derivatives **2-2a**, **2-2b**, **2-2c** and **2-2d** cover a large potential range from –2.14 to –2.80 V with varying $R_2$ (Figure 2-28). In this case, the reduction potential increases with increasing electron-withdrawing character of substituent $R_2$. Furthermore the derivatives containing at least one electron-withdrawing substituent, such as CN or COOEt, exhibit a second reduction potential between –2.4 and –2.8 V.

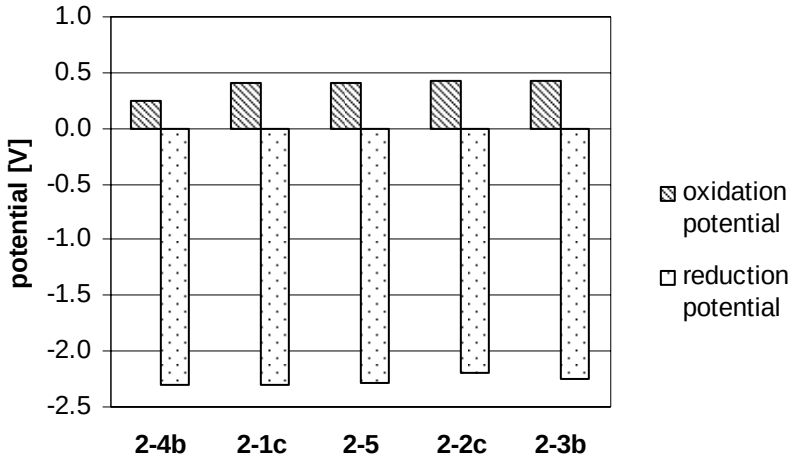


**Figure 2-27.** Oxidation and reduction potential of the pyrazoline derivatives with the same ethyl carboxylate-phenyl substituent $R_2$ group.

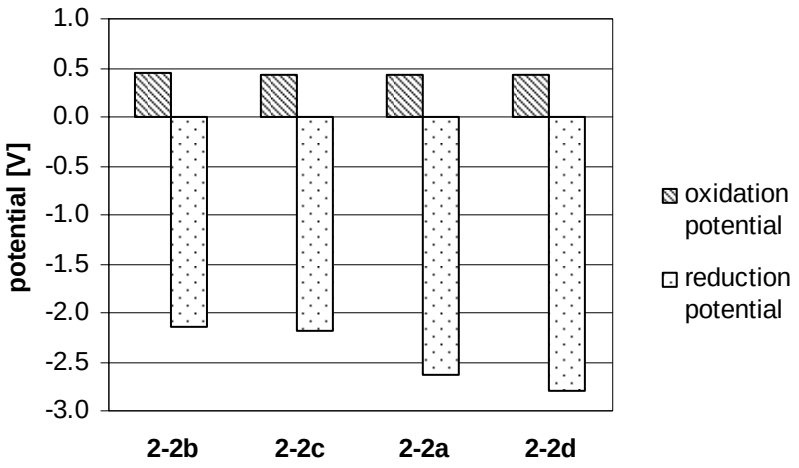


**Figure 2-28.** Oxidation and reduction potential of the pyrazoline derivatives with the same *p*-cyano-phenyl substituent $R_1$ group.

### *2.4.4.2.Photoinduced Electron-Transfer Thermodynamics*

Based on the spectroscopic data and redox potentials, the free energy change $\Delta G_{ET}$ of the photoinduced electron-transfer reaction for pyrazoline derivatives **2-1** to **2-5** were calculated according to the Rehm-Weller equation (2-1). The resulting data are listed in Table 2-9 and the quantum yield and the fluorescence enhancement factors are also included for convenience. Furthermore, a comparison of the free energy change $\Delta G_{ET}$ and the corresponding quantum yields is plotted in Figure 2-29. As expected, a very negative $\Delta G_{ET,}$ corresponding to a strong driving force for the electron transfer process, yields very efficient fluorescence quenching. For example, the quantum yields of **2-2a**, **2-2b**, **2-2c**, **2-3a** and **2-3b** in neutral methanolic solution are all very small (less than 0.01) while the corresponding $\Delta G_{ET}$ values are exceedingly negative.

**Table 2-9.** Electron Transfer Parameters and Quantum Yields of Pyrazolines **2-1** to **2-5** in Methanol.

| compd | $\Delta G_{00}$[a] [eV] | $e^*E_{1/2}$[b] ($D^+/D$) [eV] | $e^*E_{1/2}$[b] ($A/A^-$) [eV] | $\Delta G_{ET}$[c] [eV] | $\Phi$[d] | ef[e] |
|---|---|---|---|---|---|---|
| **2-1a** | 3.05 | 0.37 | -2.82 | 0.10 | 0.11 | 2 |
| **2-1b** | 2.76 | 0.41 | -2.27 | -0.12 | 0.04 | 20 |
| **2-1c** | 2.74 | 0.4 | -2.3 | -0.09 | 0.02 | 37 |
| **2-2a** | 3.20 | 0.42 | -2.63 | -0.19 | 0.01 | 50 |
| **2-2b** | 2.92 | 0.44 | -2.14 | -0.38 | 0.01 | 40 |
| **2-2c** | 2.89 | 0.43 | -2.19 | -0.31 | 0.01 | 55 |
| **2-2d** | 3.19 | 0.43 | -2.80 | -0.00 | 0.03 | 6 |
| **2-3a** | 3.71 | 0.42 | -2.70 | -0.63 | 0.004 | 1 |
| **2-3b** | 3.16 | 0.43 | -2.24 | -0.53 | 0.004 | 160 |
| **2-4a** | 2.58 | 0.29 | -2.28 | -0.05 | 0.12 | 1 |
| **2-4b** | 2.58 | 0.24 | -2.30 | -0.08 | 0.11 | 1 |
| **2-5** | 2.77 | 0.41 | -2.29 | -0.11 | 0.03 | 14 |

[a] Estimated from normalized absorption and emission spectra.[b] Half-way potential measured in acetonitrile/0.1 M $Bu_4NPF_6$ vs $Fc/Fc^+$.[c] Quantum yield in methanol.[e] Fluorescence enhancement factor upon protonation (0.1% trifluoroacetic acid in methanol).

As shown in Table 2-9, the two substituents $R_1$ and $R_2$ influence $\Delta G_{ET}$ in different ways. For a given substituent $R_1$, the reduction potential $E_{1/2}(A/A^-)$ increases while $\Delta G_{00}$ decreases with increasing electron-withdrawing character of substituent $R_2$. The changes of these two terms are opposite and the overall effect on the free energy change depends on their relative change. For a series with identical substituent $R_1$, for example **2-1a**, **2-1b** and **2-1c**, the quantum yields of the substituted derivatives **2-1b** and **2-1c** are smaller compared to the unsubstituted derivative **2-1a**. Derivatives **2-1b** and **2-1c** contain an electron withdrawing ester group, which increases the reduction potential by around 0.5 V and decreases the $\Delta G_{00}$ by 0.3 V compared to the unsubstituted **2-1a**. As a result, the driving force $-\Delta G_{ET}$ is increasing by 0.2 V, and the ET quenching process for **2-1b** and **2-1c** is more favorable, which is reflected by the lower quantum yield of 0.04 and 0.02 in neutral methanol. Likewise, the positive value for $\Delta G_{ET}$ of **2-1a** reflects an unfavorable ET driving force, which also agrees with the increased fluorescence quantum yield of 0.11. A similar effect is observed for the derivatives **2-2a**, **2-2b** and **2-2c**. The $\Delta G_{00}$ of **2-2b** and **2-2c** is by about 0.3 eV smaller, and the reduction potential is by 0.4 V less negative compared to **2-2a**. The ET driving force $-\Delta G_{ET}$ for all of these derivatives is favorable (greater than 0.19 eV), which is reflected in the comparatively low quantum around 0.01. Derivative **2-2d** containing an electron-rich methoxy substituent reveals a significantly reduced reduction potential (–2.8 V compared to –2.6 V of **2-2a**), which increases the ET energy level and reduces the ET driving force. In general, the change of reduction potential is larger than the change of $\Delta G_{00}$ with variations of $R_2$, which is consistent with the previously discussed results.

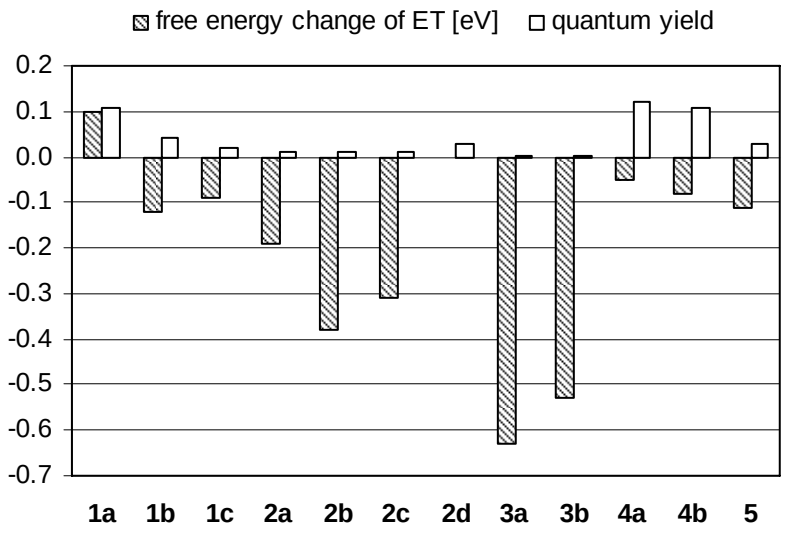


**Figure 2-29.** Comparison $\Delta G_{ET}$ and quantum yields for all synthesized pyrazoline derivatives.

In contrast, series with identical substituents $R_2$ but varying $R_1$ show different trends. For the unsubstituted derivatives **2-1a**, **2-2a** and **2-3a**, $\Delta G_{00}$ increases from 3.05, 3.20 to 3.71eV with increasing electron-withdrawing character of $R_1$. Interestingly, the reduction potential of the fluorophore also increases slightly, from –2.82 to –2.62 and –2.70 V. Consistent with previous discussion, the reduction potential is primarily determined by the nature of substituent $R_2$, while the excited state equilibrium energy $\Delta G_{00}$ is determined by the nature of substituent $R_1$. For example, $\Delta G_{00}$ changes by 0.66 eV while the reduction potential varies only by 0.20 eV with varying $R_1$. The free energy change $\Delta G_{ET}$ of **2-1a**, **2-2a,** and **2-3a** decreases from 0.10, -0.19 to –0.63 eV as the electron-withdrawing character of $R_1$ increases (within the series **2-1a**, **2-2a 2-3a**, $R_1$ changes from phenyl, *p*-cyanophenyl to pentaflurophenyl). The emission quantum yields in neutral methanol follows the same trend, and decreases from 0.11, 0.01 to 0.004.

Likewise, the ET driving force $-\Delta G_{ET}$ increases from 0.09, 0.11, 0.31 to 0.53 V for the pyrazoline series **2-1c**, **2-5**, **2-2c** and **2-3b** which all contain an ethyl ester substituent.

Interestingly, the two 1-*N*-anisyl-substituted derivatives **2-4a** and **2-4b** exhibit a different behavior. The quantum yield does not undergo any changes upon protonation with trifluoroacetic acid. Since the electron-rich 1-aryl group increases the charge transfer character of the $^1$LE state, the equilibrium energy $\Delta G_{00}$ is substantially lower (2.58 eV) compared to all other derivatives (> 2.74 eV). On the other hand, the oxidation potentials of these two electron-rich derivatives are 0.29 and 0.24 V, which is substantially lower than expected for removal of an electron from the diethylamino donor group (around 0.40V). The emission quenching process is not due to ET from the diethylamino group, therefore protonation of the diethylamino nitrogen does not influence the quenching pathway.

In summary, the substituents $R_1$ and $R_2$ influence the photoinduced electron transfer driving force $-\Delta G_{ET}$ by differentially changing the excited state equilibrium energy $\Delta G_{00}$ and the reduction potential $E_{1/2}$ ($A/A^-$), respectively. The pyrazoline platform allows therefore tuning of the electron transfer thermodynamics in a rather unique way by varying the nature of the substituents $R_1$ and $R_2$.

## 2.5. Quantum Chemical Calculation[28,29]

Since the $^1$ET state undergoes only nonemissive deactivation, it is not possible to measure its energy spectroscopically. Instead, quantum chemical calculations can be used to rationalize the observed fluorescence changes upon protonation. For example, Rurack et al. reported molecular orbital calculations to estimate the ET thermodynamics of donor-substituted 1,3,5-triaryl pyrazolines at the semiempirical level using AM1-optimized geometries (ZINDO//AM1).[7] To explore the electronic properties and ordering of the excited state energy levels, detailed quantum chemical calculations were performed on derivatives **2-1** to **2-6** at the B3LYP/6-31G*//B3LYP/6-31G* level of theory.

### *2.5.2. Geometry-Optimized Structure*

An overlay of all geometry-optimized structures for **2-1** to **2-5** is shown in Figure 2-30. The X-ray-structure coordinates of **2-2b** served as a "template" for the calculations. The substituents $R_1$ and $R_2$ were attached using standard bond lengths and angles and the resulting structures were geometrically optimized. The computed structural parameters (Table 2-10) agree well with the experimental crystal structure geometries (Table 2-2). While the geometry and orientation of the 3-aryl substituent is similar for all derivatives, the substituents in the 1- and 5-position exhibit significant differences. As can be seen from Figure 2-30, the orientation of the aryl-substituent attached to N1 influences not only the geometry of the pyrazoline ring but also the conformation of the substituent on C5.

**Tabel 2-10.** Selected Computed[a] Structural Data for 1,3,5-Triaryl Pyrazolines **2-1** to **2-5**.

| compd | C(6)-N(1) (Å) | N(1)-N(2) (Å) | N(2)-C(3) (Å) | C(3)-C(12) (Å) | $\Sigma_1$[b] (deg) | $\Sigma_2$[c] (deg) |
|---|---|---|---|---|---|---|
| **2-1a** | 1.399 | 1.366 | 1.294 | 1.463 | 357.10 | 359.99 |
| **2-1b** | 1.399 | 1.353 | 1.298 | 1.456 | 359.59 | 360.0 |
| **2-1c** | 1.397 | 1.356 | 1.298 | 1.458 | 359.79 | 360.0 |
| **2-2a** | 1.383 | 1.368 | 1.294 | 1.463 | 359.55 | 359.99 |
| **2-2b** | 1.387 | 1.359 | 1.296 | 1.459 | 359.95 | 359.99 |
| **2-2c** | 1.385 | 1.363 | 1.295 | 1.460 | 359.82 | 360.0 |
| **2-2d** | 1.381 | 1.372 | 1.294 | 1.460 | 354.22 | 359.99 |
| **2-3a** | 1.394 | 1.375 | 1.293 | 1.464 | 354.93 | 359.97 |
| **2-3b** | 1.386 | 1.363 | 1.295 | 1.460 | 359.82 | 360.0 |
| **2-4a** | 1.404 | 1.352 | 1.299 | 1.456 | 358.41 | 360.0 |
| **2-4b** | 1.404 | 1.356 | 1.298 | 1.456 | 357.90 | 360.0 |
| **2-5** | 1.399 | 1.358 | 1.297 | 1.458 | 358.55 | 360.0 |

[a] Geometry-optimized structures from DFT calculations (B3LYP/6-31G*).[b] Sum of bond angles at N1 (N2-N1-C5, N2-N1-C6, C5-N1-C6).[c] Sum of bond angles at C3 (N2-C3-C12, C4-C3-C12, N2-C3-C4).

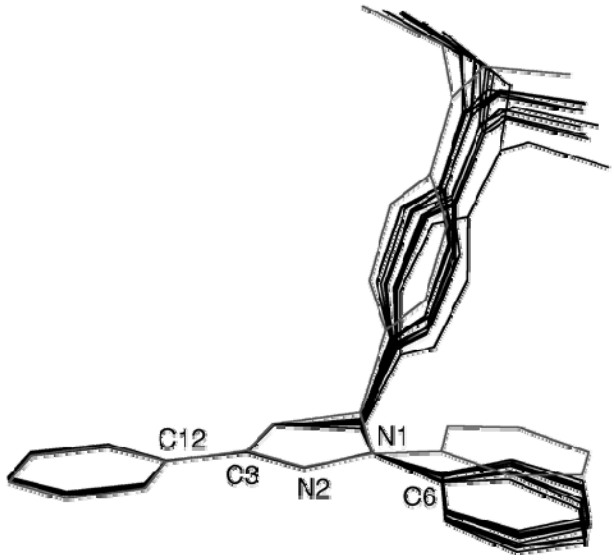


**Figure 2-30.** Overlay of the calculated geometry-optimized structures for pyrazolines **2-1** to **2-5** at the B3LYP/6-31G* level (grey, predicted geometry for **2-3b**).

The sum of the bond angles at C3 ($\sum_2$) is 360° for all computed structures, which indicates a coplanar geometry of the 3-aryl and pyrazoline ring. The sum of bond angles at N1 ($\sum_1$) is smaller than 360° for most derivatives, illustrating a partly tetrahedral geometry. Both of the conformations of the substituents on the N1 and C3 are agree with the experimentally determined geometry. In contrast, the sum of bond angles at N1 (Σ1) is smaller than 360° for most derivatives, reflecting a partly tetrahedral conformation, which is in line with the experimentally determined geometries.

As previously discussed for the crystal structure geometries, the substituents $R_1$ and $R_2$ influence the bond lengths of the pyrazoline ring, which is particularly apparent for the bond lengths of N1-N2 and N1-C6. For example, in the series **2-2d**, **2-2a** and **2-2b**, the N1-N2 bond lengths decrease from 1.372, 1.368 to 1.359 Å, while the neighboring N1-C6 bond lengths shows the opposite trend and increase slightly from 1.381, 1.383, and 1.387 Å. The change of bond lengths reflects again the degree of electronic delocalization for the ground state structures. Both changes are consistent with an increased charge delocalization toward $R_2$, which is best reflected by the Lewis structure **III** shown in Figure 2-16. On the other hand, with increasing electron-withdrawing character of $R_1$, the bond lengths of N1-C6 are decreasing and the bond lengths N1-N2 are increasing slightly. For example, in the series **2-4a**, **2-1b** and **2-2b**, the bond lengths of N1-N6 are 1.404, 1.399 and 1.387 Å, respectively; while the N1-N2 bond lengths are only slightly increasing from 1.352, 1.353, to 1.359 Å. In this case, the charge delocalization is best described by Lewis structure **I** (Figure 2-16).

### *2.5.3. Ground- and Excited-State Electronic Structures*

The computational analysis of the ground-state electronic structures provided the energy range for the HOMO and LUMO frontier orbitals, as illustrated by Figure 2-31a. Furthermore, the six lowest singlet transition energies are shown in Figure 2-31b. HOMO and LUMO are substantially separated from all other MOs with exception of the HOMO-1. The HOMO energy levels are similar for most derivatives and parallel the small variations observed for the experimental oxidation potentials. The changes of the LUMO energies are consistent with variations in the first reduction potentials.

To further elucidate the nature of the two lowest excited states $^1$ET and $^1$LE, time-dependent density functional theory (TD-DFT) was used to calculate the gas-phase Franck-Condon vertical excitation energies at the B3LYP/6-31G* level. According to these calculations, the two lowest-energy singlet states are energetically well separated from the other higher lying states across all derivatives (Figure 2-31b). Among these two states, only one state shows a large oscillator strength around 1.0 (Table 2-11), indicating an allowed transition. As shown in Table 2-11, the calculated energies of $^1$LE agree within 0.1 - 0.2 eV with the lowest-energy absorption band of the UV-vis spectra. The $S_0$ to $^1$LE transition can be most likely attributed to this band, which involves excitation into the LUMO.

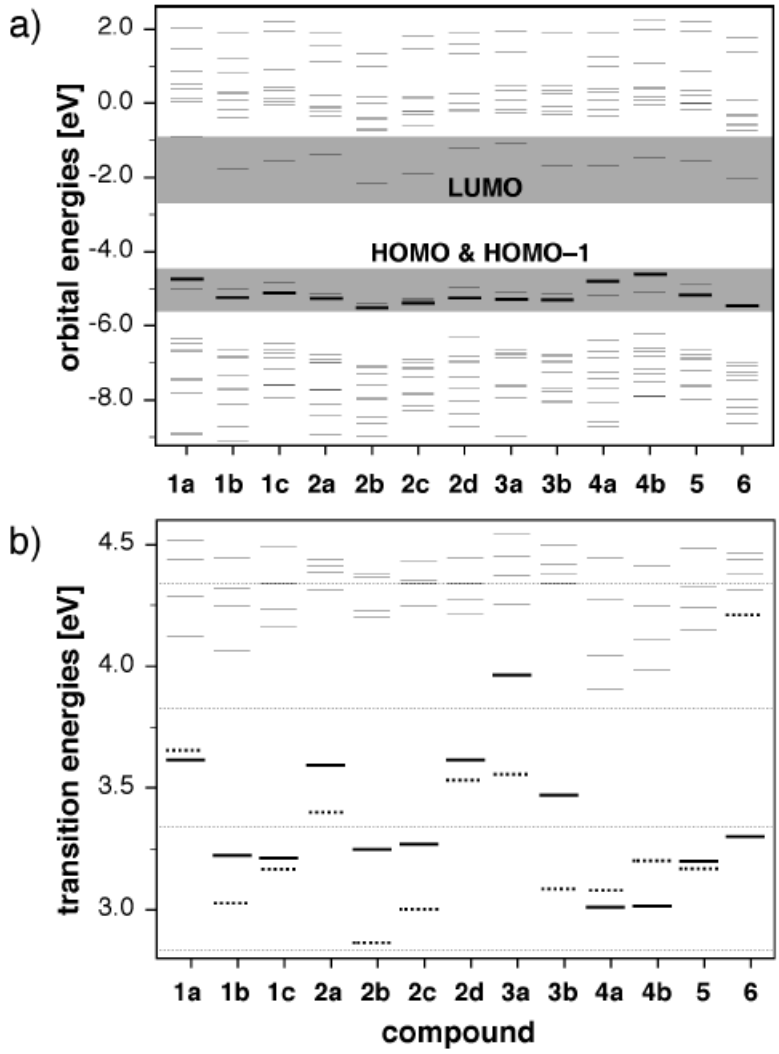


**Figure 2-31.** Results of TD-DFT calculations for pyrazolines **2-1** to **2-6**: (a) orbital energy diagram covering all MOs between HOMO-10 and LUMO+10, (b) transition energies for the six lowest-lying singlet states (LE state: bold lines, ET state: dotted lines).

**Table 2-11.** Calculated Transition Energies for the Lowest Two Excited States in Pyrazolines **2-1** to **2-6**.

| compd | abs exp[a] [eV] | $^1LE^{gas\ b}$ [eV] | $f^c$ | $^1ET^{gas\ b}$ [eV] | $f^c$ | $^1ET - {}^1LE$ [eV] | ($^1ET$ - $^3ET$) [eV] |
|---|---|---|---|---|---|---|---|
| **2-la** | 3.47 | 3.61 | 0.757 | 3.65 | 0.009 | 0.04 | 0.00 |
| **2-1b** | 3.08 | 3.22 | 0.974 | 3.03 | 0.017 | -0.19 | 0.02 |
| **2-1c** | 3.12 | 3.21 | 0.883 | 3.17 | 0.106 | -0.04 | 0.07 |
| **2-2a** | 3.41 | 3.59 | 1.030 | 3.40 | 0.028 | -0.19 | 0.03 |
| **2-2b** | 3.18 | 3.25 | 1.124 | 2.86 | 0.022 | -0.39 | 0.02 |
| **2-2c** | 3.18 | 3.26 | 1.119 | 3.00 | 0.019 | -0.26 | 0.02 |
| **2-2d** | 3.41 | 3.61 | 1.168 | 3.53 | 0.106 | -0.08 | 0.04 |
| **2-3a** | 3.91 | 3.96 | 0.867 | 3.56 | 0.081 | -0.40 | 0.07 |
| **2-3b** | 3.57 | 3.47 | 1.027 | 3.09 | 0.049 | -0.38 | 0.01 |
| **2-4a** | 2.98 | 3.01 | 0.820 | 3.08 | 0.070 | 0.07 | 0.02 |
| **2-4b** | 3.03 | 3.01 | 0.850 | 3.20 | 0.020 | 0.19 | 0.02 |
| **2-5** | 3.15 | 3.20 | 0.918 | 3.17 | 0.012 | -0.03 | 0.02 |
| **2-6** | 3.23 | 3.30 | 1.102 | 4.21 | 0.011 | 0.91 | 0.11 |

[a]Taken from solution spectrum in methanol at 25 °C. [b]DFT calculation (B3LYP/6-G*//B3LYP/6-31G*), state assignment based on orbital surface plots. [c] Oscillator strength.

The orbital densities for the HOMO-1, HOMO, and LUMO of selected derivatives are shown in Figure 2-32. Notably, the LUMO densities for all derivatives are essentially identical. Likewise, the HOMO and HOMO-1 densities are very similar; however, their relative energy ordering differs as a function of $R_1$ and $R_2$. For example, for derivative **2-2b**, the HOMO is localized on the diethylaminophenyl moiety, while the HOMO of **2-4a** and **2-6** are mostly concentrated on the phenyl ring in the 1-position.

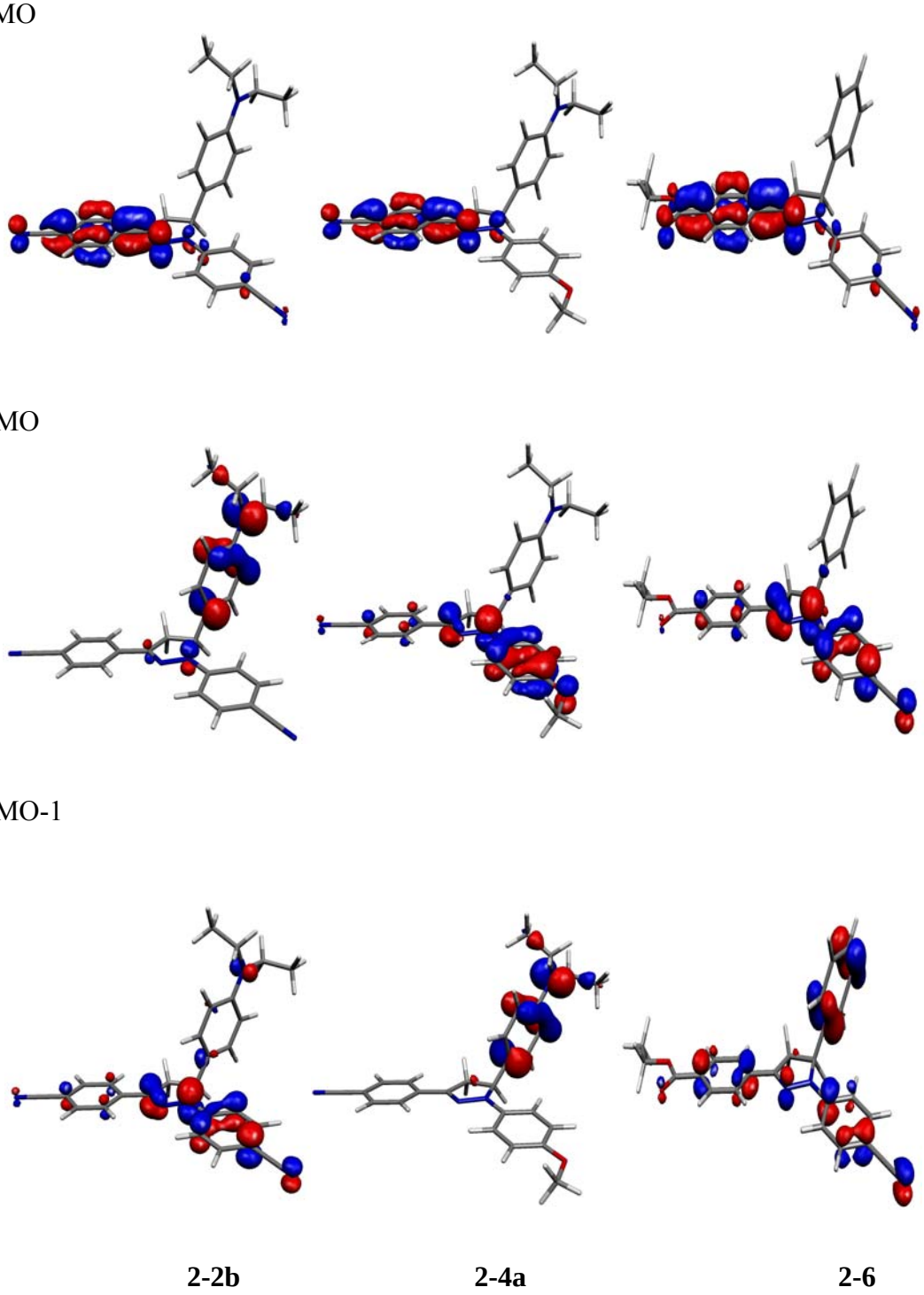


**Figure 2-32.** Molecular orbital density plots for the HOMO-1, HOMO and LUMO of pyrazoline derivatives **2-2b**, **2-4a**, **2-6**.

The MO contributions for the two lowest-energy states are best visualized with the corresponding detachment-attachment density plots as shown in Figure 2-33. There are essentially two types of density changes involved. The allowed transition, corresponding to excitation into $^1$LE, has the detachment densities (blue) localized on the 1-phenyl ring as well as on N1, N2 and C3, and the attachment densities (red) are concentrated on the 3-phenyl ring and further expand to C3 and N1. There is a significant overlap between the detachment and attachment densities, which is in agreement with the large oscillator. Furthermore, the density changes reflect well the charge transfer character as observed on basis of the previously discussed solvatochromic shift analysis. The second, not-allowed transition with very small oscillator strength, shows the attachment density mostly localized on the 3-phenyl ring, and the detachment density on the 5-diethylamino-substituted phenyl ring. Hence, this transition corresponds to the electron transfer pathway from nitrogen donor moiety to the pyrazoline fluorophore. The small energy gap between this state and the neighboring triplet state further supports the highly delocalized nature of this state.

In agreement with the experimental data, the energy ordering of the $^1$LE and $^1$ET state varies as the function of substituents $R_1$ and $R_2$. For **2-2b**, the first excited singlet state $S_1$ corresponds to the electron transfer state $^1$ET and the second excited singlet state $S_2$ can be assigned to the locally excited state $^1$LE. $^1$ET is at lower energy compared to $^1$LE, therefore the electron transfer process is efficient, as reflected by the low emission quantum yield (0.01). In case of derivative **2-4a**, the energy order of these two states is reversed. Here, $^1$LE is lower than $^1$ET, and thus, the electron transfer process is not favored, as experimentally reflected by the significantly higher quantum yield of 0.12.

Since derivative **2-6** lacks the diethylamino donor group, the energy gap between S1 and S2 is very large, suggesting that no photoinduced electron transfer process will be involved for this derivative.

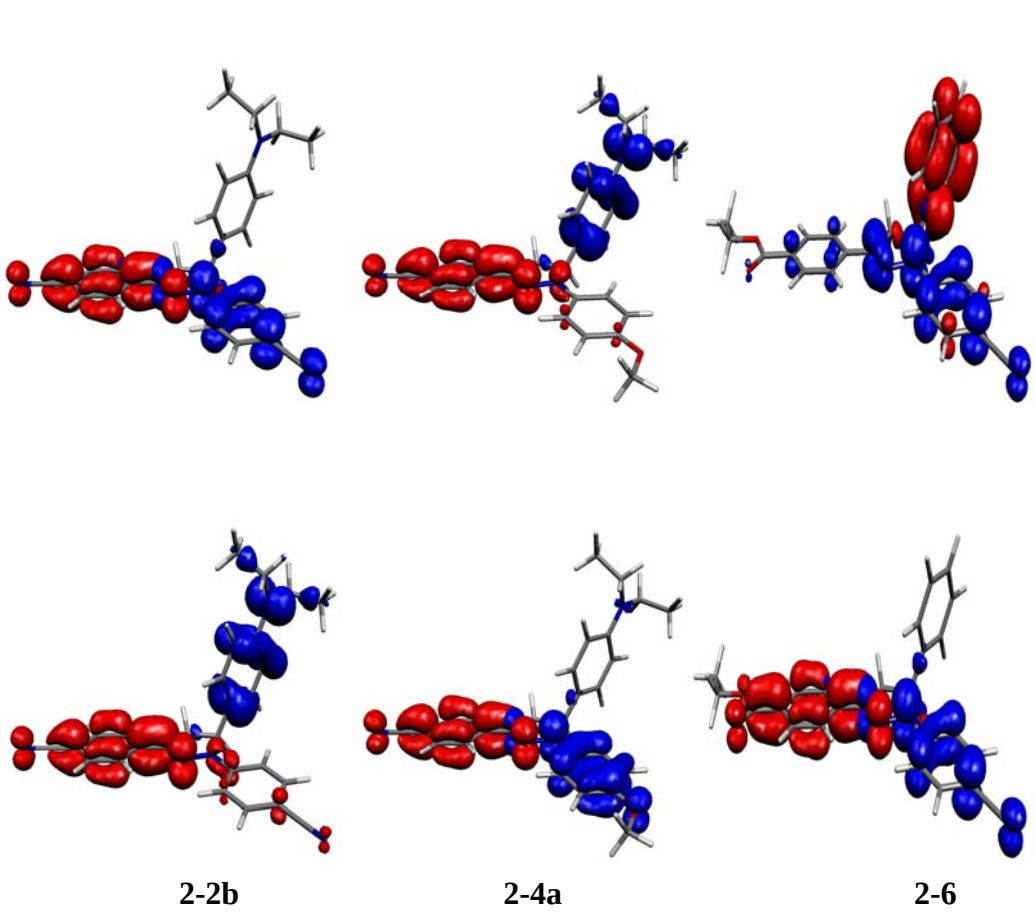


**Figure 2-33.** Detachment (blue) and attachment (red) density plots for the first ($S_1$) and second ($S_2$) excited states of pyrazoline derivatives **2-2b**, **2-4a**, **2-6**.

As shown in the Figure 2-31, the $^1$ET state (dashed lines) is below the $^1$LE state (bold lines) for most of the derivatives. Compounds **2-1a**, **2-4a** and **2-4b** are exceptions, all of which showing a reversed energy ordering. The observed significantly increased quantum yields for these three compounds (0.11, 0.12, 0.11, respectively, Table 2-4) agrees well with the energetically less favorable ET process as suggested by the quantum chemical calculations.

In a first approximation, the energy gap between the $^1$LE and $^1$ET states indicates the driving force for the ET process. Figure 2-34 shows that the calculated excited-state energy differences are in surprisingly good correlation with the experimental free energy changes of the ET process. It is important to keep in mind, that the calculated driving force is based on the vertical Franck-Condon excitation energies in the gas phase at 0 K, while the experimental data are based on the vibrationally relaxed states in a polar solvent at room temperature. The charge-separated property of ET has a large dipole moment compared to LE and may be more stabilized in the polar solvent, and important aspect that must be taken into consideration. For example, both of the pentafluoro substituted derivatives **2-3a** and **2-3b** show very negative $\Delta G_{ET}$, –0.63 and –0.53ev, respectively, while only **2-3b** has a large fluorescence enhancement factor of 160 upon protonation. The excited-state dipole moment of **2-3b** is twice as large compared to **2-3a**. The LE state of **2-3b** is more stabilized in polar solvent, and therefore reducing the gap of LE and ET states. The energy ordering of the ET and LE states can be reversed and the emission is "switched on" after protonation; however, for **2-3a**, the energy gap of ET and LE state is apparently too large to be reversed upon protonation.

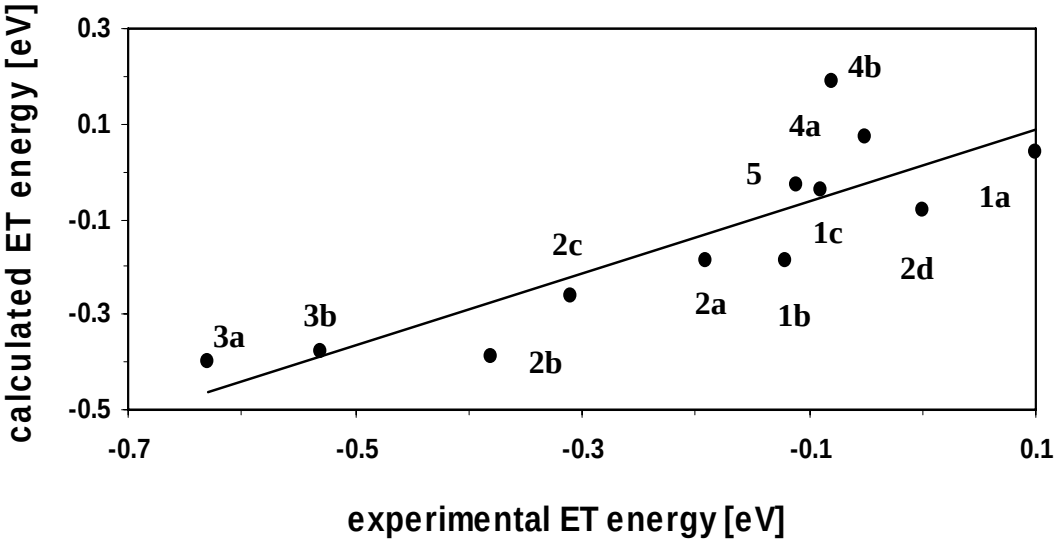


**Figure 2-34.** Correlation of the experimentally estimated free energy change of the photoinduced ET process ($\Delta G_{ET}$) vs the calculated energy difference of the $^1$LE and $^1$ET states (B3LYP/6-31G*//B3L YP /6-31G*).

## 2.6. Characterization under Physiological Conditions and Cell Biological Studies.

To evaluate the suitability of pyrazoline fluorophores as sensor platforms in a biological environment, the membrane permeability, toxicity and subcellular distribution were investigated in detail. Since the pyrazoline derivatives show pH-dependent emission quantum yield, they might be possibly usedul as markers of acidic organelles. Derivative **2-2c** displays a weak emission (quantum yield 0.01) in neutral methanol and a large fluorescence enhancement factor of 55 upon protonation. **2-2c** was used for physiological and cell studies. To improve the water solubilities, ester **2-2c** was hydrolyzed to give acid **2-2e**.

### *2.6.2. Potentiometry*

The p*K* value for protonation of the diethylamino group of **2-2e** was measured by fluorometric pH titration (Figure 2-35). Upon protonation of the diethyl amino group, the quantum yield increases from 0.02 to 0.30. The emission maximum of **2-2e** is shifted to lower energy (21,053 $cm^{-1}$) compared to **2-2c** (21,368 $cm^{-1}$), because the negatively charged carboxylate anion has weaker electron-withdrawing properties compared to the ethylester group of **2-2c**. Using the SPECFIT software for nonlinear least-squares fitting,[30] a $pK_a$ value of 6.56 ± 0.02 was extracted from the titration shown in Figure 2-36. Based on these data the basicity of the diethylamino group lies in the appropriate range for a lysosomotropic dye, and the membrane permeable derivative **2-2c** might be suitable to track intracellular pH gradients.

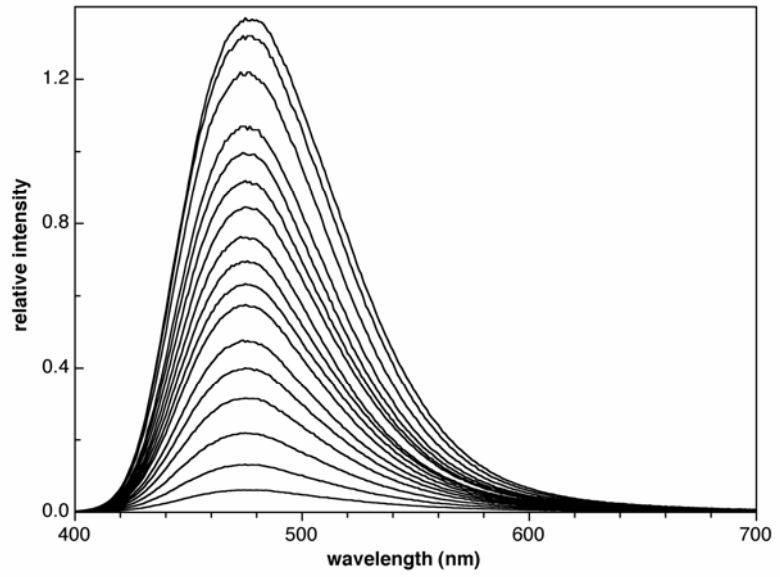


**Figure 2-35.** Fluorescence emission of pyrazoline **2-2e** as a function of pH (0.1 M KCl, 25 ºC).

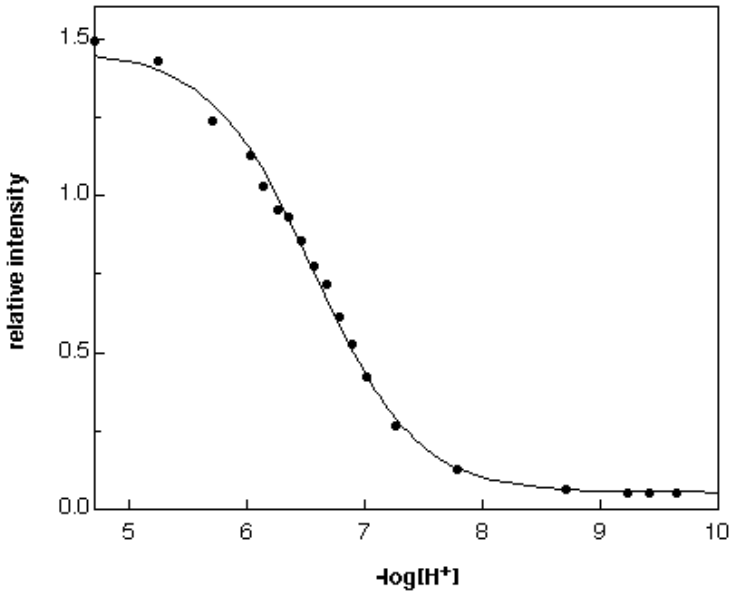


**Figure 2-36.** Fluorescence intensity at 475 nm and curve fit for determination of the protonation equilibrium constant ($pK_a$).

### *2.6.3. In-Vivo Evaluation*[28,29]

Incubation of HeLa cells with pyrazoline **2-2c** revealed a perinuclear punctate staining pattern (Figure 2-37, middle). The carboxylate ester readily diffuses across the cell membrane and exhibits a surprisingly low toxicity. In a separate experiment the cells were incubated for 3 h at a concentration of 5 μM showing no visible signs of toxic effects. To further elucidate the nature of the stained compartments HeLa cells were co-incubated with Lysotracker Red, a commercially available fluorophore which specifically stains acidic organelles (Figure 2-37, right). Surprisingly, the false-color micrograph reveals no co-localization between Lysotracker and pyrazoline **2-2c**, suggesting that the observed stained pattern with **2-2c** is not due to accumulation in acidic organelles. To further investigate whether the observed staining pattern with **2-2c** is due to an ion trapping mechanism by organelles that were not stained by the Lysotracker probe, we HeLa cells were prequilibrated with nigericin. Incubation for 30 min with media containing 0.5-1 μM of this drug is generally sufficient to destroy intracellular pH gradients.[31] Indeed, the Lysotracker specific fluorescence disappeared completely in pH equilibrated cells; however, the characteristic **2-2c** specific staining remained unchanged (Figure 2-37b), suggesting a pH independent mechanism.

To assess quantitatively the fluorescence changes averaged over a large cell population, flow cytometric analysis was performed (Figure 2-38). Cells were incubated for 90 min with a mixture of Lysotracker Red and pyrazoline **2-2c**, and after measurement of the initial fluorescence intensity for a population of 10,000 nigericin was added at a concentration of 1 μM. As shown in Figure 2-38b and c the fluorescence signal of the Lysotracker probe underwent a dramatic change, whereas the average

fluorescence emission of **2-2c** remained unchanged. It is noteworthy that the flow cytometric analysis identifies two distinct cell populations upon treatment with nigericine. After an individual cell has taken up the drug, intracellular pH gradients are apparently quickly neutralized and the emission of the Lysotracker probe drops instantaneously.

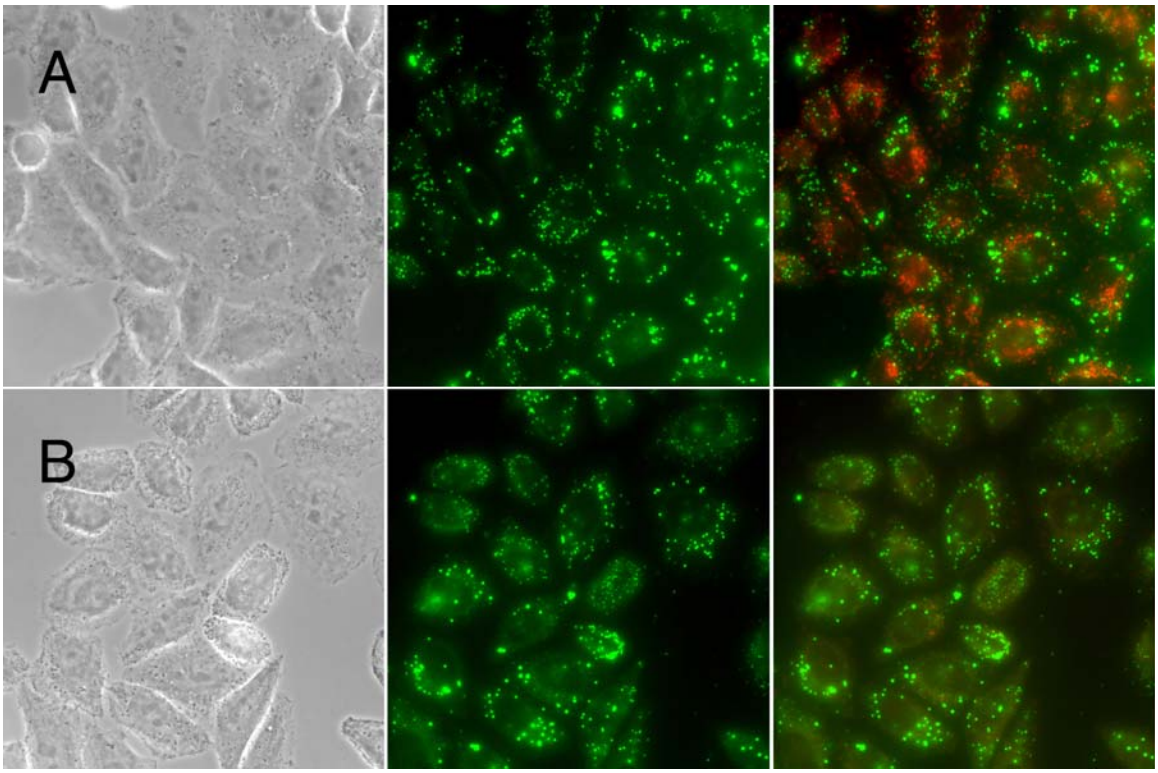


**Figure 2-37.** Phase images (left) and fluorescence micrographs for incubation of HeLa cells with pyrazoline **2-2c** (middle) and overlays with Lysotracker (right, false color image). (a) No pretreatment; (b) preincubation with 1 μM nigericin for 30 min at 37 ºC.

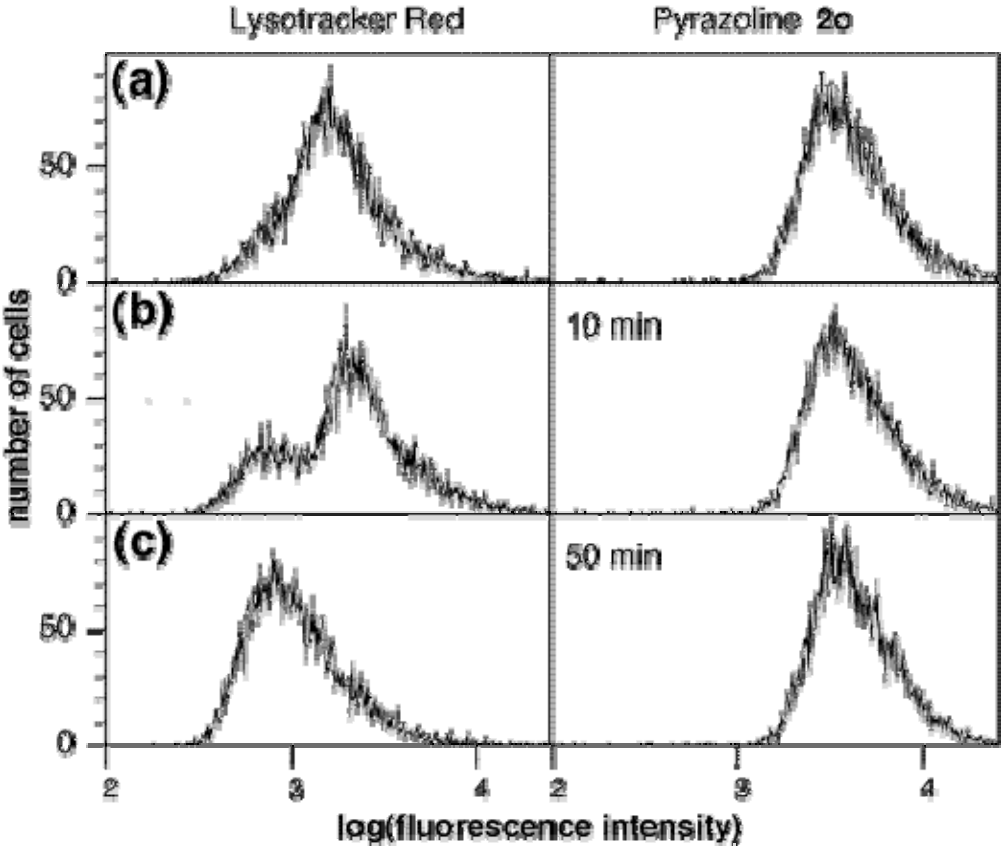


**Figure 2-38.** Flow cytometric analysis of HeLa cells incubated with Lysotracker (left) or pyrazoline **2-2c** (right) showing the effect of nigericin. The plots represent histograms of the fluorescence intensity distribution (population of 10 000 cells). (a) Control without nigericin. (b) 10 and (c) 50 min after addition of 1 μM nigericin to the cell suspension.

### *2.6.4. Model Studies with Liposomes*

The *in-vivo* experiments suggest that the intracellular staining pattern is not due to accumulation in low pH organelles. Since the thermodynamics of the electron transfer quenching process is strongly dependent on the solvent polarity, the fluorescence enhancement might be due to partitioning of the dye into intracellular membrane structures. Because of the lower polarity of the membrane environment the ET state might be sufficiently destabilized and rise above the emissive LE state. To test this hypothesis, the fluorescence intensity of **2-2c** was measured in the presence and absence of synthetic phospholipid vesicles (liposomes). Indeed, addition of pyrazoline **2-2c** to an aqueous solution of liposomes at pH 7.20 caused a 3-fold enhancement of the fluorescence intensity over the period of 2 hours (Figure 2-39). A control experiment without liposomes showed a decrease of the fluorescence emission, which is presumably due to photodecomposition of the fluorophore.

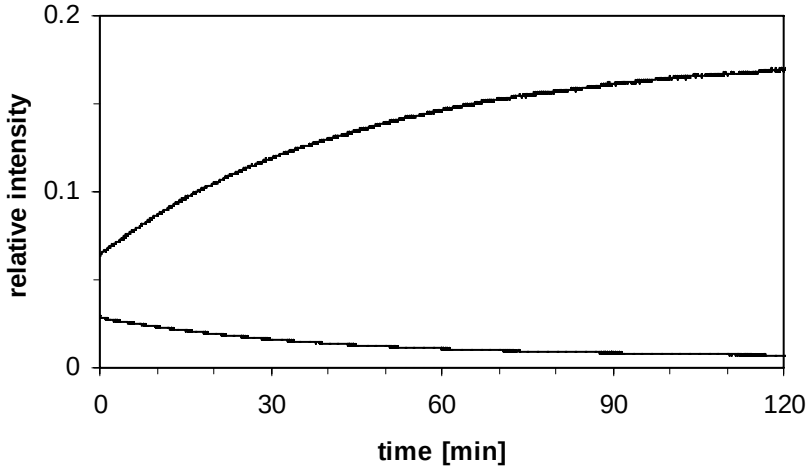


**Figure 2-39.** Fluorescence emission intensity of pyrazoline **2-2c** (20 μM) in the presence (upper line) and absence (bottom line) of liposomes (1 mg/mL, PIPES 10 mM, 0.1 M KCl, pH 7.20, 25 ºC).

## 2.7. Conclusions

Triaryl pyrazolines represent a promising class fluorophores, which combine unique photophysical properties with great synthetic flexibility. Furthermore, preliminary *in-vivo* studies suggest that the fluorophore platform is suitable for biological applications due to sufficient cell permeablity and low toxicity. Most important, the substituents $R_1$ and $R_2$ influence the photoinduced electron-transfer thermodynamics in substantially different ways. The reduction potential of the fluorophore is determined by $R_2$, while the excited state equilibrium energy $\Delta E_{00}$ is influenced by $R_1$. This property allows for selective tuning of the photophysical properties with large flexibility. The evaluation *in vivo* of a water soluble pyrazoline derivative indicates the attractive properties of the fluorophore for biological application. The study of this chapter provided a solid

foundation for the design of a fluorescence probe for the detection of monovalent copper in a biological environment.

## 2.8. Experimental Section

### *2.8.2. Materials and Reagents*

All synthetic starting materials and reagent were commercially available and used without further purification. All solvents used for absorption and fluorescence experiments were spectroscopic grade. The acetonitrile used for the cyclic voltammetry was freshly distilled over calcium hydride.

Phenyl hydrazine (Aldrich, 97%), *p*-cyano phenyl hydrazine (Aldrich, 97%), *p*-methoxy phenyl hydrazine (Aldrich, 98%), pentafluorophenyl hydrazine (Aldrich 97%), *p*-fluorophenyl hydrazine (Aldrich, 97%), ethyl 4-acetylbezoate (Aldrich, 99%), 4-acetyl benzonitrile (Aldrich, 99%), 4-acetyl-anisole (Aldrich, 99%), acetophenone (Aldrich, 99%).

Merck silica gel (70-230 mesh) was used for flash chromatography (FC). Thin layer chromatography (TLC) was 0.25 mm, Merck silica gel 60 $F_{254}$, visualizing at 254 nm or with 2% $KMnO_4$ solution.

The liposoms was prepared by evaporation of 1.0 mL of lipid solution (20 mg/mL 1,2-dioleoyl-*sn*-glycero-3-phosphocholine in chloroform). The lipid residue was added into 2.0 mL PIPES buffer solution. The mixture was hydrated for 1 h, and then ultrasonicated until the solution clarified. The experiment was performed at a lipid concentration of 1 mg/mL PIPES buffer solution (10 mM PIPES, 0.1 $KNO_3$).

### *2.8.3. Instrumentation*

Nuclear magnetic resonance (NMR) spectra were acquired with a Varian Gemini 300 MHz spectrometer. Chemical shifts are reported in delta (δ) unit per million (ppm) downfield tetramethylsilane. Splitting patterns are abbreviated as follows: s, singlet; d, doublet; t, triplet; q, quartet; m, multiplet; br, broad.

The final product was purified by reversed-phase HPLC, Varian ProStar system with UV detector. Acetonitrile-water, gradient 20% → 2% water, was used as solvent.

UV spectra were acquired by Varian Cary Bio50 UV-vis spectrometer with a constant-temperature accessory. Steady-state fluorescence spectra were recorded on PTI fluorimeter and FELIX software. All sample solutions were filtered through 0.45 μm Teflon membrane filters to remove dust particles or fibers. The path length of cell was 1 cm with volume of 3.0 mL. Quantum yields were calculated using quinine sulfate dihydrate in 1.0 N $H_2SO_4$ as a fluorescence standard ($\Phi_f = 0.54 \pm 0.05$).[32]

pK titration were performed with an Orion combination glass microelectrode (model 9802BN). The electrode was calibrated for $-\log[H_3O^+]$ by titration of a standardized HCl solution (Aldrich, 0.1 N volumetric standard) with KOH (Aldrich, 0.1 N volumetric standard) at 25 ºC and 0.1 M ionic strength (KCl). The end point, *E*º, and slope were determined using Gran's method[33] as implemented in the software GLEE.[34] The electrode potential was measured with the Corning pH/Ion Analyzer 355, and the emf measurements were reproducible with ± 0.1 mV accuracy.

The cyclic voltammograms were acquired on a CH-Instruments potentiostat (model 600A) with a Platinum working and counter electrode and an Ag/AgCl reference electrode. Solvent acetonitrile was distilled and electrolyte $Bu_4NPF_6$ was recrystallized.

The concentration of $Bu_4NPF_6$ used was 0.1 M. The samples were measured under nitrogen at a concentration of 3 mM. The half-wave potentials were referenced to ferrocene as the internal standard, and the measurements were performed with 500 mV $s^{-1}$ scan rate.

The X-ray data were collected on a Siemens SMART 1K CCD diffractometer with graphite-monochromated Mo Kα radiation (λ= 0.71073 Å). The programs SADABS (Sheldrick)[35] and SAINT 6.22 (Bruker)[36] were used for absorption corrections. The structure was solved by direct methods and refined by least-squares calculations with the SHELXTL 5.10 software package.[36] Hydrogen atoms were added using ideal geometries with a fixed C-H bond distance of 0.96 Å. The crystallographic parameters and data are included in the Appendix, Section A. Crystals of **2-1b**, **2-2a** to **2-d**, and **2-3b** suitable for X-ray structural analysis were grown from acetonitrile-water by slow evaporation of the solvent over a period of several days.

All calculations were carried out with the Q-Chem electronic structure calculation suite of programs. The geometries of ground-state structures were optimized by the density functional method using Becke's gradient corrected three-parameter exchange functional[37] with the correlation functional of Lee, Yang, and Parr[38] (B3LYP). The split-valence polarized 6-31G* (6-31G(d)) basis set was used for all geometry optimizations. Single point energies were computed at the B3LYP/6-31G* level using the optimized geometry (B3LYP/6-31G*//B3LYP/6-31G*). To obtain estimates of the vertical electronic excitation energies which include some account of electron correlation, time-dependent density functional theory (TD-DFT)[39] calculations with the B3LYP functional and 6-31G* basis set were performed. The calculation of ground-state potential curves is

based on relaxed geometries with the corresponding constraints of dihedral angles. The coordinates of the geometry-optimized structures are provided with Appendix, Section B.

The staining pictures of cells were taken using an Olympus microscope (BX40, plan apo 60x, 1.40) with a standard fluorescence excitation filter set. A Becton-Dickinson LSR flow cytometer was used for quantization of the fluorescence intensity over a large cell population (10 000 counts). HeLa cells were cultivated in Dulbecco's modified Eagle medium (DMEM) supplemented with 5% calf serum and 200 mM L-glutamine. For the uptake experiments, cells were coincubated with 50 nM Lysotracker Red (Molecular Probes) and 5 μM pyrazoline **2-2c** for 60 min at 37 ºC, washed 3 times with PBS, and fixed with 3.7% paraformaldehyde for 30 min before mounting on slides with Fluoromount (Molecular Probes). To equilibrate intracellular pH gradients, cells were incubated with 1 μM nigericin (Sigma) for 30 min prior to incubation with the dyes.

### *2.8.4. Synthesis*

Pyrazoline derivatives **2-1** to **2-6** were synthesized according to the following procedure: A solution of the corresponding hydrazine derivative (1 mmol), the chalcone (0.33 mmol), and 98% sulfuric acid (0.5 mmol) in 2.0 mL absolute ethanol was heated at reflux temperature for 8 hours. The reaction mixture was neutralized with saturated aq. $NaHCO_3$ and extracted twice with ethyl acetate. The combined organic phase was dried with anhydrous $MgSO_4$, concentrated and the residue purified by flash chromatography on silica gel to provide final product. The final product was further purified with reversed phase HPLC.

**a) [4-(2,5-Diphenyl-3,4-dihydro-2H-pyrazol-3-yl)-phenyl]-diethyl-amine (2-1a):** Yield: 50%. mp 51-53 °C. *Rf* 0.40 (10:1 hexane:EtOAc). $^1$H-NMR ($CDCl_3$, 300

MHz) δ 1.13 (t, *J* = 7.1 Hz, 6H), 3.13 (dd, *J* = 17.0, 7.1 Hz, 1H), 3.31 (q, *J* = 7.1 Hz, 4H), 3.77 (dd, *J* = 17.0, 12.6 Hz, 1H), 5.17 (dd, *J* = 12.6, 7.1 Hz, 1H), 6.61 (d, *J* = 8.8 Hz, 2H), 6.76 (t, *J* = 7.1 Hz, 1H), 7.08-7.21 (m, 5H), 7.30-7.40 (m, 4H), 7.72 (d, *J* = 7.1 Hz, 3H). MS (70 eV) 369.2 ($M^+$, 100), 221 (68). EI-HRMS, m/e: calculated for ($M^+$) $C_{25}H_{27}N_3$ 369.22050, found 369.21789.

**b) 4-[5-(4-Diethylamino-phenyl)-1-phenyl-4, 5-dihydro-1H-pyrazol-3-yl]-benzonitrile (2-1b):** Yield: 50%. mp 78-80 °C. *Rf* 0.40 (3:1 hexane:EtOAc). $^1$H-NMR ($CDCl_3$, 300 MHz) δ 1.13 (t, *J* = 7.1 Hz, 6H), 3.11 (dd, *J* = 17.0, 7.1 Hz, 1H), 3.31 (q, *J* = 7.1 Hz, 4H), 3.75 (dd, *J* = 17.0, 12.6 Hz, 1H), 5.28 (dd, *J* = 12.6, 7.1 Hz, 1H), 6.60 (d, *J* = 8.8 Hz, 2H), 6.82 (t, *J* = 7.1 Hz, 1H), 7.08-7.23 (m, 5H), 7.63 (d, *J* = 8.8 Hz, 2H), 7.76 (d, *J* = 8.8 Hz, 3H). MS (70 eV) 394.2 ($M^+$, 100), 302 (35), 246 (52). EI-HRMS, m/e: calculated for ($M^+$) $C_{26}H_{26}N_4$ 394.21575, found 394.21533.

**c) 4-[5-(4-Diethylamino-phenyl)-1-phenyl-4, 5-dihydro-1H-pyrazol-3-yl]-benzoic acid ethyl ester (2-1c):** Yield: 52%. mp 139-141 °C. *Rf* 0.33 (3:1 hexane:EtOAc). $^1$H-NMR ($CDCl_3$, 300 MHz) δ 1.13 (t, *J* = 7.1 Hz, 6H), 1.41 (t, *J* = 7.1 Hz, 3H), 3.14 (dd, *J* = 17.0, 7.1 Hz, 1H), 3.31 (q, *J* = 7.1 Hz, 4H), 3.78 (dd, *J* = 17.0, 12.1 Hz, 1H), 4.38 (q, *J* = 7.1 Hz, 2H), 5.25 (dd, *J* = 12.1, 7.1 Hz, 1H), 6.61 (d, *J* = 8.8 Hz, 3H), 6.80 (t, *J* = 7.1 Hz, 1H), 7.08-7.22 (m, 5H), 7.75 (d, *J* = 8.8 Hz, 2H), 8.03 (d, *J* = 8.8 Hz, 2H). MS (70 eV) 441.2 ($M^+$, 100), 293 (19). EI-HRMS, m/e: calculated for ($M^+$) $C_{28}H_{31}N_3O_2$ 441.24163, found 441.24202.

**d) 4-[5-(4-Diethylamino-phenyl)-3-phenyl-4, 5-dihydro-pyrazol-1-yl]-benzonitrile (2-2a):** Yield: 43%. mp 206-208 °C. *Rf* 0.25 (10:1 hexane:EtOAc). $^1$H-NMR ($CDCl_3$, 300 MHz) δ 1.13 (t, *J* = 7.1 Hz, 6H), 3.20 (dd, *J* = 17.6 Hz, 5.5 Hz, 1H)

3.31 (q, *J* = 7.1 Hz, 4H), 3.84 (dd, *J* = 17.6, 12.1 Hz, 1H), 5.24 (dd, *J* = 12.1, 5.5 Hz, 1H), 6.60 (d, *J* = 8.8 Hz, 2H), 7.06 (d, *J* = 8.8 Hz, 2H), 7.10 (d, *J* = 8.8 Hz, 2H), 7.37-7.44 (m, 5H), 7.74 (d, *J* = 7.7 Hz, 2H). MS (70 eV) 394.1 ($M^+$, 100), 307 (44). EI-HRMS, m/e: calculated for ($M^+$) $C_{26}H_{26}N_4$ 394.21575, found 395.21562.

**e) 4-[5-(4-Diethylamino-phenyl)-1-(4-cyano-phenyl)-4, 5-dihydro-1H-pyrazol-3-yl]-benzonitrile (2-2b):** Yield: 41%. mp 92-94 °C. *Rf* 0.31 (3:1 hexane:EtOAc). $^1$H-NMR ($CDCl_3$, 300 MHz) δ 1.13 (t, *J* = 7.1 Hz, 6H), 3.19 (dd, *J* = 17.0 Hz, 6.0 Hz, 1H), 3.32 (q, *J* = 7.1 Hz, 4H), 3.82 (dd, *J* =17.0, 12.1 Hz, 1H), 5.33 (dd, *J* = 12.1, 6.0 Hz, 1H), 6.60 (d, *J* = 8.8 Hz, 2H), 7.03 (d, *J* = 8.8 Hz, 2H), 7.13 (d, *J* = 8.8 Hz, 2H), 7.43 (d, *J* = 8.8 Hz, 2H), 7.67 (d, *J* = 8.3 Hz, 2H), 7.80 (d, *J* = 8.3 Hz, 2H). MS (70 eV) 419.1 ($M^+$, 100), 271 (34). EI-HRMS, m/e: calculated for ($M^+$) $C_{27}H_{25}N_5$ 419.21100, found 419.21268.

**f) 4-[1-(4-Cyano-phenyl)-5-(4-diethylamino-phenyl)-4, 5-dihydro-1H-pyrazol-3-yl]-benzoic acid ethyl ester (2-2c):** Yield: 60%. mp 88-90 °C. *Rf* 0.23 (3:1 hexane:EtOAc). $^1$H-NMR ($CDCl_3$, 300 MHz) δ 1.13 (t, *J* = 7.1 Hz, 6H), 1.41(t, *J* = 7.1 Hz, 3H), 3.22 (dd, *J* = 17.0, 6.0 Hz, 1H), 3.31 (q, *J* = 7.1 Hz, 4H), 3.84 (dd, *J* = 17.0, 12.1 Hz, 1H), 4.38 (q, *J* = 7.1 Hz, 2H), 5.29 (dd, *J* = 12.1, 6.0 Hz, 1H), 6.60 (d, *J* = 8.8 Hz, 2H), 7.05 (d, *J* = 8.8 Hz, 2H), 7.13 (d, *J* = 8.8 Hz, 2H), 7.42 (d, *J* = 8.8 Hz, 2H), 7.77 (d, *J* = 8.8 Hz, 2H), 8.06 (d, *J* = 8.8 Hz, 2H). MS (70 eV) 466.1 ($M^+$, 100), 419.2 (44), 275.1 (38). EI-HRMS, m/e: calculated for ($M^+$) $C_{29}H_{30}N_4O_2$ 466.23688, found 466.23879.

**g) 4-[5-(4-Diethylamino-phenyl)-3-(4-methoxy-phenyl)-4, 5-dihydro-pyrazol-1-yl]-benzonitrile (2-2d):** Yield: 74%. mp 181-183 °C. *Rf* 0.80 (3:1 hexane:EtOAc). $^1$H-

NMR ($CDCl_3$, 300 MHz) δ 1.14 (t, *J* = 7.1 Hz, 6H), 3.16 (dd, *J* = 17.0, 6.0 Hz, 1H), 3.30 (q, *J* = 7.1 Hz, 4H), 3.84 (s, 3H), 4.11 (dd, *J* = 12.1, 6.0 Hz, 1H), 5.19 (dd, *J* = 12.1, 6.0 Hz, 1H), 6.59 (d, *J* = 8.8 Hz, 2H), 6.92 (d, *J* = 8.8 Hz, 2H), 7.05 (d, *J* = 8.8 Hz, 2H), 7.06 (d, *J* = 8.8 Hz, 2H), 7.39 (d, *J* = 8.8 Hz, 2H), 7.66 (d, *J* = 8.8 Hz, 2H). MS (70 eV) 424.3 ($M^+$, 82), 175 (69), 160.1 (100). EI-HRMS, m/e: calculated for ($M^+$) $C_{27}H_{28}N_4O$ 424.22631, found 424.22652.

**h) 4-[1-(4-Cyano-phenyl)-5-(4-diethylamino-phenyl)-4, 5-dihydro-1H-pyrazol-3-yl]-benzoic acid (2-2e):** Yield: 81%. mp 203-205 °C. *Rf* 0.62 ( pure EtOAc). $^1$H-NMR ($CDCl_3$, 300 MHz) δ d 1.13 (t, *J* = 7.1 Hz, 6H), 3.21 (dd, *J* = 17.0, 6.0 Hz, 1H), 3.31 (q, *J* = 7.1 Hz, 4H), 3.84 (dd, *J* = 17.0, 12.1 Hz, 1H), 5.29 (dd, *J* = 12.1, 6.0 Hz, 1H), 6.61 (d, *J* = 8.8 Hz, 2H), 7.04 (d, *J* = 8.8 Hz, 2H), 7.13 (d, *J* = 8.8 Hz, 2H), 7.42 (d, *J* = 8.8 Hz, 2H), 7.80 (d, *J* = 7.7 Hz, 2H), 8.14 (d, *J* = 7.7 Hz, 2H). MS (70 eV) 438.2 ($M^+$, 63), 160.1 (91), 116.1 (64). EI-HRMS, m/e: calculated for ($M^+$) $C_{27}H_{26}N_4O_2$ 438.20558, found 438.20575.

**i) Diethyl-[4-(2-pentafluorophenyl-5-phenyl-3, 4-dihydro-2H-pyrazol-3-yl)-phenyl]-amine (2-3a):** Yield: 52%. mp 115-117 °C. *Rf* 0.65 (3:1 hexane:EtOAc). $^1$H-NMR ($CDCl_3$, 300 MHz) δ 1.14 (t, *J* = 7.1 Hz, 6H), 3.29 (q, *J* = 7.1 Hz, 4H), 3.38 (dd, *J* = 16.5, 8.2 Hz, 1H),3.68 (dd, J = 16.5, 11.0 Hz, 1H), 5.30 (dd, *J* = 11.0, 8.2 Hz, 1H), 6.54 (d, *J* = 9.34 Hz, 2H), 7.11 (d, *J* = 8.8 Hz, 2H), 7.35-7.41 (m, 3H), 7.68-7.72 (m, 2H). MS (70eV) 459.2($M^+$, 63), 277.2 (32), 175.2 (51), 160.1 (100). EI-HRMS, m/e: calculated for ($M^+$) $C_{25}H_{22}N_3F_5$ 459.17339, found 459.17544.

**j) 4-[5-(4-Diethylamino-phenyl)-1-pentafluorophenyl-4, 5-dihydro-1H-pyrazol-3-yl]-benzoic acid ethyl ester (2-3b):** Yield: 76%. mp 48-50 °C *Rf* 0.71 (5:1

hexane:EtOAc). $^1$H-NMR ($CDCl_3$, 300 MHz) δ 1.14 (t, *J* = 7.1 Hz, 6H), 1.41 (t, *J* = 7.1 Hz, 3H), 3.30 (q, *J* = 7.1Hz, 4H), 3.33 (dd, *J* = 11.0, 7.1 Hz, 1H), 3.70 (dd, *J* = 17.0 HZ, 11.0 Hz, 1H), 4.40 (q, *J* = 7.1 Hz, 2H), 5.36 (dd, *J* = 11.0, 7.1 Hz, 1H), 6.54 (d, *J* = 8.8 Hz, 2H), 7.10 (d, *J* = 8.8 Hz, 2H), 7.74 (d, *J* = 8.8 Hz, 2H), 8.06 (d, *J* = 8.8 Hz, 2H). MS (70 eV) 531 ($M^+$, 48), 160 (100), 130 (30). EI-HRMS, m/e: calculated for ($M^+$) $C_{28}H_{26}F_5N_3O_2$ 531.19452, found 531.19379.

**k) 4-[5-(4-Diethylamino-phenyl)-1-(4-methoxy-phenyl)-4, 5-dihydro-1H-pyrazol-3-yl]-benzonitrile (2-4a):** Yield: 57%. *Rf* 0.50 (3:1 hexane:EtOAc). $^1$H-NMR ($CDCl_3$, 300 MHz) δ 1.14 (t, *J* = 7.1 Hz, 6H), 3.09 (dd, *J* = 17.0, 8.2 Hz, 1H), 3.32 (q, *J* = 7.1 Hz, 4H), 3.72 (dd, *J* = 17.0, 12.6 Hz, 1H), 3.73 (s, 3H), 5.20 (dd, *J* = 12.6, 8.2 Hz, 1H), 6.61 (d, *J* = 8.8 Hz, 2H), 6.77 (d, *J* = 8.2 Hz, 2H), 7.05 (d, *J* = 8.8 Hz, 2H), 7.11 (d, *J* = 8.8 Hz, 2H), 7.62 (d, *J* = 8.2 Hz, 2H), 7.73 (d, *J* = 8.8 Hz, 2H). MS (70 eV) 424.2($M^+$, 100), 160.1 (79), 121.1 (80). EI-HRMS, m/e: calculated for ($M^+$) $C_{27}H_{28}N_4O$ 424.22631, found 424.22652.

**l) 4-[5-(4-Diethylamino-phenyl)-1-(4-methoxy-phenyl)-4, 5-dihydro-1H-pyrazol-3-yl]-benzoic acid ethyl (2-4b):** Yield: 51%. mp 114-116 °C. *Rf* 0.25 (10:1 hexane:EtOAc). $^1$H-NMR ($CDCl_3$, 300 MHz) δ 1.14 (t, *J* = 7.1Hz, 6H), 1.41 (t, *J* = 7.1 Hz, 3H), 3.12 (dd, *J* = 17.0, 7.8 Hz, 1H), 3.32 (q, *J* = 7.1 Hz, 4H), 3.73 (s, 3H), 3.82 (dd, *J* = 17.0, 12.1 Hz, 1H), 4.38 (q, *J* = 7.1 Hz, 2H), 5.16 (dd, *J* = 12.1, 7.8 Hz, 1H), 6.62 (d, *J* = 8.8 Hz, 2H), 6.77 (d, *J* = 8.8 Hz, 2H), 7.08 (d, *J* = 8.8 Hz, 2H), 7.14 (d, *J* = 8.8 Hz, 2H), 7.73 (d, J = 8.2 Hz, 2H), 8.03 (d, *J* = 8.2 Hz, 2H). MS (70 eV) 471.3 ($M^+$, 45), 160.1 (24), 121.1 (100). EI-HRMS, m/e: calculated for ($M^+$) $C_{29}H_{33}N_3O_3$ 471.25219, found 471.25198.

**m) 4-[5-(4-Diethylamino-phenyl)-1-(4-fluoro-phenyl)-4, 5-dihydro-1H-pyrazol-3-yl]-benzoic acid ethyl ester (2-5):** Yield: 50%. mp 102-104 °C. *Rf* 0.78 (3:1 hexane:EtOAc). $^1$H-NMR ($CDCl_3$, 300 MHz) δ 1.14 (t, *J* = 7.1 Hz, 6H), 1.41(t, *J* = 7.1 Hz, 3H), 3.14 (dd, *J* = 17.0 Hz, 7.1 Hz, 1H), 3.32 (q, *J* = 7.1 Hz, 4H), 3.78 (dd, *J* = 17.0, 12.1 Hz, 1H), 4.38 (q, *J* = 7.1 Hz, 2H), 5.17 (dd, *J* = 12.1, 7.1 Hz, 1H), 6.61 (d, *J* = 8.2 Hz, 2H), 6.89 (t, *J* = 8.2 Hz, 2H), 7.05 (d, *J* = 8.2 Hz, 2H), 7.11 (d, *J* = 8.8 Hz, 2H), 7.04-7.14 (m, 4H), 7.73 (d, *J* = 8.8 Hz, 2H), 8.04 (d, *J* = 8.2 Hz, 2H). MS (70 eV) 459.2 ($M^+$, 60), 160.1 (73), 109 (100). EI-HRMS, m/e: calculated for ($M^+$) $C_{28}H_{30}FN_3O_2$ 459.23221, found 459.23207.

**n) 4-[1-(4-Cyano-phenyl)-5-phenyl-4, 5-dihydro-1H-pyrazol-3-yl]-benzoic acid ethyl ester (2-6):** Yield: 92%. mp 153-155 °C. *Rf* 0.53 (3:1 hexane:EtOAc). $^1$H-NMR ($CDCl_3$, 300 MHz) δ 1.41 (t, *J* = 7.1 Hz, 3H), 3.24 (dd, *J* = 17.6 Hz, 6.0 Hz, 1H), 3.93 (dd, *J* = 17.6, 12.6 Hz, 1H), 4.40 (q, *J* = 7.14, 2H), 5.40 (dd, *J* = 12.6, 6.0 Hz, 1H), 7.08 (d, *J* = 8.8 Hz, 2H), 7.23-7.51 (m, 7H), 7.78 (d, *J* = 8.8 Hz, 2H), 8.07 (d, *J* = 8.8 Hz, 2H), MS (70 eV) 395.2 ($M^+$, 61), 116.1 (100), 102 (22). EI-HRMS, m/e: calculated for ($M^+$) $C_{25}H_{21}N_3O_2$ 395.16338, found 395.16420.

**o) 4-[3-(4-Diethylamino-phenyl)-acryloyl]-benzoic acid ethyl ester (2-14):** A mixture of 4-(diethylamino)benzaldehyde (500 mg, 2.8 mmol ), ethyl 4-acetylbenzoate (538 mg, 2.8 mmol), and 0.5 mL sulfuric acid (98%) in 5mL acetic acid was stirring at room temperature for 3 days. The reaction mixture was poured into water and neutralized with $NaHCO_3$ solution. After extraction with EtOAc, the organic phase was dried over anhydrous $MgSO_4$ and evaporated to dryness. The crude product was purified by flash chromatography on silica gel (gradient 30:1 –>10:1, hexane:EtOAc) providing 615 mg

(1.75 mmol, 63%) of chalcone **2-14** as yellow solid. Yield: 63%. mp 105-107 °C. *Rf* 0.32 (10:1 hexane:EtOAc). $^1$H-NMR ($CDCl_3$, 300 MHz) δ 1.21 (t, *J* = 7.1 Hz, 6H), 1.42 (t, *J* = 7.1 Hz, 3H), 3.43 (q, *J* = 7.1 Hz, 4H), 4.41 (q, *J* = 7.1 Hz, 2H), 6.66 (d, *J* = 8.8 Hz, 2H), 7.27 (d, *J* = 15.6 Hz, 1H), 7.53 (d, *J* = 8.8 Hz, 2H), 7.78 (d, *J* = 15.6 Hz, 1H), 8.02 (d, *J* = 8.8 Hz, 2H), 8.14 (d, *J* = 8.8 Hz, 2H). MS (70 eV) 352.1 ($M^+$, 100), 336 (50). EI-HRMS, m/e: calculated for $(M+H)^+$ $C_{22}H_{26}NO_3$ 352.19127, found 352.19039.

**p) 3-(4-Diethylamino-phenyl)-1-phenyl-propenone** (**2-15**): from 4-(diethylamino)benzaldehyde and acetophenone following the procedure for **2-14**. Yield: 64%. *Rf* 0.40 (10:1 hexane:EtOAc). $^1$H-NMR ($CDCl_3$, 300 MHz) δ 1.21 (t, *J* = 7.1 Hz, 6H), 3.41 (q, *J* = 7.1 Hz, 4H), 6.66 (d, *J* = 8.8 Hz, 2H), 7.30 (d, *J* = 15.4 Hz, 1H), 7.45-7.54 (m, 4H), 7.73 (t, *J* = 8.8 Hz, 1H), 7.78 (d, *J* = 15.4 Hz, 1H), 8.00 (d, *J* = 8.2 Hz, 2H). MS (70 eV) 279.2 ($M^+$, 100), 264.2 (65), 105.1 (40). EI- HRMS, m/e: calculated for ($M^+$) $C_{19}H_{21}NO$ 279.16231, found 279.16282.

**q) 4-[3-(4-Diethylamino-phenyl)-acryloyl]-benzonitrile** (**2-16**): from 4-(diethylamino)benzaldehyde and 4-cyano-acetophenone following the procedure for **2-14**. Yield: 59%. mp 167-169 °C. *Rf* 0.36 (10:1 hexane:EtOAc). $^1$H-NMR ($CDCl_3$, 300 MHz) δ 1.21 (t, *J* = 7.1 Hz, 6H), 3.43 (q, *J* = 7.1 Hz, 4H), 6.66 (d, *J* = 8.8 Hz, 2H), 7.22 (d, *J* = 15.4 Hz, 1H), 7.53 (d, *J* = 8.8 Hz, 2H), 7.78 (d, *J* = 8.8 Hz, 2H), 7.80 (d, *J* = 15.4 Hz, 1H), 8.05 (d, *J* = 8.8 Hz, 2H). MS (70 eV) 289.1 ($M^+$, 100), 130.1 (34), 102 (28). EI-HRMS, m/e: calculated for ($M^+$) $C_{20}H_{20}N_2O$ 304.15756, found 304.15761.

**r) 3-(4-Diethylamino-phenyl)-1-(4-methoxy-phenyl)-propenone (2-17):** Yield: 41%. mp 100-103 °C. *Rf* 0.25 (10:1 hexane:EtOAc). $^1$H NMR ($CDCl_3$, 300 MHz) δ1.20 (t, *J* = 7.1 Hz, 6H), 3.41 (q, *J* = 7.1 Hz, 4H), 3.88 (s, 3H), 6.65 (d, *J* = 8.8 Hz, 2H), 6.97

(d, $J$ = 8.8 Hz, 2H), 7.33 (d, $J$ = 15.4 Hz, 1H), 7.53 (d, $J$ = 8.8 Hz, 2H), 7.78 (d, $J$ = 15.4 Hz, 1H), 8.03 (d, $J$ = 8.8 Hz, 2H), MS (70 eV) 309.1 ($M^+$, 60), 294.1 (100), 102 (22). EI-HRMS, m/e: calculated for ($M^+$) $C_{20}H_{23}NO_2$ 309.17288, found 309.17357.

**s) 4-(3-Phenyl-acryloyl)-benzoic acid ethyl ester (2-18)**: from benzaldehyde and ethyl 4-acetylbenzoate. Yield: 34%. $Rf$ 0.32 (10:1 hexane:EtOAc). $^1$H NMR ($CDCl_3$, 300 MHz) δ 1.42 (t, $J$ = 7.1, 3H), 4.42 (q, $J$ = 7.1, 2H), 7.21-7.24 (m, 1H), 7.40-7.55 (m, 4H), 7.64-7.68 (m, 2H), 7.83 (d, $J$ = 15.9Hz, 1H), 8.05 (d, $J$ = 8.2 Hz, 2H), 8.18 (d, $J$ = 8.8Hz, 2H); MS (70 eV) 279.1 ($M^+$, 100), 207.1 (60), 131.1 (84). FAB HRMS *m/e* calculated for ($M^+$) $C_{18}H_{16}O_3$ 280.10994, found 280.10905.

## 2.9. References


1. McClure, D. S., *J. Chem. Phys.* **1952,** 20, (4), 682.
2. de Silva, A.; Gunaratne, H.; Gunnlaugsson, T.; Huxley, A.; Mccoy, C.; Rademacher, J.; Rice, T., *Chem. Rev.* **1997,** 97, (5), 1515.
3. Varnes, A. W.; Wehry, E. L.; Dodson, R. B., *J. Am. Chem. Soc.* **1972,** 94, (3), 946.
4. Gutteridge, J., *Biochem. J.* **1984,** 218, (3), 983.
5. Aragoni, M. C.; Arca, M.; Demartin, F.; Devillanova, F. A.; Isaia, F.; Garau, A.; Lippolis, V.; Jalali, F.; Papke, U.; Shamsipur, M.; Tei, L.; Yari, A.; Verani, G., *Inorg. Chem.* **2002,** 41, (25), 6623.
6. Rurack, K.; Kollmannsberger, M.; Resch-Genger, U.; Daub, J., *J. Am. Chem. Soc.* **2000,** 122, (5), 968.
7. Rurack, K.; Bricks, J. L.; Schulz, B.; Maus, M.; Reck, G.; Resch-Genger, U., *J. Phys. Chem. A* **2000,** 104, (26), 6171.
8. Karolin, J.; Johansson, L. B. A.; Strandberg, L.; Ny, T., *J. Am. Chem. Soc.* **1994,** 116, (17), 7801.
9. Fahrni, C. J.; Henary, M. M., unpublished results.

10. Ambundo, E.; Deydier, M.; Grall, A.; Aguera-Vega, N.; Dressel, L.; Cooper, T.; Heeg, M.; Ochrymowycz, L.; Rorabacher, D., *Inorg. Chem.* **1999,** 38, (19), 4233.

11. Westerby, B.; Juntunen, K.; Leggett, G.; Pett, V.; Koenigbauer, M.; Purgett, M.; Taschner, M.; Ochrymowycz, L.; Rorabacher, D., *Inorg. Chem.* **1991,** 30, (9), 2109.

12. de Silva, A.; De Silva, S.; Dissanayake, A.; Sandanayake, K., *J. Chem. Soc. Chem. Commun.* **1989**, (15), 1054.

13. de Silva, A.; Gunaratne, H.; Gunnlaugsson, T.; Nieuwenhuizen, M., *Chem. Commun.* **1996**, (16), 1967.

14. de Silva, A.; Gunaratne, H.; Maguire, G., *J Chem. Soc. Chem. Comm.* **1994**, (10), 1213.

15. de Silva, A.; Gunaratne, H.; Lynch, P., *J. Chem. Soc. Perkin. Trans. 2* **1995**, (4), 685.

16. de Silva, A.; Gunaratne, H.; Kane, A.; Maguire, G., *Chem. Lett.* **1995**, (2), 125.

17. Rurack, K.; Resch-Genger, U.; Bricks, J. L.; Spieles, M., *Chem. Commun.* **2000**, (21), 2103.

18. Yoon, J. Y.; Ohler, N. E.; Vance, D. H.; Aumiller, W. D.; Czarnik, A. W., *Tetrahedron Lett.* **1997,** 38, (22), 3845.

19. Prodi, L.; Bargossi, C.; Montalti, M.; Zaccheroni, N.; Su, N.; Bradshaw, J. S.; Izatt, R. M.; Savage, P. B., *J. Am. Chem. Soc.* **2000,** 122, (28), 6769.

20. Ramachandram, B.; Samanta, A., *J. Phys. Chem. A* **1998,** 102, (52), 10579.

21. Rehm, D.; Weller, A., *Isr. J. Chem.* **1970,** 8, (2), 259.

22. Gusten, H.; Heinrich, G., *Ber. Bunsen-Ges. Phys. Chem.* **1977,** 81, (9), 810.

23. Rivett, D. E.; Rosevear, J.; Wilshire, J. F. K., *Aust. J. Chem.* **1983,** 36, (8), 1649.

24. Lippert, E., *Z. Elektrochem.* **1957,** 61, (8), 962.

25. Lippert, E., *Z. Naturforsch., A: Phys.Sci.* **1955,** 10, (7), 541.

26. Mataga, N.; Kaifu, Y.; Koizumi, M., *Bull. Chem. Soc. Jpn.* **1956,** 29, (4), 465.

27. Onsager, L., *J. Am. Chem. Soc.* **1936,** 58, 1486.

28. Fahrni, C. J., Experiment data.

29. Fahrni, C.; Yang, L.; Vanderveer, D., *J. Am. Chem. Soc.* **2003,** 125, (13), 3799.

30. Specfit; Binstead, R. A.; Zuberbuhler, A. D., Spectrum Software Associates, Marlborough MA 01752 **2001**.

31. Millot, C.; Millot, J.; Morjani, H.; Desplaces, A.; Manfait, M., *J. Histochem. Cytochem.* **1997,** 45, (9), 1255.

32. Demas, J.; Crosby, G., *J. Phys. Chem.* **1971,** 75, (8), 991.

33. Gran, G., *Analyst* **1952,** 77, (920), 661.

34. Gans, P.; O'Sullivan, B., *Talanta* **2000,** 51, (1), 33.

35. Blessing, R., *Acta Crystallogr., Sect. A* **1995,** 51, **33.**

36. SHELXTL 5.10; Bruker: Madison, WI, **1998**.

37. Becke, A., *J. Chem. Phys.* **1993,** 98, (7), 5648.

38. Lee, C.; Yang, W.; Parr, R., *Phys. Rev. B: Condens. Matter* **1988,** 37, (2), 785.

39. Stratmann, R.; Scuseria, G.; Frisch, M., *J. Chem. Phys.* **1998,** 109, (19), 8218.

# CHAPTER III

# PARALLEL SYNTHESIS OF A FLUOROPHORE LIBRARY

## 3.1. Introduction

As discussed in chapter 2, the aryl substituents attached to the 1- and 3-position of the pyrazoline ring influence the photophysical properties of the fluorophore in distinctly different ways, and can be utilized to selectively tune the excited state electron transfer thermodynamics. In order to design a sensor with optimal fluorescence enhancement upon Cu(I) binding, the photophysical and electrochemical property of the fluorophore must be adjusted to the redox potential of the copper receptor. To explore the scope of the differential tuning properties of triaryl-substituted fluorophores in more detail, a fluorophore library covering a broad range of excited state energies and redox potentials was synthesized, and the photophysical and electrochemical properties of the library compounds were studied in detail.

## 3.2. Fluorophore Library

### *3.2.1. Synthesis*

The pyrazoline fluorophores were synthesized following the method discussed in chapter II, Section 2.2.

The first series of fluorophores (**3-1** and **3-2**) are shown in the Figure 3-1 and the respective structure key is given in Table 3-1. A hydrolysable ethyl carboxylate group was introduced in the 4-position of the 1-phenyl ring in order to increase the water solubility of the fluorophores. For substituent $R_2$ a hydrogen or cyano-group was chosen, whereas $R_1$ was varied with an increasing number of fluoro-substituents attached to

different positions on the aryl-ring, thus altering the degree of electron withdrawing ability over a broad range.

Another second series of fluorophores was synthesized lacking the ethyl carboxylate group attached to the 4-position of the 1-phenyl ring, as shown in the Figure 3-1 and Table 3-2.

All crude products were purified by column chromatography and reversed-phase HPLC (Varian ProStar system with UV detector, acetonitrile -water, gradient 15% to 2% water). The chemical structures of the synthesized compounds were confirmed by $^{1}H$ NMR, MS and high revolution mass spectrometry (HRMS). Descriptions of the detailed analytical data are provided in the experimental section.

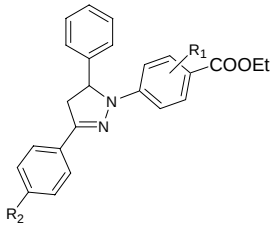


**3-1** $R_2$ = H

**3-2** $R_2$ = CN

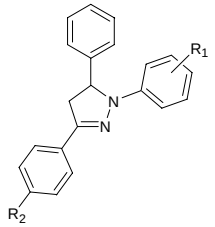


**3-3** $R_2$ = H

**3-4** $R_2$ = CN

**Figure 3-1.** Structures of pyrazolines used for the fluorophore library.

**Table 3-1.** Substituent Key for Pyrazolines **3-1a** to **3-2g**.

| comp | $R_1$ | $R_2$ |
|---|---|---|
| **3-1a** | H | H |
| **3-1b** | 2-F | |
| **3-1c** | 3-F | |
| **3-1d** | 2,5-2F | |
| **3-1e** | 2,6-2F | |
| **3-1f** | 2,3,5-3F | |
| **3-1g** | 2,3,5,6-4F | |
| | | |
| **3-2a** | H | CN |
| **3-2b** | 2-F | |
| **3-2c** | 3-F | |
| **3-2d** | 2,5-2F | |
| **3-2e** | 3,5-2F | |
| **3-2f** | 2,3,5-3F | |
| **3-2g** | 2,3,5,6-4F | |

**Table 3-2.** Substituent Key for Pyrazolines **3-3a** to **3-4h**.

| | $R_1$ | $R_2$ |
|---|---|---|
| **3a** | 2-F | H |
| **3b** | 3-F | |
| **3c** | 4-F | |
| **3d** | 2,4-2F | |
| **3e** | 2,5-2F | |
| **3f** | 3,5-2F | |
| **3g** | 2,3,5,6-4F | |
| **3h** | 2,3,4,5,6-5F | |
| | | |
| **4a** | 2-F | CN |
| **4b** | 3-F | |
| **4c** | 4-F | |
| **4d** | 2,4-2F | |
| **4e** | 2,5-2F | |
| **4f** | 3,5-2F | |
| **4g** | 2,3,5,6-4F | |
| **4h** | 2,3,4,5,6-5F | |

### *3.2.2. Photophysics*

Steady state absorption and fluorescence emission were recorded in acetonitrile at room temperature. All relevant data are given in Table 3-3 and 3-4.

The combined series of compounds cover absorption maxima ranging between 25,000 $cm^{-1}$ to 31,000 $cm^{-1}$. The changes in absorption energies as a function of the substituents are consistent with the discussion in the chapter II, Section 2.4.2.1. The absorption energy increases with increasing electron-withdrawing character of R and decreases with increasing electron-withdrawing character of the substituent $R_2$. In general, substituent $R_2$ has a greater influence on the absorption energy compared to substituent $R_1$. Substitution with a cyano group in the *para*-position of the 3-phenyl ring shifts the absorption maximum by about 2000 $cm^{-1}$, while attachment of a single fluoro-substituent on the 1-phenyl ring changes the absorption maximum by less than 1000 $cm^{-1}$. Specifically, for the series containing an ethyl carboxylate group (**3-1** and **3-2**), the 3-position of 1-phenyl ring is more sensitive to the substitution compared to the other position on the phenyl ring. For example, **3-1c** exhibits an absorption energy that is by 1000 $cm^{-1}$ higher compared to **3-1b**. Similarly, the energy of **3-1e** is higher compared to **3-1d**. The same trend can be observed in the series of **3-2** but with smaller differences of about 400 $cm^{-1}$. However, this phenomenon was not observed for the derivatives **3-3** and **3-4**, both of which are lacking the ethyl carboxylate group.

For biological applications, the absorption maximum energy of the sensor should be lower than 28,600 $cm^{-1}$, not only to minimize the UV cell damage but also to be compatible with the transmission characteristics of standard microscope lenses. In case of the compound series **3-1** containing the unsubstituted aryl ring ($R_2$ = H), the absorption

energy is for all derivatives significantly higher than the desired cutoff, except for the mono fluoro- and carbopxylate derivatives **3-1a** and **3-1b**, respectively. Similarly, the absorption maxima of derivatives **3-3 (a-h)** are also greater than 28 600 $cm^{-1}$, except for **3-3b** and **3-3c**, which have maxima of 28,400 and 28,000 $cm^{-1}$, respectively. For the cyano-substituted series **3-2** and **3-4**, the absorption maxima are below 28 600 $cm^{-1}$, except for **4i**. Hence, the derivatives with an electron-withdrawing group $R_2$ are preferred candidates for the design of biological sensors.

**Table 3-3.** Photophysical Data of **3-1a** to **3-2g** in Acetonitrile at Room Temperature.

| comp | $\nu_{abs}$ [$cm^{-1}$] | $\varepsilon$ [$M^{-1}cm^{-1}$] | $\nu_{em}$ [$cm^{-1}$] | $\nu_{abs}$- $\nu_{em}$ [$cm^{-1}$] | $E_{00}$ [$cm^{-1}$] | $G_{00}$ [eV] | $\Phi$ |
|---|---|---|---|---|---|---|---|
| **3-1a** | 27,397 | 47,284 | 23,256 | 4,141 | 25,327 | 3.12 | 0.65 |
| **3-1b** | 27,778 | 22,309 | 23,810 | 3,968 | 25,794 | 3.18 | 0.06 |
| **3-1c** | 28,818 | 16,466 | 23,529 | 5,289 | 26,174 | 3.23 | 0.04 |
| **3-1d** | 27,778 | 31,682 | 24,213 | 3,565 | 25,995 | 3.21 | 0.03 |
| **3-1e** | 29,070 | 19,889 | 24,272 | 4,798 | 26,671 | 3.29 | 0.07 |
| **3-1f** | 28,571 | 19,110 | 24,213 | 4,358 | 26,392 | 3.26 | 0.00 |
| **3-1g** | 28,986 | 35,021 | 25,000 | 3,986 | 26,993 | 3.33 | 0.00 |
| | | | | | | | |
| **3-2a** | 25,253 | 46,408 | 20,747 | 4,506 | 23,000 | 2.84 | 0.61 |
| **3-2b** | 26,042 | 32,505 | 21,053 | 4,989 | 23,547 | 2.91 | 0.64 |
| **3-2c** | 26,455 | 26,000 | 21,277 | 5,178 | 23,866 | 2.94 | 0.46 |
| **3-2d** | 26,316 | 17,871 | 21,598 | 4,718 | 23,957 | 2.96 | 0.50 |
| **3-2e** | 26,810 | 22,703 | 21,786 | 5,023 | 24,298 | 3.00 | 0.54 |
| **3-2f** | 27,322 | 33,686 | 22,727 | 4,595 | 25,025 | 3.09 | 0.05 |
| **3-2g** | 27,855 | 26,940 | 23,256 | 4,599 | 25,555 | 3.15 | 0.02 |

**Table 3-4.** Photophysical Data of **3-3a** to **3-4h** in Acetonitrile at Room Temperature.

| comp | $\nu_{abs}$ [$cm^{-1}$] | $\varepsilon$ [$M^{-1}cm^{-1}$] | $\nu_{em}$ [$cm^{-1}$] | $\nu_{abs}$- $\nu_{em}$ [$cm^{-1}$] | $E_{00}$ [$cm^{-1}$] | $G_{00}$ [eV] | $\Phi$ |
|---|---|---|---|---|---|---|---|
| **3-3a** | 29,061 | 13,785 | 22,523 | 6,539 | 25,792 | 3.18 | 0.60 |
| **3-3b** | 28,409 | 12,032 | 22,831 | 5,578 | 25,620 | 3.16 | 0.63 |
| **3-3c** | 28,011 | 14,347 | 22,124 | 5,887 | 25,068 | 3.09 | 0.58 |
| **3-3d** | 29,240 | 16,961 | 22,573 | 6,666 | 25,907 | 3.20 | 0.60 |
| **3-3e** | 28,986 | 23,097 | 23,256 | 5,730 | 26,121 | 3.22 | 0.62 |
| **3-3f** | 28,818 | 26,321 | 23,529 | 5,289 | 26,174 | 3.23 | 0.68 |
| **3-3g** | 30,874 | 21,364 | 25,063 | 5,811 | 27,968 | 3.45 | 0.41 |
| **3-3h** | 31,857 | 14,587 | 24,814 | 7,043 | 28,336 | 3.50 | 0.00 |
| **3-4a** | 26,448 | 32,996 | 20,202 | 6,246 | 23,325 | 2.88 | 0.59 |
| **3-4b** | 25,773 | 29,130 | 20,408 | 5,365 | 23,091 | 2.85 | 0.59 |
| **3-4c** | 25,439 | 26,768 | 19,455 | 5,984 | 22,447 | 2.77 | 0.52 |
| **3-4d** | 26,738 | 17,462 | 19,920 | 6,818 | 23,329 | 2.88 | 0.53 |
| **3-4e** | 26,589 | 17,506 | 20,704 | 5,885 | 23,646 | 2.92 | 0.58 |
| **3-4f** | 26,247 | 32,842 | 21,008 | 5,238 | 23,628 | 2.92 | 0.61 |
| **3-4g** | 28,482 | 27,625 | 22,422 | 6,060 | 25,452 | 3.14 | 0.70 |
| **3-4h** | 29,155 | 19,954 | 22,422 | 6,733 | 25,788 | 3.18 | 0.67 |

For the fluorescence spectra, the influence of the substituents $R_1$ and $R_2$ on the emission maxima is similar compared to the influence on the absorption maxima. With increasing electron withdrawing character of $R_2$ the emission energy decreases, while with increasing electron withdrawing character of $R_1$ the emission energy increases. Furthermore, the Stokes' shift increases with increasing electron withdrawing character of $R_1$ and decreases with increasing electron withdrawing character of $R_2$.

Based on the absorption and emission spectra, the excited state equilibrium energy $\Delta G_{00}$ was calculated (shown in Table 3-3 and Table 3-4). $\Delta G_{00}$ increases with increasing electron withdrawing character of $R_1$ and decreases with increasing electron withdrawing character of group $R_2$. In general, substitution with a cyano group for $R_2$ changes the $\Delta G_{00}$ by about 0.30 eV compared to the corresponding unsubstituted derivative. Furthermore, $\Delta G_{00}$ increases with increasing electron withdrawing character of $R_1$, covering a range of 0.30 eV across the mono to the pentafluoro substituted derivatives.

### *3.2.3. Reduction Potentials*

The cyclic voltammograms of all derivatives were acquired in acetonitrile (freshly distilled over calcium hydride), 0.1M $Bu_4NPF_6$ was used as electrolyte. The half-wave potentials were referenced to ferrocene. The data are listed in the Table 3-5 and Table 3-6 and also shown as bar graph (Figure 3-2 and Figure 3-3) for better comparison.

The oxidation potential is most likely due to oxidation of the electron-rich aryl substituent in the 1-position of pyrazoline ring. Because the electron-withdrawing group in the 1- and 3-position of the ring reduces the electron density of the π-system, the oxidation potential increases with increasing electron-withdrawing character of $R_1$ and

$R_2$. The influence of the substituents on the reduction potential of the fluorophore follows the same trend as already described in chapter 2. The reduction potential increases with increasing electron-withdrawing character of $R_2$. For example, when comparing derivatives **3-3** and **3-4**, the **3-3** series has an average reduction potential around -2.7 V while the potential for the **3-4** series is lower and invariably lies around -2.2 V. The reduction potential increases by 0.6 eV. Most important, variation of $R_1$ has no significant effect on the reduction potential, except for **1f** and **1g.**

**Table 3-5.** Redox Potentials for Pyrazolines **3-1a** to **3-2g** in Acetonitrile/0.1 M $Bu_4NPF_6$ vs $Fc/Fc^+$.

| comp | $E_{ox}$[V] | | $E_{red}$[V] | |
|---|---|---|---|---|
| **3-1a** | 0.61 | | -2.65 | |
| **3-1b** | 0.81 | | -2.58 | |
| **3-1c** | 0.71 | | -2.70 | |
| **3-1d** | 0.77 | | -2.48 | |
| **3-1e** | 0.81 | | -2.64 | |
| **3-1f** | 0.84 | 1.53 | -2.30 | |
| **3-1g** | 0.91 | 1.54 | -2.23 | -2.79 |
| | | | | |
| **3-2a** | 0.68 | | -2.14 | -2.50 |
| **3-2b** | 0.78 | | -2.12 | -2.48 |
| **3-2c** | 0.81 | | -2.17 | -2.63 |
| **3-2d** | 0.90 | | -2.08 | -2.40 |
| **3-2e** | 0.90 | | -2.13 | -2.59 |
| **3-2f** | 0.98 | 1.41 | -2.14 | -2.39 |
| **3-2g** | 1.04 | | -2.13 | -2.41 |

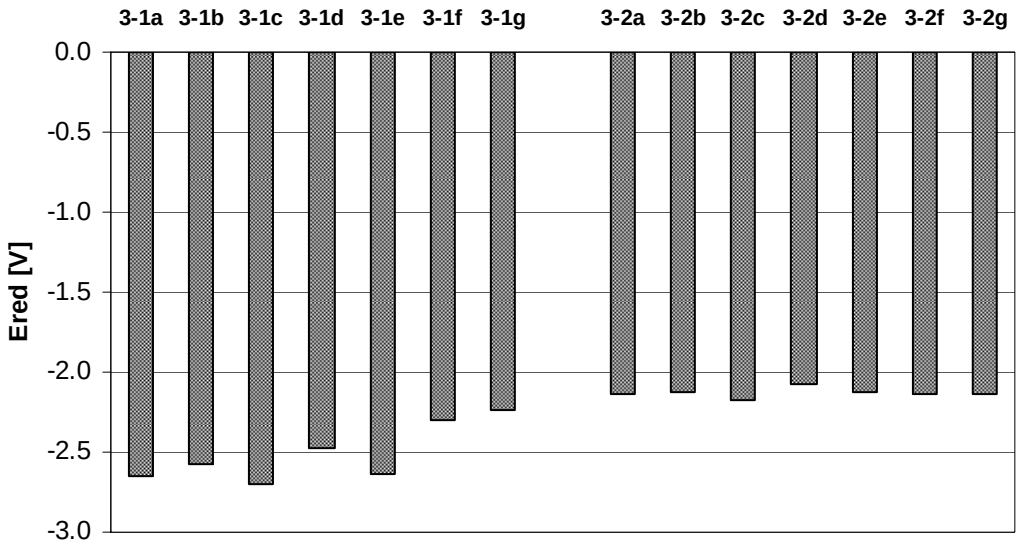


**Figure 3-2.** Reduction potentials for pyrazolines **3-1a** to **3-2g** in acetonitrile/0.1 M $Bu_4NPF_6$ vs $Fc/Fc^+$.

**Table 3-6.** Potentials for Pyrazolines **3-3a** to **3-4h** in Acetonitrile/0.1 M $Bu_4NPF_6$ vs $Fc/Fc^+$.

| comp | $E_{ox}$[V] | $E_{red}$[V] | |
|---|---|---|---|
| **3-3a** | 0.63 | -2.80 | |
| **3-3b** | 0.71 | -2.75 | |
| **3-3c** | 0.84 | -2.76 | |
| **3-3d** | 0.60 | -2.76 | |
| **3-3e** | 0.74 | -2.70 | |
| **3-3f** | 0.73 | -2.71 | |
| **3-3g** | 0.84 | -2.72 | |
| **3-3h** | 0.82 | -2.64 | |
| | | | |
| **3-4a** | 0.64 | -2.22 | |
| **3-4b** | 0.65 | -2.21 | -2.77 |
| **3-4c** | 0.62 | -2.24 | -2.76 |
| **3-4d** | 0.67 | -2.21 | -2.74 |
| **3-4e** | 0.78 | -2.18 | -2.73 |
| **3-4f** | 0.78 | -2.16 | -2.63 |
| **3-4g** | 0.97 | -2.21 | -2.73 |
| **3-4h** | 1.06 | -2.22 | -2.77 |

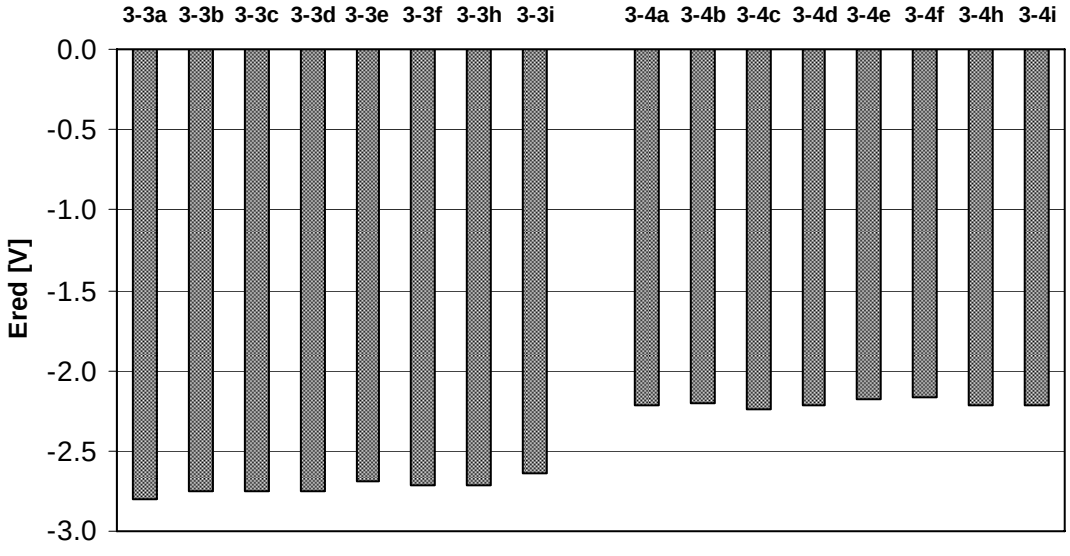


**Figure 3-3.** Reduction potentials for pyrazolines **3-3a** to **3-4h** in acetonitrile/0.1 M $Bu_4NPF_6$ vs $Fc/Fc^+$.

### *3.2.4. Electron Transfer Thermodynamic*

The free energy change $\Delta G_{ET}$ of the excited-state electron-transfer reaction in the pyrazoline derivatives **3-1** to **3-4** were calculated based on the spectroscopic and reduction potential data using the Rehm-Weller equation. Compared to the diethyl amino substituted derivatives characterized in chapter II, the unsubstituted phenyl ring has a considerably higher oxidation potential (greater than 0.6 V besides **3-3c**), and thus the photoinduced electron transfer process should be substantially less favorable. The free energy change $\Delta G_{ET}$ for all fluorophores is indeed very positive (except **3-1f** and **3-1g**) indicating that the electron transfer quenching pathway is not favorable. However, the quantum yields of compounds **3-1b** to **3-1e** are surprisingly low, suggesting another mode of nonradiative deactivation. According to the literature, the fluorescence emission can be potentially quenched by low-lying nonemissive $^3(n, \pi^*)$ states.[1] This triplet state might be potentially introduced through the carbonyl oxygen lone pair of the ethyl carboxylate substituent. If the $^3(n, \pi^*)$ state is at lower energy level compared to the emissive locally excited state, which corresponds to a $^1(\pi, \pi^*)$ state, the fluorescence emission would be effectively quenched, as illustrated in Figure 3-4. Such a $^3(n, \pi^*)$ quenching mechanism might explain the low quantum yields of the compounds containing the ethyl carboxylate substituent. For compounds **3-3** and **3-4**, which are lacking the ethyl carboxylate group, the $^3(n, \pi^*)$ state quenching cannot occur and the quantum yields are indeed higher (> 0.50, except **3-3h**) compared to compounds **3-1**, as shown in the Table 3-8. In conclusion, for design of a fluorescent sensor, the carboxyl acid group should not be attached immediately to the fluorophore π-system to avoid the

unexpected fluorescence quenching. In order to improve water solubility of the sensor, the carboxyl acid group could be link to the receptor moiety or attached via a non-conjugated spacer group.

**Table 3-7.** Electron Transfer Data and Quantum Yields of **3-1a** to **3-2g** in Acetonitrile.

| comp | $E_{ox}$ [V] | $E_{red}$ [V] | $E_{ox}$-$E_{red}$ [eV] | $\Delta G_{00}$ [eV] | $\Delta G_{ET}$ [eV] | $\Phi$ |
|---|---|---|---|---|---|---|
| **3-1a** | 0.61 | -2.65 | 3.26 | 3.12 | 0.14 | 0.65 |
| **3-1b** | 0.81 | -2.58 | 3.39 | 3.18 | 0.21 | 0.06 |
| **3-1c** | 0.71 | -2.70 | 3.41 | 3.23 | 0.18 | 0.04 |
| **3-1d** | 0.77 | -2.48 | 3.25 | 3.21 | 0.04 | 0.03 |
| **3-1e** | 0.81 | -2.64 | 3.45 | 3.29 | 0.15 | 0.07 |
| **3-1f** | 0.84 | -2.30 | 3.14 | 3.26 | -0.12 | 0.00 |
| **3-1g** | 0.91 | -2.23 | 3.14 | 3.34 | -0.20 | 0.00 |
| | | | | | | |
| **3-2a** | 0.68 | -2.14 | 2.82 | 2.84 | -0.02 | 0.61 |
| **3-2b** | 0.78 | -2.12 | 2.90 | 2.91 | 0.00 | 0.64 |
| **3-2c** | 0.81 | -2.17 | 2.98 | 2.94 | 0.04 | 0.46 |
| **3-2d** | 0.90 | -2.08 | 2.97 | 2.96 | 0.02 | 0.50 |
| **3-2e** | 0.90 | -2.13 | 3.03 | 3.00 | 0.04 | 0.54 |
| **3-2f** | 0.98 | -2.14 | 3.12 | 3.09 | 0.03 | 0.05 |
| **3-2g** | 1.04 | -2.13 | 3.17 | 3.15 | 0.02 | 0.02 |

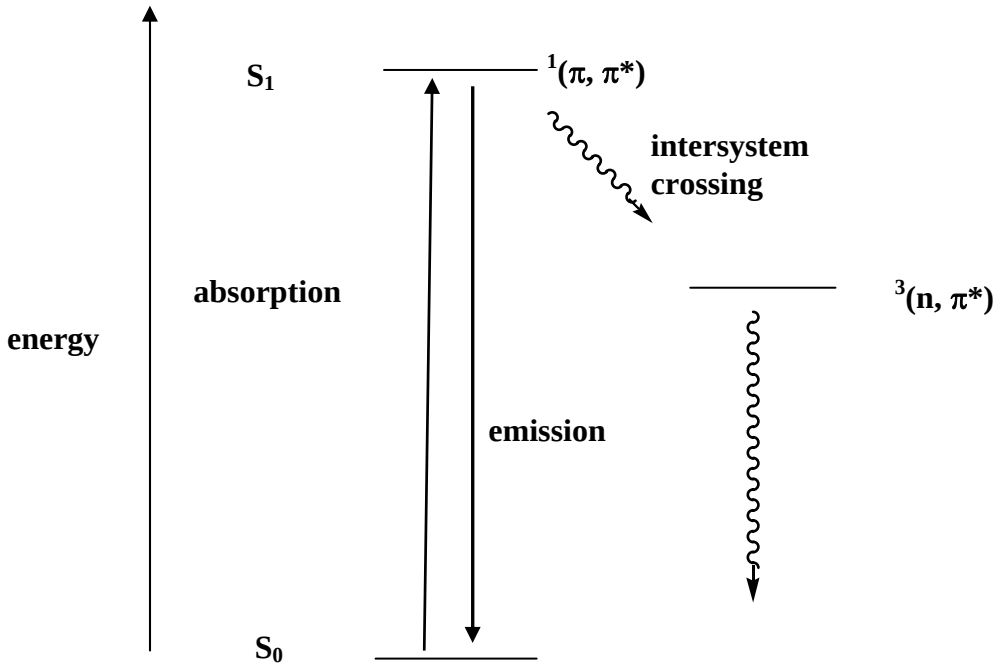


**Figure 3-4.** Simplified energy diagram for $^{3}(n, \pi^*)$ quenching mechanism.

**Table 3-8.** Electron Transfer Data and Quantum Yields of **3-3a** to **3-4h** in Acetonitrile.

| comp | $E_{ox}$ [V] | $E_{red}$ [V] | $E_{ox}$-$E_{red}$ [eV] | $\Delta G_{00}$ [eV] | $\Delta G_{ET}$ [eV] | Φ |
|---|---|---|---|---|---|---|
| **3-3a** | 0.63 | -2.80 | 3.37 | 3.18 | 0.19 | 0.60 |
| **3-3b** | 0.71 | -2.75 | 3.33 | 3.16 | 0.17 | 0.63 |
| **3-3c** | 0.84 | -2.76 | 3.23 | 3.09 | 0.14 | 0.58 |
| **3-3d** | 0.60 | -2.76 | 3.36 | 3.20 | 0.16 | 0.60 |
| **3-3e** | 0.74 | -2.70 | 3.44 | 3.22 | 0.22 | 0.62 |
| **3-3f** | 0.73 | -2.71 | 3.44 | 3.23 | 0.21 | 0.68 |
| **3-3g** | 0.84 | -2.72 | 3.56 | 3.45 | 0.11 | 0.41 |
| **3-3h** | 0.82 | -2.64 | 3.46 | 3.50 | -0.04 | 0.00 |
| | | | | | | |
| **3-4a** | 0.64 | -2.22 | 2.86 | 2.88 | -0.02 | 0.59 |
| **3-4b** | 0.65 | -2.21 | 2.86 | 2.85 | 0.01 | 0.59 |
| **3-4c** | 0.62 | -2.24 | 2.86 | 2.77 | 0.09 | 0.52 |
| **3-4d** | 0.67 | -2.21 | 2.88 | 2.88 | 0.00 | 0.53 |
| **3-4e** | 0.78 | -2.18 | 2.96 | 2.92 | 0.04 | 0.58 |
| **3-4f** | 0.78 | -2.16 | 2.94 | 2.92 | 0.02 | 0.61 |
| **3-4g** | 0.97 | -2.21 | 3.18 | 3.14 | 0.04 | 0.70 |
| **3-4h** | 1.06 | -2.22 | 3.28 | 3.18 | 0.10 | 0.67 |

### *3.2.5. Calculation of $\Delta G_{ET}$ with a Cu(I) receptor*

To design a Cu(I) sensor, the receptor ligand must match the reduction potential and excited state energy of the pyrazoline fluorophore. By combining the reduction potential and the excited state equilibrium energy $\Delta G_{00}$ of the fluorophores with the oxidation potential of the ligand (chapter 4), the $\Delta G_{ET}$ can be calculated to estimate the free energy change of the excited state electron transfer of the prospective sensors. The oxidation potentials of the free ligand and the copper complex used for calculation were 0.46 V and 0.50 V, respectively. The resulting data were listed in Table 3-9.

Free energy of electron transfer for compounds containing fluorophore **3-3a** to **3-3f** is around 0 eV and will be more negative in water. They might be suitable for the Cu(I) sensor with receptor oxidation potential of 0.46 V. Compounds containing fluorophore **3-3g**, **3-3h**, **4a**, **4b** and **4d-4h** give very negative $\Delta G_{ET}$ and would only match receptors with high oxidation potentials (greater than 0.7 eV).

**Table 3-9.** Electron Transfer Data of Compounds Containing Fluorophore **3-3a** to **3-4h** and a Ligand with Oxidation Potential 0.46 eV.

| fluorophore | $E_{ox}$ [V] | $E_{red}$ [V] | $E_{ox}$-$E_{red}$ [eV] | $\Delta G_{00}$ [eV] | $\Delta G_{ET}$ [eV] |
|---|---|---|---|---|---|
| **3-3a** | 0.46 | -2.80 | 3.26 | 3.18 | 0.08 |
| **3-3b** | 0.46 | -2.75 | 3.21 | 3.16 | 0.05 |
| **3-3c** | 0.46 | -2.76 | 3.22 | 3.09 | 0.12 |
| **3-3d** | 0.46 | -2.76 | 3.22 | 3.20 | 0.02 |
| **3-3e** | 0.46 | -2.70 | 3.16 | 3.22 | -0.07 |
| **3-3f** | 0.46 | -2.71 | 3.17 | 3.23 | -0.06 |
| **3-3g** | 0.46 | -2.72 | 3.18 | 3.45 | -0.27 |
| **3-3h** | 0.46 | -2.64 | 3.10 | 3.50 | -0.40 |
| | | | | | |
| **3-4a** | 0.46 | -2.22 | 2.68 | 2.88 | -0.20 |
| **3-4b** | 0.46 | -2.21 | 2.67 | 2.85 | -0.18 |
| **3-4c** | 0.46 | -2.24 | 2.70 | 2.77 | -0.07 |
| **3-4d** | 0.46 | -2.21 | 2.67 | 2.88 | -0.21 |
| **3-4e** | 0.46 | -2.18 | 2.64 | 2.92 | -0.28 |
| **3-4f** | 0.46 | -2.16 | 2.62 | 2.92 | -0.30 |
| **3-4g** | 0.46 | -2.21 | 2.67 | 3.14 | -0.47 |
| **3-4h** | 0.46 | -2.22 | 2.68 | 3.18 | -0.50 |

In conclusion, this study provides important information about the electron transfer thermodynamic data of a series of pyrazoline fluorophores. The derivatives cover a broad range of excited state equilibrium energies $\Delta G_{00}$ and reduction potentials. By choosing the appropriate copper receptor, the key parameters governing the electron transfer thermodynamics can be differentially adjusted. This approach is expected to yield then the best possible emission enhancement for a given receptor moiety.

## 3.3. Experimental Section

**a) Ethyl 4-(4,5-dihydro-3,5-diphenylpyrazol-1-yl)benzoate (3-1a):** Yield: 63%. mp 128-131 °C. *Rf* 0.42 (3:1 hexane:EtOAc). $^1$H-NMR ($CDCl_3$, 400 MHz) δ 1.34 (t, *J* = 7.1 Hz, 3H), 3.20 (dd, *J* = 17.3, 6.0 Hz 1H), 3.89 (dd, *J* = 17.3, *J* = 12.3 Hz, 1H), 4.30 (q, *J* = 7.1 Hz, 2H), 5.38 (dd, *J* = 12.3, 6.0 Hz, 1H), 7.05 (d, *J* = 8.8 Hz, 2H), 7.27 (d, *J* = 5.7 Hz, 3H), 7.31-7.43 (m, 5H), 7.75 (dd, *J* = 8.2, 1.4 Hz, 2H), 7.86 (d, *J* = 8.9 Hz, 2H). MS (70 eV) 370.2 ($M^+$, 100), 356.2 (13), 293.2 (23). EI-HRMS *m/e* calculated for ($M^+$) $C_{24}H_{22}N_2O_2$ 370.1681, found 370.1572.

**b) 4-(3,5-Diphenyl-4,5-dihydro-pyrazol-1-yl)-3-fluoro-benzoic acid ethyl ester (3-1b):** Yield: 54%. *Rf* 0.65 (4:1 hexane:EtOAc). $^1$H-NMR ($CDCl_3$, 400 MHz) δ 1.34 (t, *J* = 7.1 Hz, 3H), 3.29 (dd, *J* = 17.0, 3.7 Hz, 1H), 3.83 (dd, *J* = 17.0, 11.7 Hz, 1H), 4.29 (q, *J* = 7.1 Hz, 2H), 5.79 (td, *J* = 11.7, 3.7 Hz, 1H), 7.14-7.24 (m, 3H), 7.36-7.44 (m, 2H), 7.52 (dd, *J* = 13.2, 1.5 Hz, 1H), 7.72-7.74 (m, 2H), 7.76-7.79 (m, 2H). MS (70 eV) 388.2 ($M^+$, 100). EI-HRMS *m/e* calculated for ($M^+$) $C_{24}H_{21}N_2O_2F$ 388.1587, found 388.1579.

**c) 4-(3,5-Diphenyl-4,5-dihydro-pyrazol-1-yl)-2-fluoro-benzoic acid ethyl ester (3-1c):**[2] Yield: 64%. *Rf* 0.35 (5:1 hexane:EtOAc). $^1$H-NMR ($CDCl_3$, 400 MHz) δ 1.28 (t, *J* = 7.1 Hz, 3H), 3.18 (dd, *J* = 17.0, 7.7 Hz, 1H), 3.80 (dd, *J* = 17.0, 11.5 Hz, 1H), 4.33 (q, *J* = 7.1 Hz, 2H), 5.37 (dd, *J* = 11.5, 7.7 Hz, 1H), 6.43 (dd, *J* = 11.5, 2.2 Hz, 1H), 6.50 (dt, *J* = 8.2, 2.7 Hz, 1H), 7.25-7.39 (m, 8H), 7.43 (dd, *J* = 8.2, 6.0 Hz, 1H), 7.64 (dd, *J* = 8.2, 1.6 Hz, 2H). MS (70 eV) 388.2 ($M^+$, 100). EI-HRMS *m/e* calculated for ($M^+$) $C_{24}H_{21}N_2O_2F$ 388.1587, found 388.1578.

**d) 4-(3,5-Diphenyl-4,5-dihydro-pyrazol-1-yl)-2,5-difluoro-benzoic acid ethyl ester (3-1d):**[2] Yield: 39%. *Rf* 0.35 (5:1 hexane:EtOAc). $^1$H-NMR ($CDCl_3$, 400 MHz) δ 1.33 (t, *J* = 6.6 Hz, 3H), 3.29 (dd, *J* = 17.6, 3.8 Hz, 1H), 3.83 (dd, *J* = 17.6, 12.1 Hz, 1H), 4.30 (q, *J* = 7.1 Hz, 2H), 5.78 (td, *J* = 12.1, 3.8 Hz, 1H), 7.12 (d, *J* = 6.6 Hz, 1H), 7.20-7.25 (m, 4H), 7.39-7.50 (m, 4H), 7.76 (dd, *J* = 8.2, 2.2 Hz, 2H). MS (70 eV) 406.1 ($M^+$, 100). EI-HRMS *m/e* calculated for ($M^+$) $C_{24}H_{20}N_2O_2F_2$ 406.1493, found 406.1496.

**e) 4-(3,5-Diphenyl-4,5-dihydro-pyrazol-1-yl)-2,6-difluoro-benzoic acid ethyl ester (3-1e):**[2] Yield: 56%. *Rf* 0.41 (5:1 hexane:EtOAc). $^1$H-NMR ($CDCl_3$, 400 MHz) δ 1.32 (t, *J* = 7.1 Hz, 3H), 3.15 (dd, *J* = 17.0, 7.1 Hz, 1H), 3.81 (dd, *J* = 17.0, 11.5 Hz, 1H), 4.42 (q, *J* = 7.1 Hz, 2H), 5.28 (dd, *J* = 12.1, 7.1 Hz, 1H), 5.96 (td, *J* = 11.0, 1.7 Hz, 1H), 6.25 (dt, *J* = 8.8, 2.2 Hz, 1H), 7.29-7.38 (m, 8H), 7.61 (dd, *J* = 7.7, 1.7 Hz, 2H). MS (70 eV) 406.2 ($M^+$, 38), 302.1 (75), 230.1 (100). EI-HRMS m/e calculated for ($M^+$) $C_{24}H_{20}N_2O_2F_2$ 406.1493, found 406.1459.

**f) 4-(3,5-Diphenyl-4,5-dihydro-pyrazol-1-yl)-2,3,5-trifluoro-benzoic acid ethyl ester (3-1f):**[2] Yield: 7%. *Rf* 0.46 (5:1 hexane:EtOAc). $^1$H-NMR ($CDCl_3$, 400 MHz) δ 1.35 (t, *J* = 7.1 Hz, 3H), 3.31 (dd, *J* = 17.0, 6.0 Hz, 1H), 3.81 (dd, *J* = 17.0, 12.1 Hz, 1H),

4.32 (q, *J* = 7.1 Hz, 2H), 5.68 (dd, *J* = 12.1, 7.1 Hz, 1H), 7.25 (s, 5H), 7.41 (d, *J* = 7.7 Hz, 4H), 7.74 (dd, *J* = 8.2, 1.7 Hz, 2H). MS (70 eV) 406.2 ($M^+$, 38), 302.1 (75), 230.1 (100). EI-HRMS m/e calculated for ($M^+$) $C_{24}H_{19}N_2O_2F_3$424.1493, found 424.1459.

**g) 4-(3,5-Diphenyl-4,5-dihydro-pyrazol-1-yl)-2,3,5,6-tetrafluoro-benzoic acid ethyl ester (3-1g):**[2] Yield: 8%. *Rf* 0.80 (1:1 hexane:EtOAc). $^1$H-NMR ($CDCl_3$, 400 MHz) δ 1.35 (t, *J* = 7.1 Hz, 3H), 3.18 (dd, *J* = 17.0, 6.0 Hz, 1H), 3.82 (dd, *J* = 17.0, 12.1 Hz, 1H), 4.36 (q, *J* = 7.1 Hz, 2H), 5.68 (dd, *J* = 12.1, 6.0 Hz, 1H), 7.23-7.26 (m, 4H), 7.39-7.44 (m, 4H), 7.74 (dd, *J* = 7.7, 1.7 Hz, 2H). MS (70 eV) 422.1 ($M^+$, 100), 135.1 (60). EI-HRMS *m/e* calculated for ($M^+$) $C_{24}H_{18}N_2O_2F_4$ 442.1304, found 422.1333.

**h) 4-[3-(4-Cyano-phenyl)-5-phenyl-4,5-dihydro-pyrazol-1-yl]-benzoic acid ethyl ester (3-2a):** Yield: 59%. *Rf* 0.44 (3:1 hexane:EtOAc). $^1$H-NMR ($CDCl_3$, 400 MHz) δ 1.34 (t, *J* = 7.1 Hz, 3H), 3.17 (dd, *J* = 17.6, 6.0 Hz, 1H), 3.86 (dd, *J* = 17.6, 12.6 Hz, 1H), 4.30 (q, *J* = 7.1 Hz, 2H), 5.45 (dd, *J* = 12.6, 6.0 Hz, 1H), 7.06 (d, *J* = 8.8 Hz, 2H), 7.23-7.34 (m, 5H), 7.66 (d, *J* = 8.2 Hz, 2H), 7.79 (d, *J* = 8.2 Hz, 2H), 7.87 (d, *J* = 8.8 Hz, 2H). MS (70 eV) 396 ($M^+$, 100). EI-HRMS *m/e* calculated for ($M^+$) $C_{25}H_{21}N_3O_2$ 396.17120, found 396.17300.

**i) 4-[3-(4-Cyano-phenyl)-5-phenyl-4,5-dihydro-pyrazol-1-yl]-3-fluoro-benzoic acid ethyl ester (3-2b):** Yield: 28%. *Rf* 0.56 (4:1 hexane:EtOAc). $^1$H-NMR ($CDCl_3$, 400 MHz) δ 1.34 (t, *J* = 7.2 Hz, 3H), 3.37 (dd, *J* = 17.0, 3.8 Hz, 1H), 3.82 (dd, *J* = 17.0, 12.1 Hz, 1H), 4.29 (q, *J* = 7.2 Hz, 2H), 5.84 (td, *J* = 12.1, 3.8 Hz, 1H), 7.13 (dd, *J* = 7.7, 1.6 Hz, 2H), 7.20-7.24 (m, 3H), 7.54 (dd, *J* = 13.7, 1.6 Hz, 1H), 7.68-7.76 (m, 4H), 7.83 (d, *J* = 8.8 Hz, 2H). MS (70 eV) 413 ($M^+$, 100). EI-HRMS *m/e* calculated for ($M^+$) $C_{25}H_{20}N_3O_2F$ 413.1540, found 413.1526.

**j) 4-[3-(4-Cyano-phenyl)-5-phenyl-4,5-dihydro-pyrazol-1-yl]-2-fluoro-benzoic acid ethyl ester (3-2c):** Yield: 69%. $R_f$ 0.56 (4:1 hexane:EtOAc). $^1$H-NMR ($CDCl_3$, 400 MHz) δ 1.34 (t, *J* = 7.1 Hz, 3H), 3.20 (dd, *J* = 17.0, 8.2 Hz, 1H), 3.81 (dd, *J* = 17.0, 12.1 Hz, 1H), 4.31 (q, *J* = 7.1 Hz, 2H), 5.50 (dd, *J* = 12.1, 8.2 Hz, 1H), 6.49 (dd, *J* = 11.0, 2.2 Hz, 1H), 6.58 (dt, *J* = 15.9, 2.2 Hz, 1H), 7.29-7.36 (m, 5H), 7.47 (dd, *J* = 8.8, 6.6 Hz, 1H), 7.65 (d, *J* = 8.2 Hz, 2H), 7.70 (d, *J* = 8.2 Hz, 2H). MS (70 eV) 413 ($M^+$, 100). EI-HRMS *m/e* calculated for ($M^+$) $C_{25}H_{20}N_3O_2F$ 413.1540, found 413.1551.

**k) 4-[3-(4-Cyano-phenyl)-5-phenyl-4,5-dihydro-pyrazol-1-yl]-2,5-difluoro-benzoic acid ethyl ester (3-2d):** Yield: 48%. $R_f$ 0.33 (4:1 hexane:EtOAc). $^1$H-NMR ($CDCl_3$, 400 MHz) δ 1.34 (t, *J* = 7.1 Hz, 3H), 3.29 (dd, *J* = 17.6, 3.8 Hz, 1H), 3.84 (dd, *J* = 17.6, 12.1 Hz, 1H), 4.31 (q, *J* = 7.1 Hz, 2H), 5.85 (td, *J* = 12.1, 3.8 Hz, 1H), 7.11 (dd, *J* = 8.2, 2.2 Hz, 2H), 7.21-7.26 (m, 3H), 7.43 (dd, *J* = 6.6, 1.7 Hz, 1H), 7.46 (d, *J* = 6.6 Hz, 1H), 7.70 (d, *J* = 8.2 Hz, 2H), 7.84 (d, *J* = 8.2 Hz, 2H). MS (70 eV) 431.1 ($M^+$, 24), 302 (83), 230 (100). EI-HRMS *m/e* calculated for ($M^+$) $C_{25}H_{19}N_3O_2F_2$ 431.1445, found 431.1438.

**l) 4-[3-(4-Cyano-phenyl)-5-phenyl-4,5-dihydro-pyrazol-1-yl]-2,6-difluoro-benzoic acid ethyl ester (3-2e):** Yield: 38%. $R_f$ 0.38 (4:1 hexane:EtOAc). $^1$H-NMR ($CDCl_3$, 400 MHz) δ 1.33 (t, *J* = 7.1 Hz, 3H), 3.17 (dd, *J* = 17.0, 7.1 Hz, 1H), 3.82 (dd, *J* = 17.0, 12.1 Hz, 1H), 4.39 (q, *J* = 7.1 Hz, 2H), 5.39 (dd, *J* = 12.1, 7.1 Hz, 1H), 6.02 (td, *J* = 11.0, 1.7 Hz, 1H), 6.33 (dt, *J* = 9.3, 2.2, 1H), 7.30-7.40 (m, 7H), 7.67 (s, 2H). MS (70 eV) 431.1 ($M^+$, 24), 302 (83), 230 (100). EI-HRMS *m/e* calculated for ($M^+$) $C_{25}H_{19}N_3O_2F_2$ 431.1445, found 431.1438.

**m) 4-[3-(4-Cyano-phenyl)-5-phenyl-4,5-dihydro-pyrazol-1-yl]-2,3,5-trifluoro-benzoic acid ethyl ester (3-2f):**[2] Yield: 7%. $R_f$ 0.31 (5:1 hexane:EtOAc). $^1$H-NMR ($CDCl_3$, 400 MHz) δ 1.35 (t, *J* = 7.1 Hz, 3H), 3.30 (dd, *J* = 17.0, 6.0 Hz, 1H), 3.80 (dd, *J* = 17.0, 12.1 Hz, 1H), 4.33 (q, *J* = 7.1 Hz, 2H), 5.73 (dd, *J* = 12.1, 6.0 Hz, 1H), 7.22-7.26 (m, 6H), 7.34 (ddd, *J* = 11.5, 5.5, 1.7 Hz, 1H), 7.68 (d, *J* = 8.2 Hz, 2H), 7.80 (d, *J* = 8.2 Hz, 2H). MS (70 eV) 449.1 ($M^+$, 100). EI-HRMS m/e calculated for ($M^+$) $C_{24}H_{19}N_2O_2F_3$449.1351, found 449.1361.

**n) 4-[3-(4-Cyano-phenyl)-5-phenyl-4,5-dihydro-pyrazol-1-yl]-2,3,5,6-tetrafluoro-benzoic acid ethyl ester (3-2g):** Yield: 24%. $R_f$ 0.39 (4:1 hexane:EtOAc). $^1$H-NMR ($CDCl_3$, 400 MHz) δ 1.36 (t, *J* = 7.1 Hz, 3H), 3.31 (dd, *J* = 17.6, 6.0 Hz, 1H), 3.81 (dd, *J* = 17.6, 12.1 Hz, 1H), 4.37 (q, *J* = 7.1 Hz, 2H), 5.73 (dd, *J* = 12.1, 6.0 Hz, 1H), 7.22-7.30 (m, 5H), 7.69 (d, *J* = 8.2 Hz, 2H), 7.81 (d, *J* = 8.2 Hz, 2H). MS (70 eV) 467 ($M^+$, 100), 231 (40). EI-HRMS *m/e* calculated for ($M^+$) $C_{25}H_{17}N_3O_2F_4$ 467.1257, found 467.1264.

**o) 1-(2-Fluoro-phenyl)-3,5-diphenyl-4,5-dihydro-1H-pyrazole (3-3a):**[2] Yield: 91%. $R_f$ 0.83 (5:1 hexane:EtOAc). $^1$H-NMR ($CDCl_3$, 400 MHz) δ 3.25 (dd, *J* = 17.0, 4.1 Hz, 1H), 3.74 (dd, *J* = 17.0, 11.5 Hz, 1H), 5.63 (dd, *J* = 11.5, 4.1 Hz, 1H), 6.71-6.76 (m, 1H), 6.83 (dd, *J* = 12.9, 8.2 Hz, 1H), 6.98 (t, *J* = 7.6 Hz, 1H), 7.11-7.20 (m, 5H), 7.29-7.39 (m, 3H), 7.61 (t, *J* = 8.2 Hz, 1H), 7.74 (d, *J* = 7.1 Hz, 2H). MS (70 eV) 316.1 ($M^+$, 100), 239 (50), 109 (65). EI-HRMS *m/e* calculated for ($M^+$) $C_{21}H_{17}N_2F$ 316.1376, found 316.1375.

**p) 1-(3-Fluoro-phenyl)-3,5-diphenyl-4,5-dihydro-1H-pyrazole (3-3b):**[2] Yield: 90%. $R_f$ 0.72 (5:1 hexane:EtOAc). $^1$H-NMR ($CDCl_3$, 400 MHz) δ 3.12 (dd, *J* = 17.0, 6.6

Hz, 1H), 3.80 (dd, *J* = 17.0, 12.1 Hz, 1H), 5.20 (dd, *J* = 12.1, 6.6 Hz, 1H), 6.44 (dt, *J* = 8.2, 2.2 Hz, 1H), 6.69 (dd, *J* = 8.2, 2.2 Hz, 1H), 6.87 (td, *J* = 12.1, 2.2 Hz, 1H), 7.05 (td, *J* = 8.2, 6.6 Hz, 1H), 7.22-7.38 (m, 8H), 7.70 (td, *J* = 7.1, 1.7 Hz, 2H), MS (70 eV) 316.1 ($M^+$, 100), 239 (45), 109 (40). EI-HRMS *m/e* calculated for ($M^+$) $C_{21}H_{17}N_2F$ 316.1376, found 316.1363.

**q) 1-(4-Fluoro-phenyl)-3,5-diphenyl-4,5-dihydro-1H-pyrazole (3-3c):**[2] Yield: 30%. $R_f$ 0.71 (5:1 hexane:EtOAc). $^1$H-NMR ($CDCl_3$, 400 MHz) δ 3.11 (dd, *J* = 17.0, 8.2 Hz, 1H), 3.80 (dd, *J* = 17.0, 12.1 Hz, 1H), 5.16 (dd, *J* = 12.1, 8.2 Hz, 1H), 6.85 (t, *J* = 8.2 Hz, 2H), 6.97-7.00 (m, 2H), 7.25-7.38 (m, 8H), 7.69 (d, *J* = 7.1 Hz, 2H). MS (70 eV) 316.1 ($M^+$, 100), 239.1 (45), 109 (60). EI-HRMS *m/e* calculated for ($M^+$) $C_{21}H_{17}N_2F$ 316.1376, found 316.1359.

**r) 1-(2,4-Difluoro-phenyl)-3,5-diphenyl-4,5-dihydro-1H-pyrazole (3-3d):**[2] Yield: 96%. $R_f$ 0.66 (5:1 hexane:EtOAc). $^1$H-NMR ($CDCl_3$, 400 MHz) δ 3.30 (dd, *J* = 16.5, 4.9 Hz, 1H), 3.75 (dd, *J* = 16.5, 11.5 Hz, 1H), 5.56 (dtd, *J* = 11.5, 4.9, 1.7 Hz, 1H), 6.66 (dt, *J* = 8.8, 2.7 Hz, 1H), 6.75 (ddt, *J* = 10.4, 2.7, 1.1 Hz, 1H), 7.18-7.24 (m, 5H), 7.35-7.44 (m, 3H), 7.50-7.56 (m, 1H), 7.77 (dd, *J* = 8.2, 1.7 Hz, 2H). MS (70 eV) 334 ($M^+$, 100), 257 (42), 127 (70). EI-HRMS *m/e* calculated for ($M^+$) $C_{21}H_{16}N_2F_2$ 334.1282, found 334.1276.

**s) 1-(2,5-Difluoro-phenyl)-3,5-diphenyl-4,5-dihydro-1H-pyrazole (3-3e):**[2] Yield: 80%. $R_f$ 0.45 (3:1 hexane:EtOAc). $^1$H-NMR ($CDCl_3$, 400 MHz) δ 3.27 (dd, *J* = 17.0, *J* = 3.8 Hz, 1H), 3.78 (dd, *J* = 17.0, 11.5 Hz, 1H), 5.69 (td, *J* = 11.5, 3.8 Hz, 1H), 6.36-6.42 (m, 1H), 6.71-6.78 (m, 1H), 7.14-7.23 (m, 4H), 7.33-7.43 (m, 4H), 7.35 (dd, *J*

= 8.2, 1.7 Hz, 2H). MS (70 eV) 334.1 ($M^+$, 100), 127 (40). EI-HRMS *m/e* calculated for ($M^+$) $C_{21}H_{16}N_2F_2$ 334.1282, found 334.1287.

**t) 1-(3,5-Difluoro-phenyl)-3,5-diphenyl-4,5-dihydro-1H-pyrazole (3-3f):**[2] Yield: 79%. $R_f$ 0.68 (5:1 hexane:EtOAc). $^1$H-NMR ($CDCl_3$, 400 MHz) δ 3.13 (dd, *J* = 17.0, 6.6 Hz, 1H), 3.82 (dd, *J* = 17.0, 12.1 Hz, 1H), 5.17 (dd, *J* = 12.1, 6.6 Hz, 1H), 6.17 (tt, *J* = 8.8, 2.2 Hz, 1H), 6.54 (dd, *J* = 9.9, 2.2 Hz, 2H), 7.26 (dt, *J* = 8.8, 1.7 Hz, 3H), 7.31-7.40 (m, 5H), 7.69 (dd, *J* = 8.2, 1.6 Hz, 2H). MS (70 eV) 334.1 ($M^+$, 100), 257.1 (35). EI-HRMS *m/e* calculated for ($M^+$) $C_{21}H_{16}N_2F_2$ 334.1282, found 334.1282.

**u) 3,5-Diphenyl-1-(2,3,5,6-tetrafluoro-phenyl)-4,5-dihydro-1H-pyrazole (3-3h):**[2] Yield: 73%. $R_f$ 0.80 (3:1 hexane:EtOAc). $^1$H-NMR ($CDCl_3$, 400 MHz) δ 3.30 (dd, *J* = 17.0, 7.1 Hz, 1H), 3.76 (dd, *J* = 17.0, 11.5 Hz, 1H), 5.52 (dd, *J* = 11.5, 7.1 Hz, 1H), 6.58-6.66 (m, 1H), 7.20-7.30 (m, 5H), 7.35-7.42 (m, 3H), 7.71 (d, *J* = 8.2, 1.1 Hz, 2H). MS (70 eV) 370.1 ($M^+$, 100), 163 (38). EI-HRMS *m/e* calculated for ($M^+$) $C_{21}H_{14}N_2F_4$ 370.1093, found 370.1105.

**v) 1-Pentafluorophenyl-3,5-diphenyl-4,5-dihydro-1H-pyrazole (3-3g):**[2] Yield: 70%. $R_f$ 0.43 (4:1 hexane:EtOAc). $^1$H-NMR ($CDCl_3$, 400 MHz) δ 3.29 (dd, *J* = 17.0, 8.2 Hz, 1H), 3.73 (dd, *J* = 17.0, 11.5 Hz, 1H), 5.37 (dd, *J* = 11.5, 8.2 Hz, 1H), 7.23-7.31 (m, 5H), 7.37 (d, *J* = 7.1 Hz, 3H), 7.69 (dd, *J* = 8.2, 1.7 Hz, 2H). MS (70 eV) 388.1 ($M^+$, 100), 181 (60). EI-HRMS *m/e* calculated for ($M^+$) $C_{21}H_{13}N_2F_5$ 388.0999, found 388.1015.

**w) 4-(1-(2-fluorophenyl)-4,5-dihydro-5-phenyl-1H-pyrazol-3-yl)benzonitrile (3-4a):** Yield: 80%. $R_f$ 0.40 (3:1 hexane:EtOAc). $^1$H-NMR ($CDCl_3$, 400 MHz) δ 3.27 (dd, *J* = 17.0, 4.9 Hz, 1H), 3.79 (dd, *J* = 17.0, 12.6 Hz, 1H), 5.74 (td, *J* = 12.6, 4.9 Hz, 1H), 6.80-6.91 (m, 2H), 7.03 (dt, *J* = 8.2, 1.7 Hz , 1H), 7.16-7.25 (m, 5H), 7.58 (dt, *J* =

8.2, 1.7 Hz, 1H), 7.66 (d, *J* = 8.2 Hz, 2H), 7.81 (d, *J* = 8.2 Hz, 2H). MS (70 eV) 341.1 ($M^+$, 100), 264.1 (50), 109 (48). EI-HRMS *m/e* calculated for ($M^+$) $C_{22}H_{16}N_3F$ 341.1328, found 341.1338.

**x) 4-[1-(3-Fluoro-phenyl)-5-phenyl-4,5-dihydro-1H-pyrazol-3-yl]-benzonitrile (3-4b):** Yield: 87%. *Rf* 0.40 (3:1 hexane:EtOAc). $^1$H-NMR ($CDCl_3$, 400 MHz) δ 3.15 (dd, *J* = 17.0, 7.1 Hz, 1H), 3.86 (dd, *J* = 17.0, 12.6 Hz, 1H), 5.36 (dd, *J* = 12.6, 6.6 Hz, 1H), 6.51 (dt, *J* = 8.2, 2.2 Hz, 1H), 6.73 (dd, *J* = 8.2, 2.2 Hz, 1H), 6.89 (td, *J* = 11.5, 2.2 Hz, 1H), 7.10 (m, 1H), 7.28-7.31 (m, 3H), 7.36 (t, *J* = 7.1 Hz, 2H), 7.66 (d, *J* = 8.2 Hz, 2H), 7.78 (d, *J* = 8.2 Hz, 2H). MS (70 eV) 341.1 ($M^+$, 100), 264.1 (50), 109 (48). EI-HRMS *m/e* calculated for ($M^+$) $C_{22}H_{16}N_3F$ 341.1328, found 341.1338.

**y) 4-[1-(4-Fluoro-phenyl)-5-phenyl-4,5-dihydro-1H-pyrazol-3-yl]-benzonitrile (3-4c):** Yield: 80%. *Rf* 0.40 (3:1 hexane:EtOAc). $^1$H-NMR ($CDCl_3$, 400 MHz) δ 3.14(dd, *J* = 17.0, *J* = 7.7 Hz, 1H), 3.84 (dd, *J* = 17.0, 12.1 Hz, 1H), 5.33 (dd, *J* = 12.1, 7.7 Hz, 1H), 6.89 (t, *J* = 8.8 Hz, 2H), 7.27-7.38 (m, 5H), 7.64 (d, *J* = 8.8 Hz, 2H), 7.76 (d, *J* = 8.2 Hz, 2H). MS (70 eV) 341.1 ($M^+$, 100), 264.1 (50), 109 (48). EI-HRMS *m/e* calculated for ($M^+$) $C_{22}H_{16}N_3F$ 341.1328, found 341.1338.

**z) 4-[1-(2,4-Difluoro-phenyl)-5-phenyl-4,5-dihydro-1H-pyrazol-3-yl]-benzonitrile (3-4d):** Yield: 76%. *Rf* 0.44 (3:1 hexane:EtOAc). $^1$H-NMR ($CDCl_3$, 400 MHz) δ 3.29 (dd, *J* = 17.0, 5.5 Hz, 1H), 3.77 (dd, *J* = 17.0, 12.1 Hz, 1H), 5.63 (ddd, *J* = 12.1, 5.5, 3.3 Hz, 1H), 6.67 (ddd, *J* = 12.1, 8.2, 2.7 Hz, 1H), 6.76 (ddt, *J* = 7.7, 2.7, 1.7 Hz, 1H), 7.15-7.24 (m, 4H), 7.45-7.51 (m, 1H), 7.67 (d, *J* = 8.8 Hz, 2H), 7.80 (d, *J* = 8.8 Hz, 2H). MS (70 eV) 359.1 ($M^+$, 100), 282 (40), 127 (50). EI-HRMS *m/e* calculated for ($M^+$) $C_{22}H_{15}N_3F_2$ 359.1234, found 359.1189.

**aa) 4-[1-(2,5-Difluoro-phenyl)-5-phenyl-4,5-dihydro-1H-pyrazol-3-yl]-benzonitrile (3-4e):** Yield: 87%. $R_f$ 0.45 (3:1 hexane:EtOAc). $^1$H-NMR ($CDCl_3$, 400 MHz) δ 3.26 (dd, *J* = 17.0, 3.8 Hz, 1H), 3.80 (dd, *J* = 17.0, 12.1 Hz, 1H), 5.77 (td, *J* = 12.1, 3.8 Hz, 1H), 6.44-6.50 (m, 1H), 6.77-6.83 (m, 1H), 7.14 (dd, *J* = 8.2, 2.2 Hz, 2H), 7.21-7.25 (m, 3H), 7.34-7.39 (m, 1H), 7.68 (d, *J* = 8.8 Hz, 2H), 7.81 (d, *J* = 8.2 Hz, 2H). MS (70 eV) 359.1 ($M^+$, 100), 282 (40), 127 (50). EI-HRMS *m/e* calculated for ($M^+$) $C_{22}H_{15}N_3F_2$ 359.1234, found 359.1189.

**bb) 4-[1-(3,5-Difluoro-phenyl)-5-phenyl-4,5-dihydro-1H-pyrazol-3-yl]-benzonitrile (3-4f):** Yield: 76%. $R_f$ 0.45 (3:1 hexane:EtOAc). $^1$H-NMR ($CDCl_3$, 400 MHz) δ 3.16 (dd, *J* = 17.6, 6.6 Hz, 1H), 3.87 (dd, *J* = 17.6, 12.6 Hz, 1H), 5.32 (dd, *J* = 12.6, 6.6 Hz, 1H), 6.25 (tt, *J* = 8.8, 2.2 Hz, 1H), 6.56 (dd, *J* = 9.9, 2.2 Hz, 2H), 7.24-7.39 (m, 4H), 7.67 (d, *J* = 8.8 Hz, 2H), 7.79 (d, *J* = 8.8 Hz, 2H). MS (70 eV) 359.1 ($M^+$, 100), 282 (40), 127 (50). EI-HRMS *m/e* calculated for ($M^+$) $C_{22}H_{16}N_3F$ 359.1234, found 359.1189.

**cc) 4-[5-Phenyl-1-(2,3,5,6-tetrafluoro-phenyl)-4,5-dihydro-1H-pyrazol-3-yl]-benzonitrile (3-4h):** Yield: 70%. $R_f$ 0.53 (3:1 hexane:EtOAc). $^1$H-NMR ($CDCl_3$, 400 MHz) δ 3.31 (dd, *J* = 17.0, *J* = 7.1 Hz, 1H), 3.78 (dd, *J* = 17.0, 12.1 Hz, 1H), 5.60 (dd, *J* = 12.1, 7.1 Hz, 1H), 6.67-6.75 (m, 1H), 7.28-7.29 (m, 5H), 7.68 (d, *J* = 8.2 Hz, 2H), 7.79 (d, *J* = 8.8 Hz, 2H). MS (70 eV) 395.1 ($M^+$, 100), 231 (45), 163 (55). EI-HRMS *m/e* calculated for ($M^+$) $C_{22}H_{13}N_3F_4$ 395.1046, found 395.1069.

**dd) 4-(1-Pentafluorophenyl-5-phenyl-4,5-dihydro-1H-pyrazol-3-yl)-benzonitrile (3-4g)**: Yield: 70%. $R_f$ 0.53 (3:1 hexane:EtOAc). $^1$H-NMR ($CDCl_3$, 400 MHz) δ 3.31 (dd, *J* = 17.0, 7.1 Hz, 1H), 3.78 (dd, *J* = 17.0, 12.1 Hz, 1H), 5.60 (dd, *J* =

12.1, 7.1 Hz, 1H), 6.67-6.75 (m, 1H), 7.28-7.29 (m, 5H), 7.68 (d, *J* = 8.2 Hz, 2H), 7.79 (d, *J* = 8.8 Hz, 2H). MS (70 eV) 395.1 ($M^+$, 100), 231 (45), 163 (55). EI-HRMS *m/e* calculated for ($M^+$) $C_{22}H_{13}N_3F_4$ 395.1046, found 395.1069.

## 3.4. References


1. de Melo, J.; Becker, R.; Macanita, A., *J. Phys. Chem.* **1994,** 98, (24), 6054.
2. Cody, J. Experimental data.

# CHAPTER IV

# SYNTHESIS AND THERMODYNAMIC CHARACTERIZATION OF SELECTED THIOETHER LIGANDS

## 4.1. Introduction

For the design of a copper selective fluorescence probe, the cation receptor moiety plays a critical role. The following list summarizes the most important points that must be considered for the optimization of the receptor unit:

***1) Binding Affinity.*** Because Cu(I) is believed to be coordinated to a yet unknown endogenous ligand in the cellular environment, the receptor unit of the fluorescence probe must be able to effectively compete for copper binding

***2) Exchange Kinetics.*** The kinetics of the copper exchange reaction between receptor and endogenous ligand must be fast to provide accurate visualization of the intracellular copper distribution.

***3) Selectivity.*** The receptor moiety should exhibit a high copper selectivity and should effectively discriminate towards other biologically relevant cations, in particular calcium, magnesium, and zinc.

***4) Redox Properties.*** Because kinetically labile, cellular copper is believed to be present in its monovalent oxidation state, the receptor moiety should effectively stabilize Cu(I) towards oxidation or disproportionation reactions. Furthermore, the fluorescence enhancement factor upon binding of Cu(I) is directly related to the decrease of the driving force ($-\Delta G_{ET}$) of the photoinduced electron transfer quenching process. As outlined in Section 2.1.3, Chapter 2, the change in donor oxidation potential is the sole parameter that is affected by metal binding (Rehm-Weller formalism, equation 2.1). Conclusively, optimization of the difference between the oxidation potential of free vs

Cu(I)-bound ligand is one of the most critical challenges to guarantee a bright fluorescence enhancement upon Cu(I) binding.

### *4.1.1. Coordination Chemistry of Monovalent Copper*

The thermodynamic stabilization of Cu(I) is best achieved by choosing a ligand that effectively *destabilizes Cu(II).* As a $d^9$ system, Cu(II) prefers to adopt a six-coordinate octahedral or four-coordinate square planar geometry, both of which provide substantial ligand field stabilization energies. In contrast, Cu(I) has a completely filled d-shell, and therefore, electronic stabilization effects are absent. The coordination geometry is primarily governed by electrostatic and steric interactions, rendering tetrahedral or trigonal planar geometries the most favorable. In order to stabilize Cu(I) over Cu(II), a ligand must provide a tetrahedral geometry instead of octahedral geometry.

Polythioether ligands have been extensively studied by Ochrymowycz and Rorabacher.[1,2] Their studies showed that polythioether ligands are very selective for coordination of a small group of metal cations, in particular Cu(II), Cu(I), Pd(II), Ag(I), Pt(II), Au(I), and Hg(II), also referred to as the "Copper Triangle". Among this set of cations, copper is the only biologically important element. Hence, polythioether derivatives are ideal ligand candidates for the detection of Cu(I) in a cellular environment, and should effectively prevent interference of other more abundant cations, such as Ca(II), Mg(II), or Zn(II).

Figure 4-1 shows the molecular structures and thermodynamic data for selected copper ligands that have been previously characterized.[3] Macrocyclic polythioether ligands with three to five sulfur donor atoms exhibit impressive affinities for Cu(I), with stability constants ranging from log$K$=10 to greater than 15.[3,4] In general, a sulfur-rich

coordination environment stabilizes Cu(I), whereas the presence of nitrogen donor atoms favors the Cu(II) redox state.[5,6] This phenomenon might be due to the greater stability of the Cu(II)-N bond compared to Cu(I)-N. Furthermore, tripodal ligands show greater affinities toward Cu(I) compared to macrocyclic ligands with the same set of donor atoms, since tripodal ligands are more flexible to provide a tetrahedron coordination geometry.[3]

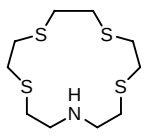
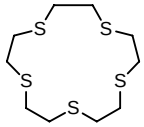
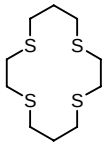

| | [15]aneNS$_4$ | [15]aneS$_5$ | [14]aneS$_4$ |
|---|---|---|---|
| log $K_{Cu(II)}$ | 9.8 | 4.2 | 4.3 |
| log $K_{Cu(I)}$ | 15.6 | 13.6 | 12.0 |
| $E^o$[V] | 0.46 | 0.68 | 0.58 |

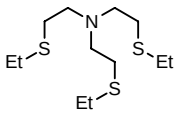
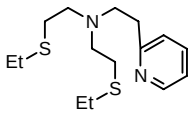
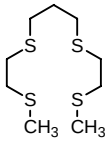

| | TEMEA | PMAS | Me$_2$-3,2,3-S$_4$ |
|---|---|---|---|
| log $K_{Cu(II)}$ | 6.4 | 10.5 | 1.2 |
| log $K_{Cu(I)}$ | 15.5 | 15.0 | 13.0 |
| $E^o$[V] | 0.67 | 0.40 | 0.83 |

**Figure 4-1.** Structures and thermodynamic data for selected copper ligands.[3]

### *4.1.2. Binding Affinity and Redox Stability*

There are a number of well-established techniques available to measure stability constants of metal ion chelators, including potentiometry,[4,7,8] spectrophotometry,[2,9,10] calorimetry,[11] or mass spectroscopy. However, the determination of stability constants of Cu(I) complexes in aqueous solution is often very challenging. Firstly, the hydrated Cu(I) (aqua) complex is unstable towards disproportionation, even at relatively low concentrations in the micro- to nanomolar range.[12] At the same time, the signal-to-noise ratio of standard analytical methods, such as potentiometry, UV-vis spectrometry, or calorimetry, is typically too small for reliable measurements at submicromolar concentrations. The second problem lies in the fact that the receptor ligand inherently must have a very high binding affinity for Cu(I) ($\log K > 10$) to sufficiently stabilize the cation towards disproportionation, and to effectively compete with the endogenous cellular chelator for Cu(I) binding. With such a high affinity, simple ligand-metal titration curves will yield a straight line at micromolar ligand concentrations, because almost all of the added Cu(I) is being bound to the ligand. However, above 80% fractional saturation of the ligand with the metal cation, the error for extracting the stability constant from a simple titration curve is exponentially increasing, thus rendering such data useless for deduction of the corresponding binding constants. An elegant solution to this problem is provided by taking advantage of the thermodynamic cycle outlined in Figure 4-2. Because the ligand is expected to effectively stabilize Cu(I), the stability constant $K_{Cu(II)}$ is substantially smaller compared to $K_{Cu(I)}$ and can be measured with standard methods. The Cu(I) stability constant can then be estimated on basis of the LCu(I/II) redox potential using Nernst's equation (4.1):

$$E_{Cu(II/I)L} = E_{aq}{}^{0} - \frac{RT}{F} \ln \frac{K_{Cu(II)L}}{K_{Cu(I)L}} \qquad (4.1)$$

where $E_{aq}{}^{0}$ = 0.37 V, $R$ = universal gas constant, $F$ = Faraday constant, T = temperature, $K_{Cu(II)L}$ = stability constant of Cu(II)L and $K_{Cu(I)L}$ = stability constant of Cu(I)L.

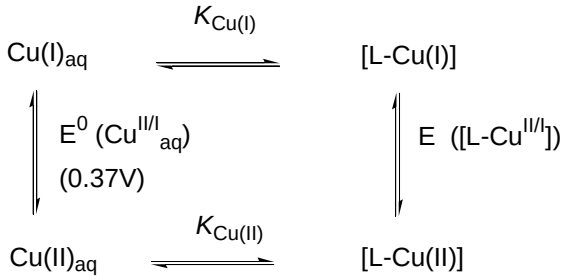


**Figure 4-2.** The thermodynamic cycle of Cu(I) and Cu(II) between aqua and certain ligand L complex.

For the determination of Cu(I) stability constants Zuberbuehler and coworkers have developed a kinetic method that is based on scavenging Cu(I) by dioxygen, a process that can be electrochemically monitored using an oxygen-sensitive electrode.[13,14] Similarly, a cobalt(III) complex was used as redox reporter for copper(I). In this case, the rate of disappearance of the cobalt(III) complex was spectrophotometrically monitored in visible or near-ultraviolet spectral region.[15]

### *4.1.3. Exchange Kinetics*

Numerous studies have been reported on the mechanism and kinetics of Cu(II) ligand binding and dissociation reactions. For example, Rorabacher and coworkers studied the kinetics for formation of copper(II) complexes in great detail using stopped-flow spectrophotometry data.[6,16,17] In contrast, literature reports on the kinetics of complex formation or metal-ligand exchange with monovalent copper are sparse. Among the few reported studies, the ligand exchange rate between free glutathione (GSH) and the corresponding Cu(I) complex was determined to be 13 $s^{-1}$ in aqueous solution by 2D rotation-frame overhauser effect spectroscopy (ROESY).[18]

Because Cu(I) is diamagnetic, dynamic NMR methods (DNMR) are particularly attractive to study the kinetics of metal or ligand exchange reactions with this cation. DNMR can provide information about the kinetics of chemical exchange processes due to the fact that the chemical shift and coupling constants of proton nuclei vary as a function of metal coordination. Depending on the rate of the exchange process compared to the NMR time scale, the spectrum shows either separate signals for the free and metal bound ligand (slow exchange limit), a single set of signals with averaged chemical shifts (fast exchange limit), or strongly broadened signals from which the exchange rate can be extracted on basis of the Bloch equations. If the exchange rates are measured at a set of different temperatures, the activation enthalpy and entropy for the exchange process can be estimated using the Eyring equation (4.2):

$$-R\ln\left(\frac{k_{obs}h}{k_B T}\right) = \frac{\Delta H^{\neq}}{T} - \Delta S^{\neq} \qquad (4.2)$$

where R stands for universal gas constant, $h$ is Plank constant , $k_B$ is Boltzmann constant, $k_{obs}$ is exchange rate at temperature T, $\Delta H^{\neq}$ is activation enthalpy ($kJmol^{-1}$), $\Delta S^{\neq}$ is activation entropy ($Jmol^{-1}K^{-1}$).

The NMR timescale is such that first-order or pseudo-first-order rate constants in the range from $10^5$ $s^{-1}$ to $10^{-1}$ $s^{-1}$ (10 μs to 10 s lifetime) with associated activation energies in the range from 20 to 100 $kJmol^{-1}$ can be measured. DNMR has been widely applied to study the kinetics of ligand or metal exchange reactions of alkaline and earthalkaline complexes.[19-24] For example, A. Popov and M. Shamsipur used Cs-133 DNMR to study the Cs(I) complexation mechanism and kinetics for various crown ethers,[25,26] including dibenzo-21-crown-7 (DB21C7), dibenzo-24-crown-8 (DB24C8), and dibenzo-30-crown-10.[20,21]

### *4.1.4. Experimental Design*

As described in Section 4.1.1, ligand **TEMEA** has a very high binding affinity for Cu(I) ($\log K_{Cu(I)}$ = 15.5) over Cu(II) ($\log K_{Cu(II)}$ = 6.4), Figure 4-1. Oxidation potential for **TEMEA** is 0.67 V. Aliphatic donor atoms usually have a higher oxidation potential compared to aromatic donor atoms, therefore a benzene ring is used to link the tripodal ligand with pyrazoline moiety. Tripodal **I** is the **TEMEA** analogue with aromatic ring, show in Figure 4-3. The nitrogen atom is conjugated with aromatic ring and the oxidation potential should be smaller.

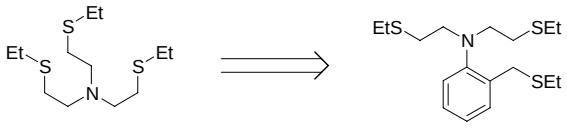


**TEMEA** **I**

**Figure 4-3.** The design of a tripodal ligand **I** based on **TEMEA**.

Using the same idea, thiaza crown ether ligand **II** is designed based on the **[15]aneNS$_4$** (Figure 4-4), which has stability constant log $K_{Cu(I)}$ = 15.6 and log $K_{Cu(II)}$ = 9.8.

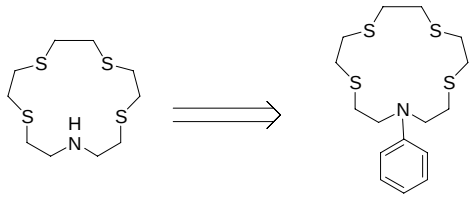


**[15]aneNS$_4$** **II**

**Figure 4-4.** The design of a tripodal ligand **II** based on **[15]aneNS$_4$**.

Using above rational, the tripodal aniline ligand **4-1** was synthesized and characterized, as well as the thiaza crownether ligands **4-2** to **4-6** containing one nitrogen and three or four sulfur donor atoms (Figure 4-5). Variations in ring size are expected to substantially influence the binding affinity for Cu(I) vs Cu(II) and thus yield a range of different redox potentials as described above (Section 4.1.2).

The binding affinity of selective ligands **4-1** to **4-3** was measured by 1H NMR titration. Kinetics of Cu(I) ligand self exchange was studied by dynamic NMR.

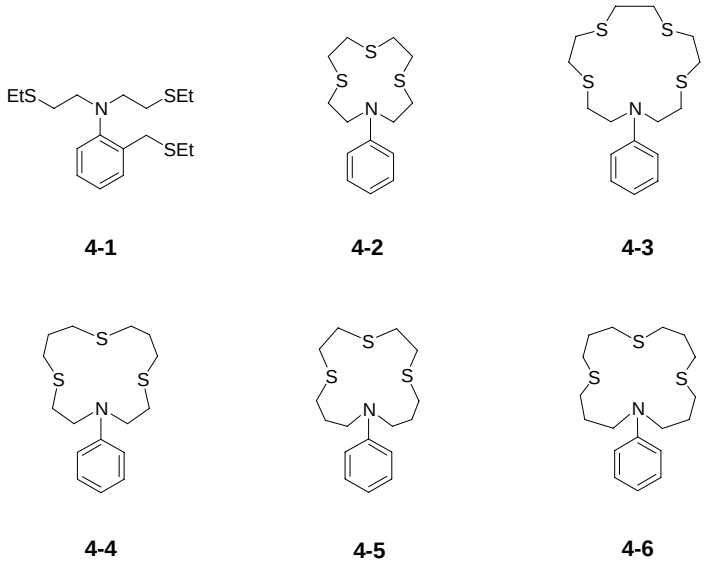


**Figure 4-5.** Molecular structures of the synthesized ligands **4-1** to **4-6**.

## 4.2. Ligand Synthesis

### *4.2.1. Tripodal Aniline Ligand*

The tripodal ligand **4-1** was synthesized in three steps as outlined in Figure 4-6. Commercially available 2-hydroxymethylaniline **4-7** was reacted with ethylene oxide under acidic conditions to provide N,N-bis(2-hydroxyethyl)-2-hydroxy-methyl-aniline in 89% yield.[27] Hydroxyl groups were converted to chloride by refluxing with thionyl

chloride in chloroform. Finally, nucleophilic substitution of the three alkylchoride moieties with ethanethiol under basic conditions provided the desired ligand **4-1** with 90% yield.

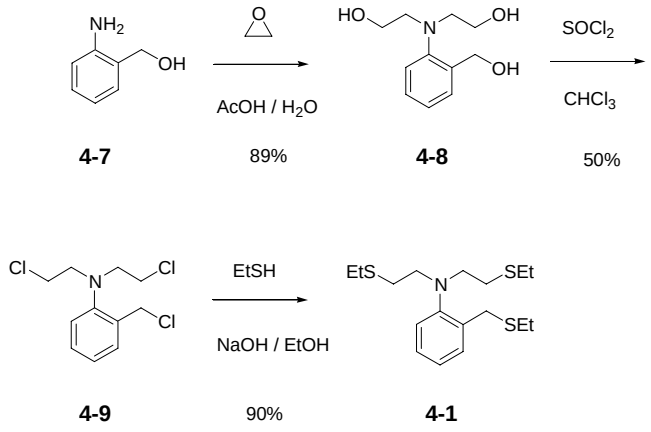


**Figure 4-6.** Synthesis of ligand **4-1**.

### *4.2.2. Thiazacrownether Ligands*

In general, thiazacrownether ligands **4-2** to **4-6** were prepared by the corresponding cyclization reaction following the method developed by J. Ishikawa *et al*.[28] Details for the synthesis of the various derivatives are shown in Figure 4-7 and 4-8.

To obtain a suitable leaving group for nucleophilic substitution with the corresponding dithiols, the hydroxy functionality of commercially available 2-[(2-hydroxy-ethyl)-phenyl-amino]-ethanol **4-10** was converted to the diiodo derivative **4-12** via tosylate intermediate **4-11** in 88% overall yield (Figure 4-7). To minimize oligomer formation the ring closing reaction was carried out in high dilution using cesium carbonate as base, which might provide some degree of templating for formation of the

macrocycle. With this method ligands **4-2** and **4-3** were both obtained in satisfactory yield, while the ring closing reaction for formation of **4-4** occurred only with 25% yield. Probably, cesium ion is not a good template for the thiol **4-15** with three carbons between the sulfur and thus ring closure is not efficient. TLC plate indicated a significant amount of byproducts produced. NMR spectrum is not clean to identify the structure of the byproducts. This phenomenon also happens with the synthesis of another sensor **4-6**, which also used **4-15** as precursor (Figure 4-8).

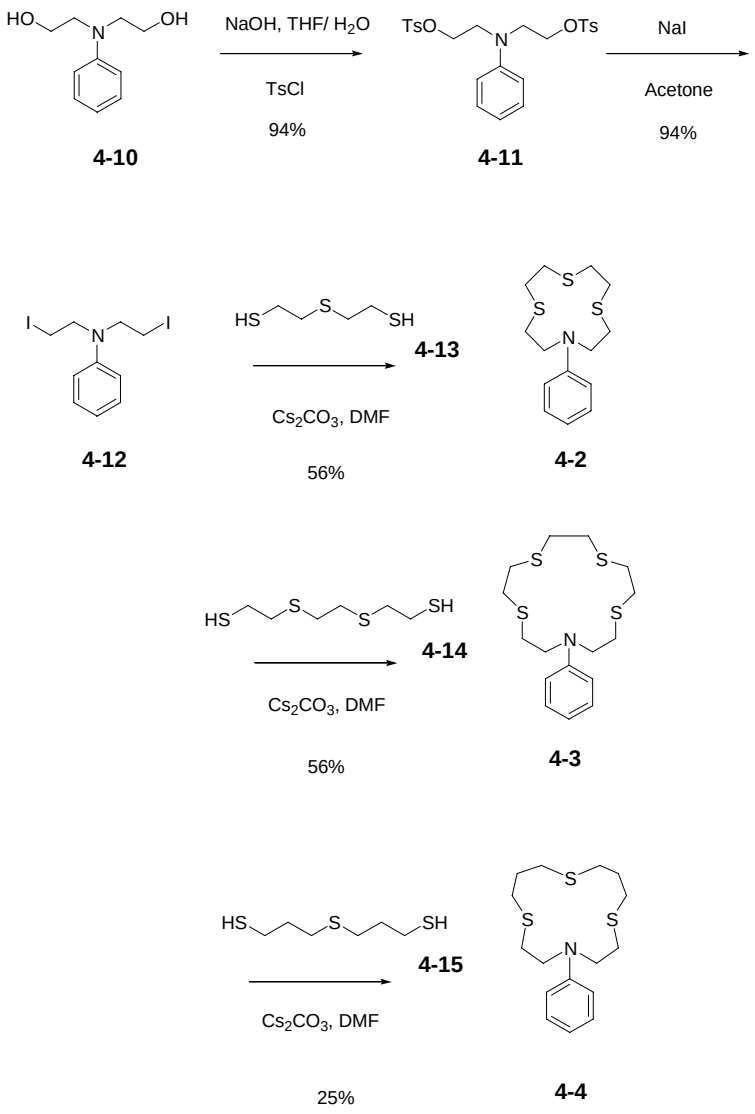


**Figure 4-7.** Synthesis of thiazacrownether ligands **4-2** to **4-4**.

While 2-(2-mercapto-ethylsulfanyl)-ethanethiol **4-13** is commercially available, the dithiols 2-[2-(2-mercapto-ethylsulfanyl)-ethylsulfanyl]-ethanethiol **4-14** and 3-(3-mercapto-propylsulfanyl)-propane-1-thiol **4-15** were prepared via nucelophilic substitution from the corresponding diols **4-16** and **4-17** with thiourea followed by hydrolysis under strong basic conditions (Figure 4-8).

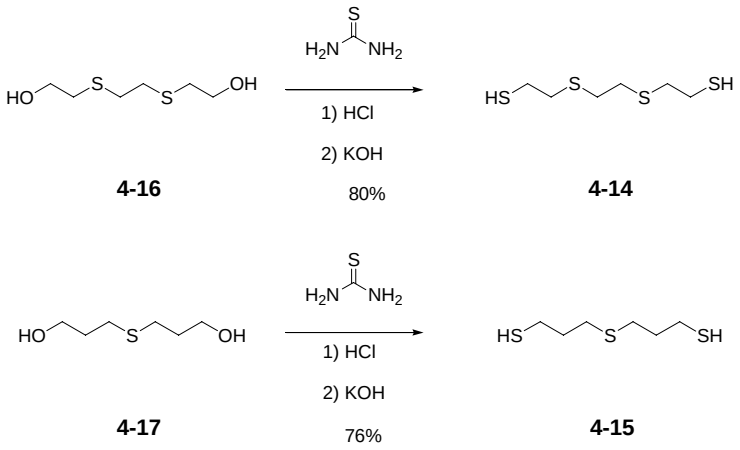


**Figure 4-8.** Synthesis of dithiols **4-14** and **4-15**.

For the synthesis of ligand **4-5** and **4-6**, the corresponding dithiols were reacted with bis(chloropropyl)aniline **4-21** as outlined in Figure 4-9. The latter was obtained from commercially available aniline **4-18** via nucleophilic substitution with 3-chloropropanol **4-19**[29] followed by reaction with thionyl chloride.

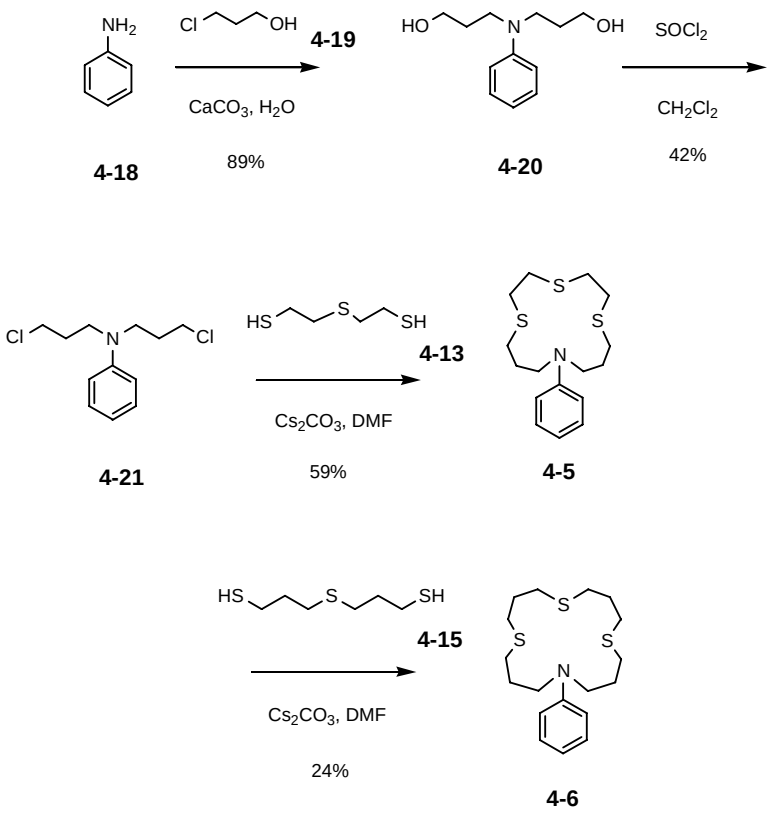


**Figure 4-9.** Synthesis of thiazacrown ether ligands **4-5** and **4-6**.

All ligands were obtained in analytical pure form, either by flash chromatography purification or in case of ligands **4-1**, **4-2** and **4-3** by reversed phase HPLC. All chemical structures of the synthesized compounds, including all intermediates, were confirmed by $^{1}$H NMR, MS and high resolution mass spectrometry (HRMS). A description of all syntheses and detailed analytical data are provided in the experimental section.

## 4.3. Evaluation of Cu(I) Binding Stoichiometries

### *4.3.1. Proton NMR Studies*

To investigate the Cu(I) coordination mode and binding stoichiometries of ligands **4-1** to **4-3**, a series of $^{1}$H NMR titrations were performed in deuterated acetonitrile at 298 K.

***Tripodal Ligand 4-1.*** As shown in Figure 4-11, the $^{1}$H NMR spectra for titration of ligand **4-1** with tetrakis(acetonitrile)copper(I) hexafluorophospahte in acetonitrile exhibit a single set of well-resolved resonances throughout the entire titration range, suggesting a fast dynamic exchange equilibrium with regard to the NMR time scale according to equation (4.3):

$$L^{*} + ML \rightleftharpoons L + ML^{*} \qquad (4.3)$$

Interestingly, an analogous titration in $D_4$-methanol revealed a single set of *broadened* resonance signals, indicating a significantly slower exchange kinetics (see Section 4.4). A molratio plot for the chemical shifts of individual proton resonances reveals an essentially linear slope up to an equimolar amount of Cu(I), being consistent with a high degree of fractional saturation and thus at least submicromolar binding affinity. Further addition of Cu(I) has no effect on the chemical shift, suggesting formation of a complex with 1:1 metal-ligand stoichiometry.

In acetonitrile, the resonance signals for the protons $H^{a}$, $H^{b}$, and $H^{c}$ shift gradually downfield, whereas the $H^{d}$ resonance shifts in the reverse direction upon addition of

Cu(I). Interestingly, the chemical shift for the aliphatic proton next to the aniline nitrogen remains essentially unaffected by addition of Cu(I), moving only by a small amount from 3.21 to 3.23 (Figure 4-12). Apparently, Cu(I) interacts primarily with the three sulfur atoms, but only weakly with the aniline nitrogen. It is possible, that the fourth coordination site is occupied by acetonitrile, which is not only present in high concentration as solvent molecule but represents also an excellent ligand for Cu(I) coordination. This conclusion is further supported by the fact that the analogous titration in $D_4$-methanol revealed a substantially larger shift from 3.20 to 3.46 for the same proton. In this solvent, the aniline nitrogen is apparently involved in coordination to Cu(I), while the solvent molecule is not interacting in the first coordination sphere of the complex.


**Figure 4-10.** Proposed coordination mode of the tripodal ligand **4-1** with $Cu(CH_3CN)_4PF_6$ in $CD_3CN$ (left) and $CD_3OD$ (right).

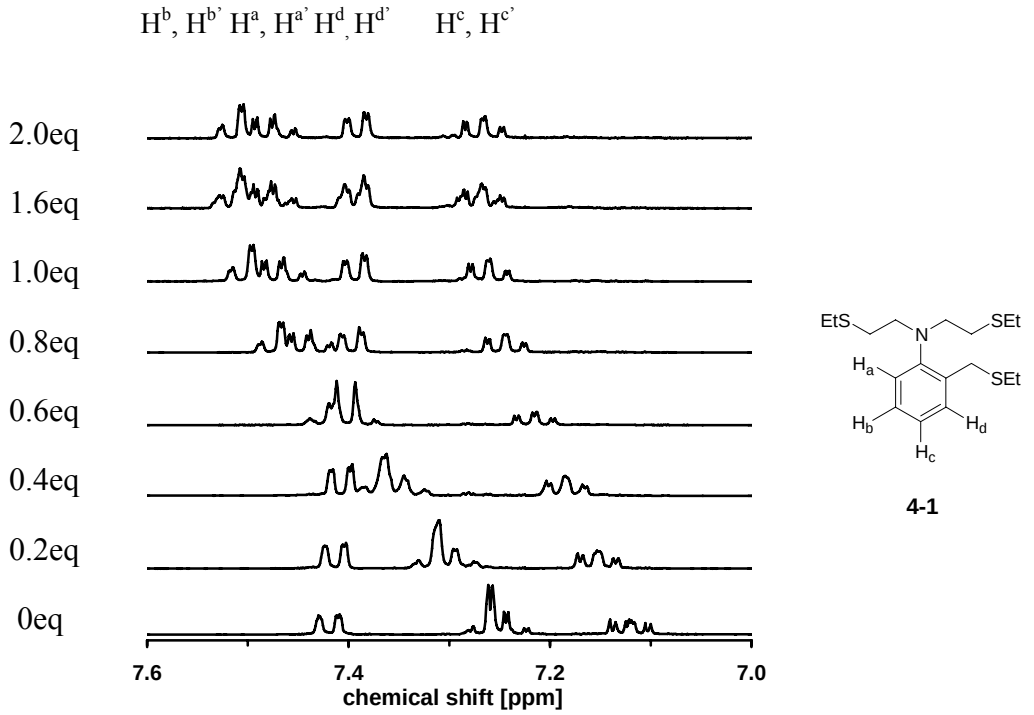


**Figure 4-11.** Aromatic proton resonances for $^1$H NMR titration of ligand **4-1** (9.3 mM) with $Cu(CH_3CN)_4PF_6$ (0.16 M stock solution in $CD_3CN$) in $CD_3CN$ at room temperature.

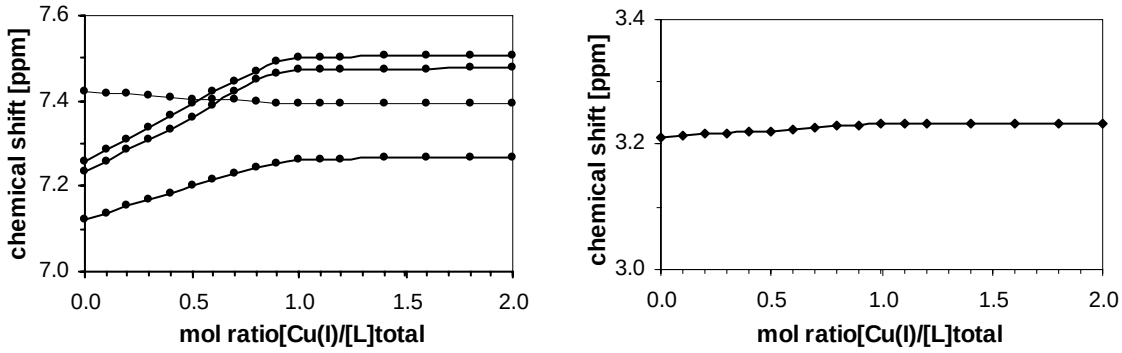


**Figure 4-12.** Variation of the $^1$H chemical shift of ligand **4-1** (9.3 mM) aromatic proton as a function of $Cu^+$/ligand mol-ratio in $CD_3CN$. Left: chemical shift change of the aromatic ring protons. Right: chemical shift change of methylene protons next to the aniline nitrogen.

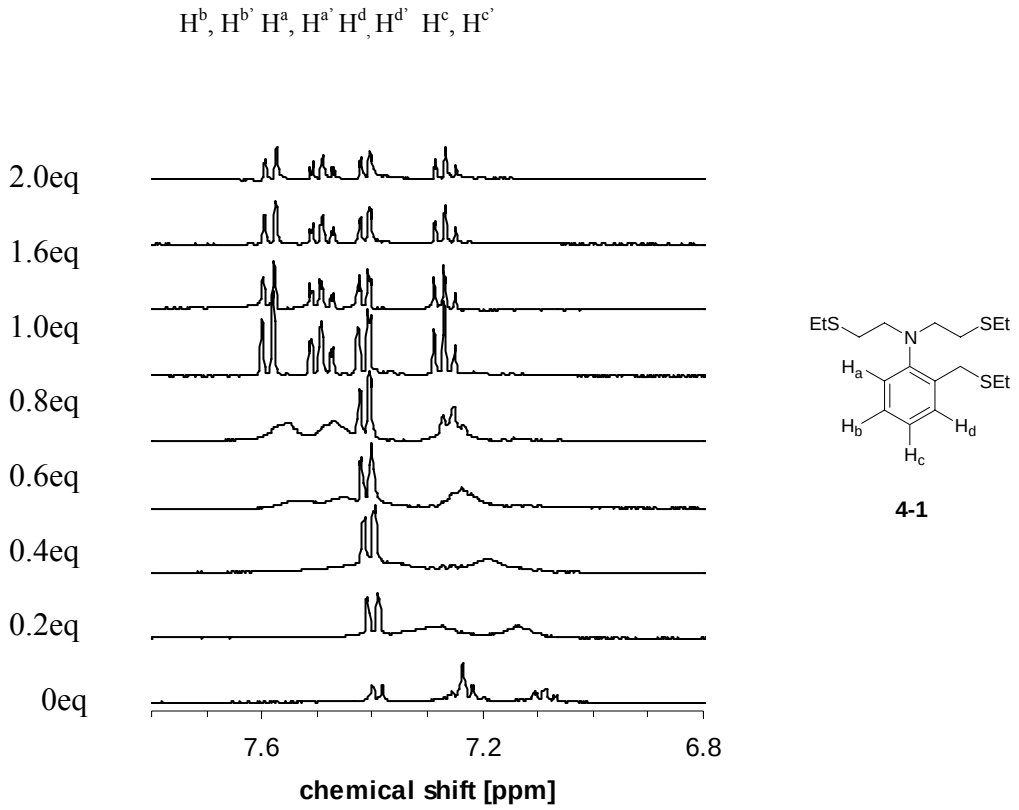


**Figure 4-13.** Aromatic proton resonances for $^1$H NMR titration of ligand **4-1** (9.0 mM) with $Cu(CH_3CN)_4PF_6$ (0.16 M stock solution in $CD_3CN$) in $CD_3OD$ at room temperature.

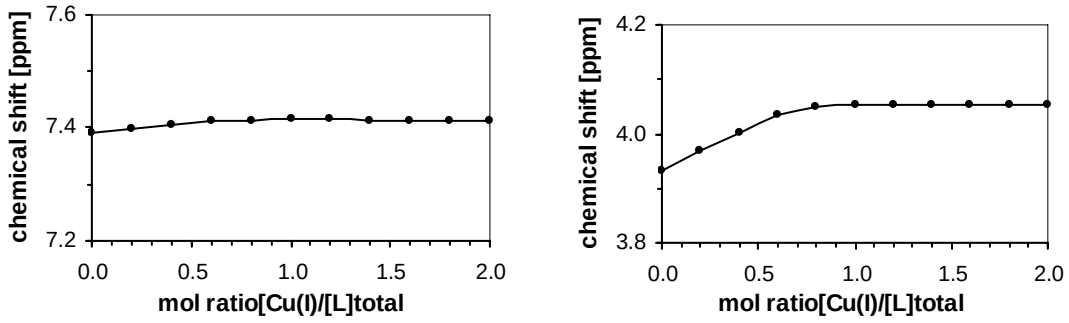


**Figure 4-14.** Variation of the $^1$H chemical shift of ligand **4-1** aromatic proton as a function of $Cu^+$/ligand mol-ratio in $CD_3OD$. Total ligand concentration: 9.0 mM. Left: chemical shift change of the aromatic ring proton $H^d$. Right: chemical shift change of the methylene proton next to the aromatic ring.

***Thiazacrown Ether Ligands.*** The $^1$H NMR titration for ligand **4-2** with Cu(I) in $CD_3CN$ is shown in Figure 4-15. As already observed with tripodal ligand **4-1**, all proton resonances move linearly until one molar equivalent Cu(I) has been added, suggesting again strong binding as well as a 1:1 metal-ligand complex stoichiometry. However, in contrast to the titration of ligand **4-1**, the proton signals are broadened, suggesting a significantly slower exchange rate in acetonitrile at room temperature. Presumably due to the increased rigidity of the crownether ring compared to the more flexible tripodal framework, conformational changes that are required for the metal exchange reaction are energetically less favorable. As a consequence, the activation barrier for Cu(I) exchange is significantly higher for the crownether compared to the tripodal ligand.

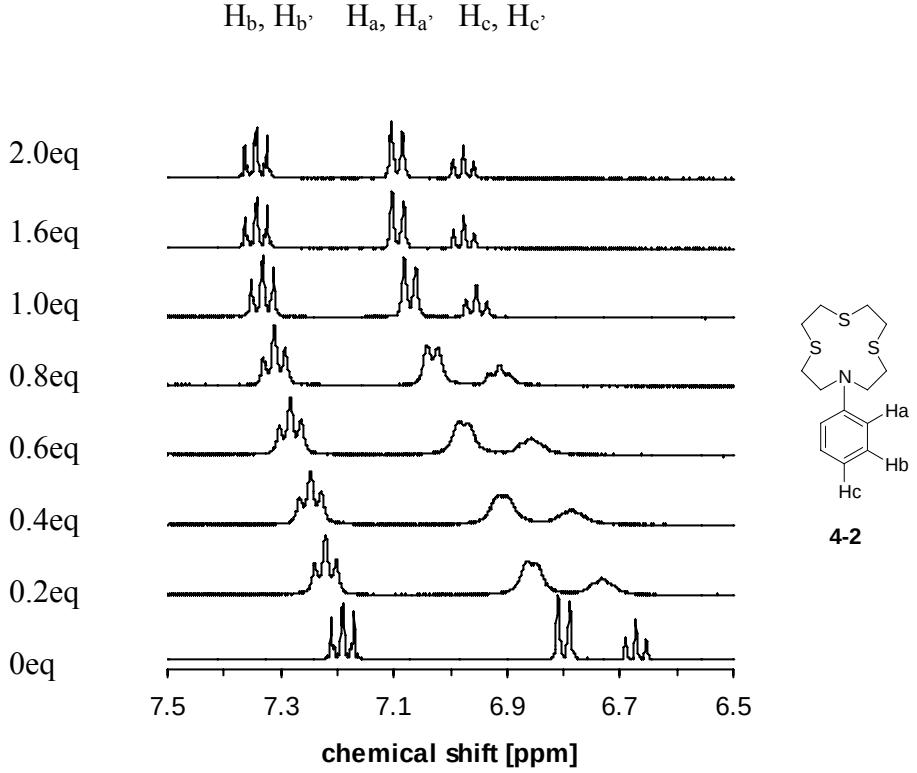


**Figure 4-15.** $^1$H NMR titration of ligand **4-2** (11.8 mM) with $Cu(CH_3CN)_4PF_6$ (83 mM stock solution in $CD_3CN$) in $CD_3CN$.

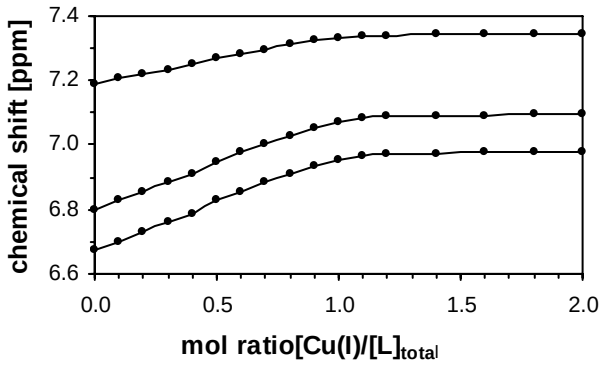


**Figure 4-16.** Variation of the $^1$H chemical shift of ligand **4-2** as a function of $Cu^+$/ligand mol-ratio**.**

The $^1$H NMR titration for ligand **4-3** revealed also a single set of well-resolved, sharp proton resonances, consistent with a fast exchange kinetics with regard to the NMR timescale (Figure 4-17). With increasing Cu(I) concentration the ring proton resonances for $H^a$, $H^b$, and $H^c$ gradually underwent a downfield shift.

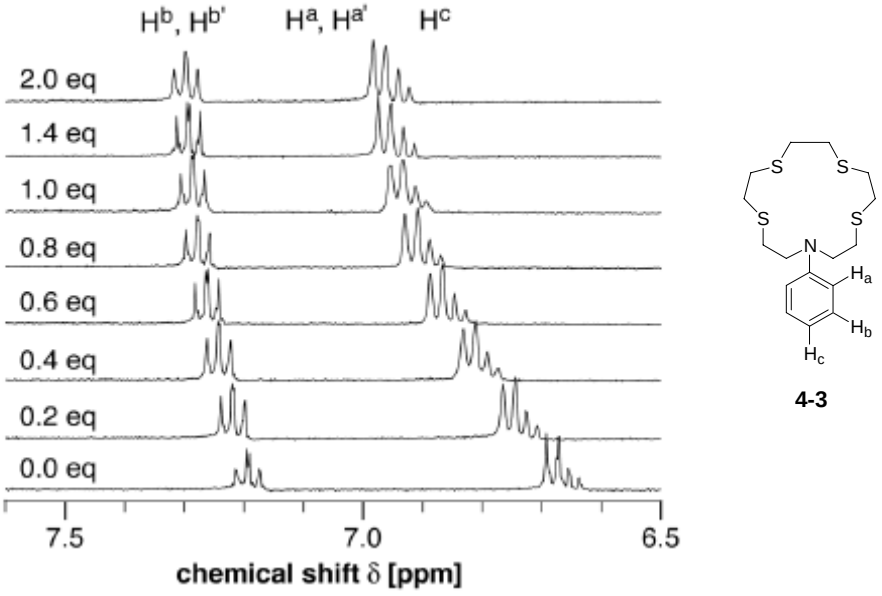


**Figure 4-17.** $^1$H NMR titration of ligand **4-3** (10 mM) with $Cu(CH_3CN)_4PF_6$ (0.1 M in $CD_3CN$) in $CD_3CN$ at 298K.

Molratio plots of the chemical shift changes for selected protons show again an almost linear response up to 0.8 molar equivalent of Cu(I) (Figure 4-18), suggesting a fractional saturation (ratio between the complex concentration and total metal concentration) near unity at each titration point. As previously outlined in Section 4.1.2, data with fractional saturation of greater than 80% are inevitably associated with a significant error, therefore, the NMR titration experiment is not suitable to provide a quantitatively *accurate* stability constant. Nevertheless, because this ligand has been extensively used as receptor moiety for biological studies (see Section 5.4, Chapter 5), the titration data were used to extract at least an *approximate* stability constant on the basis of the following treatment:

At the fast exchange limit the observed chemical shift $\delta_{obs}$ for a set of exchanging protons of free ligand L and complexed ligand ML is given by

$$\delta_{obs} = \chi_L \delta_L + \chi_{ML} \delta_{ML} \tag{4.4}$$

where $\delta_L$ and $\delta_{ML}$ refer to the chemical shifts of free and complexed ligand, respectively, and $\chi_L$ and $\chi_{ML}$ are the corresponding molfractions of exchangeable protons. With an equal number of exchangeable protons of the two species, the mol-fractions can be defined on basis of the corresponding concentrations [L] (= free ligand), [ML] (= complexed ligand), and $[L]_{tot}$ (total ligand concentration).

$$\chi_L = \frac{[L]}{[L]_{tot}} \quad \text{and} \quad \chi_{ML} = \frac{[ML]}{[L]_{tot}} \tag{4.5}$$

Finally, assuming a complex equilibrium with 1:1 stoichiometry the stability constant $K$ is given by

$$K = \frac{[ML]}{[L][M]} \quad \text{with} \tag{4.6}$$

$$[L] = [L]_{tot} - [ML] \quad \text{and} \tag{4.7}$$

$$[M] = [M]_{tot} - [ML] \tag{4.8}$$

Substituting equation (4.6) with equations (4.7) and (4.8) and solving for [ML] gives

$$[ML] = \frac{1 + K([M]_{tot} + [L]_{tot}) + \sqrt{(K[M]_{tot} + K[L]_{tot} + 1)^2 - 4K^2[M]_{tot}[L]_{tot}}}{2K} \tag{4.9}$$

Hence, equation (4.4) can be written as a function of $[M]_{tot,}$ $[L]_{tot}$ and $K$ by substituting with equations (4.5), (4.7), (4.8), and (4.9). From the plot of $\delta_{obs}$ vs $[M]_{tot}$ as shown in Figure 4-18 the stability constant log$K$ = 3.7 ±0.1 was obtained via non-linear least squares fitting. The data are clearly consistent with a 1:1 metal-ligand stoichiometry. The binding affinity of this ligand was further investigated by means of fluorescence titration of the corresponding fluorescent sensor **5-3b**.

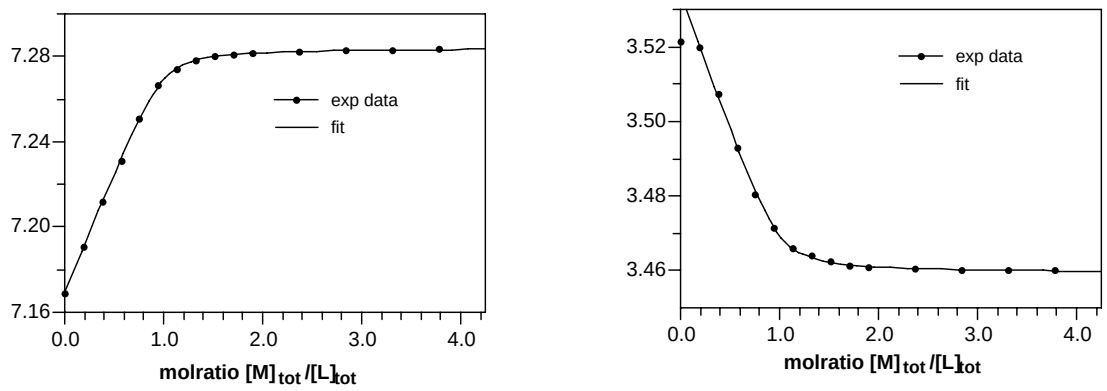


**Figure 4-18.** Molratio plot of $\delta_{obs}$ vs $[M]_{tot}/[L]_{tot}$ for the $^{1}H$ NMR titration of **4-3** (10 mM) with $Cu(CH_3CN)_4PF_6$ in $CD_3CN$. The data were fitted to equation (4.9) by non-linear least squares fitting as described in the text. Left: chemical shift change of the aromatic ring proton $H^a$. Right: chemical shift change of the methylene protons next to the aniline nitrogen.

### *4.3.2. Mass Spetrometric Characterization*

Electrospray mass spectrometry data unequivocally confirmed the formation of complexes with 1:1 ligand-metal binding stoichiometries for all studied ligands, even in the presence of excess Cu (I) cations. At 0.5 molar equivalent of Cu(I), both the masses of free ligand and copper complex were observed, as shown in Figure 4-19. After saturation with 1 molar equivalent of Cu(I), only a single signal consistent with the molecular mass of the complex ($M^+$) could be observed.

**Table 4-1.** ESI-MS Data for Cu(I) Complexes with Ligands **4-1** to **4-3**.

| | Observed Mass | | |
|---|---|---|---|
| | ligand **4-1** | ligand **4-2** | ligand **4-3** |
| 0.0eq Cu(I) | 344.0 | 300.0 | 360.1 |
| 0.5eq Cu(I) | 344.0 | 300.0 | 360.1 |
| | 372.0 | 362.1 | 422.0 |
| 1.0eq Cu(I) | 372.0 | 362.1 | 422.0 |
| 2.0eq Cu(I) | 372.0 | 362.1 | 422.0 |

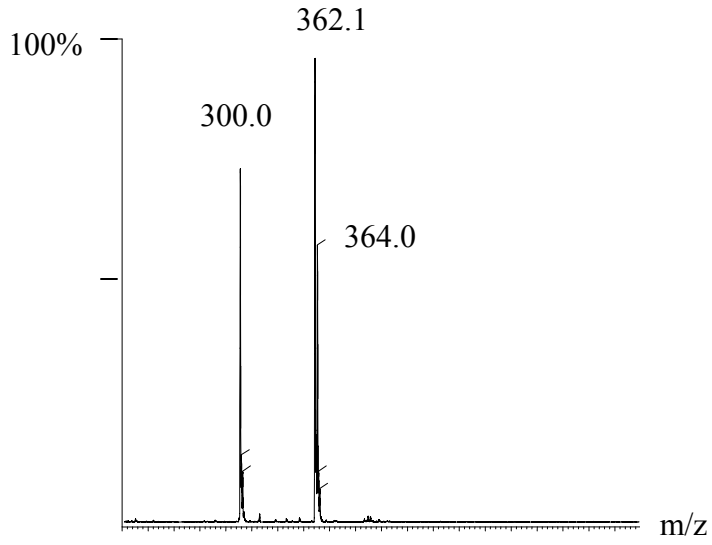


**Figure 4-19.** Mass spectrum of ligand **4-2** acetonitrile solution containing 0.5 equivalent of Cu(I).

## 4.4. Exchange Kinetics and Mechanistic Studies

The dynamic selfexchange equilibrium between a ligand L (or solvated metal cation M) and the corresponding complex ML can be described by the following equation:

$$L + ML^{*} \rightleftharpoons L^{*} + ML \tag{4.10}$$

As proposed by Shchori *et al.*, such a dynamic selfexchange reaction can principally occur by means a dissociative pathway (4.11a) a bimolecular exchange mechanism (4.11b).[30,31]

$$M + L \underset{k_{-1}}{\overset{k_1}{\rightleftharpoons}} ML \tag{4.11a}$$

$$ML + L^{*} \overset{k_2}{\rightleftharpoons} ML^{*} + L \tag{4.11b}$$

The expression for the mean life time of the ligand in these two mechanisms is given by[25,26,32-34]

$$\frac{1}{\tau} = k_{obs} = k_{-1}\frac{[ligand]_{tot}}{[ligand]_{f}} + k_2[ligand]_{tot} \tag{4.12}$$

where $[ligand]_{tot}$ and $[ligand]_f$ are the total ligand concentration and free ligand concentration, respectively.

Full line shape analysis of the corresponding $^1H$ NMR provides the *rate* for the exchange process, which depends on the concentration of ligand and complex present in solution. On basis of these data the rate constant $k_{obs}$ is then calculated as the sum of the forward and the reverse process:

$$k_{obs} = k_{-1} + k_1 = \frac{rate}{[ligand]_f} + \frac{rate}{[complex]} \tag{4.13}$$

where *rate* refers to the NMR exchange rate, and [*complex*] and $[ligand]_f$ are the concentration of the complex and free ligand, respectively. Both of the concentrations were also obtained by full line shape curve-fitting, which slightly deviates from the calculated concentration according to the molar ratios. A compilation of all obtained parameters is given in Table 4-2.

If the rate constant $k_{obs}$ is determined at various molar ratios of free ligand and complex, the characteristic rate constants for the dissociative ($k_{-1}$) and associative ($k_2$) mechanism can be obtained according to equation (4.12). For a given temperature, a plot of $k_{obs}$ /$[ligand]_{tot}$ *vs.* $1/[ligand]_f$ will then provide the contributions ($k_{-1}$) and ($k_2$) for the two mechanisms on basis of equation (4.14), a rearranged version of equation (4.12):

$$\frac{k_{obs}}{[ligand]_{tot}} = \frac{k_{-1}}{[ligand]_f} + k_2 \tag{4.14}$$

On the basis of this rational the mechanism for the dynamic exchange of ligands **4-1**, **4-2** and **4-3** with their respective Cu(I) complexes was investigated in more detail. Furthermore, variable temperature studies provided further insights into the activation enthalpy and entropy of the exchange process (see also Section 4.1.3).

A series of solutions with identical ligand concentration but different Cu(I)/ligand mol-ratios of 0.3, 0.4, 0.5 and 0.6 were prepared in $CD_3CN$, and the corresponding $^1H$ NMR spectra were acquired in 10 $^oC$ intervals between –30 $^oC$ and room temperature. The exchange rates for each combination of mol-ratio and temperature was obtained by full line-shape analysis using the gNMR software package.[35] This software calculates the full bandshape of signals that are broadened as a result of chemical exchange, the method developed by Binsch.[36,37] Although the lowest possible temperature setting was insufficient to determine the reference chemical shifts at the slow exchange limit required for curve fitting, the shifts and line widths were still obtained by acquiring a set of $^1H$ NMR spectra of the free and Cu(I)-saturated ligand at each temperature point. From the NMR exchange rates, the rate constants $k_{obs}$ were calculated, and the rate constants $k_{-1}$ and $k_2$ for the dissociative and associative pathway, respectively, were obtained from the slopes and the intercepts of the plots according to equation (4.14).

To illustrate the overall procedure, a set of variable temperature spectra for the titration of each ligand **4-1** to **4-3** with Cu(I) at a constant 0.5 Cu(I)/ligand mol-ratio is shown in Figures 4-22 to Figure 4-24, respectively. The simulated spectra that were obtained by means of full line shape analysis are reproduced to the right of each NMR trace. According to the previous titration studies, all ligands bind Cu(I) with submicromolar affinity. Therefore, the fractional saturation for each titration point is near

unity and the actual concentration of free ligand and complex can be assumed to be identical with the calculated Cu(I)/ligand mol-ratios.

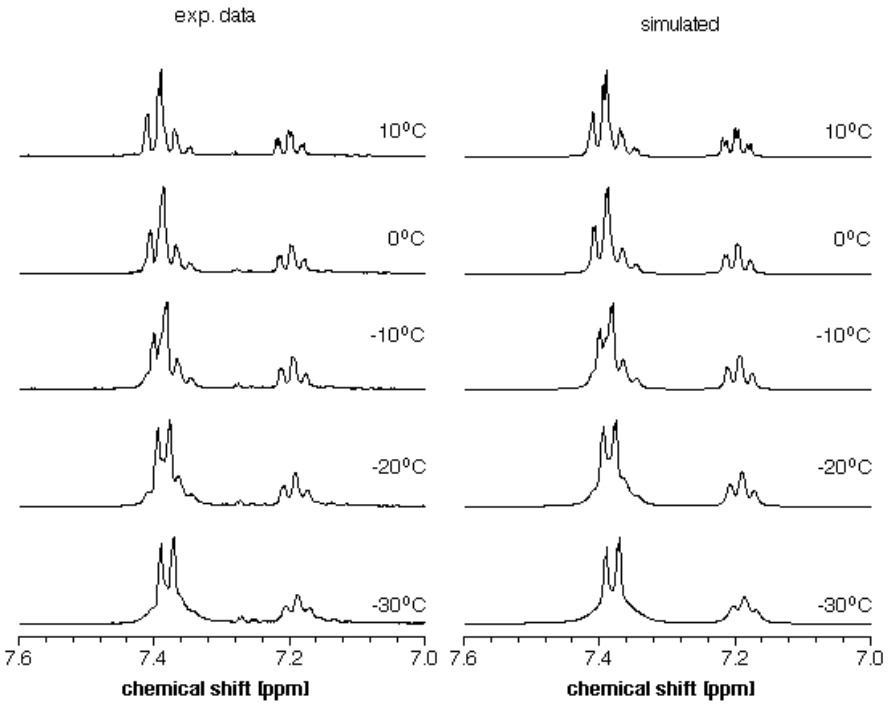


**Figure 4-20.** Experimental (left) and simulated (right) $^{1}$H NMR spectra at various temperatures for ligand **4-1** (total concentration 24 mM) in $CD_3CN$ at a constant Cu(I)/ligand mole ratio of 0.5.

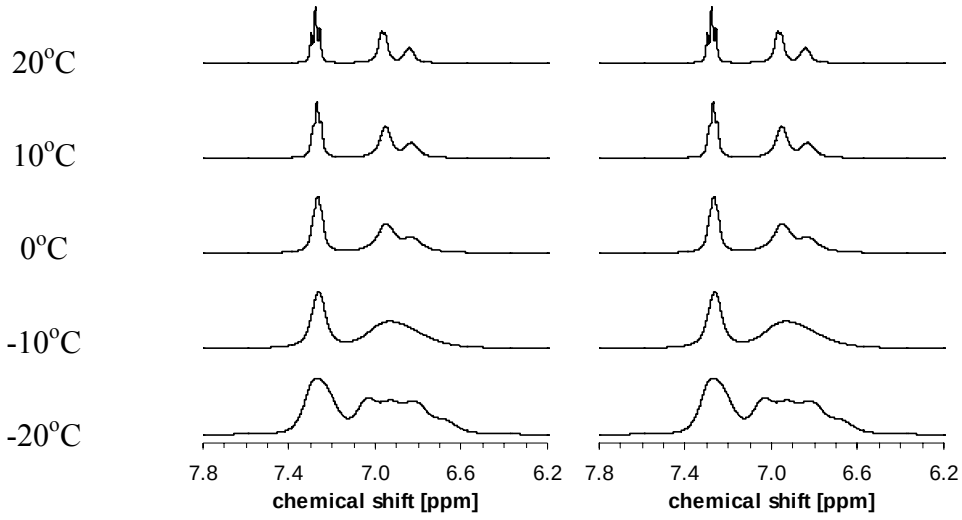


**Figure 4-21.** Experimental (left) and simulated (right) $^{1}H$ NMR spectra at various temperatures for ligand **4-2 (**total concentration 38 mM) in $CD_3CN$ at a constant Cu(I)/ligand mole ratio of 0.5.

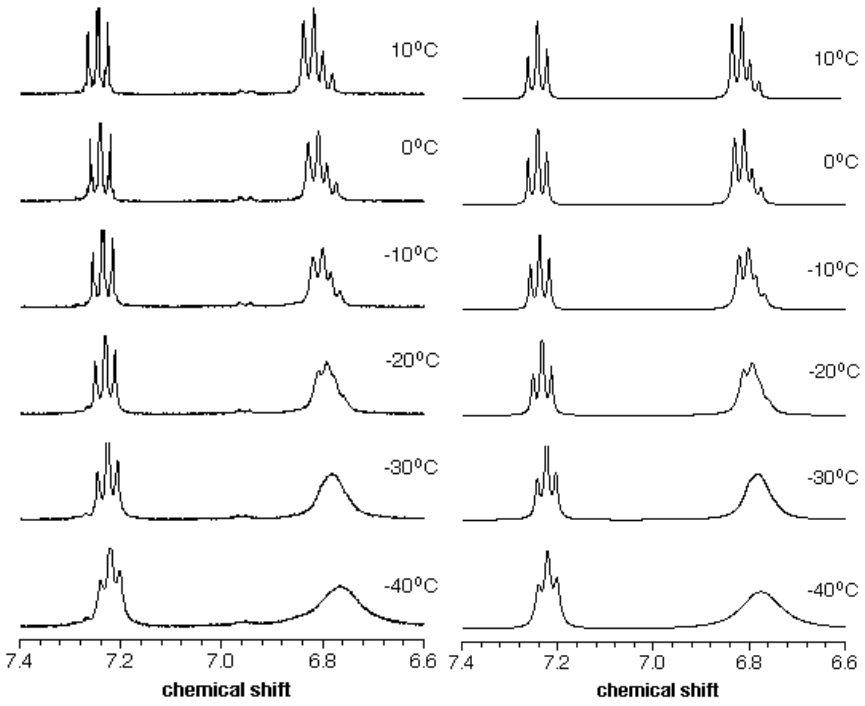


**Figure 4-22.** Experimental (left) and simulated (right) $^{1}H$ NMR spectra at various temperatures for ligand **4-3** (total concentration 12 mM) in $CD_3CN$ at a constant Cu(I)/ligand mole ratio of 0.5.

A compilation of the rate constants $k_{obs}$ obtained from variable temperature studies at a 1:1 molar ratio of free ligand and complex is given in the Table 4-2. As expected, $k_{obs}$ is increasing with increasing temperature. At room temperature, the exchange rate is fastest for the tripodal ligand **4-1** (66,000 $s^{-1}$) and the larger crown ether ligand **4-3** (43,800 $s^{-1}$), whereas the smaller sized crown ether **4-2** exhibits a significantly slower exchange rate (4,800 $s^{-1}$). As previously mentioned, the differences in exchange kinetics are most likely due to differences in conformational flexibility of the Cu(I)-ligand complex. The tripodal ligand **4-1** has clearly the most flexible structure, whereas the smallest crown ether ligand is most rigid and thus exhibits the slowest exchange kinetics. Most important, all ligands provide *very fast exchange rates* with average lifetimes (=1/$k_{obs}$) ranging between 15 to 208 μs at 283 K.

Figure **4-24 to 4-26** illustrate the dependence of the rate constant $k_{obs}$ from the molar ratio of free ligand and complex, plotted for a set of 5 different temperatures.

**Table 4-2.** Variable Temperature Rate Constants $k_{obs}$ Obtained from Full Line Shape Analysis at a 1:1 Molar Ratio of Free Ligand and Complex.

| | $k_{obs}[10^3 s^{-1}]$ | | |
|---|---|---|---|
| T[K] | **4-1** | **4-2** | **4-3** |
| 283 | 66.0 | 4.8 | 43.8 |
| 273 | 25.4 | 3.3 | 22.8 |
| 263 | 13.2 | 2.1 | 11.5 |
| 253 | 6.7 | 1.4 | 5.8 |
| 243 | 3.1 | | 2.7 |
| 233 | | | 1.1 |

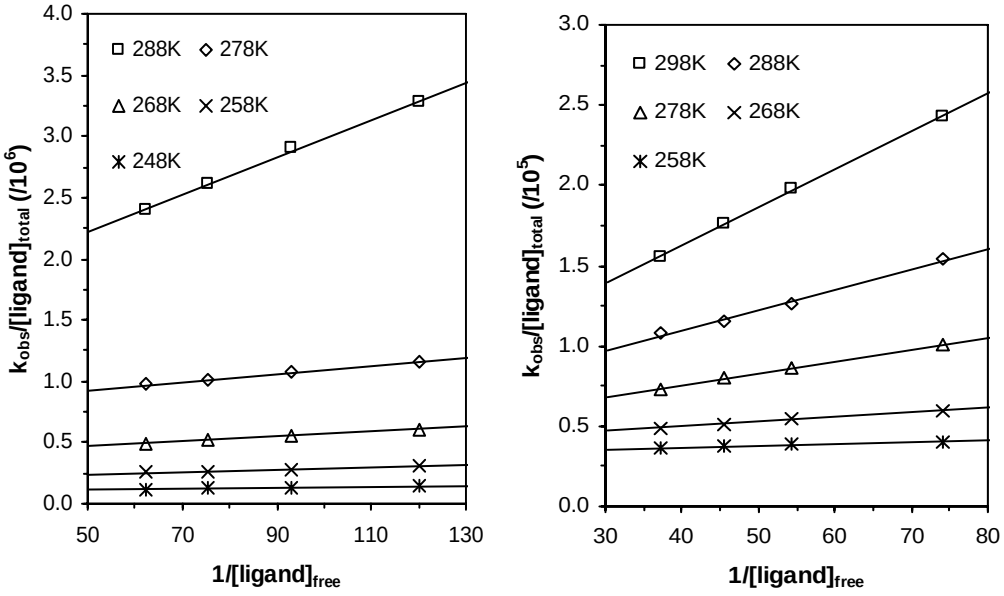


**Figure 4-23.** Plots of $k_{obs}/[ligand]_{total}$ vs $1/[ligand]_{free}$ at various temperatures in acetonitrile, ligand **4-1** (left), ligand **4-2** (right).

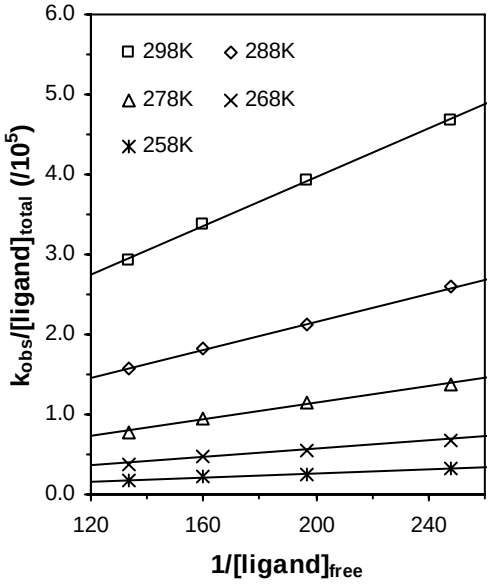


**Figure 4-24.** Plots of $k_{obs}/[ligand]_{total}$ vs $1/[ligand]_{free}$ at various temperatures in acetonitrile, ligand **4-3**.

The respective rate constants for the dissociative and associative exchange as obtained from the slope and intercept of each linear curve fit is given in Table 4-3. For all the systems studied, both of the two mechanisms appear to be involved in the exchange processes. With increasing temperature the rate constants for both mechanisms are increasing. Most importantly, the bimolecular exchange rate constants for all studied ligands are more than ten times faster compared to the dissociative rates. Conclusively, although a dissociative mechanism appears to partially participate in the exchange process, the bimolecular exchange mechanism is clearly predominant. In case of the conformationally restricted crownethers, the transition state involves most likely formation of a "sandwich"-like structure as also observed for alkali-metal crownether complexes in the gas-phase.[38]

**Table 4-3.** Simulated Rate Constants for Two Mechanisms.

| | **4-1** | | **4-2** | | **4-3** | |
|---|---|---|---|---|---|---|
| T [K] | $k_{-1}$ [$10^3 s^{-1}$] | $k_2$ [$10^3 Lmol^{-1}s^{-1}$] | $k_{-1}$ [$10^3 s^{-1}$] | $k_2$ [$10^3 Lmol^{-1}s^{-1}$] | $k_{-1}$ [$10^3 s^{-1}$] | $k_2$ [$10^3 Lmol^{-1}s^{-1}$] |
| 243 | 0.43 | 94.87 | | | | |
| 253 | 0.87 | 200.35 | 0.12 | 1.82 | 0.12 | 2.21 |
| 263 | 1.95 | 376.22 | 0.26 | 4.22 | 0.26 | 4.22 |
| 273 | 3.18 | 773.60 | 0.51 | 11.80 | 0.52 | 10.08 |
| 283 | | | 0.88 | 39.26 | 0.88 | 39.26 |
| 293 | | | 1.51 | 93.49 | 1.51 | 93.49 |

According to the Eyring equation (4.2) the activation parameter $\Delta H^{\neq}$, $\Delta S^{\neq}$ for each of the two mechanisms can be obtained by plotting -Rln($k_{obs}$h/ $k_B$T) *vs.* 1/T. The corresponding plots are shown in the Figure 4-25 and Figure 4-26, and the activation parameters are summarized in the Table 4-4. Consistent with a predominant bimolecular exchange mechanism, the entropy of activation is negative for all ligands studied.

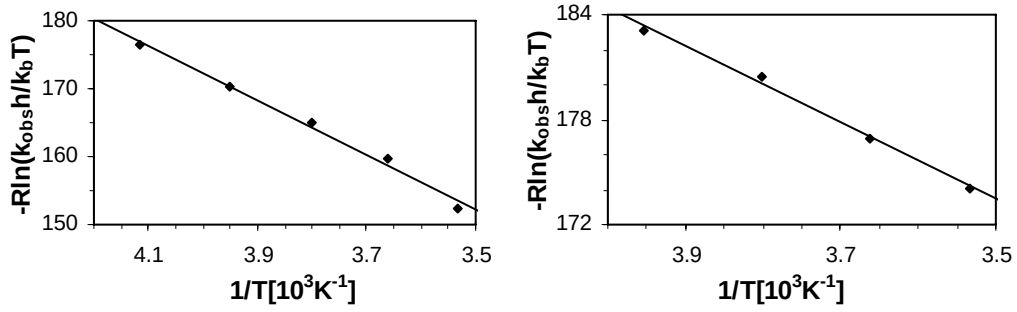


**Figure 4-25.** Eyring plots of -Rln($k_{obs}$h/$k_B$T) *vs.* 1/T, ligand **4-1** (left), ligand **4-2** (right).

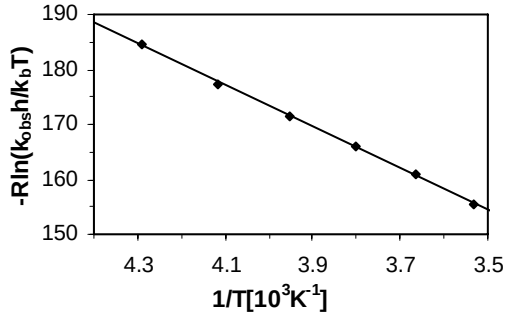


**Figure 4-26**. Eyring plots of -Rln($k_{obs}$h/$k_B$T) *vs.* 1/T, ligand **4-3**.

**Table 4-4.** Thermodynamic Activation Parameters for the Dynamic Cu(I)-ligand Exchange Reactions with Thioether Ligands **4-1, 4-2,** and **4-3**.

| compd. | $\Delta H^{\neq}$ [$kJmol^{-1}$] | $\Delta S^{\neq}$ [$Jmol^{-1}K^{-1}$] | $\Delta G^{\neq}$ (298K) [$kJmol^{-1}$] |
|---|---|---|---|
| **4-1** | 40.1 ± 2.1 | -12 ± 8 | 44 ± 3.2 |
| **4-2** | 21.8 ± 1.1 | -97 ± 4 | 51 ± 1.6 |
| **4-3** | 37.8 ± 0.4 | -22 ± 2 | 44 ± 0.7 |

In summary, the ligands studied in this chapter undergo rapid metal exchange reactions at room temperature, exhibit small activation barrier between 40-50 $kJmol^{-1}$ at room temperature, and should be well suited for dynamic measurements of intercellular copper.

## 4.5. Redox Potentials

The redox properties of ligands **4-1** to **4-6** were evaluated by means of cyclic voltammetry in acetonitrile using 0.1 M tetrabutyl exafluorophosphate as electrolyte. Since ligand **4-2** can not stabilize Cu(I) in aqueous condition, the oxidation potential was not measured.

Surprisingly, ligand **4-1** exhibits the most positive oxidation potential of 0.65 V. Presumably, the C-N bond between the aniline nitrogen and the aromatic ring is rotated out of plane, such that the lone pair electrons on the nitrogen are no further in conjugation with the aryl π-system. Upon removal of an electron, the resulting positive charge is not

as well stabilized as in case of a coplanar geometry. Although the corresponding Cu(I) complex is very well stabilized ($E_{ox}$ = 0.67 V), the large positive oxidation potential of the free ligand is not suitable for the design of a Cu(I) fluorescence sensor. As outlined in Section 2.1.3., according to the Rehm-Weller formalism the fluorescence enhancement factor directly parallels the increase of the electron donor oxidation potential upon binding of Cu(I). In case of ligand **4-1**, this increase is very small ($\Delta E$ = 20 mV), such that no significant change in fluorescence intensity is expected upon binding of Cu(I), even if the ET thermodynamics is carefully tuned to the electrochemical potential of the ligand. Likewise, the oxidation potential of ligand **4-4** does not change upon binding to Cu(I), while ligand **4-5** and **4-6** exhibit somewhat larger changes around 40 mV. Nevertheless, ligand **4-3** exhibits a similar stabilization for Cu(I) as ligand **4-1** ($E_{ox}$ = 0.67 V), but is significantly easier to oxidize in absence of Cu(I), thus providing a potential window of approximately 110 mV.

**Table 4-5.** Oxidation Potentials of Free Ligands and the Corresponding Copper(I) Complexes in Acetonitrile/0.1 M $Bu_4NPF_6$ vs $Fc/Fc^+$ (all units are given in Volt).

| compd | free ligand | Cu(I) complex |
|---|---|---|
| **4-1** | 0.65 | 0.67 |
| **4-3** | 0.56 | 0.67 |
| **4-4** | 0.53 | 0.53 |
| **4-5** | 0.46 | 0.50 |
| **4-6** | 0.46 | 0.50 |

All the ligands synthesized have high Cu(I) binding affinity, fast self exchange kinetics. However, only ligand **4-3** exhibits a large oxidation potential change upon binding to Cu(I). The sensor based on this ligand will be studied in Chapter V.

## 4.6. Experimental Section

### *4.6.1. Ligand Synthesis*

Azacrown ethers **2-6** were synthesized by cyclization reaction of correspondent thiol and (haloalkyl) aniline in the presence of $Cs_2CO_3$ as base in DMF.[39]

**a) Bis-(2-ethylsulfanyl-ethyl)-(2-ethylsulfanylmethyl-phenyl)-amine (ligand 4-1):** To a solution of bis-(2-chloro-ethyl)-(2-chloromethyl-phenyl)-amine (1.6 g, 6.04 mmol) in 10 mL EtOH, EtSH solution (1.87 g, 2.34 mL, 30.2 mmol) in NaOEt solution (2.4 g NaOH in 128 mL EtOH) was added dropwise at ice bath. Upon complete addition of the EtSH solution, the ice bath was removed. The mixture refluxed at 90$^o$C for 2h. All the solvent was removed and the residue was neutralized by 1N HCl. The reaction mixture was extracted twice with EtOAc, dried over anhydrous $MgSO_4$ and evaporated to dryness. The crude product was purified by silica gel, gradient 30:1 and 20:1 hexane: EtOAc, providing 1.3 g of product brown yellow oil (3.8 mmol, 62% yield). $R_f$ 0.25 (20:1 hexane:EtOAc); $^1$H NMR ($CDCl_3$, 400 MHz) δ 1.18-1.29 (m, 9H), 2.46-2.60 (m, 10H), 3.18-3.23 (m, 4H), 3.90 (s, 2H), 7.09-7.27 (m, 3H), 7.43 (dd, $J$ = 1.65, 7.69 Hz, 1H); MS (70 eV) 344 ($M^+$, 100). FAB HRMS m/e: calculated for $C_{17}H_{30}NS_3$ $(M+H)^+$ 344.15404, found 344.15594.

**b) 4-Phenyl-1,7,11-trithia-4-aza-cyclotetradecane (4-4):** To dry DMF (200 mL) was added $Cs_2CO_3$ (3.5 g, 10.74 mmol) and the solution stirred at 60 °C under nitrogen

atmosphere. Then dry DMF solution (10 mL) containing 3-(3-mercapto-propylsulfanyl)-propane-1- thiol (0.95 g, 5.21 mmol) and bis-(3-iodo-propyl)-phenyl-amine (2.0 g, 4.99 mmol), respectively, was added dropwise over 24 h. After the addition was complete, the mixture was stirred at 60 °C for 24 h. After the reaction, the mixture was concentrated, and then 100 mL water was added. The solution was extracted with $CHCl_3$ (60 mL×4) and the combined extract wash twice with water, a 20% $Na_2S_2O_3$ aqueous solution and water. The extract was dried over $MgSO_4$ and evaporated *in vacuo*. The residue was purified by column chromatography (silica gel, gradient 30:1 and 20:1 hexane:EtOAc ), providing 550 mg white solid. Yield: 25%. *Rf* 0.21 (10:1 hexane:EtOAc); $^1$H-NMR ($CDCl_3$, 400 MHz) δ 1.97 (quintet, *J* = 7.3 Hz, 4H), 2.69-2.81 (m, 12H), 3.63 (t, *J* = 7.3 Hz, 4H), 6.64-6.742 (m, 3H), 7.21-7.25 (m, 2H). MS (70 eV) 327.1 ($M^+$, 100), 106 (42). EI-HRMS, m/e: calculated for ($M^+$) $C_{16}H_{25}NS_3$ 327.11492, found 327.11571.

**c) 11-Phenyl-1,4,7-trithia-11-aza-cyclotetradecane (4-5):** method as **4-4**. Yield: 59%. *Rf* 0.21 (10:1 hexane:EtOAc); $^1$H-NMR ($CDCl_3$, 400 MHz) δ 1.96 (quintet, *J* = 7.3 Hz, 4H), 2.64 (t, *J* = 7.7 Hz, 4H), 2.74-2.79 (m, 8H), 3.41 (t, *J* = 7.3 Hz, 4H), 6.70-6.74 (m, 3H), 7.21-7.25 (m, 2H). MS (70 eV) 327.1 ($M^+$, 83), 206.1 (37), 179 (100). EI-HRMS, m/e: calculated for ($M^+$) $C_{16}H_{25}NS_3$ 327.11492, found 327.11647.

**d) 13-Phenyl-1,5,9-trithia-13-aza-cyclohexadecane (4-6):** method as **4-4**. Yield: 24%. *Rf* 0.21 (10:1 hexane:EtOAc); $^1$H-NMR ($CDCl_3$, 400 MHz) δ 1.92 (quintet, *J* = 7.1 Hz, 4H), 2.62 (t, *J* = 7.4 Hz, 4H), 2.67-2.71 (m, 8H), 3.46 (t, *J* = 7.4 Hz, 4H), 6.67-6.79 (m, 3H), 7.22 (t, *J* = 7.8 Hz, 2H). MS (70 eV) 355.2 ($M^+$, 100), 146.1 (78). EI-HRMS, m/e: calculated for ($M^+$) $C_{18}H_{29}NS_3$ 355.14622, found 355.14602.

### *4.6.2. Dynamic $^1$H NMR Experiments*

Proton NMR spectra (400 MHz) were recorded on a Varian Mercury VX400 spectrometer**.** The temperature of the sample was adjusted with a temperature control unit using liquid nitrogen as cooling medium. Prior to acquisition of each spectrum, the sample tube was allowed to equilibrate for at least 20 min to reach the desired temperature. The standard methanol sample was used for temperature calibration. The methanol sample was equilibrated for sufficient time in desired temperature and a spectrum was obtained. The temperature was calculated and displayed based on the difference frequency between the two resonances.[40] At all the temperature used, the accuracy of temperature measurements was ±0.1$^o$C. TMS was used as an internal standard. A set of $^1$H NMR spectra of the free and Cu(I)-saturated ligand at each temperature point were obtained and used as reference spectra. The raw FID was processed with the gNMR software package. The spectra of various molar ratio Cu(I)/ligand were fitting based on the chemical shift and the line width of the reference spectra. The software calculates the full bandshape of signals that are broadened as a result of chemical exchange and thus provides the exchange rate and the molar ratio of Cu(I)/ligand.

### *4.6.3. Redox Potentials*

The cyclic voltammograms of ligands **4-1** and compounds containing fluorophores and ligand **4-3** to **4-6** in the presence and absence of one molar equivalent Cu(I) were acquired in acetonitrile (freshly distilled over calcium hydride), 0.1 M $Bu_4NPF_6$ (recrystalized in water) was used as electrolyte. The same instrument was used as described in Section 2.7.2. The half-wave potentials were referenced to ferrocene and

the measurements were typically performed with 500 mV $s^{-1}$ scan rate at room temperature in inert gas environment. The sample concentration was 1 mM.

## 4.7. References


1. Cooper, T.; Mayer, M.; Leung, K.; Ochrymowycz, L.; Rorabacher, D., *Inorg. Chem.* **1992,** 31, (18), 3796.

2. Sokol, L.; Ochrymowycz, L.; Rorabacher, D., *Inorg. Chem.* **1981,** 20, (10), 3189.

3. Ambundo, E.; Deydier, M.; Grall, A.; Aguera-Vega, N.; Dressel, L.; Cooper, T.; Heeg, M.; Ochrymowycz, L.; Rorabacher, D., *Inorg. Chem.* **1999,** 38, (19), 4233.

4. Bernardo, M.; Heeg, M.; Schroeder, R.; Ochrymowycz, L.; Rorabacher, D., *Inorg. Chem.* **1992,** 31, (2), 191.

5. Westerby, B.; Juntunen, K.; Leggett, G.; Pett, V.; Koenigbauer, M.; Purgett, M.; Taschner, M.; Ochrymowycz, L.; Rorabacher, D., *Inorg. Chem.* **1991,** 30, (9), 2109.

6. Ambundo, E.; Deydier, M.; Ochrymowycz, L.; Rorabacher, D., *Inorg. Chem.* **2000,** 39, (6), 1171.

7. Hemmerich, P.; Sigwart, C., *Experientia* **1963,** 19, (9), 488.

8. Manahan, S.; Iwamoto, R., *J. Electroanal. Chem.* **1967,** 14, (2), 213.

9. McConnell, H.; Davidson, N., *J. Am. Chem. Soc.* **1950,** 72, (7), 3164.

10. Young, I.; Ochrymowycz, L.; Rorabacher, D., *Inorg. Chem.* **1986,** 25, (15), 2576.

11. Wernimont, A.; Yatsunyk, L.; Rosenzweig, A., *J. Biol. Chem.* **2004,** 279, (13), 12269.

12. Cotton, F. A.; Wilkinson, G.; Murillo, C. A.; Bochmann, M., *Adv. Inorg. Chem.* **1999**.

13. Gunter, A.; Zuberbuh.A, *Chimia* **1970,** 24, (9), 340.

14. Zuberbuh.A, *Helv. Chim. Acta* **1970,** 53, (3), 473.

15. Kamau, P.; Jordan, R., *Inorg. Chem.* **2001,** 40, (16), 3879.

16. Krylova, K.; Jackson, K.; Ochrymowycz, L.; Rorabacher, D., *Inorg. Chem.* **1997,** 36, 6216.

17. Aronne, L.; Yu, Q.; Ochrymowycz, L.; Rorabacher, D., *Inorg. Chem.* **1995,** 34, (7), 1844.

18. Corazza, A.; Harvey, I.; Sadler, P., *Eur. J. Biochem.* **1996,** 236, (2), 697.

19. Shamsipur, M.; Talebpour, Z.; Alizadeh, N., *J. Solution Chem.* **2003,** 32, (3), 227.

20. Shamsipur, M.; Alizadeh, N., *J. Chin. Chem. Soc.* **1998,** 45, (2), 241.

21. Shamsipur, M.; Karkhaneei, E.; Afkhami, A., *J. Coord. Chem.* **1998,** 44, (1-2), 23.

22. Hilmersson, G., *Chem.-Eur. J.* **2000,** 6, (16), 3069.

23. Alizadeh, N.; Shamsipur, M., *J. Chem. Soc. Faraday Trans.* **1996,** 92, (22), 4391.

24. Alizadeh, N.; Shamsipur, M., *J. Solution Chem.* **1996,** 25, (10), 1029.

25. Shamsipur, M.; Popov, A., *J. Phys. Chem.* **1988,** 92, (1), 147.

26. Strasser, B.; Shamsipur, M.; Popov, A., *J. Phys. Chem.* **1985,** 89, (22), 4822.

27. Palmer, B.; Wilson, W.; Pullen, S.; Denny, W., *J. Med. Chem.* **1990,** 33, (1), 112.

28. Ishikawa, J.; Sakamoto, H.; Nakamura, M.; Doi, K.; Wada, H., *J. Chem. Soc. Dalton Trans.* **1999**, (2), 191.

29. Jones, G.; Chapman, B.; Mathews, J., *J. Org. Chem.* **1998,** 63, (9), 2928.

30. Shchori, E.; Jagurgro.J; Luz, Z.; Shporer, M., *J. Am. Chem. Soc.* **1971,** 93, (26), 7133.

31. Shchori, E.; Jagurgro.J; Shporer, M., *J. Am. Chem. Soc.* **1973,** 95, (12), 3842.

32. Shamsipur, M.; Popov, A., *J. Phys. Chem* **1986,** 90, (22), 5997.

33. Szczygiel, P.; Shamsipur, M.; Hallenga, K.; Popov, A., *J. Phys. Chem* **1987,** 91, (5), 1252.

34. Shamsipur, M.; Popov, A., *J. Phys. Chem.* **1987,** 91, (2), 447.

35. *gNMR* Version 4.1,Cherwell Scientific Limited, The Magdalen Centre Oxford Science Park, Oxford OX3 4GA (UK).

36. Binsch, G., *J. Am. Chem. Soc.* **1969,** 91, (6), 1304.

37. Stephenson, D.; Binsch, G., *J. Magn. Reson.* **1978,** 30, (3), 625.

38. Chu, I.; Zhang, H.; Dearden, D., *J. Am. Chem. Soc.* **1993,** 115, (13), 5736.

39. Sakamoto, H.; Ishikawa, J.; Mizuno, T.; Doi, K.; Otomo, M., *Chem. Lett.* **1993**, (4), 609.

40. Varian Liquids NMR User Guide.

# CHAPTER V

# PYRAZOLINE-BASED CU(I)-SELECTIVE SENSORS FOR CELLULAR IMAGING

## 5.1. Introduction

The photophysical studies of the pyrazoline fluorophore in Chapter 2 and 3 have provided detailed information regarding the influence of the two aryl-substituents on the energetics of the electron transfer quenching pathway. For the design of a Cu(I)-selective sensor that can be used in an aqueous biological environment, the two substituents must be now carefully chosen to match best the oxidation potential of the Cu(I) receptor unit, and thus to achieve the best possible fluorescence enhancement upon binding of Cu(I). As discussed in Section 2.6, Chapter II, the quantum yield of pH sensor **2-2c** is less than 0.01 in methanol (Table 2-4), and the corresponding electron transfer driving force $-\Delta G_{ET}$ is very large (0.31 eV, Table 2-9). Because the polarity of water is significantly greater compared to methanol, the electron transfer state $^1$ET is even more stabilized, and might reside at a level that cannot sufficiently rise above the locally excited state upon binding of Cu(I). For a given electron donor, the ET driving force $-\Delta G_{ET}$ can be reduced by either decreasing the excited state equilibrium energy $\Delta G_{00}$, or by decreasing the reduction potential $E_{red}$ (see Rehm-Weller equation, equation 2.1).[1] The latter is best accomplished by using for example an unsubstituted phenylring attached to the 3-position of the pyrazoline fluorophore.

A second important point for biological application is the water-solubility of the sensor. This can be best improved by incorporating at least one carboxylic ester group that can be hydrolyzed by unspecific esterases within the cellular environment. Attaching an electron withdrawing ester group to the aryl substituent in the 3-position of the

pyrazoline ring ($R_2$ as in Figure 2-8) will increase the reduction potential and thus lower the energy level of the electron transfer state. In contrast, an ester group attached to the aryl substituent in the 1-position of the pyrazoline ring ($R_1$ as in Figure 2-8) is expected to increase the excited state equilibrium energy $\Delta G_{00}$ and therefore to increase $\Delta G_{ET}$.

In conclusion, for design of a first-generation set of Cu(I)-selective pyrazoline-based sensors **5-1** to **5-6,** we utilized a combination of an unsubstituted phenyl ring in the 3-position, and a benzoic ester moiety in the 1-position of the pyrazoline fluorophore (Figure 5-1). Compared to the pH sensor **2-2c**, which contains a cyano group for $R_1$ and an ester group for $R_2$, the synthesized sensors contain a less electron withdrawing group in the 3-position, providing a more negative reduction potential, and an ester group with similar electron withdrawing ability compared to the cyano substituent. Hence, the sensors are expected to exhibit a lower driving force $-\Delta G_{ET}$ compared to **2-2c**, and hopefully a matching excited state electron transfer energetics to rise the ET state above LE upon binding to Cu(I). As Cu(I)-selective receptor units, various chelators were combined with this particular pyrazoline. To experimentally evaluate the ET switching properties with various receptor moieties, the pyrazoline fluorophore was combined with either a tripodal chelating moiety (**5-1**) or thiaza crownethers of various sizes (**5-2** to **5-8**).

All sensors were characterized in terms of their photophysical properties, and the lead compound was further tested in a cellular environment for the visualization of kinetically labile copper pools.

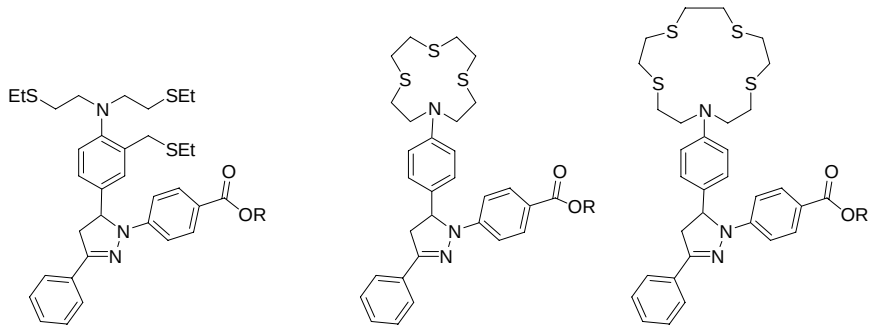

**5-1**



**5-2**



**5-3**

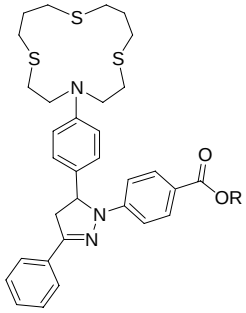

**5-4**

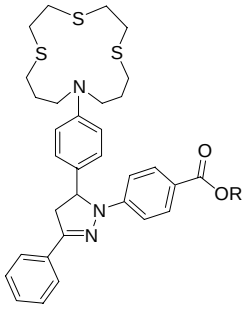

**5-5**

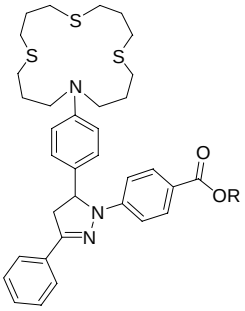

**5-6**

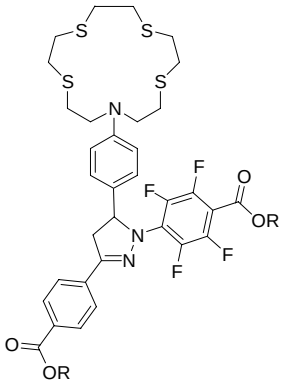

**5-7**

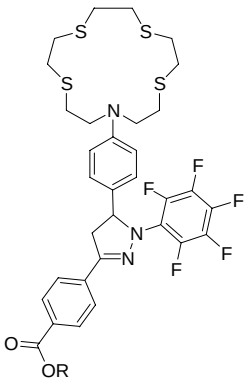

**5-8**

**Figure 5-1.** Structures of synthesized pyrazoline-based Cu(I) sensors (numbering in text with **a**: R = Et (ethyl ester), and **b:** R = H (free carboxylic acid).

## 5.2. Synthesis

### *5.2.1. Pyrazoline Sensors with Tripodal Thioether Receptor*

Figure 5-2 shows a complete retrosynthetic analysis for the tripodal thioether-receptor-substituted pyrazoline sensor of type **I**. Although the fluorophore structure might appear to be rather simple, the underlying molecular framework poses significant synthetic challenges. The first retrosynthetic step **a** yields the formyl-derivative of the aryl-thioether ligand **II** together with the corresponding aryl ketone and phenyl hydrazine derivatives. As previously outlined in Figure 2-9 (Chapter II), the pyrazoline fluorophore is readily synthesized from these components via an aldol condensation followed by cyclization with the corresponding hydrazine derivative. The aldehyde functionality in intermediate **II** could be either directly introduced via Vilsmeyer formylation of the azathioether **III**, or by means of lithium-halogen exchange at low temperature, followed by electrophilic attack of a substituted formamide derivative, starting with the bromo-substituted precursor **IV** (path **b**). Intermediate **III** in turn can be further retro-synthetically disconnected to give a secondary thioalkyl amine and the corresponding fluoro-substituted aryl compound **V** (path **d**). To increase the reactivity of **V** towards nucleophilic aromatic substitution with the secondary amine, the thiomethyl-substituent is best introduced via the more electronwithdrawing benzaldehyde precursor. Alternatively, intermediate **III** could be obtained from the corresponding chloroalkyl-substituted aniline precursor **VI** via nucleophilic substitution with ethanethiol (path **e**). Following further along the pathway of the bromo-substiuted intermediate **IV**, a similar alkyl chloride precursor **VII** is obtained through retrosynthetic step **g**. Alternatively, intermediate **IV** might be directly accessible via electrophilic aromatic bromination of **III**; however, this

strategy will require careful choice of the bromination reagent to avoid oxidative decomposition of the thioether functionality. Finally, the aldehyde functionality of intermediate **II** could be also introduced prior to substitution with ethanethiol, requiring the corresponding alkyl chloride precursor **VIII** (pathway **c**). However, this strategy might give rise to potential problems through reaction of ethanethiol with the aldehyde to give the corresponding thioacetal. Nevertheless, with careful control of the reaction conditions this route might be still a viable solution to the synthetic challenge. The required intermediate **VIII** should be readily accessible from the corresponding aniline by reaction with ethylene oxide followed by Vilsmeyer formylation (pathway **h**).

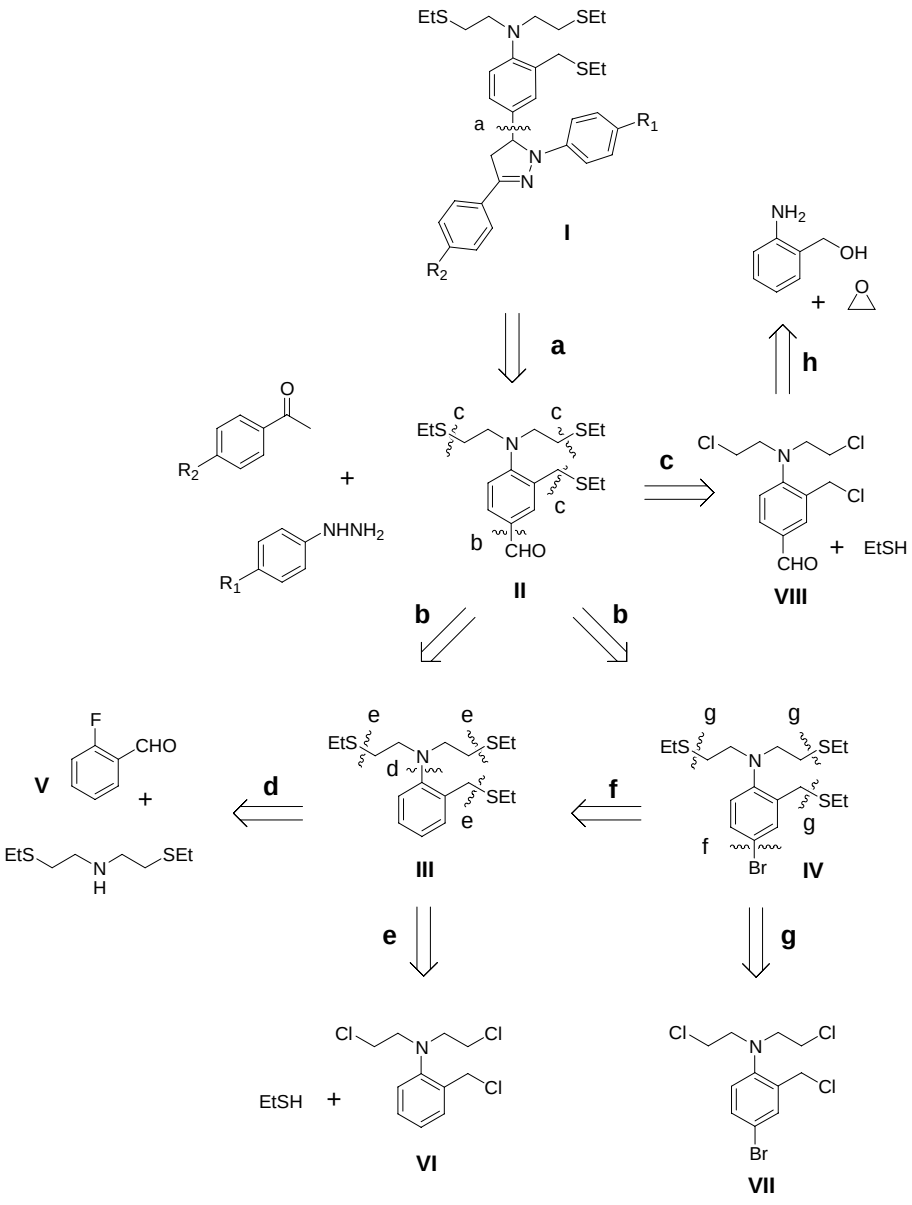


**Figure 5-2.** Retrosynthetic analysis for the molecular framework of pyrazoline sensors containing **a** tripodal thioether receptor unit.

### *5.2.1.1.Synthesis via Retrosynthetic Pathways b, d, and e*

First attempts for the synthesis of intermediate **II** focused on path **d** and **e** (Figure 5-2). Initial trials to react 2-fluoro-benzaldehyde with the corresponding secondary amine failed (path **d**), presumably due to insufficient electrophilicity of the aromatic ring to overcome the steric constraints of the secondary amine. As already described in Section 4.2.1, Chapter 4 (Figure 4-6), nucleophilic substitution of the corresponding alkylchloride precursor provided compound **4-1** with high yield (path **e**); however, several attempts to introduce the aldehyde group via Vilsmeyer formylation were not successful (path **b**, left). While no reaction was observed at 0 deg C, the ring closure product 3-ethylsulfanylmethyl-4-thiomorpholin-4-yl-benzaldehyde (**5-10**) was formed when the reaction mixture was heated, but none of the desired product **5-9** could be isolated (Figure 5-3). The unusually low nucleophilicity of aniline derivative **4-1** might be due to the steric constraints imposed by the neighboring *ortho*-ethylthiomethyl substituent. If the aniline nitrogen is rotated out-of-plane, the nitrogen lone pair electrons are no longer available to activate the aromatic ring.

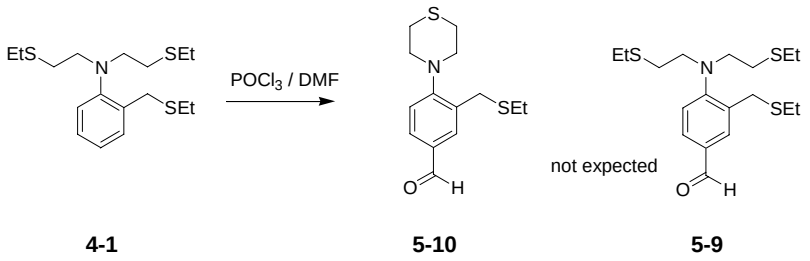


**Figure 5-3.** Reaction of aniline derivative **4-1** under Vilsmeyer formylation conditions.

To overcome this problem, the introduction of the formyl group was attempted via lithium-halogen exchange of the bromo-substituted precursor **5-14**. Because direct bromination of **4-1** was not successful (path **f**), the required *p*-bromo derivative **5-14** was synthesized as outlined in Figure 5-4.

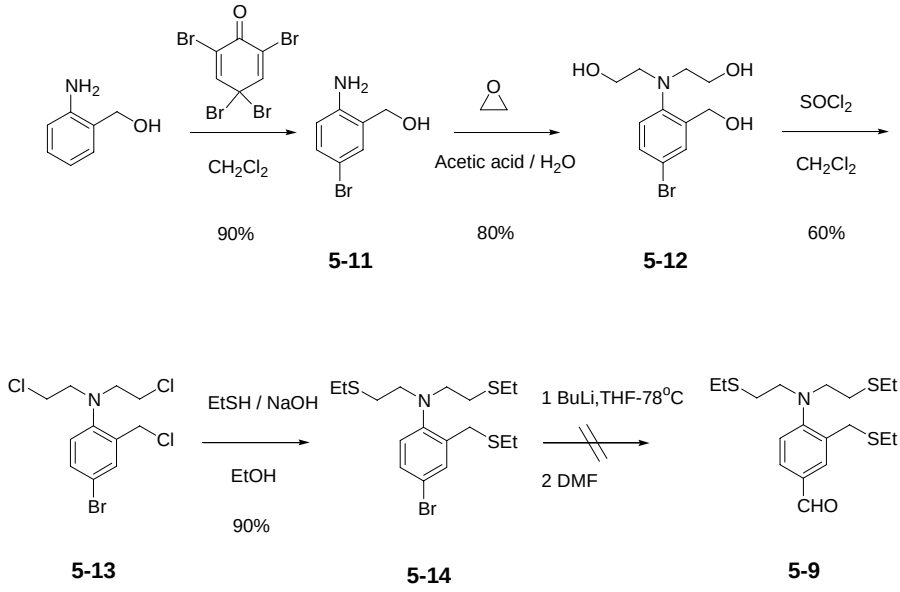


**Figure 5-4.** Synthesis and attempted formylation of precursor **5-14** to give **5-9**.

Bromination of commercially available 2-aminobenzylalcohol yielded (2-Amino-5-bromo-phenyl)-methanol **5-11** according to a literature precedure.[2] The ethylthioalkyl-substituted aniline derivative **5-14** was then obtained according to the same strategy as already successfully used for the synthesis of compound **4-1** (Figure 4-6, Chapter IV). However, the subsequent key step for introduction of the aldehyde proved to be unsuccessful. No reaction when butyl lithium or a Grignard reagent was added to bromo derivative **5-14** at –78 deg C.

### *5.2.1.2. Synthesis via Retrosynthetic Pathway c and h*

Although Vilsmeyer formylation of **4-1** did not yield the desired product, the reaction conditions at elevated temperature proved to be principally successful to introduce the aldehyde functionality. To avoid the undesired cyclization reaction of the thioether moiety, the aldehyde functionality was installed prior to conversion of the chloroalkyl group to the thioether (path **c** and **h**). Aldehyde **5-15** was indeed accessible through Vilsmeyer formylation; however, reaction of **5-15** with ethanethiol lead to formation of the thioacetal derivative **5-16** as the main product instead of the desired product **5-9** (Figure 5-5).

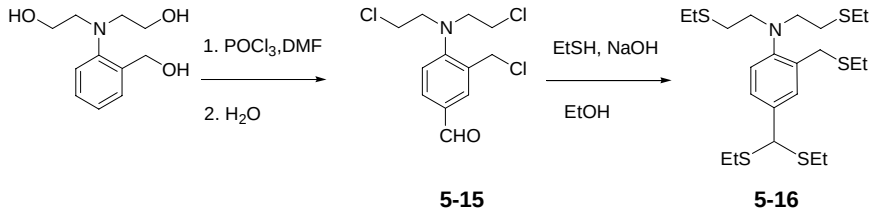


**5-15** **5-16**

**Figure 5-5.** Reaction of precursor **5-15** with ethanethiol.

While the aldehyde group in **5-15** might be principally protected through formation of the corresponding acetal, a simple change of the reaction conditions using aqueous DMF as solvent already eliminated the problem. Apparently, under these reaction conditions, the aldehyde reacts with water to form the corresponding hydrate, which is not sufficiently reactive towards nucleophilic substitution with the thiol (Figure 5-6). After having successfully synthesized indermediate **5-17**, the remaining synthetic steps to access pyrazoline **5-1a** proved to be straight forward and revealed no further surprises.

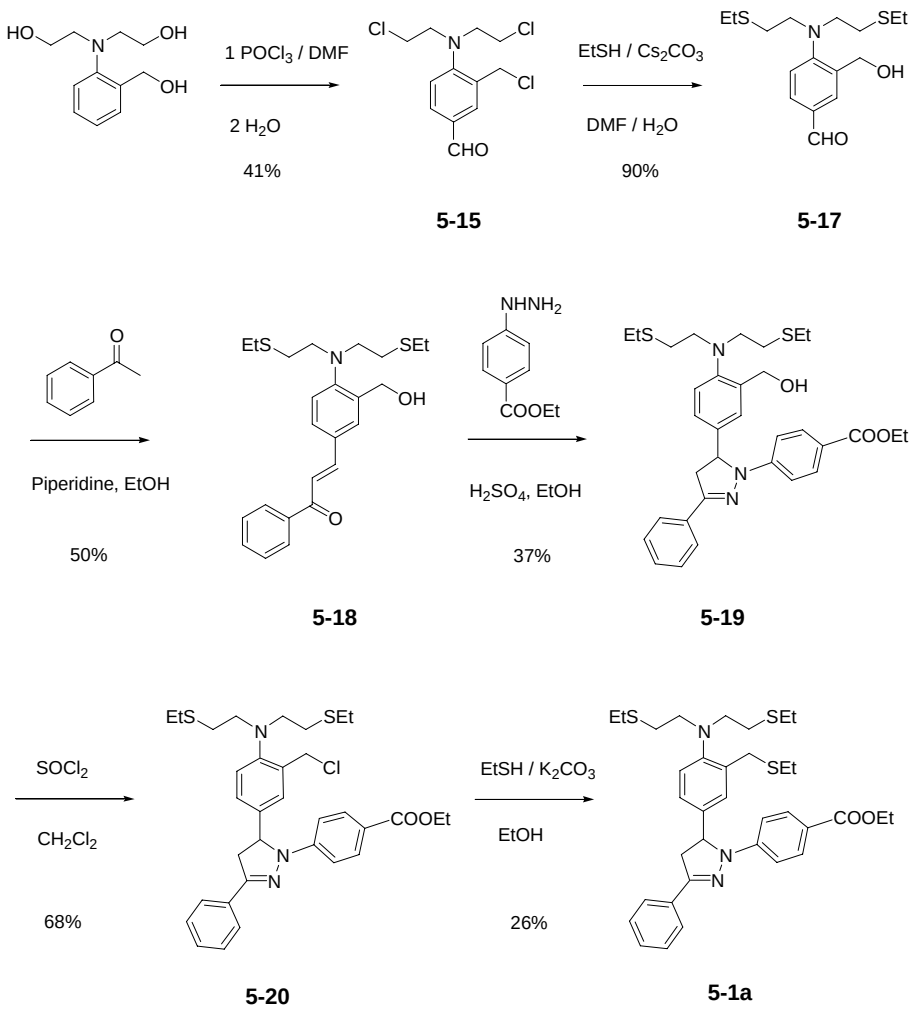


**Figure 5-6.** Successful synthesis of pyrazoline sensor **5-1a**.

### *5.2.2. Pyrazoline Sensors with Thiazacrown Ether Receptors*

As illustrated by Figure 5-7, the retrosynthetic disconnection of thiazacrown ether receptor pyrazoline sensors of type **I** can be accomplished analogously to the approached outlined for the tripodal ligand in Section 5.2.1. Here, the introduction of the aldehyde group via Vilsmeyer formylation starting from **III** is well documented in the literature for similar derivatives. [3]

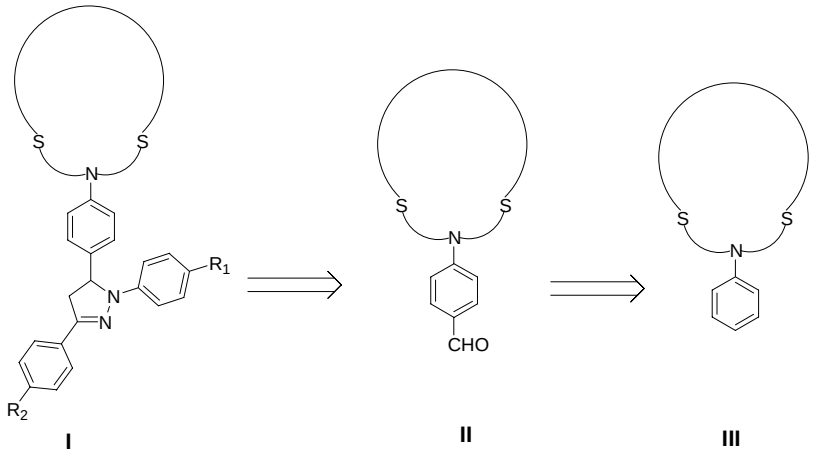


**Figure 5-1.** Retrosynthetic scheme of pyrazoline sensors with thiazacrown ether receptors.

Compounds **5-2** to **5-8** were successfully synthesized according to this strategy as exemplified with the synthetic scheme for sensor **5-3** (Figure 5-7). The synthesis of the corresponding thiaza crown ether ligands has been already discussed in Section 4.2.2 of Chapter 4.

All crude final products were purified by column chromatography and by reversed phase HPLC to give spectroscopically pure samples. The chemical structures of all synthesized products and intermediates were confirmed by $^{1}$H NMR, MS and high resolution mass spectrometry (HRMS). Description of the syntheses and the detailed analytical data are provided in the experimental section.

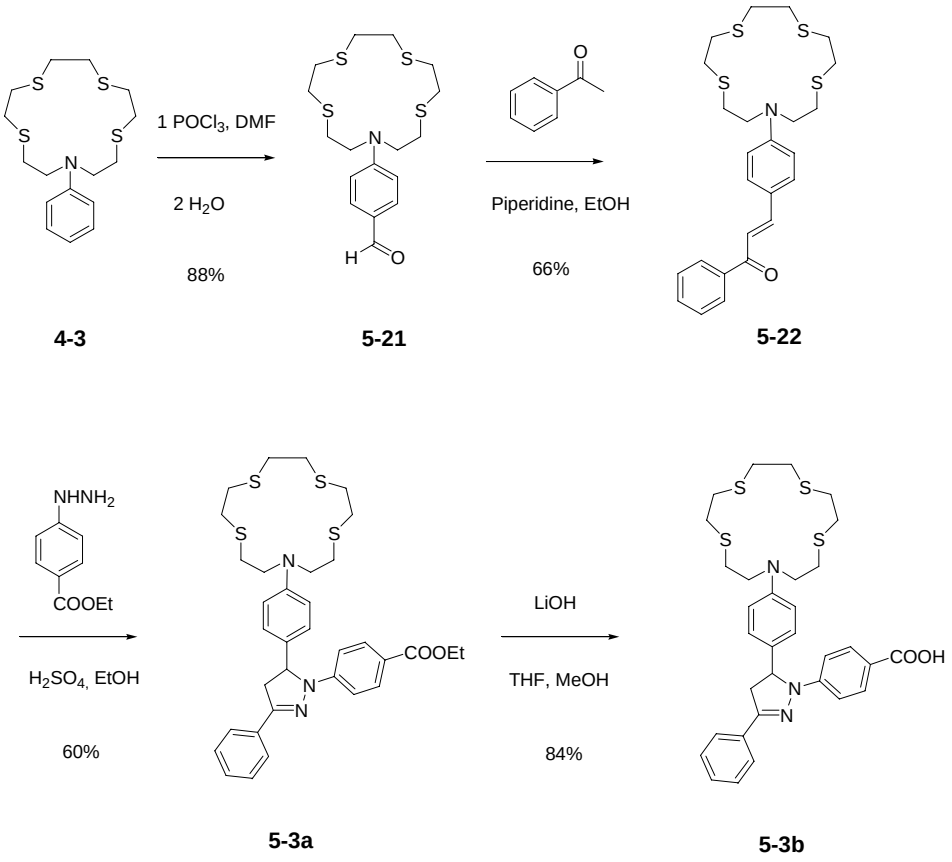


**Figure 5-2.** Synthesis of sensor **5-3a** and **5-3b**.

## 5.3. Photophysical and Thermodynamic Characterization

### *5.3.1. Fluorescence Emission and Quantum Yields*

All of the synthesized sensors undergo a Cu(I)-dependent change of the fluorescence intensity, however, the degree of emission enhancement varies significantly as a function of the receptor group (Table 5-1). As expected, the peak emission wavelengths for sensors **5-1** through **5-6** are very similar (within 10 nm difference), since all of these derivatives contain identical substituents on the pyrazoline fluorophore system. Derivatives **5-7** and **5-8** are substituted with electron withdrawing aryl groups on 1- and 3- position of pyrazoline and also have similar emission maxima.

**Table 5-1.** Fluorescence Emission Maxima and Quantum Yields for Sensors **5-1a** through **5-8a** in Methanol in the Absence and Presence of 1 Molar Equivalent $[Cu(I)(CH_3CN)_4]PF_6$ (based on quinine sulfate in 1.0 N $H_2SO_4$ as quantum yield standard).

| Sensor | $\lambda_{max}$ | $\Phi_f$ | $\lambda_{max}$ (+1 eq Cu(I)) | $\Phi_f$ (+1 eq Cu(I)) |
|---|---|---|---|---|
| **5-1a** | 427 | 0.04 | 427 | 0.05 |
| **5-2a** | 442 | 0.17 | 445 | 0.34 |
| **5-3a** | 442 | 0.13 | 443 | 0.34 |
| **5-4a** | 432 | 0.04 | 432 | 0.06 |
| **5-5a** | 431 | 0.04 | 432 | 0.32 |
| **5-6a** | 428 | 0.04 | 428 | 0.12 |
| **5-7a** | 420 | 0.002 | 424 | 0.005 |
| **5-8a** | 434 | 0.03 | 445 | 0.03 |

The degree of fluorescence enhancement in methanol solution parallels the increase in oxidation potentials (Tabel 4-5, Chapter IV) and/or excited state equilibrium energy, thus directly reflecting the change in the electron transfer quenching driving force according to the Rehm-Weller equation (Section 2.1.3, Chapter II). For example, sensor **5-1a** and **5-4a** exhibit both a very small change in oxidation potential, and thus the emission quantum yield increases only by a small amount. For **5-7a** and **5-8a**, both of which contain strong electron withdrawing aryl groups, the fluorescence quantum yield is very weak (less than 0.03), even in the presence of an equimolar amount of Cu(I). The electron withdrawing group of the susbtituent in the 1-position significantly increases the excited state equilibrium energy $\Delta E_{00}$, rendering the electron transfer free energy change $\Delta G_{ET}$ more exothermic according to Rehm-Weller equation (Section 2.1.3, Chapter II). Because the electron transfer driving force is substantially more favorable compared to other derivatives, binding of Cu(I) does not induce a significant change of the fluorescence emission intensity. Furthermore, the significantly lower quantum yield of compound **5-7a** might be due to a low-lying $^3(n\text{-}\pi^*)$ state, as observed in case of the unsubstituted model compounds described in Chapter III (Section 3.2.4).

Although the quantum yields have been acquired in methanol for improved solubility, the data set provides already valuable information to extrapolate the fluorescence emission properties towards an aqueous, physiological environment. Compared to the locally excited state, the quenching electron transfer state inherently has a much greater dipole moment, which yields a significantly better stabilization in a more polar solvent such as water. If the quantum yield of the sensor is already low in methanol, the driving force for the electron transfer process $-\Delta G_{ET}$ will be even more favorable in a

higher polarity environment, and thus prevent from effective fluorescence switching upon binding of Cu(I) to the receptor unit. This reasoning has been confirmed by the observation that the corresponding water-soluble carboxylic acid derivatives of sensors **5-4a**, **5-5a**, **5-6a**, exhibit a change in fluorescence emission upon binding of Cu(I) in PIPES buffered aqueous solution (pH 7.20). Only sensors **5-2a** and **5-3a** have reasonable quantum yields in methanol and are therefore viable candidates for biological applications.

Interestingly, the fluorescence intensity of acid derivative **5-2b** does not change with addition of Cu(I) in PIPES-buffered solution, and even decreases at Cu(I) concentrations higher than 1 molar equivalent. The resulting yellow solution indicates the formation of Cu(II). Presumably, the small ring of **5-2b** is too rigid to provide the optimal tetrahedral coordination geometry for effective stabilization of Cu(I). In contrast, sensor **5-3b** undergoes a bright emission enhancement with Cu(I) in aqueous solution and thus represents a promising Cu(I) sensor for biological applications. For future reference, compound **5-3b** will be referred to as **CTAP-1** (TAP = triarylpyrazoline).[4] Given the superior photophysical properties of **CTAP-1** compared to all other synthesized derivatives, the following studies were carried out exclusively with this compound.

### *5.3.2. Determination of the Cu(I)-Binding Affinity*

To determine the binding affinity of **CTAP-1** for Cu(I) under simulated physiological conditions, a stepwise fluorescence titration was performed in 10 mM PIPES-buffered solution at pH 7.20 (Figure 5-9). A 5 μM solution of **CTAP-1** was titrated with 0.1 molar aliquots of $[(Cu(I)(CH_3CN)_4]PF_6$, added from a 30 mM stock solution in $CH_3CN$. The emission spectra were acquired with excitation at 365 nm. In the

absence of Cu(I), the fluorescence emission is almost completely quenched with a quantum yield of 3%. After saturation with Cu(I) the emission intensity at 485 nm increased approximately 4.6 fold and the quantum yield reached 14%. As illustrated by the mol-ratio plot in Figure 5-10, the emission increased with a linear response, indicating tight binding with a fractional saturation near unity at each titration point. Since the fractional saturation should be less than 80% to provide a reliable binding constant (See Section 4.2.2, Chapter IV), the mol-ratio plot of fluorescence titration is not suitable to determine the Cu(I) affinity. Nevertheless, when assuming a fractional saturation of greater than 99%, the dissociation constant $K_d$ can be estimated to be $< 10^{-7}$ from the titration data. Also, the fluorescence signal is not saturated at 1 molar equivalent Cu(I) and continues to increase with a smaller slope. The tetrathiaza crown receptor is either coordinating to more than one equivalent of Cu(I), or the fluorescence increase might be due to associative/dissociative changes of the fluorophore moiety.

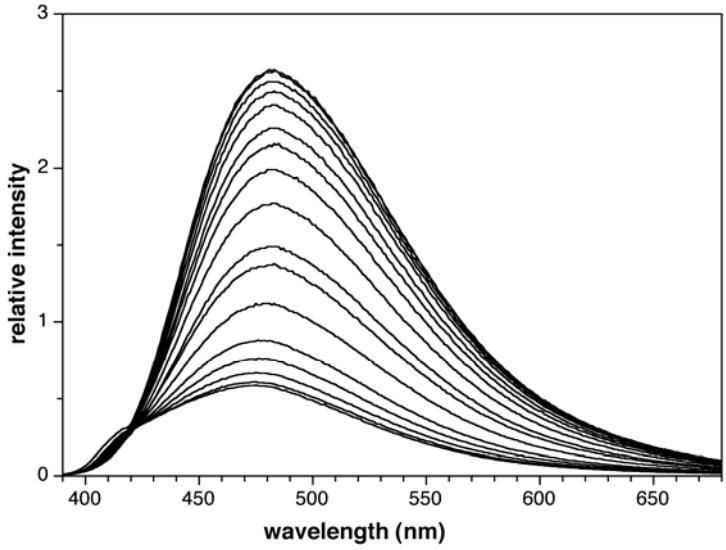


**Figure 5-9.** Fluorescence emission spectra of **CTAP-1** as a function of the Cu(I) concentration. (5 µM **5-3b**, 10 mM PIPES, pH 7.20, excitation at 365 nm).

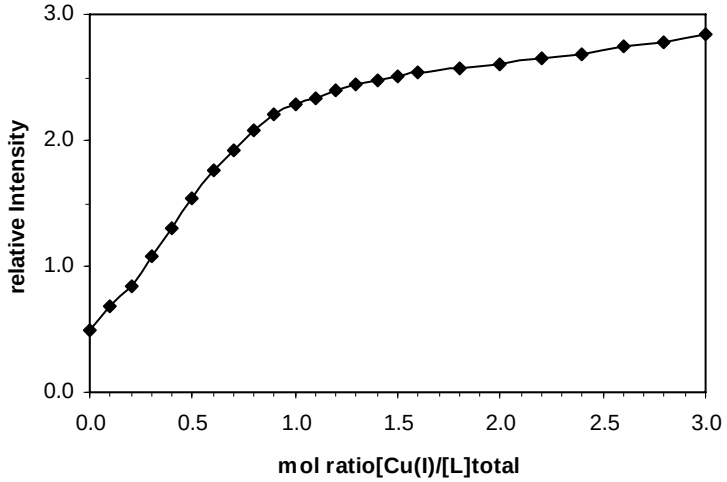


**Figure 5-10.** Relative fluorescence emission intensity of **5-3b** at 480 nm vs mol-ratio of Cu(I). (5 µM **5-3b**, 10 mM PIPES, pH 7.20).

To determine the binding affinity more accurately, a 10-fold diluted solution of **CTAP-1** (0.5 μM) containing 320 mM $CH_3CN$ for stabilization of Cu(I)[5] was titrated with 0.2 molar equivalent aliquots of $[(Cu(I)(CH_3CN)_4]PF_6$. Compared to the NMR titration of the receptor moiety **4-3** in neat $CD_3CN$ (Figure 4-17, Section 4.3.1, Chapter IV), as well as the previous fluorescence titration in absence of $CH_3CN$ (Figure 5-10), the observed binding isotherm revealed now a non-linear slope ("bent" curve), suggesting a significantly smaller fractional saturation (Figure 5-11). In this case, the data are suitable for a reliable determination of the stability constant. Thus, the spectra were analyzed by non-linear least squares fitting using the SPECFIT software package.[6] The data are consistent with a 1:1 binding stoichiometry and yielded a conditional binding affinity of $\log K = 6.88 \pm 0.05$. Taking into account that acetonitrile is an effective competitor-ligand for Cu(I) with $\log\beta_1 = 2.63$, $\log\beta_2 = 4.02$, $\log\beta_3 = 4.29$,[5] the stability constant of **CTAP-1** was estimated to be $\log K' = 10.4 \pm 0.1$.

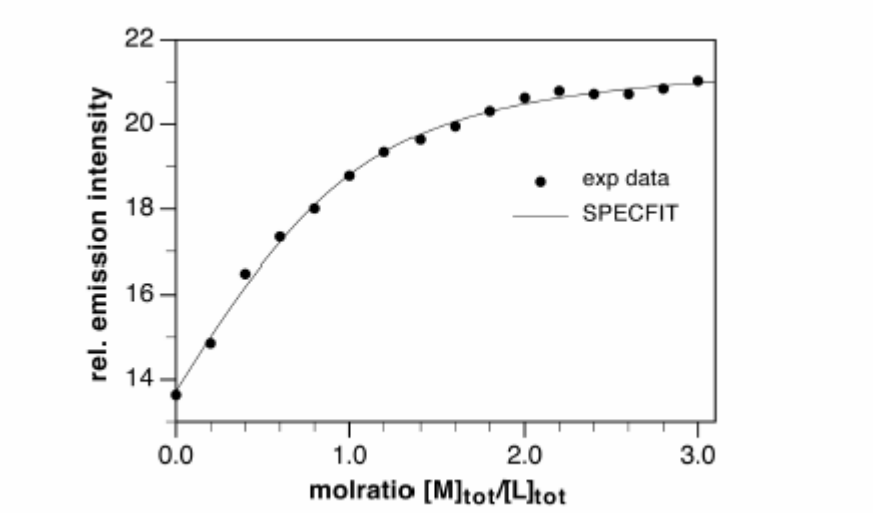


**Figure 5-11.** Plot of the relative emission intensity at 480 nm vs Cu(I)/[L]total. 0.5 μM **5-3b** in a solution of 10 mM PIPES and 320 mM $CH_3CN$ (pH 7.20); $[(Cu(I)(CH_3CN)_4]PF_6$ stock solution in $CH_3CN$. Although the plot shows only the intensity change at a single wavelength, the data were analyzed over the entire spectral range by non-linear least squares fit using the SPECFIT software package.

### *5.3.3. Metal Ion Selectivity of the Fluorescence Response*

The fluorescence emission of **CTAP-1** was measured in the presence of other transition metal ions in aqueous solution at neutral pH. As shown in Figure 5-12, significant fluorescence emission enhancement was only observed in the case of Cu(I) among all tested metal cations. Most importantly, the emission intensity is not affected by the presence of millimolar concentrations of Ca(II) or Mg(II). Furthermore, the fluorescence intensity upon addition of Cu(I) is altered by further addition of millimolar concentrations of Ca(II) or Mg(II). Hence, the sensor response and selectivity fulfills the requirements expected for biological applications.

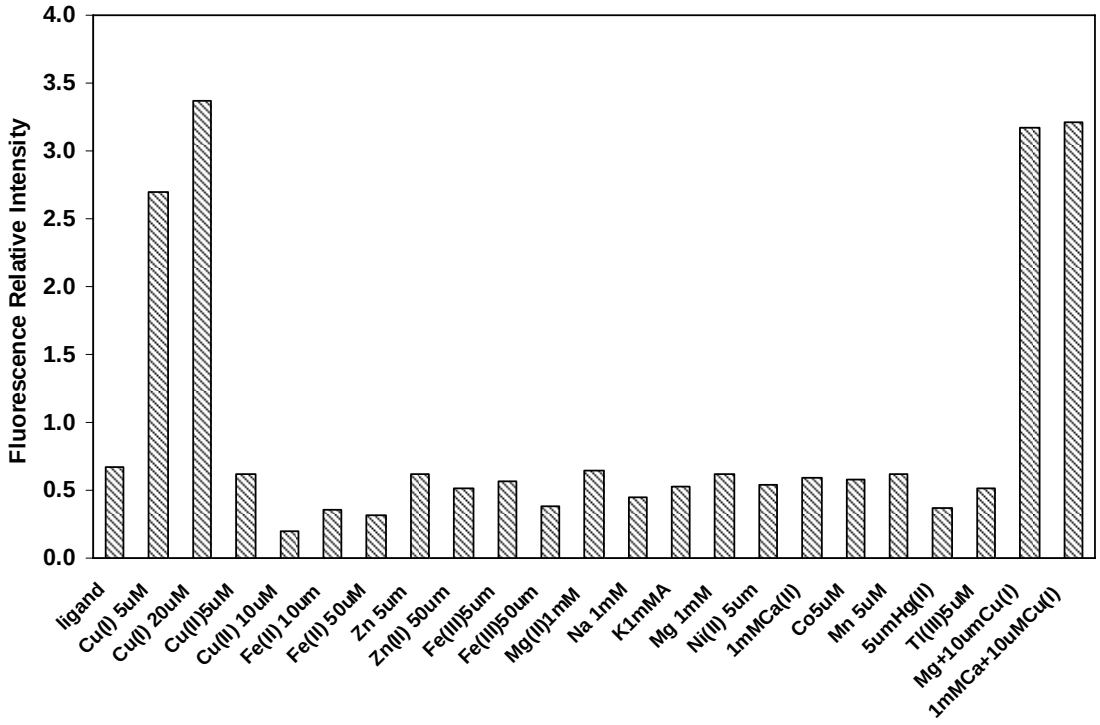


**Figure 5-12.** Fluorescence intensity of **CTAP-1** at 480 nm with various metal cations. (5 μM **CTAP-1**, 10 mM PIPES, pH 7.20).

### *5.3.4. pH Dependence*

The influence of pH on the fluorescence emission intensity was studied by titration of **CTAP-1** (10 μM in 0.1 M aqueous KCl as ionic background) with HCl (Figure 5-13). Interestingly, the titration revealed an overall enhancement with increasing pH. Assuming a p$K_a$ around 6-7 for the aniline nitrogen of **CTAP-1**, the emission intensity would be expected to decrease upon deprotonation of the nitrogen lone pair. At the same time, the emission maximum shifts to longer wavelength from 465 nm to 480nm. The decrease in fluorescence intensity upon acidification might be attributed to the fact, that the carboxyl acid moiety is protonated at acidic pH, which is expected to

increase the electron its withdrawing character, and thus to increase the excited state equilibrium energy as reflected in the blue shift of the peak fluorescence emission. The increased excited state equilibrium energy in turn provides a stronger driving force $-\Delta G_{ET}$ for the electron transfer quenching pathway, thus decreasing the fluorescence emission upon acidification. In context of biological applications, it is important to note that the fluorescence emission is not switched on at the slightly acidic pH found in the Golgi apparatus (pH = 6.5)[7-9] or by the more acidic environment of lysosomes or other acidic compartments (pH 4.5-5).[10] It is therefore not likely, that significant artifacts due to changes in protonation state are produced with **CTAP-1** in cell biological experiments.

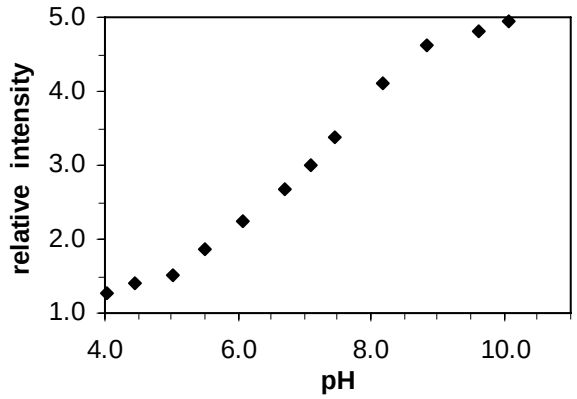


**Figure 5-13.** Relative fluorescence intensity as a function of pH. (**5-3b** 10 μM in 0.1 M KCl).

## 5.4. Cell Culture Studies[11]

### *5.4.1. In vivo Evaluation*

Incubation of mouse NIH 3T3 fibroblast cells with 10 μM **CTAP-1** produced a weak perinuclear staining pattern (Figure 5-14, top row). Supplementation of the growth medium with 150 μM $CuCl_2$ for 12 hours resulted in an approximately two- to three fold stronger emission intensity compared to cells cultured in basal medium (Figure 5-14, bottom row). The staining is particularly strong in proximity to the nuclear envelope and appears to co-localize with the Golgi apparatus. To quantitatively assess differences in emission intensities between the two growth conditions, the depicted fluorescence micrographs were acquired with a high-resolution 12-bit CCD camera using precisely identical exposure times and microscope settings. For better comparison, the profile of the average emission intensity across the x-coordinate of each fluorescence micrograph is shown to the right of Figure 5-14. Incubation in medium supplemented with 150 μM bathocuproin sulfonate (BCS), a copper-selective membrane-impermeable extracellular chelator, led to a relatively small decrease of the fluorescence intensity compared to basal conditions (data not shown). These results correlate well with literature data acquired by means of metabolic labeling with $^{64}Cu$ or atomic absorption spectroscopy, showing approximately a 3-5-fold increase at 100 μM $CuCl_2$ and 30% decrease upon incubation with 200 μM BCS.[12]

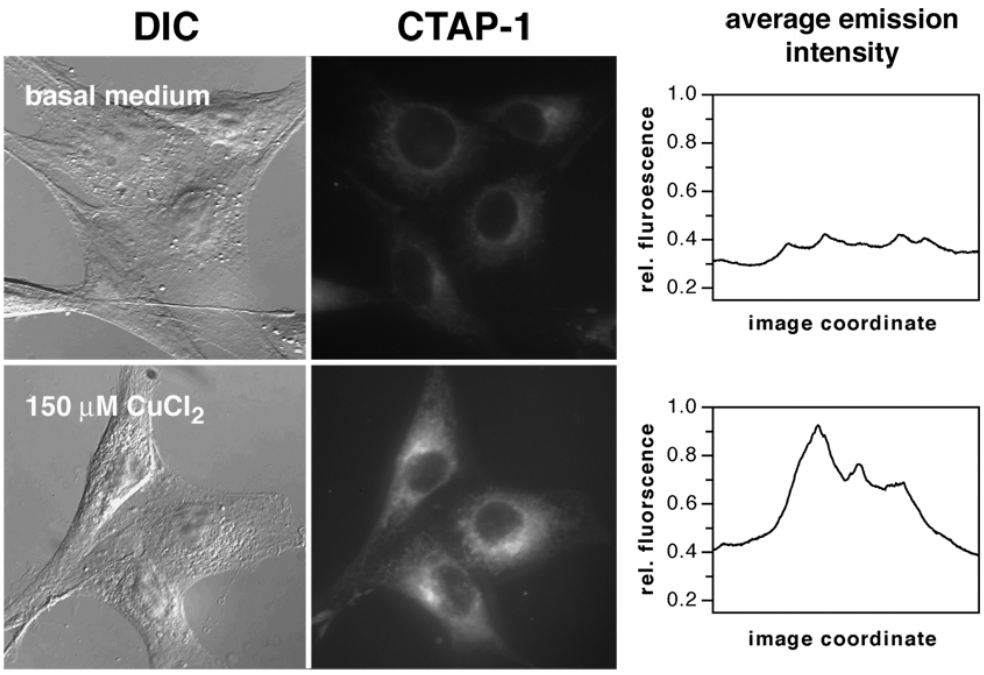


**Figure 5-14.** Fluorescence micrographs of NIH 3T3 cells incubated with 10 μM **CTAP-1** for 50 min. Influence of the extracellular copper concentration. Top row: Cells were grown in basal medium. Bottom row: Medium supplemented with 150 μM $CuCl_2$ for 8h. The graph to the right of each panel depicts the average intensity profile along the x-coordinate of the fluorescence micrographs (DIC = differential interference contrast image).

To identify organelles or compartments that might be associated with the observed staining pattern, we performed immunofluorescence colocalization experiments with a series of cellular markers. As shown in Figure 5-15 (top row), the copper-dependent staining pattern of **CTAP-1** matches the subcellular localization of the Golgi apparatus; however, additional, weaker stained areas can be detected throughout the cytoplasm. Visualization of the intracellular mitochondria distribution revealed a high degree of co-localization with this weaker pattern (Figure 5-15, bottom row). Because the net charge of **CTAP-1** at physiological pH is either neutral or negative, staining artifacts through accumulation within the negatively charged environment of the mitochondrial matrix are less probable. Other staining artifacts could be introduced through the mildly acidic lumenal pH of the Golgi apparatus ($pH_G$ = 6.40),[10] potentially leading to protonation induced fluorescence enhancements;[1] however, the emission intensity of an aqueous solution of **CTAP-1** (0.1 M KCl ionic background) decreases upon acidification from pH 7.2 to 4.5 (Figure 5-13), indicating that the observed perinuclear staining pattern is not due to protonation of **CTAP-1**. In an additional control experiment we tested whether the intracellular fluorescence of **CTAP-1** observed under high-copper growth conditions is reversed upon addition of an exogenous Cu(I) chelator. For this purpose, NIH 3T3 fibroblast cells were cultured first for 12 hours in medium supplemented with 150 μM of copper(II) chloride, and then treated with 2 μM **CTAP-1** in the presence or absence of 10 mM 3,6-dithia-1,8-octanediol (DTO) as exogenous chelator. Quantitative image analysis of the fluorescence micrographs revealed that the average intracellular fluorescence intensity of the control cells was approximately 50% higher (40 cells; $p < 0.0001$, Student's t-test) compared to DTO-treated cells (data not shown). Furthermore, a

set of cell-free fluorescence experiments in buffer solution demonstrated that DTO is able to competitively remove Cu(I) from **CTAP-1**.

In summary, the data suggest that under copper-supplemented growth conditions the fibroblast cells accumulate copper predominantly in the Golgi region and the mitochondria. The latter observation is corroborated through recent studies by Winge and coworkers, who recently demonstrated the existence of a non-proteinaceous copper pool in the mitochondrial matrix of yeast cells.[13]

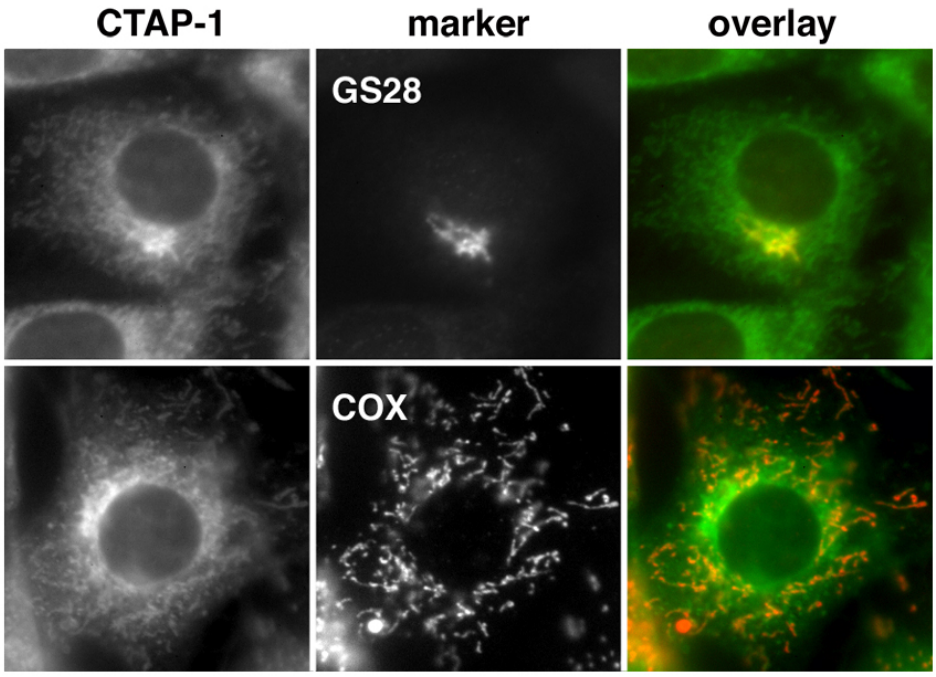


**Figure 5-15.** Fluorescence micrographs of NIH 3T3 cells incubated with 10 μM **CTAP-1** for 50 min.Immunofluorescence colocalization of the **CTAP-1** staining pattern (left) with two cellular marker antibodies (middle): Top row: anti-GS28 to visualize the Golgi apparatus. Bottom row: anti-OxPhos Complex V to visualize mitochondria (for details see experimental section). Right: false color overlay (**CTAP-1** green; antibody: red; areas of colocalization appear in orange/yellow).

### *5.4.2. Synchrotron X-ray Fluorescence Microprobe*[4,14]

To study the subcellular distribution of copper with an independent technique, we performed a series of synchrotron x-ray fluorescence microprobe (micro-XRF) experiments at the Advanced Photon Source of the Argonne National Laboratory. This technique has a detection limit of approximately $10^{-19}$ mol $\mu m^{-2}$ for Mn, Fe, Cu or Zn and a spatial resolution of 200 nm, rendering it well-suited for quantitative elemental mapping of single cells with subcellular resolution.[15,16] Two-dimensional maps of element distributions were compared with light and epifluorescence micrographs to further elucidate the role of these elements in cellular functions.

Cells, which were cultured in medium supplemented with 150 μM $CuCl_2$, yielded an approximately 20-fold increased Cu Kα signal at 8.0 keV compared to cells grown in basal medium (Figure 5-16). The perinuclear intensity distribution of the XRF copper map strongly resembles the staining pattern observed with **CTAP-1**. Interestingly, the ratio between the average emission intensity of copper and zinc appears reversed, however, the total amount of zinc varies only little between the two samples.

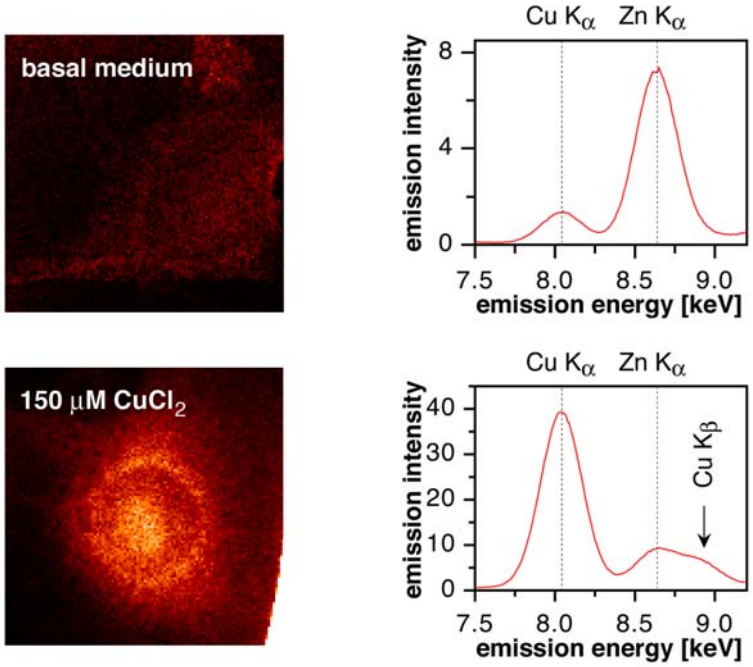


**Figure 5-16.** XRF copper maps of NIH 3T3 cells grown in basal medium (top) or in medium supplemented with 150 μM $CuCl_2$ (bottom). The emission intensity of each pixel was normalized using the beam intensity as reference. The maps are reproduced on the following intensity scales: basal medium 0.0002-0.0104 μg/cm$^2$; high copper medium 0.0017-0.1634 μg/cm$^2$). Right: x-ray emission spectra for Cu and Zn averaged over the entire area of the corresponding cell (normalized to beam intensity).

To assess the degree of co-localization between the epifluorescence staining pattern of **CTAP-1** and the subcellular copper topography obtained by means of micro-XRF, cells were grown in medium supplemented with 150 μM $CuCl_2$, incubated with **CTAP-1**, and inspected by optical and synchrotron x-ray fluorescence microscopy (Figure 5-17). Although drying of the cells, which is required to perform the micro-XRF experiments, caused some distortion of the overall structure, the micrographs indicate a high degree of colocalization. Interestingly, because the cells were fixed in methanol/acetone rather than formaldehyde, **CTAP-1** also stained the nucleoli, which in agreement with the x-ray fluorescence map appear to contain elevated levels of copper. A comparison between the copper and sulfur topography reveals a significant colocalization, suggesting that copper might be primarily coordinated by sulfur-donor ligands.

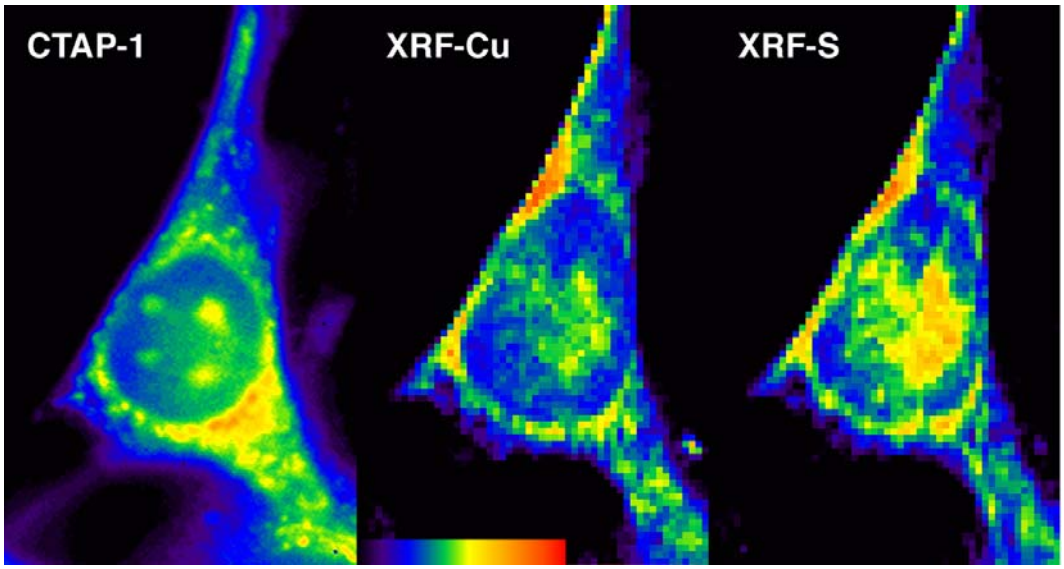


**Figure 5-17.** False-color micrographs of a single NIH 3T3 fibroblast cell grown in medium supplemented with 150 μM $CuCl_2$. Left: Epifluorescence image acquired with a DAPI filter set. Middle: SXRF copper map. Right: SXRF sulfur map. The relative intensities increase in the order blue-green-yellow-orange-red.

### *5.4.3. Microprobe X-ray Absorption Near-Edge Structure (micro-XANES)*[4,14]

The energy and shape of the near-edge x-ray absorption band of copper complexes is very sensitive towards variations in oxidation state and coordination environment. Whereas Cu(I) complexes exhibit a pre-edge feature centered around 8984 eV characteristic for the 1s –> 4p transition,[17] the analogous transition of Cu(II) complexes occurs at significantly higher energy (8986 eV). Micro-XANES was performed by scanning the energy of the incident x-ray near the Cu Kα edge (~ 8.979 keV) in the selected area. The zone plate and the specimen remained stationary during the measurement, which ensured that the illuminated area was fixed during the energy scan, although slight defocusing increased the spot size to about (0.25 μm). Microprobe XANES performed on a copper-loaded NIH 3T3 cell revealed at all tested subcellular locations a near-edge feature that is characteristic for monovalent copper (Figure 5-18A). Given the higher edge energy of Cu(II), the observed band shape does not exclude the presence of Cu(II); nevertheless, the spectrum demonstrates that a significant portion of the total copper is present as Cu(I). Due to the complex mixture of potentially coordinating endogenous ligands, a detailed interpretation of the XANES spectra is not possible; however, qualitative comparison with two reference compounds suggests a low-coordinate linear or trigonal geometry (Figure 5-18B). According to literature reports, neither metallothionein nor glutathione exhibit the observed, characteristic XANES near-edge feature,[18-20] and are therefore most likely not the prevalent endogenous ligands for coordination of kinetically labile copper in these pools.

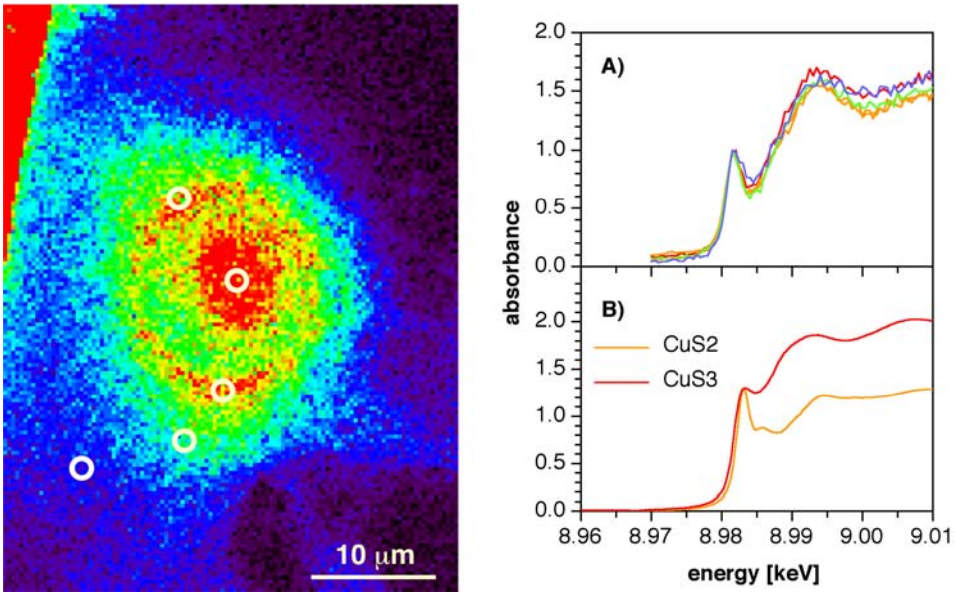


**Figure 5-18**. NIH 3T3 fibroblast cell grown in medium supplemented with 150 μM $CuCl_2$. Left: False-color SXRF micrograph showing the copper distribution (color code as Figure 5-17). Right: A) XANES spectra acquired at various locations (marked with white rings in the micrograph to the left). B) XANES reference spectra: CuS2 = $[Cu(SC_{10}H_{13})_2][N(C_3H_7)_4]$, and CuS3 = $[Cu(SC_6H_5)_3][P(C_6H_5)_4]$.[21]

## 5.5. Conclusion

Copper-selective fluorescence sensing combined with SXRF imaging microscopy provided a coherent picture regarding the subcellular localization of copper in the studied NIH 3T3 cell line. The copper-dependent intracellular staining pattern observed with **CTAP-1** and SXRF microscopy strongly supports the existence of the hypothesized labile copper pool, which appears to be localized in mitochondria and the Golgi apparatus. Microprobe XANES experiments confirmed the predominance of low-coordinate, monovalent copper throughout the cell, and are inconsistent with predominant coordination to metallothionein or glutathione. At present, the nature of the endogenous ligand is elusive; however, Winge and coworkers provided recently first evidence, that kinetically labile, mitochondrial copper is coordinated to a non-proteinaceous, low-molecular weight ligand carrying a negative net complex charge.[13] It is critical to note that the fluorescent sensor cannot provide actual quantitative concentration information. Because copper must be assumed to be coordinated to this yet unknown endogenous ligand, the sensor is inevitably engaged in a competitive metal exchange equilibrium, which position depends not only on the relative binding affinities but also the local concentrations of the sensor and endogenous ligand. While SXRF microscopy can provide quantitative information about the total copper concentration regardless of its kinetic availability, copper-selective fluorescence sensing complements this technique in a synergistic fashion, thus representing a powerful partnership for the investigation of the biological chemistry of labile copper pools and their possible role in cellular homeostasis.

## 5.6. Experimental Data

### *5.6.1. Synthesis*

**Materials and Reagents.** Acetophenone (Aldrich, 99%), NMR: δ in ppm vs $SiMe_4$ (0 ppm, 1H, 400 MHz). MS: selected peaks; m/z. Melting points are uncorrected. Flash chromatography: Merck silica gel (70-230 mesh). TLC: 0.25 mm, Merck silica gel 60 F254, visualizing at 254 nm or with 2% $KMnO_4$ solution. 4-Hydrazino-benzoic acid ethyl ester,[22] 4-(1,4,7,10-tetrathia-13-aza-cyclopentadec-13-yl)-benzene **4-3**, and 4-(1,4,7,10-tetrathia-13-aza-cyclopentadec-13-yl)-benzaldehyde **5-21** were synthesized as described in the literature.[3]

**a) 4-(5-{4-[Bis-(2-ethylsulfanyl-ethyl)-amino]-3-ethylsulfanylmethyl-phenyl}-3-phenyl-4,5-dihydro-pyrazol-1-yl)-benzoic acid ethyl ester (5-1a):** Yield: 26%. *Rf* 0.55 (3:1 hexane:EtOAc). $^1$H NMR ($CDCl_3$, 400 MHz) δ 1.14 (t, *J* = 7.3 Hz, 6H), 1.17 (t, *J* = 7.3 Hz, 3H), 1.34 (t, *J* = 7.3 Hz, 3H), 2.36 (q, J = 7.3 Hz, 2H), 2.47 (q, *J* = 7.3 Hz, 4H), 2.48-2.55 (m, 4H), 3.17 (t, *J* = 7.3 Hz, 4H), 3.19 (dd, *J* = 16.9 Hz, 5.9 Hz, 1H), 3.81 (q, *J* = 7.3 Hz, 2H), 3.87 (dd, *J* = 16.9 Hz, 12.5 Hz, 1H), 4.30 (q, *J* = 7.3 Hz, 2H), 5.36 (dd, *J* = 12.5 Hz, 5.9 Hz, 1H), 7.04 (d, *J* = 8.3 Hz, 2H), 7.08 (d, *J* = 4.4 Hz, 2H), 7.31 (s, 1H) 7.35-7.41 (m, 3H), 7.75 (d, *J* = 8.8 Hz, 2H), 7.86 (d, *J* = 8.8 Hz, 2H). MS (70 eV), 636.3 $(M+1)^+$, 20). EI-HRMS, m/e: calculated for $M^+$ $C_{35}H_{45}N_3O_2S_3$ 635.26739, found 635.26612.

**b) 4-{3-Phenyl-5-[4-(1,4,7-trithia-10-aza-cyclododec-10-yl)-phenyl]-4,5-dihydro-pyrazol-1-yl}-benzoic acid ethyl ester (5-2a):** Yield: 70%. *Rf* 0.30 (4:1 hexane:EtOAc). $^1$H-NMR ($CDCl_3$, 400 MHz) δ 1.36 (t, *J* = 6.6 Hz, 3H), 2.78-2.86 (m,

12H), 3.17 (dd, *J* = 17.6 Hz, 5.9 Hz, 1H), 3.52 (t, *J* = 7.3 Hz, 4H), 3.83 (dd, *J* = 17.6 Hz, 12.5 Hz, 1H), 4.30 (q, *J* = 7.3 Hz, 2H), 5.30 (dd, *J* = 12.5 Hz, 5.9 Hz, 1H), 6.65 (d, *J* = 8.8 Hz, 2H), 7.06 (d, *J* = 8.8 Hz, 2H), 7.10 (d, *J* = 8.8 Hz, 2H), 7.33-7.42 (m, 3H), 7.73 (d, *J* = 7.3 Hz, 2H), 7.85 (d, *J* = 8.8 Hz, 2H). MS (70 eV) 592.1 ($M^+$, 20). EI-HRMS, m/e: calculated for $(M+H)^+$ $C_{32}H_{37}N_3O_2S_3$ 591.2048, found 591.2076.

**c) 4-{3-Phenyl-5-[4-(1,4,7-trithia-10-aza-cyclododec-10-yl)-phenyl]-4,5-dihydro-pyrazol-1-yl}-benzoic acid (5-2b):** Yield: 63%. *Rf* 0.25 ( pure EtOAc). $^1$H-NMR ($CDCl_3$, 400 MHz) δ 2.78-2.84 (m, 16H), 3.19 (dd, *J* = 17.6, 5.1 Hz, 1H), 3.50-3.50 (m, 4H), 3.85 (dd, *J* = 17.6, 11.7 Hz, 1H), 5.31 (dd, *J* = 11.7, 5.1 Hz, 1H), 6.66 (d, *J* = 8.1 Hz, 2H), 7.09 (d, *J* = 8.8 Hz, 4H), 7.34-7.42 (m, 3H ), 7.74 (d, *J* = 8.1 Hz, 2H), 7.89 (d, *J* = 8.8 Hz, 2H). MS (70 eV) 562.2 ($M^+$, 85), 387 (55), 254 (100). EI HRMS, m/e: calculated for $(M+H)^+$ $C_{30}H_{34}N_3O_2S_3$ 564.1813, found 564.1832.

**d) 4-{3-Phenyl-5-[4-(1,4,7,10-tetrathia-13-aza-cyclopentadec-13-yl)-phenyl]-4,5-dihydro-pyrazol-1-yl}-benzoic acid ethyl ester (5-3a):** A solution of 4-hydrazinobenzoic acid ethyl ester hydrochloride (133 mg, 0.612 mmol) in 2 mL of ethanol was neutralized by addition of one molar equivalent of sodium ethoxide (20% solution in ethanol). This mixture was added to a solution of chalcone **5-22** (100 mg, 0.204 mmol) and 24 µL conc. $H_2SO_4$ in abs. ethanol (2 mL), and the resulting mixture was heated at reflux for 2 hours. After cooling to room temperature the solvent was removed under reduced pressure, the residue dissolved in ethyl acetate and extracted with sat. aqueous $NaHCO_3$ solution. The organic phase was dried ($MgSO_4$), concentrated, and the residue purified on silica gel (hexane/ethyl acetate, gradient 20:1 to 5:1) yielding 88 mg (0.135 mmol, 66%) of pyrazoline ester **5-3a** as pale yellow solid. mp 174-176 °C. *Rf*

0.23 (4:1 hexane/EtOAc). $^1$H-NMR ($CDCl_3$, 400 MHz) δ 1.34 (t, *J* = 7.1 Hz, 3H), 2.69-2.78 (m, 16H), 3.15 (dd, *J* = 17.0, 6.0 Hz, 1H), 3.51 (t, *J* = 8.2 Hz, 4H), 3.81 (dd, *J* = 17.0, 12.0 Hz, 1H), 4.29 (q, *J* = 7.1 Hz, 2H), 5.28 (dd, *J* = 12.0, 6.0 Hz, 1H), 6.54 (d, *J* = 8.8 Hz, 2H), 7.01 (d, *J* = 8.8 Hz, 2H), 7.10 (d, *J* = 8.8 Hz, 2H), 7.32-7.40 (m, 3H), 7.72 (d, *J* = 7.1 Hz, 2H), 7.84 (d, *J* = 8.8 Hz, 2H). MS (70 eV) 651.3 ($M^+$, 70), 471.2 (24), 457.2 (24), 43.1 (100). EI-HRMS, m/e: calculated for $(M+H)^+$ $C_{34}H_{41}N_3O_2S_4$ 651.2081, found 651.2032.

**e) 4-{3-Phenyl-5-[4-(1,4,7,10-tetrathia-13-aza-cyclopentadec-13-yl)-phenyl]-4,5-dihydro-pyrazol-1-yl}-benzoic acid (5-3b):** To the solution of pyrazoline ester **5-3a** (20 mg, 30.7 µmol) in THF (0.4 mL) a solution of lithium hydroxide (32 mg, 0.76 mmol) in 0.8 ml of methanol/water (1:1) was added. The reaction mixture was refluxed at 90 °C for 2 h, cooled to room temperature, and the organic solvent removed under reduced pressure. The residue was diluted with water and the product precipitated by addition of HCl (1 M) providing 16 mg (25.6 µmol) of **CTAP-1** as pale yellow solid. For the photophysical characterization the fluorophore was further purified by reversed-phase HPLC (C18 column, acetonitrile-water, gradient 75% –> 98%). Yield: 84%. mp >215°C (dec.). *Rf* 0.15 (3:1 hexane/EtOAc). $^1$H-NMR (DMSO-$d_6$, 400 MHz) δ 2.64-2.77 (m, 16H), 3.12 (dd, *J* = 17.0, 5.0 Hz, 1H), 3.45-3.51 (m, 4H), 3.89 (dd, *J* = 17.0, 12.1 Hz, 1H), 5.49 (dd, *J* = 12.1, 5.0 Hz, 1H), 6.56 (d, *J* = 8.8 Hz, 2H), 7.05 (d, *J* = 8.8 Hz, 4H), 7.38-7.47 (m, 3H ), 7.72 (d, *J* = 8.8 Hz, 2H), 7.78 (d, *J* = 8.8 Hz, 2H). MS (70 eV) 624.1 ($M^+$, 65), 419.2 (82), 335.2 (100), 265.1 (82). EI-HRMS, m/e: calculated for $(M+H)^+$ $C_{32}H_{38}N_3O_2S_4$ 624.1846, found 624.1827.

**f) 4-{3-Phenyl-5-[4-(1,7,11-trithia-4-aza-cyclotetradec-4-yl)-phenyl]-4,5-dihydro-pyrazol-1-yl}-benzoic acid ethyl ester (5-4a):** Yield: 50%. $R_f$ 0.42 (3:1 hexane:EtOAc); $^1$H-NMR ($CDCl_3$, 400 MHz) δ 1.34 (t, *J* = 7.1 Hz, 3H), 1.95 (quintet, *J* = 6.6 Hz, 4H), 2.68-2.77 (m, 12H), 3.17 (dd, *J* = 17.0, 6.0 Hz, 1H), 3.59 (t, *J* = 7.7 Hz, 4H), 3.83 (dd, *J* = 17.0, 12.1 Hz, 1H), 4.29 (q, *J* = 7.1 Hz, 2H), 5.30 (dd, *J* = 12.1, 6.0 Hz, 1H), 6.57 (d, *J* = 7.1 Hz, 2H), 7.06-7.11 (m, 4H), 7.35-7.42 (m, 3H), 7.74 (d, *J* = 8.2 Hz, 2H), 7.76 (d, *J* = 8.8 Hz, 2H). MS (70 eV) 619 ($M^+$, 100), 44 (100). EI-HRMS, m/e: calculated for ($M^+$) $C_{34}H_{41}N_3O_2S_3$ 619.23609, found 619.23424

**g) 4-{3-Phenyl-5-[4-(1,4,7-trithia-11-aza-cyclotetradec-11-yl)-phenyl]-4,5-dihydro-pyrazol-1-yl}-benzoic acid ethyl ester (5-5a):** Yield: 50%. $R_f$ 0.42 (3:1 hexane:EtOAc); $^1$H-NMR ($CDCl_3$, 400 MHz) δ 1.34 (t, *J* = 7.1 Hz, 3H), 1.93 (quintet, *J* = 6.6 Hz, 4H), 2.60 (t, *J* = 7.7 Hz, 4H), 3.18 (dd, *J* = 17.6, 6.0 Hz, 1H), 3.37 (t, *J* = 7.1 Hz, 4H), 3.83 (dd, *J* = 17.6, 12.1 Hz, 1H), 4.30 (q, *J* = 7.1 Hz, 2H), 5.30 (dd, *J* = 12.1, 6.0 Hz, 1H), 6.61 (d, *J* = 8.2 Hz, 2H), 7.07-7.10 (m, 4H), 7.34-7.42 (m, 3H), 7.74 (d, *J* = 7.7 Hz, 2H), 7.86 (d, *J* = 8.8 Hz, 2H). MS (70 eV) 619 ($M^+$, 100), 44 (100). EI-HRMS, m/e: calculated for ($M^+$) $C_{34}H_{41}N_3O_2S_3$ 619.23609, found 619.23424.

**f) 4-{3-Phenyl-5-[4-(1,5,9-trithia-13-aza-cyclohexadec-13-yl)-phenyl]-4,5-dihydro-pyrazol-1-yl}-benzoic acid ethyl ester (5-6a):** Yield: 50%. $R_f$ 0.38 (3:1 hexane:EtOAc); $^1$H-NMR ($CDCl_3$, 400 MHz) δ 1.34 (t, *J* = 7.3 Hz, 3H), 1.90 (quintet, *J* = 7.3 Hz, 8H), 2.59 (t, *J* = 6.6 Hz, 4H), 2.65-2.69 (m, 8H), 3.18 (dd, *J* = 16.9, 5.9 Hz, 1H), 3.42 (t, *J* = 7.3 Hz, 4H), 3.82 (dd, *J* = 16.9, 11.7 Hz, 1H), 4.29 (q, *J* = 7.3 Hz, 2H), 5.39 (dd, *J* = 11.7, 5.9 Hz, 1H), 6.58 (d, *J* = 8.8 Hz, 2H), 7.08 (d, *J* = 8.1 Hz, 4H), 7.33-7.42 (m, 3H), 7.74 (d, *J* = 7.3 Hz, 2H), 7.86 (d, *J* = 8.8 Hz, 2H). MS (70 eV) 647 ($M^+$,

75), 174.1 (70). EI-HRMS, m/e: calculated for ($M^+$) $C_{36}H_{45}NS_3O_2$ 647.24964, found 647.26357.

**g) 4-{1-(4-ethyl-ester-tetrafluorophenyl-5-[4-(1,4,7,10-tetrathia-13-aza-cyclopentadec-13-yl)-phenyl]-4,5-dihydro-1H-pyrazol-3-yl}-benzoic acid ethyl ester (5-7a):** Yield: 42%. mp 150-153°C. *Rf* 0.20 (4:1 hexane:EtOAc). $^1$H-NMR ($CDCl_3$, 300 MHz) δ 1.36 (t, *J* = 7.1 Hz, 3H), 1.41 (t, *J* = 7.1 Hz, 3H), 3.28 (dd, *J* = 17.6, 6.0 Hz, 1H), 3.76 (dd, *J* = 17.6, 12.1 Hz, 1H), 4.37 (q, *J* = 7.1 Hz, 2H), 4.39 (q, *J* = 7.1 Hz, 2H), 5.61 (dd, *J* = 12.1, 6.0 Hz, 1H), 6.49 (d, *J* = 8.8 Hz, 2H), 7.07 (d, *J* = 8.8 Hz, 2H), 7.76 (d, *J* = 8.8 Hz, 2H), 8.07 (d, *J* = 8.8 Hz, 2H). MS (70 eV) 795.2 ($M^+$, 40), 221 (68). EI-HRMS, m/e: calculated for ($M^+$) $C_{37}H_{41}F_4N_3O_4S_4$ 795.1916, found 795.2109.

**h) 4-{1-Pentafluorophenyl-5-[4-(1,4,7,10-tetrathia-13-aza-cyclopentadec-13-yl)-phenyl]-4,5-dihydro-1H-pyrazol-3-yl}-benzoic acid ethyl ester (5-8a):** Yield: 76%. mp 140-142°C. *Rf* 0.25 (4:1 hexane:EtOAc). $^1$H-NMR ($CDCl_3$, 300 MHz) δ 1.13 (t, *J* = 7.1 Hz, 3H), 3.13 (dd, *J* = 17.0, 7.1 Hz, 1H), 3.31 (q, *J* = 7.1 Hz, 2H), 3.77 (dd, *J* = 17.0, 12.6 Hz, 1H), 5.17 (dd, *J* = 12.6, 7.1 Hz, 1H), 6.49 (d, *J* = 8.8 Hz, 2H), 7.07 (d, *J* = 8.8 Hz, 2H), 7.74 (d, *J* = 7.1 Hz, 3H), 8.05 (d, *J* = 8.8 Hz, 2H). MS (70 eV) 741.4 ($M^+$, 95), 548.3 (100). EI-HRMS, m/e: calculated for ($M^+$) $C_{34}H_{36}F_5N_3O_2S_4$ 741.1610, found 741.1652

**i) 2-[(4-Bromo-2-hydroxymethyl-phenyl)-(2-hydroxy-ethyl)-amino]-ethanol (5-12):** A mixture solution of (2-amino-5-bromo-phenyl)-methanol (5.8 g, 28.7 mmol) and ethylene oxide (8.9 g, 0.20 mol) in 1:1 acetic acid: $H_2O$ was stirring vigorously at room temp for 24 h. The reaction mixture was poured into water, neutralized with $NaHCO_3$ solid and extracted twice with EtOAc, dried over anhydrous $MgSO_4$ and

evaporated to dryness, providing 9.0 g yellow solid of **5-12**. *Rf* 0.45 (pure EtOAc); $^1$H NMR ($CDCl_3$, 300 MHz) δ 3.33 (t, *J* = 5.2 Hz, 4H), 3.78 (t, *J* = 5.2 Hz, 4H), 4.69 (s, 2H), 7.26 (s, 1H), 7.36 (d, *J* = 2.5 Hz, 1H), 7.61 (d, *J* = 2.5 Hz); MS (70 eV) 289 ($M^+$, 10), 258 (100), 117 (74). FAB HRMS, m/e: calculated for ($M^+$) $C_{11}H_{16}NO_3$ 289.03135, found 289.03071.

**j) 2-chloromethyl-4-bromo-N, N-bis(2'-chloroethyl)aniline (5-13):** To a solution of 2-[(4-bromo-2-hydroxymethyl-phenyl)-(2-hydroxy-ethyl)-amino]-ethanol (8.0 g, 0.028 mol) in 200 mL $CHCl_3$, $SOCl_2$ (20.0 g, 12.1 mL, 0.166 mol) was added. The reaction mixture was refluxed at 80 °C for 40 min. After cooling to room temp., the reaction mixture poured into water and neutralized with $NaHCO_3$ then extracted twice with EtOAc, dried over anhydrous $MgSO_4$ and evaporated to dryness. The crude product was purified by silica gel, gradient 30:1 and 20:1 hexane:EtOAc, providing 6.13 g pale yellow oil ( 0.0179 mol, 64%). *Rf* 0.68 (10:1 hexane:EtOAc); $^1$H NMR ($CDCl_3$, 300 MHz) δ 3.39-3.50 (m, 8H), 4.77 (s, 2H), 7.14 (d, *J* = 8.8 Hz, 1H), 7.44 (dd, *J* = 8.8, 2.2 Hz, 1H), 7.65 (d, *J* = 2.2 Hz, 1H); MS (70 eV) 342.9 ($M^+$, 78). FAB HRMS, m/e: calculated for ($M^+$) $C_{11}H_{13}BrCl_3N$ 342.92969, found 342.92538.

**k) (4-Bromo-2-ethylsulfanylmethyl-phenyl)-bis-(2-ethylsulfanyl-ethyl)-amine (5-14):** To a solution of 2-chloromethyl-4-bromo-N, N-bis(2'-chloroethyl)aniline ( 500 mg,1.45 mmol ) in 5 mL EtOH, EtSH solution (360 mg, 5.79 mmol) in NaOEt solution ( 572 mg NaOH in 31 mL EtOH) was added dropwise in ice bath. Upon complete addition of the EtSH solution, the ice bath was removed. The mixture refluxed at 90$^o$C for 1.5 h. All the solvent was removed and the residue was neutralized by 1N HCl. The reaction

mixture was extracted twice with EtOAc, dried over anhydrous $MgSO_4$ and evaporated the solvent. The crude product was purified by column chromatography, gradient 30:1 and 20:1 hexane:EtOAc , providing 550 mg brown yellow oil ( 1.3 mmol, yield 90% ). $R_f$ 0.60 (10:1 hexane:EtOAc); $^1$H NMR ($CDCl_3$, 300 MHz) δ 1.20 (dt, *J* = 7.1, 1.1 Hz, 6H), 1.27 (dt, *J* = 7.1, 1.1 Hz, 3H), 2.45-2.58 (m, 10H), 3.18 (t, *J* = 7.1 Hz, 4H), 3.84 (s, 2H), 7.04 (d, *J* = 8.8 Hz, 1H), 7.30 (t, *J* = 8.8 Hz, 1H), 7.58 (s, 1H); MS (70 eV), 372.1 ($M^+$, 100). FAB HRMS *m/e* calculated for $(M+H)^+$ $C_{17}H_{28}NS_3Br$ 421.05673, found 421.05616.

**l) 4-[Bis-(2-chloro-ethyl)-amino]-3-hydroxymethyl-benzaldehyde (5-15):** Yield: 41%. $R_f$ 0.35 (3:1 hexane:EtOAc). $^1$H-NMR ($CDCl_3$, 400 MHz) δ 3.56 (t, *J* = 3.3 Hz, 8H), 4.84 (s, 2H), 7.33 (d, *J* = 8.8 Hz, 1H), 7.81 (dd, *J* = 8.8, 2.2 Hz , 1H), 7.97 (d, *J* = 2.2 Hz, 1H ); MS (70 eV) 276 ($M^+$, 100), 258 (95). EI-HRMS, m/e: calculated for $(M+H)^+$ $C_{12}H_{16}NO_2$ $Cl_2$ 276.055261, found 276.05430.

**m) 4-[Bis-(2-ethylsulfanyl-ethyl)-amino]-3-hydroxymethyl-benzaldehyde (5-17):** Yield: 84%. $R_f$ 0.45 (3:1 hexane:EtOAc). $^1$H NMR ($CDCl_3$, 400 MHz) δ 1.20 (t, *J* = 7.1 Hz, 6H), 2.48 (t, *J* = 7.7 Hz, 4H), 2.63 (t, *J* = 7.3 Hz, 4H), 3.33 (t, *J* = 7.3 Hz, 4H), 4.66 (s, 2H), 7.25 (d, *J* = 8.1 Hz, 1H), 7.63 (d, *J* = 8.1 Hz, 1H), 7.89 (s, 1H), 9.91 (s, 1H); MS (70 eV), 327.2 ($M^+$, 20), 89 (100). EI-HRMS, m/e: calculated for $M^+$ $C_{16}H_{25}NO_2S_2$ 327.13269, found 327.13400.

**n) 3-{4-[Bis-(2-ethylsulfanyl-ethyl)-amino]-3-hydroxymethyl-phenyl}-1-phenyl-propenone (5-18):** Yield: 31%. $R_f$ 0.55 (2:1 hexane:EtOAc). $^1$H NMR ($CDCl_3$, 400 MHz) δ 1.22 (t, *J* = 7.3 Hz, 6H), 2.50 (q, *J* = 7.3 Hz, 4H), 2.63 (t, *J* = 7.3 Hz, 4H), 3.27 (t, *J* = 7.3 Hz, 4H), 4.79 (s, 2H), 7.24 (d, *J* = 8.8 Hz, 2H), 7.47-7.63 (m, 5H), 7.78

(d, *J* = 16.1 Hz, 1H), 8.02 (d, *J* = 8.8 Hz, 2H); MS (70 eV), 430 ($M^+$, 100). EI-HRMS, m/e: calculated for $(M+H)^+$ $C_{24}H_{32}NO_2S_2$ 430.1869, found 430.1919.

**o) 4-(5-{4-[Bis-(2-ethylsulfanyl-ethyl)-amino]-3-hydroxymethyl-phenyl}-3-phenyl-4,5-dihydro-pyrazol-1-yl)-benzoic acid ethyl ester (5-19):** Yield: 37%. *Rf* 0.28 (3:1 hexane:EtOAc). $^1$H NMR ($CDCl_3$, 400 MHz) δ 1.19 (t, *J* = 7.3 Hz, 6H), 1.35 (t, *J* = 7.3 Hz, 3H), 2.48 (q, *J* = 7.3 Hz, 4H), 2.58 (t, *J* = 8.1 Hz, 4H), 3.17 (t, *J* = 7.3 Hz, 2H), 3.22 (dd, *J* = 16.9, 5.9 Hz, 1H), 3.88 (dd, *J* = 16.9, 12.5 Hz, 1H), 4.30 (q, *J* = 7.3 Hz, 2H), 4.80 (s, 2H), 5.35 (dd, *J* = 12.5, 5.9 Hz, 1H),7.04 (d, *J* = 9.53 Hz, 2H), 7.14 (s, 2H), 7.20 (s, 1H), 7.37-7.44 (m, 3H), 7.75 (d, *J* = 6.6 Hz, 2H), 7.87 (d, *J* = 8.8 Hz, 2H); MS (70 eV), 592 ($M^+$, 100). EI-HRMS, m/e: calculated for $M^+$ $C_{33}H_{42}N_3O_3S_2$ 592.266213, found 592.2632.

**p) 4-(5-{4-[Bis-(2-ethylsulfanyl-ethyl)-amino]-3-chloromethyl-phenyl}-3-phenyl-4,5-dihydro-pyrazol-1-yl)-benzoic acid ethyl ester (5-20):** Yield: 68%. *Rf* 0.41 (5:1 hexane:EtOAc). $^1$H NMR ($CDCl_3$, 400 MHz) δ 1.18 (t, *J* = 7.3 Hz, 6H), 1.34 (t, *J* = 7.3 Hz, 3H), 2.47 (q, *J* = 7.3 Hz, 4H), 2.54 (t, *J* = 8.1 Hz, 4H), 3.21 (t, *J* = 7.3 Hz, 2H), 3.24 (dd, *J* = 16.9, 5.9 Hz, 1H), 3.90 (dd, *J* = 16.9, 11.7 Hz, 1H), 4.30 (q, *J* = 7.3 Hz, 2H), 4.81 (s, 1H), 4.83 (s, 1H), 5.37 (dd, *J* = 11.7, 5.9 Hz, 1H), 7.03 (d, *J* = 8.3 Hz, 2H), 7.14 (d, *J* = 2.9 Hz, 2H), 7.37-7.48 (m, 4H), 7.75 (d, *J* = 8.8 Hz, 2H), 7.87 (d, *J* = 8.8 Hz, 2H).

**q) 1-Phenyl-3-[4-(1,4,7,10-tetrathia-13-aza-cyclopentadec-13-yl)-phenyl]-propenone (5-22):** A mixture of 4-(1,4,7,10-tetrathia-13-aza-cyclopentadec-13-yl)-benzaldehyde **5-21** (180 mg, 0.464 mmol), acetophenone (57 mg, 0.478 mmol), and freshly distilled piperidine (87 mg, 1.02 mmol) in ethanol was heated under nitrogen at reflux temperature for 48 hours. The precipitated orange solid was filtered off, and the

product purified on silica gel (hexane/ethyl acetate, gradient 20:1 to 5:1) providing 150 mg (0.31 mmol, 66%) of chalcone **5-22** as yellow solid. mp 113-115 °C. *Rf* 0.43 (4:1 hexane/EtOAc). 1H-NMR (CDCl3, 400 MHz) δ 2.73-2.87 (m, 16H), 3.64 (t, *J* = 7.7 Hz, 4H), 6.65 (t, *J* = 8.8 Hz, 2H), 7.35 (d, *J* = 15.4 Hz, 1H), 7.48-7.58 (m, 5H), 7.78 (d, *J* = 15.4 Hz, 1H), 8.00 (d, *J* = 8.8 Hz, 2H). MS (70 eV) 489.1 ($M^+$, 44), 295.1 (100), 235.1 (38), 105 (95). EI-HRMS, m/e: calculated for ($M^+$) $C_{25}H_{31}NOS_4$ 489.1288, found 489.1281.

### *5.6.1.1. Intermediate Products of Aldehydes and Chalcones for Sensors 5-2, 5-4 to 5-6.*

**r) 4-(1,4,7-Trithia-10-aza-cyclododec-10-yl)-benzaldehyd**e: Yield: 52%. *Rf* 0.41 (3:1 hexane:EtOAc). $^1$H-NMR ($CDCl_3$, 400 MHz) δ 2.83-2.91 (m, 12H), 3.69 (t, *J* = 7.3 Hz, 4H), 6.75 (d, *J* = 8.8 Hz, 2H), 7.74 (d, *J* = 8.8 Hz, 2H), 9.74 (s, 1H). MS (70 eV) 327 ($M^+$, 100). EI-HRMS, m/e: calculated for $(M+H)^+$ $C_{15}H_{21}NOS_3$ 327.0785, found 327.0816.

**s) 1-Phenyl-3-[4-(1,4,7-trithia-10-aza-cyclododec-10-yl)-phenyl]-propenone:** Yield: 76%. *Rf* 0.67 (2:1 hexane:EtOAc). $^1$H-NMR ($CDCl_3$, 400 MHz) δ 2.81-2.90 (m, 12H), 3.65 (t, *J* = 7.3 Hz, 4H), 6.73 (d, *J* = 8.8 Hz, 2H), 7.34 (d, *J* = 15.4 Hz, 1H), 7.49 (t, *J* = 7.3 Hz, 2H), *7*.54 (d, *J* = 8.8 Hz, 3H), 7.76 (d, *J* = 15.4 Hz, 1H), 8.00 (d, *J* = 7.3 Hz, 2H). MS (70 eV) 429.1 ($M^+$, 30). EI-HRMS, m/e: calculated for $(M+H)^+$ $C_{32}H_{37}N_3O_2S_3$ 429.1255, found 429.1209.

**t) 4-(1,7,11-Trithia-4-aza-cyclotetradec-4-yl)-benzaldehyde:** Yield: 91%. *Rf* 0.78 (4:1 hexane:EtOAc); $^1$H-NMR ($CDCl_3$, 400 MHz) δ 1.97 (quintet, *J* = 6.6 Hz, 4H), 2.70-2.83 (m, 12H), 3.73 (t, *J* = 7.3 Hz, 4H), 6.68 (d, *J* = 8.8 Hz, 2H), 7.74 (d, *J* = 8.8 Hz,

2H), 9.75 (s, 1H). MS (70 eV) 355.1 ($M^+$, 100), 160.1 (58). EI-HRMS, m/e: calculated for ($M^+$) $C_{17}H_{25}NOS_3$ 355.10983, found 355.10769.

**u) 1-Phenyl-3-[4-(1,7,11-trithia-4-aza-cyclotetradec-4-yl)-phenyl]-propenone:** Yield: 47%. *Rf* 0.45 (4:1 hexane:EtOAc); $^1$H-NMR ($CDCl_3$, 400 MHz) δ 1.97 (quintet, *J* = 6.6 Hz, 4H), 2.70-2.83 (m, 12H), 3.71-3.75 (m, 4H), 6.67 (d, *J* = 9.9 Hz, 2H), 7.33 (d, *J* = 15.4Hz, 1H), 7.49 (t, *J* = 7.7 Hz, 2H), 7.55 (d, *J* = 8.8 Hz, 2H), 7.73-7.79 (m, 2H), 8.00 (d, *J* = 7.1 Hz, 2H). MS (70 eV) 458.2 ($M^+$, 25), 418 (100). EI-HRMS, m/e: calculated for ($M^+$) $C_{25}H_{31}NOS_3$ 457.15678, found 457.15824.

**v) 4-(1,4,7-Trithia-11-aza-cyclotetradec-11-yl)-benzaldehyde:** Yield: 79%. *Rf* 0.75(4:1 hexane:EtOAc); $^1$H-NMR ($CDCl_3$, 400 MHz) δ 2.02 (quintet, *J* = 7.3 Hz, 4H), 2.65 (t, *J* = 7.3 Hz, 4H), 2.80 (bs, 8H), 3.58 (t, *J* = 7.3 Hz, 4H), 6.70 (d, *J* = 8.1 Hz, 2H), 7.73 (d, *J* = 8.1 Hz, 1H), 9.74 (s, 1H). MS (70 eV) 383 ($M^+$, 25). EI-HRMS, m/e: calculated for ($M^+$) $C_{17}H_{25}NOS_3$ 355.10983, found 355.10652.

**w) 1-Phenyl-3-[4-(1,4,7-trithia-11-aza-cyclotetradec-11-yl)-phenyl]-propenone:** Yield: 56%. *Rf* 0.34 (5:1 hexane:EtOAc); $^1$H-NMR ($CDCl_3$, 400 MHz) δ 2.01 (quintet, *J* = 7.3 Hz, 4H), 2.65 (t, *J* = 7.3 Hz, 4H), 2.79 (bs, 8H), 3.53 (t, *J* = 7.3 Hz, 4H), 6.68 (d, *J* = 8.1 Hz, 2H), 7.33 (d, *J* = 15.8 Hz, 1H), 7.47-7.56 (m, 5H),7.78 (d, *J* = 15.8 Hz, 1H), 8.00 (d, *J* = 8.1 Hz, 2H), 7.73-7.79 (m, 2H), 8.00 (d, *J* = 7.1 Hz, 2H). MS (70 eV) 458.2 ($M^+$, 25), 418 (100). EI-HRMS, m/e: calculated for ($M^+$) $C_{25}H_{31}NOS_3$ 457.15678, found 457.15824.

**x) 4-(1,5,9-Trithia-13-aza-cyclohexadec-13-yl)-benzaldehyde:** Yield: 89%. *Rf* 0.13 (5:1 hexane:EtOAc); $^1$H-NMR ($CDCl_3$, 400 MHz) δ 1.90-2.01 (m, 8H), 2.64 (t, *J* = 6.6 Hz, 4H), 2.71 (q, *J* = 7.1 Hz, 8H), 3.61 (t, *J* = 7.7 Hz, 4H), 6.68 (d, *J* = 8.8 Hz, 2H),

7.72 (d, *J* = 8.8 Hz, 2H), 9.73 (s, 1H). MS (70 eV) 383.2 ($M^+$, 100), 174.1 (58). EI-HRMS, m/e: calculated for ($M^+$) $C_{19}H_{29}NS_3O$ 383.14113, found 383.14047.

**y) 1-Phenyl-3-[4-(1,5,9-trithia-13-aza-cyclohexadec-13-yl)-phenyl]-propen-one:** Yield: 71%. *Rf* 0.28 (5:1 hexane:EtOAc); $^1$H-NMR ($CDCl_3$, 400 MHz) δ 1.89-2.01 (m, 8H), 2.64 (t, *J* = 6.6 Hz, 4H), 2.70 (q, *J* = 7.1 Hz, 8H), 3.57 (t, *J* = 7.1 Hz, 4H), 6.66 (d, *J* =8.8 Hz, 2H), 7.32 (d, *J* = 15.4 Hz, 1H), 7.44-7.56 (m, 5H), *7*.75 (d, *J* = 15.4 Hz, 1H), 8.00 (d, *J* = 8.8 Hz, 2H). MS (70 eV) 485.2 ($M^+$, 75), 174.1 (70). EI-HRMS, m/e: calculated for (M+) $C_{27}H_{35}NS_3O$ 485.18808, found 485.18668.

**z) 4-{3-[4-(1,4,7,10-Tetrathia-13-aza-cyclopentadec-13-yl)-phenyl]-acryloyl}-benzoic acid ethyl ester:** Yield: 57%. *Rf* 0.625 (2:1 hexane:EtOAc). $^1$H-NMR ($CDCl_3$, 300 MHz) δ 1.13 (t, *J* = 7.1 Hz, 6H), 3.13 (dd, *J* = 17.0 Hz, 7.1 Hz, 1H), 3.31 (q, *J* = 7.1 Hz, 4H), 3.77 (dd, *J* = 17.0 Hz, 12.6 Hz, 1H), 5.17 (dd, *J* = 12.6 Hz, 7.1 Hz, 1H), 6.61 (d, *J* = 8.8 Hz, 2H), 6.76 (t, *J* = 7.1 Hz, 1H), 7.08-7.21 (m, 5H), 7.30-7.40 (m, 4H), 7.72 (d, *J* = 7.1 Hz, 3H). MS (70 eV) 561.3 ($M^+$, 70), 367.2 (65). EI-HRMS, m/e: calculated for ($M^+$) $C_{28}H_{35}NS_4O_3$ 561.1500, found 561.1456.

### *5.6.2. Steady State Fluorescence Spectroscopy*

All sample solutions were filtered through 0.2 μm Teflon membrane filters to remove interfering dust particles or fibers. Fluorescence emission spectra were recorded with a PTI fluorimeter (path length 1 cm, cell volume 3.0 mL). The fluorescence spectra have been corrected for the spectral response of the detection system (emission correction file provided by instrument manufacturer) and for the spectral irradiance of the excitation channel (via calibrated photodiode). Quantum yields were determined using quinine

sulfate dihydrate in 1.0 N $H_2SO_4$ as fluorescence standard ($\Phi_f = 0.54 \pm 0.05$).[23] Mol-ratio titration: To a 5 μM solution of CTAP-1 in 10 mM PIPES (pH 7.20, 25°C) were stepwise added 0.1 molar equiv aliquots of $[Cu(I)(CH_3CN)_4]PF_6$ (5 mM stock solution in $CH_3CN$). After each addition the solution was equilibrated with stirring until no further increase of the emission intensity at 480 nm (excitation at 365 nm) was observed (typically 10 min). To minimize photobleaching by the incident light the emission intensity was checked by short scans (2 sec) in intervals of 20 sec. Upon equilibration the emission spectrum was acquired over the entire wavelength range (0.2 sec integration time/ 1 nm stepsize). In a control experiment addition of an equivalent amount of neat acetonitrile had no effect on the emission intensity.

### *5.6.3. Cell Culture Experiments*

Mouse NIH 3T3 cells were cultivated in Dulbecco's modified Eagle's medium (DMEM) supplemented with 5% calf serum and 200 mM L-glutamine. copper uptake studies were performed in the same media, but supplemented with 150 μM copper(II) chloride. For the staining experiments cells were incubated with 10 μM **CTAP-1** (in DMEM) for 50 minutes at 37 °C, washed with phosphate buffered saline (PBS), and fixed with 3.7% paraformaldehyde for 30 min before mounting on slides with ProLong (Molecular Probes). Immuofluorescence colocalization: NIH 3T3 cells were fixed (3.7% paraformaldehyde, 30 min), permeabilized (0.2% Triton X-100, 2 min), and incubated with either mouse anti-GS28 IgG1 (Stressgen) or mouse anti-OxPhos complex V IgG1 (Molecular Probes) primary antibodies (1:500 dilution, 1h), respectively, and goat anti-mouse IgG Alexa Fluor 546 (Molecular Probes) as a secondary antibody following a standard immunofluorescence protocol. After the last washing step, the cells were further

incubated with 10 μM **CTAP-1** (in PBS, filtered) for 50 minutes at room temperature. The cells were imaged with a Zeiss Axiovert fluorescence microscope equipped with a standard filter set (DAPI, FITC, RITC).

### *5.6.4. Synchrotron X-ray Fluorescence Microscopy (micro-XRF)*

Scanning x-ray fluorescence microscopy was performed at beamline 2-ID-D of the Advanced Photon Source at the Argonne National Laboratory.[24] Incident x-rays of 10 keV energy were chosen to excite elements from P to Zn. A Fresnel zone plate focused the x-ray beam to a spot size of $(0.2\ \mu m)^2$ on the specimen which was raster scanned.[21] X-ray fluorescence from the specimen was captured with an energy dispersive Ge detector. Spectral analysis of the fluorescence spectrum of each raster pixel provided then spatial images for each element.[16] At the hard x-ray regime, biological cells do not cause significant absorption nor beam spreading, hence no specimen thinning is required, and the fluorescence image represents a two-dimensional projection of the volumetric distribution for each element. Sample preparation: Cells were allowed to attach to the formvar layer of a gold electron microscopy (EM) grid. Upon treatment with **CTAP-1** as described above, cells were washed in PBS, fixed in methanol/acetone (50/50) at –20 deg C for 2 minutes, and then air dried.

### *5.6.5. Microprobe X-ray Absorption Near-Edge Structure (micro-XANES)*

Once an interesting area was identified in the x-ray fluorescence image, micro-XANES was performed by scanning the energy of the incident x-ray near the Cu K edge (~ 8.979 keV). The zone plate and the specimen remained stationary during the

measurement, which ensured that the illuminated area was fixed during the energy scan, although slight defocusing increased the spot size to about $(0.25\ \mu m)^2$.

## 5.7. References


1. Fahrni, C.; Yang, L.; Vanderveer, D., *J. Am. Chem. Soc.* **2003,** 125, (13), 3799.

2. Pearson, N.; Broom, N.; Ohanlon, P., *Tetrahedron Lett.* **1994,** 35, (22), 3771.

3. Sakamoto, H.; Ishikawa, J.; Mizuno, T.; Doi, K.; Otomo, M., *Chem. Lett.* **1993**, (4), 609.

4. Yang, L.; McRae, R.; Henary, M. M.; Fahrni, C. J., *Proc. Nat. Acad. Sci. U.S.A.* **2005,** in press.

5. Kamau, P.; Jordan, R., *Inorg. Chem.* **2001,** 40, (16), 3879.

6. Specfit; Binstead, R. A.; Zuberbuhler, A. D., Spectrum Software Associates, Marlborough MA 01752 **2001**.

7. Seksek, O.; Biwersi, J.; Verkman, A., *J. Biol. Chem.* **1995,** 270, (10), 4967.

8. Nelson, N., *Curr. Opin. Cell Biol.* **1992,** 4, 654.

9. Mellman, I., *J. Exp. Biol.* **1992,** 172, 39.

10. Mellman, I.; Fuchs, R.; Helenius, A., *Annu. Rev. Biochem.* **1986,** 55, 663.

11. McRae, R., Experiment data.

12. Hamza, I.; Prohaska, J.; Gitlin, J., *Proc. Natl. Acad. Sci. U.S.A.* **2003,** 100, (3), 1215.

13. Cobine, P.; Ojeda, L.; Rigby, K.; Winge, D., *J. Biol. Chem.* **2004,** 279, (14), 14447.

14. Fahrni, C. J., Experiment data.

15. Twining, B.; Baines, S.; Fisher, N.; Maser, J.; Vogt, S.; Jacobsen, C.; Tovar-Sanchez, A.; Sanudo-Wilhelmy, S., *Anal. Chem.* **2003,** 75, (15), 3806.

16. Maser, J.; Lai, B.; Yun, W.; Cai, Z.; Ilinski, P.; Rodrigues, W.; Legnini, D., *Mol. Biol. Cell* **1999,** 10, 10A.

17. Kau, L.; Spirasolomon, D.; Pennerhahn, J.; Hodgson, K.; Solomon, E., *J. Am. Chem. Soc.* **1987,** 109, (21), 6433.

18. Pickering, I.; George, G.; Dameron, C.; Kurz, B.; Winge, D.; Dance, I., *J. Am. Chem. Soc.* **1993,** 115, (21), 9498.

19. Smith, T.; Lerch, K.; Hodgson, K., *Inorg. Chem.* **1986,** 25, (26), 4677.

20. Corazza, A.; Harvey, I.; Sadler, P., *Eur. J. Biochem.* **1996,** 236, (2), 697.

21. Yun, W.; Lai, B.; Cai, Z.; Maser, J.; Legnini, D.; Gluskin, E.; Chen, Z.; Krasnoperova, A.; Vladimirsky, Y.; Cerrina, F.; Di Fabrizio, E.; Gentili, M., *Rev. Sci. Instrum.* **1999,** 70, (5), 2238.

22. Cocquet, G.; Ferroud, C.; Guy, A., *Tetrahedron* **2000,** 56, (19), 2975.

23. Demas, J.; Crosby, G., *J. Phys. Chem.* **1971,** 75, (8), 991.

24. Cai, Z.; Lai, B.; Yun, W.; Ilinski, P.; Legnini, D.; Maser, J.; Rodrigues, W., *Am. Inst. Phys. Proc.* **2000,** 507, 472.

# APPENDIX A

# CRYSTALLOGTRAPHIC DATA

**Table A-1.** Atomic Coordinates and Equivalent Isotropic Displacement Parameters for **2-1b**.

| Atom | x | y | z | U(eq) [Å$^2$] |
|---|---|---|---|---|
| N1 | -0.3737(2) | -0.03954(18) | -0.0164(3) | 0.0395(11) |
| N2 | -0.3470(2) | -0.08088(19) | 0.1076(3) | 0.0378(11) |
| N24 | -0.0621(2) | 0.18362(17) | -0.2508(3) | 0.0402(11) |
| N30 | -0.1599(3) | -0.1593(2) | 0.8703(3) | 0.0499(14) |
| C3 | -0.3225(3) | -0.0266(2) | 0.2057(4) | 0.0359(14) |
| C4 | -0.3332(3) | 0.0634(2) | 0.1549(4) | 0.0379(14) |
| C5 | -0.3604(3) | 0.0536(2) | -0.0029(4) | 0.0348(14) |
| C6 | -0.4117(3) | -0.0845(2) | -0.1352(4) | 0.0329(12) |
| C7 | -0.4449(3) | -0.0444(2) | -0.2608(4) | 0.0404(14) |
| C8 | -0.4846(3) | -0.0910(2) | -0.3772(4) | 0.0441(17) |
| C9 | -0.4916(3) | -0.1772(2) | -0.3723(4) | 0.0442(16) |
| C10 | -0.4576(3) | -0.2173(2) | -0.2472(4) | 0.0453(16) |
| C11 | -0.4179(3) | -0.1727(2) | -0.1304(4) | 0.0383(12) |
| C12 | -0.2889(2) | -0.0536(2) | 0.3472(4) | 0.0322(12) |
| C13 | -0.2665(3) | -0.1385(2) | 0.3785(4) | 0.0396(14) |
| C14 | -0.2343(3) | -0.1648(2) | 0.5126(4) | 0.0403(16) |
| C15 | -0.2228(3) | -0.1068(2) | 0.6205(4) | 0.0329(12) |
| C16 | -0.2448(3) | -0.0219(2) | 0.5895(4) | 0.0371(14) |
| C17 | -0.2752(3) | 0.0036(2) | 0.4559(4) | 0.0354(12) |
| C18 | -0.2837(3) | 0.0859(2) | -0.0724(3) | 0.0313(12) |
| C19 | -0.2977(3) | 0.1579(2) | -0.1554(4) | 0.0375(14) |
| C20 | -0.2257(3) | 0.1902(2) | -0.2127(4) | 0.0358(14) |
| C21 | -0.1341(3) | 0.1525(2) | -0.1919(3) | 0.0319(12) |
| C22 | -0.1195(3) | 0.0796(2) | -0.1083(3) | 0.0347(14) |
| C23 | -0.1922(3) | 0.0485(2) | -0.0517(3) | 0.0336(14) |
| C25 | -0.0749(3) | 0.2625(2) | -0.3273(4) | 0.0409(14) |
| C26 | -0.0582(3) | 0.3387(2) | -0.2322(4) | 0.0526(16) |
| C27 | 0.0312(3) | 0.1412(2) | -0.2353(4) | 0.0459(16) |
| C28 | 0.0277(3) | 0.0690(2) | -0.3353(4) | 0.0566(17) |
| C29 | -0.1888(3) | -0.1347(2) | 0.7597(4) | 0.0391(16) |

**Table A-2.** Interatomic Distances (Å) and Angles (°) for **2-1b**.

| | | | |
|---|---|---|---|
| N1 -N2 | 1.376(4) | C20-C21 | 1.397(6) |
| N1 -C5 | 1.493(4) | C21-C22 | 1.414(4) |
| N1 -C6 | 1.384(5) | C22-C23 | 1.370(6) |
| N2 -C3 | 1.291(5) | C25-C26 | 1.523(5) |
| N24-C21 | 1.375(5) | C27-C28 | 1.513(5) |
| N24-C25 | 1.456(4) | C4 -H4A | 0.9593 |
| N24-C27 | 1.455(5) | C4 -H4B | 0.9609 |
| N30-C29 | 1.155(5) | C5 -H5 | 0.9605 |
| C3 -C4 | 1.512(5) | C7 -H7 | 0.9607 |
| C3 -C12 | 1.449(5) | C8 -H8 | 0.9596 |
| C4 -C5 | 1.542(6) | C9 -H9 | 0.9596 |
| C5 -C18 | 1.501(6) | C10-H10 | 0.9611 |
| C6 -C7 | 1.389(5) | C11-H11 | 0.9604 |
| C6 -C11 | 1.404(5) | C13-H13 | 0.9597 |
| C7 -C8 | 1.384(5) | C14-H14 | 0.9600 |
| C8 -C9 | 1.374(5) | C16-H16 | 0.9595 |
| C9 -C10 | 1.387(5) | C17-H17 | 0.9596 |
| C10-C11 | 1.371(5) | C19-H19 | 0.9600 |
| C12-C13 | 1.403(5) | C20-H20 | 0.9605 |
| C12-C17 | 1.394(5) | C22-H22 | 0.9610 |
| C13-C14 | 1.377(5) | C23-H23 | 0.9603 |
| C14-C15 | 1.398(5) | C25-H25A | 0.9600 |
| C15-C16 | 1.402(5) | C25-H25B | 0.9606 |
| C15-C29 | 1.434(5) | C26-H26A | 0.9602 |
| C16-C17 | 1.366(5) | C26-H26B | 0.9596 |
| C18-C19 | 1.399(5) | C26-H26C | 0.9594 |
| C18-C23 | 1.393(6) | C27-H27A | 0.9603 |
| C19-C20 | 1.372(6) | C27-H27B | 0.9589 |
| C28-H28A | 0.9593 | C28-H28C | 0.9598 |
| C28-H28B | 0.9596 | | |
| N2-N1-C5 | 112.8(3) | C14-C15-C29 | 119.9(3) |
| N2-N1-C6 | 119.9(3) | C16-C15-C29 | 121.3(3) |
| C5-N1-C6 | 127.2(3) | C15-C16-C17 | 120.3(3) |
| N1-N2-C3 | 109.6(3) | C12-C17-C16 | 121.6(3) |

**Table A-2.** (continued).

| | | | |
|---|---|---|---|
| C21-N24-C25 | 121.1(3) | C5-C18-C19 | 122.2(4) |
| C21-N24-C27 | 121.7(3) | C5-C18-C23 | 121.8(3) |
| C25-N24-C27 | 117.1(3) | C19-C18-C23 | 116.0(4) |
| N2-C3-C4 | 112.8(3) | C18-C19-C20 | 122.2(4) |
| N2-C3-C12 | 120.9(3) | C19-C20-C21 | 121.7(3) |
| C4-C3-C12 | 126.3(3) | N24-C21-C20 | 122.0(3) |
| C3-C4-C5 | 103.3(3) | N24-C21-C22 | 121.5(4) |
| N1-C5-C4 | 100.9(3) | C20-C21-C22 | 116.4(4) |
| N1-C5-C18 | 112.7(3) | C21-C22-C23 | 121.0(4) |
| C4-C5-C18 | 113.4(3) | C18-C23-C22 | 122.7(3) |
| N1-C6-C7 | 121.5(3) | N24-C25-C26 | 111.9(3) |
| N1-C6-C11 | 120.0(3) | N24-C27-C28 | 112.7(3) |
| C7-C6-C11 | 118.5(3) | N30-C29-C15 | 177.8(4) |
| C6-C7-C8 | 120.1(3) | C3-C4-H4A | 111.14 |
| C7-C8-C9 | 121.4(3) | C3-C4-H4B | 111.11 |
| C8-C9-C10 | 118.4(3) | C5-C4-H4A | 111.12 |
| C9-C10-C11 | 121.3(3) | C5-C4-H4B | 111.14 |
| C6-C11-C10 | 120.2(3) | H4A-C4-H4B | 108.97 |
| C3-C12-C13 | 120.6(3) | N1-C5-H5 | 109.83 |
| C3-C12-C17 | 121.5(3) | C4-C5-H5 | 109.81 |
| C13-C12-C17 | 117.9(3) | C18-C5-H5 | 109.83 |
| C12-C13-C14 | 121.0(3) | C6-C7-H7 | 119.88 |
| C13-C14-C15 | 120.3(3) | C8-C7-H7 | 119.97 |
| C14-C15-C16 | 118.8(3) | C7-C8-H8 | 119.31 |
| C9-C8-H8 | 119.28 | N24-C25-H25A | 109.22 |
| C8-C9-H9 | 120.76 | N24-C25-H25B | 109.14 |
| C10-C9-H9 | 120.79 | C26-C25-H25A | 109.35 |
| C9-C10-H10 | 119.36 | C26-C25-H25B | 109.27 |
| C11-C10-H10 | 119.30 | H25A-C25-H25B | 107.88 |
| C6-C11-H11 | 119.87 | C25-C26-H26A | 109.47 |
| C10-C11-H11 | 119.95 | C25-C26-H26B | 109.45 |
| C12-C13-H13 | 119.40 | C25-C26-H26C | 109.53 |
| C14-C13-H13 | 119.56 | H26A-C26-H26B | 109.41 |
| C13-C14-H14 | 119.83 | H26A-C26-H26C | 109.50 |

**Table A-2.** (continued).

| | | | |
|---|---|---|---|
| C15-C14-H14 | 119.90 | H26B-C26-H26C | 109.46 |
| C15-C16-H16 | 119.81 | N24-C27-H27A | 109.10 |
| C17-C16-H16 | 119.84 | N24-C27-H27B | 109.08 |
| C12-C17-H17 | 119.19 | C28-C27-H27A | 108.97 |
| C16-C17-H17 | 119.21 | C28-C27-H27B | 109.01 |
| C18-C19-H19 | 118.94 | H27A-C27-H27B | 107.84 |
| C20-C19-H19 | 118.86 | C27-C28-H28A | 109.42 |
| C19-C20-H20 | 119.19 | C27-C28-H28B | 109.45 |
| C21-C20-H20 | 119.14 | C27-C28-H28C | 109.44 |
| C21-C22-H22 | 119.43 | H28A-C28-H28B | 109.49 |
| C23-C22-H22 | 119.56 | H28A-C28-H28C | 109.53 |
| C18-C23-H23 | 118.64 | H28B-C28-H28C | 109.50 |
| C22-C23-H23 | 118.67 | | |

**Table A-3.** Anisotropic Displacement Paremeters for **2-1b**.

| Atom | U(1,1) | U(2,2) | U(3,3) | U(2,3) | U(1,3) | U(1,2) |
|---|---|---|---|---|---|---|
| N1 | 0.061(2) | 0.0247(17) | 0.0334(19) | 0.0010(15) | 0.0116(16) | -0.0115(15) |
| N2 | 0.047(2) | 0.0319(19) | 0.0350(19) | 0.0047(16) | 0.0105(16) | -0.0062(15) |
| N24 | 0.049(2) | 0.0211(17) | 0.058(2) | 0.0076(16) | 0.0277(18) | 0.0020(15) |
| N30 | 0.072(3) | 0.034(2) | 0.045(2) | 0.0032(17) | 0.016(2) | 0.0065(18) |
| C3 | 0.044(3) | 0.027(2) | 0.038(2) | -0.0022(19) | 0.012(2) | -0.0010(18) |
| C4 | 0.048(3) | 0.027(2) | 0.043(2) | -0.0001(18) | 0.019(2) | -0.0034(18) |
| C5 | 0.046(3) | 0.022(2) | 0.040(2) | -0.0011(18) | 0.017(2) | -0.0012(19) |
| C6 | 0.036(2) | 0.028(2) | 0.037(2) | -0.0005(18) | 0.0130(18) | -0.0025(18) |
| C7 | 0.050(3) | 0.031(2) | 0.042(2) | 0.002(2) | 0.014(2) | -0.0068(19) |
| C8 | 0.051(3) | 0.039(3) | 0.043(3) | 0.005(2) | 0.012(2) | -0.004(2) |
| C9 | 0.050(3) | 0.043(3) | 0.041(2) | -0.007(2) | 0.013(2) | -0.005(2) |
| C10 | 0.049(3) | 0.027(2) | 0.057(3) | -0.006(2) | 0.006(2) | -0.0026(19) |
| C11 | 0.040(2) | 0.026(2) | 0.047(2) | 0.002(2) | 0.006(2) | -0.0026(18) |
| C12 | 0.035(2) | 0.026(2) | 0.038(2) | 0.0005(18) | 0.0134(19) | -0.0031(17) |
| C13 | 0.046(3) | 0.031(2) | 0.041(2) | -0.008(2) | 0.008(2) | -0.0059(19) |
| C14 | 0.047(3) | 0.027(2) | 0.047(3) | -0.0015(19) | 0.011(2) | -0.0025(19) |
| C15 | 0.040(2) | 0.027(2) | 0.034(2) | -0.0032(18) | 0.0130(18) | -0.0024(17) |
| C16 | 0.046(3) | 0.030(2) | 0.037(2) | -0.0066(19) | 0.013(2) | -0.0008(18) |
| C17 | 0.046(2) | 0.020(2) | 0.042(2) | 0.0010(18) | 0.0137(19) | 0.0028(18) |
| C18 | 0.040(2) | 0.023(2) | 0.032(2) | 0.0007(16) | 0.0105(18) | -0.0013(18) |
| C19 | 0.042(3) | 0.024(2) | 0.048(2) | 0.0066(18) | 0.013(2) | 0.0053(18) |
| C20 | 0.047(3) | 0.018(2) | 0.045(2) | 0.0075(18) | 0.016(2) | 0.0025(18) |
| C21 | 0.047(2) | 0.018(2) | 0.034(2) | -0.0036(16) | 0.0159(19) | -0.0019(17) |
| C22 | 0.047(3) | 0.025(2) | 0.035(2) | 0.0031(17) | 0.0154(19) | 0.0079(19) |
| C23 | 0.053(3) | 0.021(2) | 0.029(2) | 0.0055(17) | 0.0137(19) | 0.0032(19) |
| C25 | 0.051(3) | 0.033(2) | 0.041(2) | 0.0049(19) | 0.015(2) | -0.0088(19) |
| C26 | 0.066(3) | 0.031(2) | 0.063(3) | -0.003(2) | 0.019(2) | -0.006(2) |
| C27 | 0.050(3) | 0.040(3) | 0.050(2) | 0.004(2) | 0.016(2) | -0.006(2) |
| C28 | 0.066(3) | 0.036(3) | 0.076(3) | 0.001(2) | 0.033(3) | 0.006(2) |
| C29 | 0.049(3) | 0.027(2) | 0.043(3) | -0.006(2) | 0.014(2) | -0.0039(19) |

**Table A-4.** Atomic Coordinates and Equivalent Isotropic Displacement Parameters for **2-2a**.

| Atom | x | y | z | U(eq) [Å$^2$] |
|---|---|---|---|---|
| N1 | 0.12412(12) | 0.63512(6) | 0.81751(11) | 0.0287(3) |
| N2 | 0.20790(12) | 0.62022(6) | 0.95010(11) | 0.0273(3) |
| N24 | -0.26959(12) | 0.89244(6) | 0.48031(12) | 0.0296(4) |
| N30 | -0.30946(16) | 0.38872(8) | 0.40844(16) | 0.0552(5) |
| C3 | 0.29633(14) | 0.67017(7) | 1.00176(14) | 0.0256(4) |
| C4 | 0.28276(15) | 0.72617(8) | 0.90395(14) | 0.0346(4) |
| C5 | 0.16613(14) | 0.69903(7) | 0.77214(14) | 0.0297(4) |
| C6 | 0.03648(14) | 0.58422(7) | 0.73484(14) | 0.0269(4) |
| C7 | -0.03804(16) | 0.59607(8) | 0.59749(14) | 0.0332(5) |
| C8 | -0.12731(16) | 0.54584(8) | 0.51550(15) | 0.0362(5) |
| C9 | -0.14514(14) | 0.48279(8) | 0.56651(15) | 0.0320(4) |
| C10 | -0.07100(15) | 0.47067(8) | 0.70279(15) | 0.0332(5) |
| C11 | 0.01818(14) | 0.52044(7) | 0.78610(14) | 0.0308(4) |
| C12 | 0.39429(14) | 0.67155(7) | 1.14388(14) | 0.0273(4) |
| C13 | 0.38501(16) | 0.62425(7) | 1.23262(15) | 0.0324(5) |
| C14 | 0.48161(17) | 0.62414(8) | 1.36531(15) | 0.0383(5) |
| C15 | 0.58925(17) | 0.67175(8) | 1.41224(16) | 0.0401(5) |
| C16 | 0.59714(16) | 0.72003(9) | 1.32669(15) | 0.0381(5) |
| C17 | 0.50046(15) | 0.72037(8) | 1.19346(15) | 0.0335(5) |
| C18 | 0.05088(14) | 0.75068(7) | 0.69984(13) | 0.0256(4) |
| C19 | 0.04711(14) | 0.78977(7) | 0.59604(13) | 0.0271(4) |
| C20 | -0.05515(14) | 0.83772(7) | 0.52557(13) | 0.0262(4) |
| C21 | -0.16335(14) | 0.84766(7) | 0.55428(13) | 0.0237(4) |
| C22 | -0.15785(15) | 0.80865(7) | 0.66158(14) | 0.0282(4) |
| C23 | -0.05321(14) | 0.76189(7) | 0.73172(14) | 0.0285(4) |
| C25 | -0.26737(16) | 0.93859(7) | 0.37989(14) | 0.0319(4) |
| C26 | -0.32056(18) | 0.90518(9) | 0.24453(15) | 0.0433(5) |
| C27 | -0.38642(15) | 0.89852(8) | 0.50381(15) | 0.0316(4) |
| C28 | -0.36356(17) | 0.94959(9) | 0.61414(17) | 0.0422(5) |
| C29 | -0.23679(17) | 0.43048(9) | 0.47899(16) | 0.0397(5) |

**Table A-5.** Interatomic Distances (Å) and Angles (°) for **2-2a**.

| | | | |
|---|---|---|---|
| N1-N2 | 1.3785(16) | C20-C21 | 1.404(2) |
| N1-C5 | 1.4821(19) | C21-C22 | 1.410(2) |
| N1-C6 | 1.3798(19) | C22-C23 | 1.379(2) |
| N2-C3 | 1.2910(19) | C25-C26 | 1.508(2) |
| N24-C21 | 1.374(2) | C27-C28 | 1.514(2) |
| N24-C25 | 1.4545(19) | C4-H4A | 0.9605 |
| N24-C27 | 1.453(2) | C4-H4B | 0.9593 |
| N30-C29 | 1.146(2) | C5-H5 | 0.9606 |
| C3-C4 | 1.499(2) | C7-H7 | 0.9596 |
| C3-C12 | 1.463(2) | C8-H8 | 0.9604 |
| C4-C5 | 1.536(2) | C10-H10 | 0.9610 |
| C5-C18 | 1.511(2) | C11-H11 | 0.9600 |
| C6-C7 | 1.401(2) | C13-H13 | 0.9603 |
| C6-C11 | 1.404(2) | C14-H14 | 0.9595 |
| C7-C8 | 1.375(2) | C15-H15 | 0.9603 |
| C8-C9 | 1.388(2) | C16-H16 | 0.9594 |
| C9-C10 | 1.391(2) | C17-H17 | 0.9596 |
| C9-C29 | 1.435(2) | C19-H19 | 0.9600 |
| C10-C11 | 1.374(2) | C20-H20 | 0.9605 |
| C12-C13 | 1.396(2) | C22-H22 | 0.9603 |
| C12-C17 | 1.394(2) | C23-H23 | 0.9602 |
| C13-C14 | 1.379(2) | C25-H25A | 0.9593 |
| C14-C15 | 1.390(3) | C25-H25B | 0.9594 |
| C15-C16 | 1.374(2) | C26-H26A | 0.9593 |
| C16-C17 | 1.384(2) | C26-H26B | 0.9605 |
| C18-C19 | 1.384(2) | C26-H26C | 0.9601 |
| C18-C23 | 1.387(2) | C27-H27A | 0.9601 |
| C19-C20 | 1.380(2) | C27-H27B | 0.9596 |
| C28-H28A | 0.9596 | C28-H28C | 0.9593 |
| C28-H28B | 0.9601 | | |
| N2-N1-C5 | 113.09(11) | C13-C14-C15 | 120.05(15) |
| N2-N1-C6 | 119.74(11) | C14-C15-C16 | 119.76(15) |
| C5-N1-C6 | 125.03(11) | C15-C16-C17 | 120.40(16) |
| N1-N2-C3 | 108.71(11) | C12-C17-C16 | 120.57(15) |

**Table A-5.** (continued).

| | | | |
|---|---|---|---|
| C21-N24-C25 | 121.77(14) | C5-C18-C19 | 119.28(15) |
| C21-N24-C27 | 121.33(13) | C5-C18-C23 | 123.67(13) |
| C25-N24-C27 | 116.82(13) | C19-C18-C23 | 117.05(14) |
| N2-C3-C4 | 113.45(13) | C18-C19-C20 | 122.36(15) |
| N2-C3-C12 | 121.58(13) | C19-C20-C21 | 120.93(13) |
| C4-C3-C12 | 124.91(13) | N24-C21-C20 | 121.53(13) |
| C3-C4-C5 | 103.33(12) | N24-C21-C22 | 121.98(15) |
| N1-C5-C4 | 101.12(11) | C20-C21-C22 | 116.49(13) |
| N1-C5-C18 | 113.40(14) | C21-C22-C23 | 121.32(16) |
| C4-C5-C18 | 114.76(12) | C18-C23-C22 | 121.79(14) |
| N1-C6-C7 | 120.17(13) | N24-C25-C26 | 114.15(12) |
| N1-C6-C11 | 121.10(13) | N24-C27-C28 | 113.27(14) |
| C7-C6-C11 | 118.72(13) | N30-C29-C9 | 179.4(2) |
| C6-C7-C8 | 120.12(14) | C3-C4-H4A | 111.08 |
| C7-C8-C9 | 121.02(14) | C3-C4-H4B | 111.09 |
| C8-C9-C10 | 119.08(14) | C5-C4-H4A | 111.07 |
| C8-C9-C29 | 120.17(14) | C5-C4-H4B | 111.08 |
| C10-C9-C29 | 120.74(14) | H4A-C4-H4B | 109.12 |
| C9-C10-C11 | 120.61(14) | N1-C5-H5 | 109.04 |
| C6-C11-C10 | 120.45(13) | C4-C5-H5 | 109.08 |
| C3-C12-C13 | 121.40(14) | C18-C5-H5 | 109.11 |
| C3-C12-C17 | 120.17(13) | C6-C7-H7 | 119.97 |
| C13-C12-C17 | 118.42(14) | C8-C7-H7 | 119.91 |
| C12-C13-C14 | 120.73(15) | C7-C8-H8 | 119.50 |
| C9-C8-H8 | 119.48 | N24-C25-H25A | 108.68 |
| C9-C10-H10 | 119.70 | N24-C25-H25B | 108.71 |
| C11-C10-H10 | 119.69 | C26-C25-H25A | 108.73 |
| C6-C11-H11 | 119.81 | C26-C25-H25B | 108.71 |
| C10-C11-H11 | 119.74 | H25A-C25-H25B | 107.66 |
| C12-C13-H13 | 119.68 | C25-C26-H26A | 109.47 |
| C14-C13-H13 | 119.59 | C25-C26-H26B | 109.46 |
| C13-C14-H14 | 120.01 | C25-C26-H26C | 109.49 |
| C15-C14-H14 | 119.95 | H26A-C26-H26B | 109.50 |
| C14-C15-H15 | 120.12 | H26A-C26-H26C | 109.43 |

**Table A-5.** (continued).

| | | | |
|---|---|---|---|
| C16-C15-H15 | 120.11 | H26B-C26-H26C | 109.47 |
| C15-C16-H16 | 119.81 | N24-C27-H27A | 108.91 |
| C17-C16-H16 | 119.79 | N24-C27-H27B | 108.92 |
| C12-C17-H17 | 119.71 | C28-C27-H27A | 108.93 |
| C16-C17-H17 | 119.72 | C28-C27-H27B | 108.94 |
| C18-C19-H19 | 118.83 | H27A-C27-H27B | 107.73 |
| C20-C19-H19 | 118.81 | C27-C28-H28A | 109.48 |
| C19-C20-H20 | 119.55 | C27-C28-H28B | 109.52 |
| C21-C20-H20 | 119.52 | C27-C28-H28C | 109.47 |
| C21-C22-H22 | 119.30 | H28A-C28-H28B | 109.52 |
| C23-C22-H22 | 119.38 | H28A-C28-H28C | 109.38 |
| C18-C23-H23 | 119.12 | H28B-C28-H28C | 109.45 |
| C22-C23-H23 | 119.09 | | |

**Table A-6.** Anisotropic Displacement Paremeters for **2-2a**.

| Atom | U(1,1) | U(2,2) | U(3,3) | U(2,3) | U(1,3) | U(1,2) |
|---|---|---|---|---|---|---|
| N1 | 0.0300(6) | 0.0252(6) | 0.0241(6) | 0.0034(5) | 0.0073(6) | 0.0015(5) |
| N2 | 0.0276(6) | 0.0271(6) | 0.0240(6) | -0.0005(5) | 0.0097(5) | 0.0048(5) |
| N24 | 0.0295(6) | 0.0308(6) | 0.0288(7) | 0.0065(5) | 0.0141(6) | 0.0056(5) |
| N30 | 0.0461(9) | 0.0563(9) | 0.0581(10) | -0.0184(8) | 0.0206(8) | -0.0148(8) |
| C3 | 0.0235(7) | 0.0249(7) | 0.0287(8) | -0.0012(6) | 0.0126(6) | 0.0045(6) |
| C4 | 0.0269(7) | 0.0338(8) | 0.0347(8) | 0.0052(7) | 0.0079(7) | -0.0001(7) |
| C5 | 0.0288(7) | 0.0292(8) | 0.0309(8) | 0.0017(6) | 0.0141(7) | 0.0011(6) |
| C6 | 0.0227(7) | 0.0275(7) | 0.0290(8) | -0.0007(6) | 0.0112(6) | 0.0046(6) |
| C7 | 0.0365(8) | 0.0305(8) | 0.0286(8) | 0.0019(6) | 0.0122(7) | 0.0006(7) |
| C8 | 0.0343(8) | 0.0434(9) | 0.0242(8) | -0.0028(7) | 0.0086(7) | 0.0008(7) |
| C9 | 0.0255(7) | 0.0330(8) | 0.0348(8) | -0.0060(7) | 0.0122(7) | -0.0009(6) |
| C10 | 0.0297(8) | 0.0294(8) | 0.0378(9) | 0.0016(7) | 0.0139(7) | 0.0018(6) |
| C11 | 0.0279(7) | 0.0316(8) | 0.0276(8) | 0.0040(6) | 0.0089(7) | 0.0037(6) |
| C12 | 0.0261(7) | 0.0256(7) | 0.0293(8) | -0.0028(6) | 0.0124(7) | 0.0052(6) |
| C13 | 0.0353(8) | 0.0284(8) | 0.0323(8) | -0.0040(6) | 0.0152(7) | -0.0002(7) |
| C14 | 0.0455(9) | 0.0370(9) | 0.0291(8) | 0.0015(7) | 0.0152(8) | 0.0035(8) |
| C15 | 0.0374(9) | 0.0467(10) | 0.0273(8) | -0.0043(7) | 0.0081(7) | 0.0053(8) |
| C16 | 0.0320(8) | 0.0393(9) | 0.0354(9) | -0.0085(7) | 0.0099(7) | -0.0045(7) |
| C17 | 0.0329(8) | 0.0321(8) | 0.0337(8) | -0.0022(7) | 0.0145(7) | -0.0001(7) |
| C18 | 0.0243(7) | 0.0249(7) | 0.0243(7) | -0.0005(6) | 0.0089(6) | -0.0016(6) |
| C19 | 0.0240(7) | 0.0311(7) | 0.0269(7) | -0.0001(6) | 0.0126(6) | -0.0026(6) |
| C20 | 0.0291(7) | 0.0268(7) | 0.0223(7) | 0.0020(6) | 0.0119(6) | -0.0029(6) |
| C21 | 0.0246(7) | 0.0219(7) | 0.0211(7) | -0.0031(5) | 0.0081(6) | -0.0040(6) |
| C22 | 0.0288(7) | 0.0298(7) | 0.0291(8) | 0.0032(6) | 0.0163(7) | 0.0015(6) |
| C23 | 0.0326(8) | 0.0278(7) | 0.0261(7) | 0.0059(6) | 0.0149(7) | 0.0003(6) |
| C25 | 0.0342(8) | 0.0276(7) | 0.0309(8) | 0.0068(6) | 0.0130(7) | 0.0030(7) |
| C26 | 0.0417(9) | 0.0539(10) | 0.0270(8) | 0.0064(7) | 0.0104(8) | -0.0057(8) |
| C27 | 0.0253(7) | 0.0319(8) | 0.0349(8) | 0.0044(7) | 0.0121(7) | 0.0046(6) |
| C28 | 0.0429(9) | 0.0437(9) | 0.0454(10) | 0.0024(8) | 0.0253(9) | 0.0094(8) |
| C29 | 0.0333(8) | 0.0425(9) | 0.0419(9) | -0.0074(8) | 0.0169(8) | -0.0029(8) |

**Table A-7.** Atomic Coordinates and Equivalent Isotropic Displacement Parameters for **2-2b**.

| Atom | x | y | z | U(eq) [Å$^2$] |
|---|---|---|---|---|
| N1 | -0.06787(9) | 0.06408(14) | 0.13864(8) | 0.0241(4) |
| N5 | 0.01634(9) | 0.07279(14) | 0.12615(8) | 0.0247(4) |
| N12 | 0.40591(10) | 0.25132(15) | 0.45541(9) | 0.0284(5) |
| N24 | 0.20154(12) | -0.52406(17) | 0.04736(10) | 0.0414(6) |
| N32 | -0.46320(11) | 0.33296(17) | 0.26853(10) | 0.0395(6) |
| C2 | -0.09325(12) | 0.18807(17) | 0.15097(10) | 0.0222(5) |
| C3 | -0.02424(11) | 0.29998(17) | 0.14718(10) | 0.0239(5) |
| C4 | 0.06126(12) | 0.21484(17) | 0.14319(10) | 0.0234(5) |
| C6 | 0.15363(12) | 0.22069(16) | 0.22428(10) | 0.0211(5) |
| C7 | 0.15014(12) | 0.19552(16) | 0.30248(10) | 0.0222(5) |
| C8 | 0.23182(11) | 0.20609(16) | 0.37815(10) | 0.0217(5) |
| C9 | 0.32414(12) | 0.24055(16) | 0.38012(10) | 0.0219(5) |
| C10 | 0.32767(12) | 0.26289(16) | 0.30086(11) | 0.0230(5) |
| C11 | 0.24385(12) | 0.25518(16) | 0.22572(10) | 0.0218(5) |
| C13 | 0.50120(13) | 0.2877(2) | 0.45846(12) | 0.0366(6) |
| C14 | 0.55878(14) | 0.1624(3) | 0.45224(14) | 0.0533(8) |
| C15 | 0.40080(13) | 0.2280(2) | 0.53638(11) | 0.0344(6) |
| C16 | 0.36868(16) | 0.3558(2) | 0.56946(13) | 0.0495(8) |
| C17 | 0.05485(12) | -0.04618(17) | 0.10755(9) | 0.0231(5) |
| C18 | 0.14079(12) | -0.04214(19) | 0.09434(10) | 0.0265(5) |
| C19 | 0.17939(12) | -0.16293(19) | 0.07868(10) | 0.0287(5) |
| C20 | 0.13405(13) | -0.29104(18) | 0.07567(10) | 0.0282(5) |
| C21 | 0.04678(13) | -0.29398(19) | 0.08611(10) | 0.0300(6) |
| C22 | 0.00697(13) | -0.17422(17) | 0.10083(10) | 0.0263(5) |
| C23 | 0.17407(13) | -0.4189(2) | 0.06097(10) | 0.0323(6) |
| C25 | -0.17858(12) | 0.21307(17) | 0.16860(10) | 0.0224(5) |
| C26 | -0.23053(12) | 0.10350(18) | 0.18467(11) | 0.0268(5) |
| C27 | -0.30661(12) | 0.13204(18) | 0.20749(11) | 0.0272(5) |
| C28 | -0.33240(12) | 0.27006(18) | 0.21354(10) | 0.0239(5) |
| C29 | -0.28374(12) | 0.37864(18) | 0.19448(10) | 0.0276(6) |
| C30 | -0.20764(12) | 0.34893(18) | 0.17216(11) | 0.0266(5) |
| C31 | -0.40607(13) | 0.30304(18) | 0.24351(10) | 0.0272(6) |

**Table A-8.** Interatomic Distances (Å) and Angles (°) for **2-2b**.

| | | | |
|---|---|---|---|
| N1-N5 | 1.373(2) | C25-C26 | 1.406(3) |
| N1-C2 | 1.296(2) | C25-C30 | 1.386(2) |
| N5-C4 | 1.496(2) | C26-C27 | 1.385(3) |
| N5-C17 | 1.379(2) | C27-C28 | 1.398(2) |
| N12-C9 | 1.374(2) | C28-C29 | 1.391(3) |
| N12-C13 | 1.454(3) | C28-C31 | 1.442(3) |
| N12-C15 | 1.456(2) | C29-C30 | 1.382(3) |
| N24-C23 | 1.153(3) | C3-H3A | 0.9604 |
| N32-C31 | 1.149(3) | C3-H3B | 0.9597 |
| C2-C3 | 1.515(2) | C4-H4 | 0.9601 |
| C2-C25 | 1.458(3) | C7-H7 | 0.9605 |
| C3-C4 | 1.549(3) | C8-H8 | 0.9593 |
| C4-C6 | 1.510(2) | C10-H10 | 0.9595 |
| C6-C7 | 1.401(2) | C11-H11 | 0.9596 |
| C6-C11 | 1.386(3) | C13-H13A | 0.9602 |
| C7-C8 | 1.377(2) | C13-H13B | 0.9599 |
| C8-C9 | 1.413(3) | C14-H14A | 0.9605 |
| C9-C10 | 1.415(2) | C14-H14B | 0.9603 |
| C10-C11 | 1.386(2) | C14-H14C | 0.9592 |
| C13-C14 | 1.513(3) | C15-H15A | 0.9604 |
| C15-C16 | 1.517(3) | C15-H15B | 0.9596 |
| C17-C18 | 1.404(3) | C16-H16A | 0.9600 |
| C17-C22 | 1.405(2) | C16-H16B | 0.9601 |
| C18-C19 | 1.374(3) | C16-H16C | 0.9603 |
| C19-C20 | 1.397(3) | C18-H18 | 0.9604 |
| C20-C21 | 1.398(3) | C19-H19 | 0.9604 |
| C20-C23 | 1.437(3) | C21-H21 | 0.9597 |
| C21-C22 | 1.369(3) | C22-H22 | 0.9603 |
| C26-H26 | 0.9598 | C29-H29 | 0.9594 |
| C27-H27 | 0.9597 | C30-H30 | 0.9597 |
| N5-N1-C2 | 108.93(14) | C18-C17-C22 | 119.02(16) |
| N1-N5-C4 | 113.21(13) | C17-C18-C19 | 120.15(17) |
| N1-N5-C17 | 119.42(14) | C18-C19-C20 | 120.76(18) |
| C4-N5-C17 | 127.10(15) | C19-C20-C21 | 118.86(17) |

**Table A-8.** (continued).

| | | | |
|---|---|---|---|
| C9-N12-C13 | 121.98(15) | C19-C20-C23 | 121.73(19) |
| C9-N12-C15 | 121.28(16) | C21-C20-C23 | 119.41(17) |
| C13-N12-C15 | 116.74(15) | C20-C21-C22 | 120.95(17) |
| N1-C2-C3 | 113.03(16) | C17-C22-C21 | 120.16(19) |
| N1-C2-C25 | 122.13(16) | N24-C23-C20 | 176.6(2) |
| C3-C2-C25 | 124.82(15) | C2-C25-C26 | 121.91(15) |
| C2-C3-C4 | 102.90(13) | C2-C25-C30 | 119.08(16) |
| N5-C4-C3 | 100.13(14) | C26-C25-C30 | 118.99(17) |
| N5-C4-C6 | 112.44(13) | C25-C26-C27 | 120.12(16) |
| C3-C4-C6 | 113.34(14) | C26-C27-C28 | 119.83(17) |
| C4-C6-C7 | 120.30(17) | C27-C28-C29 | 120.25(17) |
| C4-C6-C11 | 122.55(15) | C27-C28-C31 | 120.97(16) |
| C7-C6-C11 | 117.12(15) | C29-C28-C31 | 118.71(16) |
| C6-C7-C8 | 122.13(17) | C28-C29-C30 | 119.39(16) |
| C7-C8-C9 | 121.08(15) | C25-C30-C29 | 121.34(17) |
| N12-C9-C8 | 121.37(15) | N32-C31-C28 | 177.89(19) |
| N12-C9-C10 | 122.08(17) | C2-C3-H3A | 111.15 |
| C8-C9-C10 | 116.55(15) | C2-C3-H3B | 111.14 |
| C9-C10-C11 | 121.20(18) | C4-C3-H3A | 111.17 |
| C6-C11-C10 | 121.88(16) | C4-C3-H3B | 111.24 |
| N12-C13-C14 | 112.99(17) | H3A-C3-H3B | 109.15 |
| N12-C15-C16 | 113.19(16) | N5-C4-H4 | 110.16 |
| N5-C17-C18 | 121.35(16) | C3-C4-H4 | 110.17 |
| N5-C17-C22 | 119.63(17) | C6-C4-H4 | 110.22 |
| C6-C7-H7 | 118.98 | H15A-C15-H15B | 107.80 |
| C8-C7-H7 | 118.89 | C15-C16-H16A | 109.47 |
| C7-C8-H8 | 119.49 | C15-C16-H16B | 109.49 |
| C9-C8-H8 | 119.43 | C15-C16-H16C | 109.46 |
| C9-C10-H10 | 119.38 | H16A-C16-H16B | 109.45 |
| C11-C10-H10 | 119.42 | H16A-C16-H16C | 109.47 |
| C6-C11-H11 | 119.05 | H16B-C16-H16C | 109.48 |
| C10-C11-H11 | 119.06 | C17-C18-H18 | 119.97 |
| N12-C13-H13A | 109.03 | C19-C18-H18 | 119.88 |
| N12-C13-H13B | 108.99 | C18-C19- H19 | 119.59 |

**Table A-8.** (continued).

| | | | |
|---|---|---|---|
| C14-C13-H13A | 109.00 | C20-C19-H19 | 119.64 |
| C14-C13-H13B | 109.02 | C20-C21-H21 | 119.51 |
| H13A-C13-H13B | 107.66 | C22-C21-H21 | 119.55 |
| C13-C14-H14A | 109.45 | C17-C22-H22 | 119.90 |
| C13-C14-H14B | 109.53 | C21-C22-H22 | 119.94 |
| C13-C14-H14C | 109.48 | C25-C26-H26 | 119.90 |
| H14-C14A-H14B | 109.51 | C27-C26-H26 | 119.98 |
| H14A-C14-H14C | 109.45 | C26-C27-H27 | 120.04 |
| H14B-C14-H14C | 109.42 | C26-C27-H27 | 120.13 |
| N12-C15-H15A | 108.91 | C28-C29-H29 | 120.33 |
| N12-C15-H15B | 108.93 | C30-C29-H29 | 120.28 |
| C16-C15-H15A | 108.94 | C25-C30-H30 | 119.32 |
| C16-C15-H15B | 108.93 | C29-C30-H30 | 119.33 |

**Table A-9.** Anisotropic Displacement Paremeters for **2-2b**.

| Atom | U(1,1) | U(2,2) | U(3,3) | U(2,3) | U(1,3) | U(1,2) |
|---|---|---|---|---|---|---|
| N1 | 0.0202(8) | 0.0331(8) | 0.0197(7) | -0.0018(6) | 0.0090(6) | 0.0001(6) |
| N5 | 0.0207(7) | 0.0297(8) | 0.0253(7) | -0.0049(7) | 0.0111(6) | -0.0011(6) |
| N12 | 0.0197(8) | 0.0445(9) | 0.0205(7) | 0.0000(7) | 0.0080(6) | -0.0038(7) |
| N24 | 0.0510(11) | 0.0430(10) | 0.0354(9) | 0.0046(8) | 0.0231(9) | 0.0148(8) |
| N32 | 0.0351(10) | 0.0520(11) | 0.0386(9) | -0.0048(8) | 0.0224(8) | -0.0035(8) |
| C2 | 0.0223(9) | 0.0266(9) | 0.0154(8) | -0.0002(7) | 0.0056(7) | -0.0001(7) |
| C3 | 0.0216(9) | 0.0285(10) | 0.0200(8) | 0.0011(7) | 0.0071(7) | 0.0014(7) |
| C4 | 0.0242(9) | 0.0279(9) | 0.0192(8) | 0.0013(7) | 0.0101(8) | -0.0010(7) |
| C6 | 0.0223(9) | 0.0213(8) | 0.0198(8) | 0.0007(7) | 0.0090(7) | 0.0012(7) |
| C7 | 0.0195(9) | 0.0239(9) | 0.0243(9) | 0.0010(7) | 0.0103(8) | -0.0011(7) |
| C8 | 0.0236(9) | 0.0253(9) | 0.0189(8) | 0.0019(7) | 0.0116(7) | 0.0005(7) |
| C9 | 0.0210(9) | 0.0223(9) | 0.0210(9) | 0.0011(7) | 0.0075(7) | 0.0014(7) |
| C10 | 0.0208(9) | 0.0255(9) | 0.0248(9) | -0.0001(8) | 0.0117(8) | -0.0016(7) |
| C11 | 0.0246(9) | 0.0243(9) | 0.0202(8) | 0.0030(7) | 0.0129(8) | 0.0018(7) |
| C13 | 0.0250(10) | 0.0560(13) | 0.0251(10) | 0.0002(9) | 0.0068(8) | -0.0110(9) |
| C14 | 0.0284(11) | 0.0859(18) | 0.0483(13) | 0.0222(13) | 0.0188(10) | 0.0143(11) |
| C15 | 0.0257(10) | 0.0520(12) | 0.0208(9) | 0.0013(9) | 0.0050(8) | -0.0059(9) |
| C16 | 0.0571(14) | 0.0608(14) | 0.0419(12) | -0.0180(11) | 0.0319(11) | -0.0234(11) |
| C17 | 0.0230(9) | 0.0307(10) | 0.0123(8) | -0.0004(7) | 0.0040(7) | 0.0029(7) |
| C18 | 0.0245(9) | 0.0351(10) | 0.0189(8) | -0.0039(8) | 0.0082(8) | -0.0012(8) |
| C19 | 0.0223(9) | 0.0439(11) | 0.0180(8) | -0.0021(8) | 0.0066(8) | 0.0042(8) |
| C20 | 0.0321(10) | 0.0355(10) | 0.0155(8) | 0.0012(8) | 0.0084(8) | 0.0098(8) |
| C21 | 0.0365(11) | 0.0302(10) | 0.0244(9) | 0.0012(8) | 0.0139(9) | 0.0024(8) |
| C22 | 0.0248(9) | 0.0327(10) | 0.0226(9) | 0.0010(8) | 0.0111(8) | 0.0015(8) |
| C23 | 0.0359(11) | 0.0401(12) | 0.0209(9) | 0.0041(9) | 0.0118(9) | 0.0108(9) |
| C25 | 0.0194(9) | 0.0289(9) | 0.0159(8) | -0.0009(7) | 0.0044(7) | -0.0004(7) |
| C26 | 0.0261(9) | 0.0240(9) | 0.0296(9) | -0.0016(8) | 0.0109(8) | -0.0007(7) |
| C27 | 0.0248(9) | 0.0298(10) | 0.0273(9) | 0.0026(8) | 0.0112(8) | -0.0025(8) |
| C28 | 0.0187(9) | 0.0319(10) | 0.0188(8) | -0.0017(8) | 0.0056(7) | -0.0004(7) |
| C29 | 0.0281(10) | 0.0252(9) | 0.0310(10) | -0.0020(8) | 0.0138(8) | 0.0011(8) |
| C30 | 0.0260(9) | 0.0272(9) | 0.0284(9) | 0.0007(8) | 0.0130(8) | -0.0017(8) |
| C31 | 0.0248(10) | 0.0344(10) | 0.0217(9) | -0.0011(8) | 0.0089(8) | -0.0027(8) |

**Table A-10.** Atomic Coordinates and Equivalent Isotropic Displacement Parameters for **2-2c**.

| Atom | x | y | z | U(eq) [Å$^2$] |
|---|---|---|---|---|
| O32 | -0.0295(2) | -0.58239(12) | -0.21442(5) | 0.0444(5) |
| O33 | -0.0129(2) | -0.74960(11) | -0.18695(4) | 0.0376(5) |
| N1 | 1.0148(2) | -0.76302(13) | -0.34345(5) | 0.0325(5) |
| N2 | 0.8472(2) | -0.71625(13) | -0.32538(5) | 0.0318(5) |
| N24 | 0.9308(3) | -1.18695(14) | -0.46215(5) | 0.0377(6) |
| N30 | 1.6291(4) | -0.44899(18) | -0.45626(7) | 0.0677(8) |
| C3 | 0.7747(3) | -0.78526(15) | -0.30001(5) | 0.0290(6) |
| C4 | 0.8954(3) | -0.89120(16) | -0.29753(6) | 0.0311(6) |
| C5 | 1.0577(3) | -0.87714(15) | -0.33019(6) | 0.0292(6) |
| C6 | 1.1364(3) | -0.70035(15) | -0.36767(5) | 0.0302(6) |
| C7 | 1.3239(3) | -0.74179(16) | -0.38192(6) | 0.0333(6) |
| C8 | 1.4489(3) | -0.67773(17) | -0.40503(6) | 0.0364(6) |
| C9 | 1.3892(3) | -0.57115(17) | -0.41495(6) | 0.0397(7) |
| C10 | 1.2004(4) | -0.53098(18) | -0.40136(7) | 0.0495(8) |
| C11 | 1.0754(3) | -0.59373(17) | -0.37805(7) | 0.0427(7) |
| C12 | 0.5925(3) | -0.75729(15) | -0.27690(5) | 0.0298(6) |
| C13 | 0.4926(3) | -0.65561(16) | -0.28213(6) | 0.0351(6) |
| C14 | 0.3193(3) | -0.62996(16) | -0.26076(6) | 0.0352(6) |
| C15 | 0.2402(3) | -0.70413(15) | -0.23353(6) | 0.0299(6) |
| C16 | 0.3393(3) | -0.80501(16) | -0.22788(6) | 0.0320(6) |
| C17 | 0.5132(3) | -0.83154(16) | -0.24965(6) | 0.0322(6) |
| C18 | 1.0286(3) | -0.95644(15) | -0.36570(5) | 0.0265(5) |
| C19 | 1.1862(3) | -1.03073(15) | -0.37390(6) | 0.0316(6) |
| C20 | 1.1577(3) | -1.10609(16) | -0.40541(6) | 0.0329(6) |
| C21 | 0.9661(3) | -1.11169(15) | -0.43088(5) | 0.0296(6) |
| C22 | 0.8076(3) | -1.03500(16) | -0.42267(6) | 0.0321(6) |
| C23 | 0.8396(3) | -0.96052(15) | -0.39113(6) | 0.0312(6) |
| C25 | 1.0823(4) | -1.2714(2) | -0.47058(7) | 0.0552(8) |
| *C26' | 1.1725(5) | -1.2654(3) | -0.51115(10) | 0.0629(9) |
| C27 | 0.7315(3) | -1.18659(17) | -0.48846(6) | 0.0385(7) |
| C28 | 0.7202(4) | -1.09903(18) | -0.52127(6) | 0.0454(7) |
| C29 | 1.5218(4) | -0.50368(18) | -0.43832(7) | 0.0479(8) |

**Table A-10.** (continued).

| | | | | |
|---|---|---|---|---|
| C31 | 0.0536(3) | -0.67105(16) | -0.21126(6) | 0.0320(6) |
| C34 | -0.1908(3) | -0.72128(18) | -0.16313(6) | 0.0414(7) |
| C35 | -0.2434(4) | -0.8202(2) | -0.13965(8) | 0.0685(11) |
| *C26 | 1.0806(19) | -1.3319(10) | -0.5057(3) | 0.050(3) |

Starred Atom sites have a S.O.F less than 1.0

**Table A-11.** Interatomic Distances (Å) and Angles (°) for **2-2c**.

| | | | |
|---|---|---|---|
| O32-C31 | 1.207(2) | C16-C17 | 1.390(3) |
| O33-C31 | 1.336(2) | C18-C19 | 1.388(3) |
| O33-C34 | 1.455(2) | C18-C23 | 1.391(3) |
| N1-N2 | 1.374(2) | C19-C20 | 1.382(3) |
| N1-C5 | 1.483(2) | C20-C21 | 1.405(3) |
| N1-C6 | 1.377(2) | C21-C22 | 1.412(3) |
| N2-C3 | 1.292(2) | C22-C23 | 1.377(3) |
| N24-C21 | 1.379(2) | C25-C26' | 1.482(4) |
| N24-C25 | 1.449(3) | C25-C26 | 1.362(11) |
| N24-C27 | 1.457(3) | C27-C28 | 1.512(3) |
| N30-C29 | 1.145(3) | C34-C35 | 1.486(3) |
| C3-C4 | 1.504(3) | C4-H4A | 0.9603 |
| C3-C12 | 1.462(3) | C4-H4B | 0.9593 |
| C4-C5 | 1.543(3) | C5-H5 | 1.0003 |
| C5-C18 | 1.510(3) | C7-H7 | 0.9599 |
| C6-C7 | 1.397(3) | C8-H8 | 0.9605 |
| C6-C11 | 1.397(3) | C10-H10 | 0.9602 |
| C7-C8 | 1.378(3) | C11-H11 | 0.9594 |
| C8-C9 | 1.391(3) | C13-H13 | 0.9610 |
| C9-C10 | 1.390(3) | C14-H14 | 0.9600 |
| C9-C29 | 1.437(3) | C16-H16 | 0.9596 |
| C10-C11 | 1.373(3) | C17-H17 | 0.9604 |
| C12-C13 | 1.401(3) | C19-H19 | 0.9610 |
| C12-C17 | 1.392(3) | C20-H20 | 0.9600 |
| C13-C14 | 1.377(3) | C22-H22 | 0.9603 |
| C14-C15 | 1.391(3) | C23-H23 | 0.9606 |
| C15-C16 | 1.391(3) | C25-H25B | 1.1897 |
| C15-C31 | 1.485(3) | C25-H25C | 1.0642 |
| C26-H26C | 0.9609 | C28-H28A | 0.9594 |
| C26-H26B | 0.9601 | C28-H28B | 0.9600 |
| C26-H26A | 0.9612 | C28-H28C | 0.9598 |
| C26'-H26F | 0.9607 | C34-H34B | 0.9600 |
| C26'-H26E | 0.9593 | C34-H34A | 0.9596 |
| C26'-H26D | 0.9594 | C35-H35A | 0.9596 |

**Table A-11.** (continued).

| | | | |
|---|---|---|---|
| C27-H27A | 0.9605 | C35-H35B | 0.9597 |
| C27-H27B | 0.9599 | C35-H35C | 0.9602 |
| C31-O33-C34 | 115.82(15) | C12-C13-C14 | 120.51(18) |
| N2-N1-C5 | 113.39(14) | C13-C14-C15 | 120.81(18) |
| N2-N1-C6 | 119.56(15) | C14-C15-C16 | 119.13(18) |
| C5-N1-C6 | 126.70(15) | C14-C15-C31 | 118.08(17) |
| N1-N2-C3 | 108.87(15) | C16-C15-C31 | 122.79(17) |
| C21-N24-C25 | 123.45(18) | C15-C16-C17 | 120.23(18) |
| C21-N24-C27 | 120.63(17) | C12-C17-C16 | 120.65(18) |
| C25-N24-C27 | 115.91(17) | C5-C18-C19 | 121.83(16) |
| N2-C3-C4 | 113.44(16) | C5-C18-C23 | 121.44(17) |
| N2-C3-C12 | 120.52(16) | C19-C18-C23 | 116.70(16) |
| C4-C3-C12 | 126.04(16) | C18-C19-C20 | 122.13(17) |
| C3-C4-C5 | 103.04(15) | C19-C20-C21 | 121.49(17) |
| N1-C5-C4 | 101.04(14) | N24-C21-C20 | 123.06(17) |
| N1-C5-C18 | 112.21(15) | N24-C21-C22 | 120.91(17) |
| C4-C5-C18 | 114.23(15) | C20-C21-C22 | 116.03(16) |
| N1-C6-C7 | 120.67(17) | C21-C22-C23 | 121.48(17) |
| N1-C6-C11 | 120.48(17) | C18-C23-C22 | 122.15(17) |
| C7-C6-C11 | 118.85(17) | N24-C25-C26' | 116.1(2) |
| C6-C7-C8 | 120.54(18) | N24-C25-C26 | 126.1(5) |
| C7-C8-C9 | 120.53(18) | N24-C27-C28 | 113.87(17) |
| C8-C9-C10 | 118.69(18) | N30-C29-C9 | 178.7(2) |
| C8-C9-C29 | 120.51(18) | O32-C31-O33 | 123.10(18) |
| C10-C9-C29 | 120.8(2) | O32-C31-C15 | 123.91(18) |
| C9-C10-C11 | 121.3(2) | O33-C31-C15 | 112.98(16) |
| C6-C11-C10 | 120.06(19) | O33-C34-C35 | 107.02(17) |
| C3-C12-C13 | 120.58(16) | C3-C4-H4A | 111.18 |
| C3-C12-C17 | 120.74(17) | C3-C4-H4B | 111.16 |
| C13-C12-C17 | 118.67(17) | C5-C4-H4A | 111.09 |
| C5-C4-H4B | 111.11 | C22-C23-H23 | 118.99 |
| H4A-C4-H4B | 109.17 | N24-C25-H25B | 112.15 |
| N1-C5-H5 | 109.69 | N24-C25-H25C | 95.69 |
| C4-C5-H5 | 109.59 | H25B-C25-H25C | 143.26 |

**Table A-11.** (continued).

| | | | |
|---|---|---|---|
| C18-C5-H5 | 109.75 | H26A-C26-H26B | 109.40 |
| C6-C7-H7 | 119.78 | H26A-C26-H26C | 109.38 |
| C8-C7-H7 | 119.67 | H26B-C26-H26C | 109.38 |
| C7-C8-H8 | 119.76 | C25-C26-H26A | 109.49 |
| C9-C8-H8 | 119.70 | C25-C26-H26B | 109.62 |
| C9 C10-H10 | 119.36 | C25-C26-H26C | 109.56 |
| C11-C10-H10 | 119.34 | H26D-C26'-H26E | 109.52 |
| C6-C11-H11 | 120.00 | H26D-C26'-H26F | 109.48 |
| C10-C11-H11 | 119.94 | H26E-C26'-H26F | 109.43 |
| C12-C13-H13 | 119.73 | C25-C26'-H26D | 109.48 |
| C14-C13-H13 | 119.76 | C25-C26'-H26E | 109.50 |
| C13-C14-H14 | 119.57 | C25-C26'-H26F | 109.41 |
| C15-C14-H14 | 119.62 | C28-C27-H27A | 108.84 |
| C15-C16-H16 | 119.91 | N24-C27-H27A | 108.75 |
| C17-C16-H16 | 119.86 | N24-C27-H27B | 108.77 |
| C12-C17-H17 | 119.64 | C28-C27-H27B | 108.81 |
| C16-C17-H17 | 119.71 | H27A-C27- H27B | 107.62 |
| C18-C19-H19 | 118.91 | C27-C28-H28B | 109.42 |
| C20-C19-H19 | 118.96 | C27-C28-H28A | 109.45 |
| C19-C20-H20 | 119.26 | H28A-C28-H28B | 109.48 |
| C21-C20-H20 | 119.25 | H28A-C28- H28C | 109.48 |
| C21-C22-H22 | 119.20 | C27-C28-H28C | 109.51 |
| C23-C22-H22 | 119.33 | H28B-C28-H28C | 109.48 |
| C18-C23-H23 | 118.86 | C35-C34-H34A | 110.32 |
| C35-C34-H34B | 110.35 | C34-C35-H35A | 109.44 |
| O33-C34-H34A | 110.37 | C34-C35-H35B | 109.43 |
| O33-C34-H34B | 110.30 | C34-C35-H35C | 109.42 |
| H34A-C34-H34B | 108.48 | H35A-C35-H35B | 109.54 |
| H35B-C35-H35C | 109.53 | H35A-C35-H35C | 109.48 |

**Table A-12.** Anisotropic Displacement Paremeters for **2-2c**.

| Atom | U(1,1) | U(2,2) | U(3,3) | U(2,3) | U(1,3) | U(1,2) |
|---|---|---|---|---|---|---|
| O32 | 0.0433(8) | 0.0356(8) | 0.0563(9) | -0.0031(7) | 0.0153(7) | 0.0072(7) |
| O33 | 0.0357(8) | 0.0390(8) | 0.0398(8) | -0.0023(6) | 0.0129(6) | 0.0022(6) |
| N1 | 0.0313(9) | 0.0297(9) | 0.0377(9) | -0.0009(7) | 0.0109(7) | 0.0011(7) |
| N2 | 0.0276(8) | 0.0351(9) | 0.0330(8) | -0.0041(7) | 0.0051(7) | -0.0007(7) |
| N24 | 0.0418(10) | 0.0374(10) | 0.0336(9) | -0.0047(8) | 0.0013(8) | 0.0060(8) |
| N30 | 0.0899(17) | 0.0552(13) | 0.0615(13) | 0.0031(11) | 0.0266(12) | -0.0260(12) |
| C3 | 0.0281(10) | 0.0325(10) | 0.0264(9) | -0.0044(8) | 0.0014(8) | -0.0031(8) |
| C4 | 0.0296(10) | 0.0339(11) | 0.0300(10) | -0.0010(8) | 0.0042(8) | -0.0022(8) |
| C5 | 0.0258(10) | 0.0314(10) | 0.0304(10) | 0.0015(8) | 0.0032(8) | 0.0009(8) |
| C6 | 0.0305(10) | 0.0314(10) | 0.0288(10) | -0.0015(8) | 0.0033(8) | -0.0040(8) |
| C7 | 0.0344(10) | 0.0313(11) | 0.0348(10) | -0.0005(9) | 0.0067(8) | -0.0022(8) |
| C8 | 0.0370(11) | 0.0404(12) | 0.0328(10) | -0.0029(9) | 0.0090(9) | -0.0069(9) |
| C9 | 0.0490(13) | 0.0371(12) | 0.0340(11) | 0.0001(9) | 0.0100(9) | -0.0095(10) |
| C10 | 0.0594(14) | 0.0337(12) | 0.0575(14) | 0.0112(11) | 0.0178(12) | 0.0029(11) |
| C11 | 0.0429(12) | 0.0366(12) | 0.0503(13) | 0.0046(10) | 0.0138(10) | 0.0061(10) |
| C12 | 0.0276(10) | 0.0329(11) | 0.0287(9) | -0.0064(8) | 0.0013(8) | -0.0029(8) |
| C13 | 0.0348(11) | 0.0342(11) | 0.0370(11) | 0.0018(9) | 0.0069(9) | -0.0028(8) |
| C14 | 0.0340(11) | 0.0321(11) | 0.0399(11) | -0.0027(9) | 0.0053(9) | 0.0022(9) |
| C15 | 0.0278(10) | 0.0311(10) | 0.0308(10) | -0.0073(8) | 0.0018(8) | -0.0010(8) |
| C16 | 0.0336(11) | 0.0330(11) | 0.0298(10) | -0.0023(8) | 0.0048(8) | -0.0035(8) |
| C17 | 0.0327(10) | 0.0313(11) | 0.0327(10) | -0.0061(8) | 0.0040(8) | 0.0008(8) |
| C18 | 0.0247(9) | 0.0293(10) | 0.0262(9) | 0.0028(8) | 0.0062(7) | -0.0009(7) |
| C19 | 0.0262(10) | 0.0343(11) | 0.0344(10) | 0.0047(9) | 0.0023(8) | 0.0029(8) |
| C20 | 0.0301(10) | 0.0311(11) | 0.0381(11) | 0.0018(9) | 0.0064(9) | 0.0085(8) |
| C21 | 0.0351(10) | 0.0294(10) | 0.0253(9) | 0.0043(8) | 0.0083(8) | 0.0000(8) |
| C22 | 0.0271(10) | 0.0391(11) | 0.0300(10) | -0.0002(9) | 0.0019(8) | 0.0031(8) |
| C23 | 0.0269(10) | 0.0340(11) | 0.0333(10) | 0.0000(8) | 0.0062(8) | 0.0055(8) |
| C25 | 0.0662(16) | 0.0548(15) | 0.0448(13) | -0.0082(11) | 0.0051(12) | 0.0235(13) |
| C27 | 0.0437(12) | 0.0356(11) | 0.0363(11) | -0.0043(9) | 0.0039(9) | -0.0025(9) |
| C28 | 0.0549(14) | 0.0443(13) | 0.0362(11) | -0.0001(10) | -0.0004(10) | 0.0043(10) |
| C29 | 0.0629(15) | 0.0394(13) | 0.0433(13) | -0.0016(10) | 0.0157(11) | -0.0127(11) |
| C31 | 0.0317(11) | 0.0325(11) | 0.0316(10) | -0.0081(9) | 0.0013(8) | -0.0032(9) |
| C34 | 0.0366(12) | 0.0496(13) | 0.0397(11) | -0.0120(10) | 0.0135(10) | -0.0019(10) |

**Table A-12.** (continued).

| | | | | | | |
|---|---|---|---|---|---|---|
| C35 | 0.0733(19) | 0.0729(19) | 0.0645(17) | 0.0161(15) | 0.0368(15) | 0.0083(14) |

**Table A-13.** Atomic Coordinates and Equivalent Isotropic Displacement Parameters for **2-2d**.

| Atom | x | y | z | U(eq) [Å$^2$] |
|---|---|---|---|---|
| O31 | 0.08631(12) | -0.09925(7) | 1.24462(10) | 0.0395(4) |
| N1 | 0.28448(13) | 0.21487(8) | 0.86026(11) | 0.0288(5) |
| N2 | 0.28852(13) | 0.15212(8) | 0.92460(11) | 0.0277(5) |
| N24 | 0.35797(14) | 0.53285(8) | 1.07721(12) | 0.0351(5) |
| N30 | 0.78453(17) | 0.30317(11) | 0.53961(16) | 0.0630(7) |
| C3 | 0.18145(15) | 0.14769(9) | 0.97785(13) | 0.0256(5) |
| C4 | 0.09157(16) | 0.21161(10) | 0.95586(14) | 0.0315(5) |
| C5 | 0.17155(15) | 0.26352(10) | 0.88285(13) | 0.0275(5) |
| C6 | 0.39029(15) | 0.23515(9) | 0.80101(13) | 0.0265(5) |
| C7 | 0.38142(16) | 0.29483(10) | 0.72798(13) | 0.0284(5) |
| C8 | 0.48359(16) | 0.31186(10) | 0.66238(14) | 0.0313(6) |
| C9 | 0.59817(16) | 0.27142(10) | 0.66910(14) | 0.0336(6) |
| C10 | 0.60931(17) | 0.21408(11) | 0.74489(15) | 0.0383(6) |
| C11 | 0.50728(16) | 0.19565(10) | 0.80976(15) | 0.0339(6) |
| C12 | 0.15507(15) | 0.08473(9) | 1.04878(12) | 0.0256(5) |
| C13 | 0.24737(17) | 0.02921(10) | 1.06716(14) | 0.0330(6) |
| C14 | 0.22137(17) | -0.03057(10) | 1.13222(15) | 0.0362(6) |
| C15 | 0.10077(17) | -0.03775(10) | 1.18059(13) | 0.0301(6) |
| C16 | 0.00775(16) | 0.01579(10) | 1.16214(13) | 0.0294(6) |
| C17 | 0.03520(16) | 0.07643(10) | 1.09708(13) | 0.0284(5) |
| C18 | 0.21503(15) | 0.33514(9) | 0.93515(12) | 0.0251(5) |
| C19 | 0.17342(16) | 0.40370(10) | 0.89829(13) | 0.0279(6) |
| C20 | 0.21644(16) | 0.46885(10) | 0.94571(13) | 0.0295(6) |
| C21 | 0.30819(16) | 0.46870(10) | 1.03227(13) | 0.0279(5) |
| C22 | 0.34865(17) | 0.39881(10) | 1.07017(14) | 0.0329(6) |
| C23 | 0.30418(17) | 0.33480(10) | 1.02186(14) | 0.0321(6) |
| C25 | 0.45116(18) | 0.52964(11) | 1.16797(14) | 0.0386(6) |
| C26 | 0.39158(19) | 0.51424(11) | 1.27880(15) | 0.0430(7) |
| C27 | 0.30962(19) | 0.60519(10) | 1.04415(17) | 0.0416(7) |
| C28 | 0.1815(2) | 0.62658(12) | 1.09353(18) | 0.0528(8) |
| C29 | 0.70254(19) | 0.28904(11) | 0.59784(17) | 0.0437(7) |
| C32 | -0.03263(19) | -0.10679(12) | 1.30157(16) | 0.0456(7) |

**Table A-14.** Interatomic Distances (Å) and Angles (°) for **2-2d**.

| | | | |
|---|---|---|---|
| O31-C15 | 1.369(2) | C18-C23 | 1.388(2) |
| O31-C32 | 1.430(2) | C19-C20 | 1.381(2) |
| N1-N2 | 1.379(2) | C20-C21 | 1.404(2) |
| N1-C5 | 1.490(2) | C21-C22 | 1.405(3) |
| N1 C6 | 1.373(2) | C22-C23 | 1.373(3) |
| N2-C3 | 1.297(2) | C25-C26 | 1.525(3) |
| N24-C21 | 1.377(2) | C27-C28 | 1.515(3) |
| N24-C25 | 1.453(2) | C4-H4A | 0.9601 |
| N24-C27 | 1.453(2) | C4-H4B | 0.9596 |
| N30-C29 | 1.146(3) | C5-H5 | 0.9596 |
| C3-C4 | 1.501(2) | C7-H7 | 0.9599 |
| C3-C12 | 1.459(2) | C8-H8 | 0.9601 |
| C4-C5 | 1.545(2) | C10-H10 | 0.9598 |
| C5-C18 | 1.507(2) | C11-H11 | 0.9597 |
| C6-C7 | 1.401(2) | C13-H13 | 0.9603 |
| C6-C11 | 1.404(2) | C14-H14 | 0.9599 |
| C7-C8 | 1.373(2) | C16-H16 | 0.9599 |
| C8-C9 | 1.391(2) | C17-H17 | 0.9602 |
| C9-C10 | 1.392(3) | C19-H19 | 0.9596 |
| C9-C29 | 1.435(3) | C20-H20 | 0.9599 |
| C10-C11 | 1.372(3) | C22-H22 | 0.9599 |
| C12-C13 | 1.398(2) | C23-H23 | 0.9592 |
| C12-C17 | 1.390(2) | C25-H25A | 0.9598 |
| C13-C14 | 1.371(3) | C25-H25B | 0.9600 |
| C14-C15 | 1.395(2) | C26-H26A | 0.9598 |
| C15-C16 | 1.378(2) | C26-H26B | 0.9598 |
| C16-C17 | 1.386(2) | C26-H26C | 0.9593 |
| C18-C19 | 1.383(2) | C27-H27A | 0.9605 |
| C27-H27B | 0.9602 | C32-H32A | 0.9593 |
| C28-H28A | 0.9600 | C32-H32B | 0.9605 |
| C28-H28B | 0.9609 | C32-H32C | 0.9600 |
| C28-H28C | 0.9596 | | |
| C15-O31-C32 | 117.42(14) | C12-C13-C14 | 121.13(16) |
| N2-N1-C5 | 113.15(12) | C13-C14-C15 | 120.42(16) |

**Table A-14.** (continued).

| | | | |
|---|---|---|---|
| N2-N1-C6 | 120.34(13) | O31-C15-C14 | 115.26(15) |
| C5-N1-C6 | 125.07(14) | O31-C15-C16 | 125.38(15) |
| N1-N2-C3 | 108.72(13) | C14-C15-C16 | 119.36(16) |
| C21-N24-C25 | 120.39(15) | C15-C16-C17 | 119.88(15) |
| C21-N24-C27 | 121.53(15) | C12-C17-C16 | 121.56(16) |
| C25-N24-C27 | 117.76(15) | C5-C18-C19 | 122.89(14) |
| N2-C3-C4 | 113.11(14) | C5-C18-C23 | 120.42(15) |
| N2-C3-C12 | 121.20(15) | C19-C18-C23 | 116.66(15) |
| C4-C3-C12 | 125.67(14) | C18-C19-C20 | 122.12(15) |
| C3-C4-C5 | 103.54(13) | C19-C20-C21 | 121.33(16) |
| N1-C5-C4 | 100.30(13) | N24-C21-C20 | 122.58(16) |
| N1-C5-C18 | 110.96(13) | N24-C21-C22 | 121.26(15) |
| C4-C5-C18 | 115.72(13) | C20-C21-C22 | 116.15(16) |
| N1-C6-C7 | 119.95(14) | C21-C22-C23 | 121.38(16) |
| N1-C6-C11 | 121.10(15) | C18-C23-C22 | 122.31(16) |
| C7-C6-C11 | 118.92(15) | N24-C25-C26 | 114.33(15) |
| C6-C7-C8 | 120.24(16) | N24-C27-C28 | 114.58(16) |
| C7-C8-C9 | 120.70(16) | N30-C29-C9 | 178.9(2) |
| C8-C9-C10 | 119.20(16) | C3-C4-H4A | 111.09 |
| C8-C9-C29 | 119.73(16) | C3-C4-H4B | 111.02 |
| C10-C9-C29 | 121.07(16) | C5-C4-H4A | 111.04 |
| C9-C10-C11 | 120.73(17) | C5-C4-H4B | 111.08 |
| C6-C11-C10 | 120.12(17) | H4A-C4-H4B | 109.00 |
| C3-C12-C13 | 121.29(14) | N1-C5-H5 | 109.84 |
| C3-C12-C17 | 121.02(15) | C4-C5-H5 | 109.79 |
| C13-C12-C17 | 117.64(15) | C18-C5-H5 | 109.84 |
| C6-C7-H7 | 119.86 | C26-C25-H25A | 108.66 |
| C8-C7-H7 | 119.90 | C26-C25-H25B | 108.63 |
| C7-C8-H8 | 119.69 | H25A-C25-H25B | 107.63 |
| C9-C8-H8 | 119.62 | C25-C26-H26A | 109.46 |
| C9-C10-H10 | 119.64 | C25-C26-H26B | 109.50 |
| C11-C10-H10 | 119.62 | C25-C26-H26C | 109.49 |
| C6-C11-H11 | 119.94 | H26A-C26-H26B | 109.43 |
| C10-C11-H11 | 119.94 | H26A-C26-H26C | 109.45 |

**Table A-14.** (continued).

| | | | |
|---|---|---|---|
| C12-C13-H13 | 119.44 | H26B-C26-H26C | 109.51 |
| C14-C13-H13 | 119.43 | N24-C27-H27A | 108.59 |
| C13-C14-H14 | 119.76 | N24-C27-H27B | 108.60 |
| C15-C14-H14 | 119.82 | C28-C27-H27A | 108.64 |
| C15-C16-H16 | 120.05 | C28-C27-H27B | 108.61 |
| C17-C16-H16 | 120.08 | H27A-C27-H27B | 107.61 |
| C12-C17-H17 | 119.21 | C27-C28-H28A | 109.50 |
| C16-C17-H17 | 119.24 | C27-C28-H28B | 109.45 |
| C18-C19-H19 | 118.97 | C27-C28-H28C | 109.52 |
| C20-C19-H19 | 118.91 | H28A-C28-H28B | 109.44 |
| C19-C20-H20 | 119.37 | H28A-C28-H28C | 109.47 |
| C21-C20-H20 | 119.30 | H28B-C28-H28C | 109.43 |
| C21-C22-H22 | 119.27 | O31-C32-H32A | 109.47 |
| C23-C22-H22 | 119.35 | O31-C32-H32B | 109.47 |
| C18-C23-H23 | 118.86 | O31-C32-H32C | 109.46 |
| C22-C23-H23 | 118.83 | H32A-C32-H32B | 109.48 |
| N24-C25-H25A | 108.69 | H32A-C32-H32C | 109.49 |
| N24-C25-H25B | 108.69 | H32B-C32-H32C | 109.46 |

**Table A-15.** Anisotropic Displacement Paremeters for **2-2d**.

| Atom | U(1,1) | U(2,2) | U(3,3) | U(2,3) | U(1,3) | U(1,2) |
|---|---|---|---|---|---|---|
| O31 | 0.0406(8) | 0.0374(8) | 0.0408(7) | 0.0078(6) | 0.0087(6) | -0.0055(6) |
| N1 | 0.0291(8) | 0.0248(8) | 0.0329(8) | 0.0016(7) | 0.0080(6) | 0.0034(6) |
| N2 | 0.0292(8) | 0.0259(9) | 0.0280(7) | -0.0028(6) | 0.0026(6) | -0.0013(6) |
| N24 | 0.0363(9) | 0.0281(9) | 0.0408(9) | -0.0026(7) | -0.0011(7) | -0.0026(7) |
| N30 | 0.0488(11) | 0.0573(13) | 0.0842(14) | -0.0108(11) | 0.0322(11) | -0.0164(9) |
| C3 | 0.0256(9) | 0.0271(10) | 0.0240(8) | -0.0063(7) | -0.0007(7) | -0.0021(7) |
| C4 | 0.0289(9) | 0.0295(10) | 0.0362(9) | -0.0013(8) | 0.0041(8) | -0.0005(8) |
| C5 | 0.0246(9) | 0.0291(10) | 0.0288(9) | -0.0010(8) | 0.0019(7) | 0.0040(7) |
| C6 | 0.0267(9) | 0.0257(10) | 0.0271(8) | -0.0069(8) | 0.0016(7) | -0.0034(7) |
| C7 | 0.0279(9) | 0.0291(10) | 0.0281(9) | -0.0058(8) | 0.0012(7) | -0.0007(8) |
| C8 | 0.0352(10) | 0.0298(11) | 0.0288(9) | -0.0042(8) | 0.0018(8) | -0.0085(8) |
| C9 | 0.0285(10) | 0.0310(11) | 0.0416(10) | -0.0066(9) | 0.0077(8) | -0.0086(8) |
| C10 | 0.0268(10) | 0.0341(11) | 0.0541(12) | -0.0056(10) | 0.0055(9) | 0.0001(8) |
| C11 | 0.0298(10) | 0.0296(11) | 0.0423(10) | 0.0016(9) | 0.0022(8) | 0.0003(8) |
| C12 | 0.0258(9) | 0.0261(10) | 0.0249(8) | -0.0056(7) | -0.0013(7) | -0.0023(7) |
| C13 | 0.0264(10) | 0.0355(11) | 0.0372(10) | 0.0027(9) | 0.0062(8) | 0.0002(8) |
| C14 | 0.0299(10) | 0.0351(11) | 0.0438(10) | 0.0057(9) | 0.0046(8) | 0.0037(9) |
| C15 | 0.0340(10) | 0.0290(11) | 0.0272(9) | -0.0013(8) | 0.0003(8) | -0.0069(8) |
| C16 | 0.0259(9) | 0.0333(11) | 0.0291(9) | -0.0052(8) | 0.0033(7) | -0.0048(8) |
| C17 | 0.0257(9) | 0.0298(10) | 0.0296(9) | -0.0056(8) | -0.0007(7) | 0.0028(8) |
| C18 | 0.0240(9) | 0.0282(10) | 0.0233(8) | 0.0022(8) | 0.0024(7) | 0.0037(7) |
| C19 | 0.0257(9) | 0.0317(11) | 0.0262(9) | 0.0027(8) | -0.0017(7) | 0.0039(7) |
| C20 | 0.0313(10) | 0.0253(10) | 0.0320(9) | 0.0053(8) | 0.0013(8) | 0.0053(8) |
| C21 | 0.0252(9) | 0.0289(10) | 0.0299(9) | -0.0001(8) | 0.0056(7) | -0.0011(8) |
| C22 | 0.0335(10) | 0.0336(11) | 0.0312(9) | 0.0003(8) | -0.0088(8) | 0.0044(8) |
| C23 | 0.0392(10) | 0.0241(10) | 0.0326(9) | 0.0021(8) | -0.0058(8) | 0.0087(8) |
| C25 | 0.0328(10) | 0.0401(12) | 0.0430(11) | -0.0089(9) | 0.0023(9) | -0.0078(9) |
| C26 | 0.0449(12) | 0.0406(13) | 0.0436(11) | -0.0034(10) | 0.0010(9) | -0.0086(9) |
| C27 | 0.0457(12) | 0.0277(11) | 0.0516(12) | -0.0002(9) | 0.0070(10) | -0.0036(9) |
| C28 | 0.0511(13) | 0.0409(13) | 0.0667(14) | 0.0017(11) | 0.0090(11) | 0.0074(10) |
| C29 | 0.0371(11) | 0.0371(12) | 0.0572(13) | -0.0110(10) | 0.0113(10) | -0.0080(9) |
| C32 | 0.0456(12) | 0.0511(14) | 0.0404(11) | 0.0041(10) | 0.0097(9) | -0.0138(10) |

**Table A-16.** Atomic Coordinates and Equivalent Isotropic Displacement Parameters for **2-3b**.

| Atom | x | y | z | U(eq) [Å$^2$] |
|---|---|---|---|---|
| F29 | 0.17911(11) | 0.7089(5) | 0.04311(17) | 0.0795(18) |
| F30 | 0.11231(13) | 0.7985(5) | 0.04002(17) | 0.095(2) |
| F31 | 0.10701(15) | 1.0416(5) | 0.06128(18) | 0.119(3) |
| F32 | 0.17333(15) | 1.1929(5) | 0.08362(18) | 0.114(3) |
| F33 | 0.24028(14) | 1.1101(4) | 0.08432(15) | 0.0796(17) |
| O35 | 0.31788(15) | 0.1353(5) | 0.03738(19) | 0.0683(19) |
| O36 | 0.37568(14) | 0.2183(4) | 0.04288(16) | 0.0554(17) |
| N1 | 0.25174(16) | 0.8586(5) | 0.06934(19) | 0.051(2) |
| N2 | 0.25483(15) | 0.7352(5) | 0.06066(18) | 0.0459(19) |
| N24 | 0.37079(19) | 0.9771(6) | 0.3155(2) | 0.068(3) |
| C3 | 0.29183(19) | 0.7126(6) | 0.0673(2) | 0.043(3) |
| C4 | 0.3174(2) | 0.8291(6) | 0.0789(3) | 0.050(3) |
| C5 | 0.29409(19) | 0.9216(6) | 0.0940(2) | 0.048(3) |
| C6 | 0.2160(2) | 0.9026(8) | 0.0679(2) | 0.054(3) |
| C7 | 0.1806(2) | 0.8282(8) | 0.0559(3) | 0.060(3) |
| C8 | 0.1446(2) | 0.8763(11) | 0.0531(3) | 0.073(4) |
| C9 | 0.1418(3) | 0.9960(12) | 0.0628(3) | 0.085(4) |
| C10 | 0.1749(3) | 1.0726(10) | 0.0745(3) | 0.082(4) |
| C11 | 0.2108(2) | 1.0257(8) | 0.0762(3) | 0.063(3) |
| C12 | 0.30391(18) | 0.5909(6) | 0.0613(2) | 0.041(3) |
| C13 | 0.2775(2) | 0.4890(6) | 0.0517(2) | 0.048(3) |
| C14 | 0.28944(19) | 0.3727(7) | 0.0467(2) | 0.048(3) |
| C15 | 0.32846(18) | 0.3520(6) | 0.0503(2) | 0.041(3) |
| C16 | 0.3552(2) | 0.4517(6) | 0.0603(2) | 0.044(3) |
| C17 | 0.34308(19) | 0.5677(6) | 0.0659(2) | 0.043(3) |
| C18 | 0.31268(18) | 0.9356(6) | 0.1525(2) | 0.045(3) |
| C19 | 0.32022(18) | 0.8350(7) | 0.1849(3) | 0.047(3) |
| C20 | 0.33948(19) | 0.8481(7) | 0.2385(3) | 0.051(3) |
| C21 | 0.35212(19) | 0.9650(7) | 0.2622(3) | 0.048(3) |
| C22 | 0.34451(19) | 1.0659(7) | 0.2297(3) | 0.050(3) |
| C23 | 0.32544(18) | 1.0507(7) | 0.1761(3) | 0.050(3) |
| C25 | 0.3903(3) | 1.0968(9) | 0.3413(3) | 0.088(4) |

**Table A-16.** (continued).

| | | | | |
|---|---|---|---|---|
| C26 | 0.3602(3) | 1.1735(9) | 0.3476(3) | 0.107(5) |
| C27 | 0.3779(2) | 0.8742(8) | 0.3500(3) | 0.077(4) |
| C28 | 0.4179(2) | 0.8036(8) | 0.3642(3) | 0.091(3) |
| C34 | 0.3390(2) | 0.2255(7) | 0.0426(2) | 0.048(3) |
| C37 | 0.3901(2) | 0.0961(7) | 0.0388(3) | 0.063(3) |
| C38 | 0.3744(3) | 0.0611(8) | -0.0160(3) | 0.104(4) |
| F29' | 0.08814(11) | 0.7025(3) | 0.34763(14) | 0.0603(16) |
| F30' | 0.08540(13) | 0.4625(4) | 0.32902(16) | 0.0722(17) |
| F31' | 0.04995(13) | 0.3750(4) | 0.23004(16) | 0.0783(17) |
| F32' | 0.01757(12) | 0.5393(4) | 0.14917(15) | 0.0687(17) |
| F33' | 0.01886(11) | 0.7802(3) | 0.16691(13) | 0.0590(14) |
| O35' | 0.03152(15) | 1.4194(5) | 0.4640(2) | 0.073(2) |
| O36' | 0.01236(14) | 1.2423(4) | 0.48421(18) | 0.0576(17) |
| N1' | 0.05061(15) | 0.8762(5) | 0.2662(2) | 0.042(2) |
| N2' | 0.04633(14) | 0.9147(5) | 0.3076(2) | 0.0400(19) |
| N24' | 0.22533(16) | 0.9368(6) | 0.2647(2) | 0.075(3) |
| C3' | 0.05003(17) | 1.0329(6) | 0.3112(2) | 0.040(2) |
| C4' | 0.05951(19) | 1.0899(6) | 0.2721(3) | 0.048(3) |
| C5' | 0.06231(18) | 0.9784(6) | 0.2420(2) | 0.041(2) |
| C6' | 0.05172(17) | 0.7521(6) | 0.2577(2) | 0.036(2) |
| C7' | 0.06888(19) | 0.6654(6) | 0.2974(3) | 0.042(3) |
| C8' | 0.0679(2) | 0.5412(6) | 0.2885(3) | 0.050(3) |
| C9' | 0.0502(2) | 0.4969(6) | 0.2384(3) | 0.050(3) |
| C10' | 0.03428(19) | 0.5807(7) | 0.1984(3) | 0.046(3) |
| C11' | 0.03517(18) | 0.7029(6) | 0.2084(3) | 0.040(3) |
| C12' | 0.04524(17) | 1.0995(6) | 0.3505(2) | 0.038(2) |
| C13' | 0.03634(18) | 1.0403(6) | 0.3850(2) | 0.043(3) |
| C14' | 0.03055(18) | 1.1064(7) | 0.4209(3) | 0.047(3) |
| C15' | 0.03355(17) | 1.2346(6) | 0.4225(3) | 0.043(2) |
| C16' | 0.04317(19) | 1.2935(7) | 0.3889(3) | 0.053(3) |
| C17' | 0.04845(18) | 1.2281(6) | 0.3531(3) | 0.046(3) |
| C18' | 0.10471(17) | 0.9595(6) | 0.2474(2) | 0.039(2) |
| C19' | 0.13932(19) | 0.9261(6) | 0.2947(3) | 0.049(3) |
| C20' | 0.17883(19) | 0.9176(6) | 0.3003(3) | 0.054(3) |

**Table A-16.** (continued).

| | | | | |
|---|---|---|---|---|
| C21' | 0.18571(18) | 0.9435(7) | 0.2587(3) | 0.054(3) |
| C22' | 0.15046(19) | 0.9764(7) | 0.2110(3) | 0.057(3) |
| C23' | 0.11079(19) | 0.9822(6) | 0.2059(3) | 0.051(3) |
| C25' | 0.2627(2) | 0.9324(11) | 0.3186(3) | 0.095(4) |
| C26' | 0.2678(3) | 1.0509(12) | 0.3491(3) | 0.118(5) |
| C27' | 0.2327(2) | 0.9641(11) | 0.2217(3) | 0.084(4) |
| C28' | 0.2364(3) | 1.0992(12) | 0.2138(3) | 0.104(5) |
| C34' | 0.0260(2) | 1.3098(8) | 0.4583(3) | 0.057(3) |
| C37' | 0.0023(3) | 1.3106(8) | 0.5185(3) | 0.076(3) |
| C38' | -0.0127(3) | 1.2213(9) | 0.5426(3) | 0.105(5) |

**Table A-17.** Interatomic Distances (Å) and Angles (°) for **2-3b**.

| | | | |
|---|---|---|---|
| F29-C7 | 1.341(10) | N24'-C27' | 1.462(10) |
| F30-C8 | 1.348(11) | N24'-C21' | 1.382(10) |
| F31-C9 | 1.354(14) | C3-C12 | 1.431(9) |
| F32-C10 | 1.339(12) | C3-C4 | 1.509(10) |
| F33-C11 | 1.347(10) | C4-C5 | 1.527(10) |
| F29'-C7' | 1.352(8) | C5-C18 | 1.521(7) |
| F30'-C8' | 1.346(8) | C6-C11 | 1.387(12) |
| F31'-C9' | 1.343(8) | C6-C7 | 1.420(12) |
| F32'-C10' | 1.347(9) | C7-C8 | 1.390(13) |
| F33'-C11' | 1.356(8) | C8-C9 | 1.344(17) |
| O35-C34 | 1.210(10) | C9-C10 | 1.369(17) |
| O36-C34 | 1.351(10) | C10-C11 | 1.395(15) |
| O36-C37 | 1.455(9) | C12-C13 | 1.404(10) |
| O35'-C34' | 1.203(10) | C12-C17 | 1.404(11) |
| O36'-C37' | 1.449(11) | C13-C14 | 1.367(10) |
| O36'-C34' | 1.329(10) | C14-C15 | 1.407(11) |
| N1-C6 | 1.382(10) | C15-C16 | 1.391(10) |
| N1-C5 | 1.515(9) | C15-C34 | 1.474(10) |
| N1-N2 | 1.377(8) | C16-C17 | 1.372(10) |
| N2-C3 | 1.300(10) | C18-C19 | 1.387(10) |
| N24-C25 | 1.495(11) | C18-C23 | 1.392(10) |
| N24-C27 | 1.446(10) | C19-C20 | 1.387(11) |
| N24-C21 | 1.379(9) | C20-C21 | 1.410(11) |
| N1'-C5' | 1.496(9) | C21-C22 | 1.391(11) |
| N1'-C6' | 1.373(8) | C22-C23 | 1.390(11) |
| N1'-N2' | 1.380(8) | C25-C26 | 1.472(16) |
| N2'-C3' | 1.287(9) | C27-C28 | 1.522(12) |
| N24'-C25' | 1.500(10) | C37-C38 | 1.477(11) |
| C4-H4B | 0.9601 | C4'-C5' | 1.537(10) |
| C4-H4A | 0.9602 | C5'-C18' | 1.504(10) |
| C5-H5 | 0.9603 | C6'-C7' | 1.387(9) |
| C13-H13 | 0.9609 | C6'-C11' | 1.379(9) |
| C14-H14 | 0.9595 | C7'-C8' | 1.369(9) |
| C16-H16 | 0.9611 | C8'-C9' | 1.377(11) |

**Table A-17.** (continued).

| | | | |
|---|---|---|---|
| C17-H17 | 0.9595 | C9'-C10' | 1.371(11) |
| C19-H19 | 0.9593 | C10'-C11' | 1.354(10) |
| C20-H20 | 0.9612 | C12'-C13' | 1.380(9) |
| C22-H22 | 0.9595 | C12'-C17' | 1.398(9) |
| C23-H23 | 0.9593 | C13'-C14' | 1.386(10) |
| C25-H25A | 0.9586 | C14'-C15' | 1.393(10) |
| C25-H25B | 0.9617 | C15'-C16' | 1.372(11) |
| C26-H26A | 0.9591 | C15'-C34' | 1.472(11) |
| C26-H26B | 0.9598 | C16'-C17' | 1.370(11) |
| C26-H26C | 0.9613 | C18'-C19' | 1.391(10) |
| C27-H27A | 0.9604 | C18'-C23' | 1.380(10) |
| C27-H27B | 0.9581 | C19'-C20' | 1.384(12) |
| C28-H28A | 0.9628 | C20'-C21' | 1.408(11) |
| C28-H28B | 0.9597 | C21'-C22' | 1.406(11) |
| C28-H28C | 0.9615 | C22'-C23' | 1.395(12) |
| C37-H37A | 0.9598 | C25'-C26' | 1.528(16) |
| C37-H37B | 0.9607 | C27'-C28' | 1.500(17) |
| C38-H38A | 0.9593 | C37'-C38' | 1.467(14) |
| C38-H38B | 0.9592 | C4'-H4D | 0.9592 |
| C38-H38C | 0.9605 | C4'-H4E | 0.9598 |
| C3'-C4' | 1.502(10) | C5'-H5' | 0.9587 |
| C3'-C12' | 1.456(9) | C13'-H13' | 0.9597 |
| C14'-H14' | 0.9591 | C26'-H26F | 0.9599 |
| C16'-H16' | 0.9597 | C27'-H27D | 0.9586 |
| C17'-H17' | 0.9603 | C27'-H27E | 0.9592 |
| C19'-H19' | 0.9594 | C28'-H28D | 0.9607 |
| C20'-H20' | 0.9600 | C28'-H28E | 0.9579 |
| C22'-H22' | 0.9599 | C28'-H28F | 0.9600 |
| C23'-H23' | 0.9593 | C37'-H37D | 0.9603 |
| C25'-H25D | 0.9627 | C37'-H37E | 0.9598 |
| C25'-H25E | 0.9582 | C38'-H38D | 0.9615 |
| C26'-H26D | 0.9606 | C38'-H38E | 0.9601 |
| C26'-H26E | 0.9602 | C38'-H38F | 0.9595 |
| C34-O36-C37 | 117.3(6) | F29-C7-C8 | 116.3(8) |

**Table A-17.** (continued).

| | | | |
|---|---|---|---|
| C34'-O36'-C37' | 115.4(6) | F30-C8-C7 | 117.5(9) |
| N2-N1-C6 | 119.8(6) | F30-C8-C9 | 120.9(9) |
| C5-N1-C6 | 126.6(6) | C7-C8-C9 | 121.5(10) |
| N2-N1-C5 | 111.5(5) | F31-C9-C8 | 121.2(10) |
| N1-N2-C3 | 109.5(6) | F31-C9-C10 | 119.8(11) |
| C21-N24-C25 | 120.4(6) | C8-C9-C10 | 119.0(11) |
| C21-N24-C27 | 123.2(6) | C9-C10-C11 | 119.8(10) |
| C25-N24-C27 | 115.9(6) | F32-C10-C9 | 121.2(10) |
| N2'-N1'-C6' | 119.2(5) | F32-C10-C11 | 118.9(9) |
| C5'-N1'-C6' | 126.5(5) | F33-C11-C10 | 115.2(8) |
| N2'-N1'-C5' | 113.1(5) | C6-C11-C10 | 123.8(8) |
| N1'-N2'-C3' | 108.7(5) | F33-C11-C6 | 120.9(7) |
| C21'-N24'-C27' | 121.6(6) | C3-C12-C13 | 121.5(7) |
| C25'-N24'-C27' | 117.6(6) | C3-C12-C17 | 121.5(6) |
| C21'-N24'-C25' | 119.1(6) | C13-C12-C17 | 117.0(6) |
| N2-C3-C4 | 111.4(6) | C12-C13-C14 | 121.2(7) |
| N2-C3-C12 | 121.5(6) | C13-C14-C15 | 120.8(7) |
| C4-C3-C12 | 127.0(7) | C14-C15-C16 | 118.8(6) |
| C3-C4-C5 | 103.7(6) | C14-C15-C34 | 118.4(6) |
| N1-C5-C4 | 99.1(5) | C16-C15-C34 | 122.8(7) |
| N1-C5-C18 | 111.2(5) | C15-C16-C17 | 119.9(7) |
| C4-C5-C18 | 113.7(6) | C12-C17-C16 | 122.3(7) |
| N1-C6-C11 | 122.7(7) | C5-C18-C19 | 122.2(6) |
| C7-C6-C11 | 113.5(7) | C5-C18-C23 | 120.6(6) |
| N1-C6-C7 | 123.7(7) | C19-C18-C23 | 117.1(6) |
| F29-C7-C6 | 121.4(7) | C18-C19-C20 | 121.6(7) |
| C6-C7-C8 | 122.2(8) | C19-C20-C21 | 121.0(7) |
| N24-C21-C20 | 120.5(7) | C20-C19-H19 | 119.11 |
| N24-C21-C22 | 122.1(7) | C21-C20-H20 | 119.35 |
| C20-C21-C22 | 117.3(7) | C19-C20-H20 | 119.62 |
| C21-C22-C23 | 120.8(7) | C23-C22-H22 | 119.71 |
| C18-C23-C22 | 122.1(7) | C21-C22-H22 | 119.53 |
| N24-C25-C26 | 110.8(9) | C18-C23-H23 | 119.00 |
| N24-C27-C28 | 113.0(7) | C22-C23-H23 | 118.88 |

**Table A-17.** (continued).

| | | | |
|---|---|---|---|
| O35-C34-O36 | 122.2(7) | N24-C25-H25A | 109.48 |
| O36-C34-C15 | 113.2(6) | N24-C25-H25B | 109.42 |
| O35-C34-C15 | 124.6(7) | H25A-C25-H25B | 107.90 |
| O36-C37-C38 | 111.6(6) | C26-C25-H25A | 109.69 |
| C5-C4-H4B | 111.09 | C26-C25-H25B | 109.50 |
| C5-C4-H4A | 111.01 | H26B-C26-H26C | 109.32 |
| C3-C4-H4A | 111.06 | C25-C26-H26A | 109.55 |
| H4A-C4-H4B | 108.93 | C25-C26-H26B | 109.52 |
| C3-C4-H4B | 111.00 | C25-C26-H26C | 109.41 |
| C4-C5-H5 | 110.82 | H26A-C26-H26B | 109.53 |
| C18-C5-H5 | 110.76 | H26A-C26-H26C | 109.51 |
| N1-C5-H5 | 110.70 | N24-C27-H27B | 108.98 |
| C14-C13-H13 | 119.36 | C28-C27-H27A | 109.00 |
| C12-C13-H13 | 119.41 | C28-C27-H27B | 108.82 |
| C13-C14-H14 | 119.62 | H27A-C27-H27B | 107.92 |
| C15-C14-H14 | 119.61 | N24-C27-H27A | 109.03 |
| C15-C16-H16 | 120.07 | C27-C28-H28A | 109.50 |
| C17-C16-H16 | 120.04 | C27-C28-H28B | 109.59 |
| C12-C17-H17 | 118.78 | C27-C28-H28C | 109.64 |
| C16-C17-H17 | 118.93 | H28A-C28-H28B | 109.50 |
| C18-C19-H19 | 119.25 | H28A-C28-H28C | 109.13 |
| H28B-C28-H28C | 109.46 | F31'-C9'-C8' | 119.9(6) |
| O36-C37-H37A | 109.42 | F31'-C9'-C10' | 122.1(7) |
| O36-C37-H37B | 109.31 | C8'-C9'-C10' | 118.0(6) |
| C38-C37-H37A | 109.30 | F32'-C10'-C9' | 118.9(7) |
| H37A-C37-H37B | 107.97 | F32'-C10'-C11' | 120.8(7) |
| C38-C37-H37B | 109.21 | C9'-C10'-C11' | 120.3(7) |
| C37-C38-H38B | 109.55 | F33'-C11'-C6' | 118.9(6) |
| C37-C38-H38C | 109.46 | F33'-C11'-C10' | 117.0(7) |
| C37-C38-H38A | 109.36 | C6'-C11'-C10' | 124.0(7) |
| H38A-C38-H38C | 109.54 | C3'-C12'-C13' | 122.2(6) |
| H38B-C38-H38C | 109.43 | C3'-C12'-C17' | 119.8(6) |
| H38A-C38-H38B | 109.49 | C13'-C12'-C17' | 117.9(6) |
| N2'-C3'-C4' | 113.6(5) | C12'-C13'-C14' | 121.0(6) |

**Table A-17.** (continued).

| | | | |
|---|---|---|---|
| N2'-C3'-C12' | 120.6(6) | C13'-C14'-C15' | 120.1(7) |
| C4'-C3'-C12' | 125.7(6) | C14'-C15'-C16' | 119.0(7) |
| C3'-C4'-C5' | 103.6(5) | C14'-C15'-C34' | 122.4(7) |
| N1'-C5'-C4' | 100.6(5) | C16'-C15'-C34' | 118.6(6) |
| N1'-C5'-C18' | 112.5(5) | C15'-C16'-C17' | 120.8(7) |
| C4'-C5'-C18' | 114.5(6) | C12'-C17'-C16' | 121.2(7) |
| N1'-C6'-C7' | 123.4(5) | C5'-C18'-C19' | 121.5(6) |
| N1'-C6'-C11' | 122.4(5) | C5'-C18'-C23' | 120.4(5) |
| C7'-C6'-C11' | 114.2(6) | C19'-C18'-C23' | 118.0(7) |
| F29'-C7'-C6' | 119.9(6) | C18'-C19'-C20' | 121.1(7) |
| F29'-C7'-C8' | 117.0(6) | C19'-C20'-C21' | 121.5(7) |
| C6'-C7'-C8' | 123.1(7) | N24'-C21'-C20' | 121.3(7) |
| F30'-C8'-C7' | 119.7(7) | N24'-C21'-C22' | 121.8(7) |
| F30'-C8'-C9' | 120.0(6) | C20'-C21'-C22' | 116.8(7) |
| C7'-C8'-C9' | 120.3(7) | C21'-C22'-C23' | 120.7(7) |
| C18'-C23'-C22' | 121.7(7) | C23'-C22'-H22' | 119.58 |
| N24'-C25'-C26' | 112.3(8) | C18'-C23'-H23' | 119.09 |
| N24'-C27'-C28' | 113.9(8) | C22'-C23'-H23' | 119.19 |
| O35'-C34'-O36' | 123.3(7) | N24'-C25'-H25D | 108.95 |
| O35'-C34'-C15' | 124.6(7) | N24'-C25'-H25E | 109.18 |
| O36'-C34'-C15' | 112.1(7) | C26'-C25'-H25D | 109.12 |
| O36'-C37'-C38' | 107.3(7) | C26'-C25'-H25E | 109.32 |
| C3'-C4'-H4D | 110.97 | H25D-C25'-H25E | 107.84 |
| C3'-C4'-H4E | 110.83 | C25'-C26'-H26D | 109.51 |
| C5'-C4'-H4D | 111.08 | C25'-C26'-H26E | 109.45 |
| C5'-C4'-H4E | 111.14 | C25'-C26'-H26F | 109.50 |
| H4D-C4'-H4E | 109.13 | H26D-C26'-H26E | 109.40 |
| N1'-C5'-H5' | 109.61 | H26D-C26'-H26F | 109.65 |
| C4'-C5'-H5' | 109.60 | H26E-C26'-H26F | 109.33 |
| C18'-C5'-H5' | 109.73 | N24'-C27'-H27D | 108.66 |
| C12'-C13'-H13' | 119.47 | N24'-C27'-H27E | 108.63 |
| C14'-C13'-H13' | 119.49 | C28'-C27'-H27D | 108.90 |
| C13'-C14'-H14' | 119.98 | C28'-C27'-H27E | 108.82 |
| C15'-C14'-H14' | 119.93 | H27D-C27'-H27E | 107.75 |

**Table A-17.** (continued).

| | | | |
|---|---|---|---|
| C15'-C16'-H16' | 119.54 | C27'-C28'-H28D | 109.44 |
| C17'-C16'-H16' | 119.66 | C27'-C28'-H28E | 109.46 |
| C12'-C17'-H17' | 119.42 | C27'-C28'-H28F | 109.44 |
| C16'-C17'-H17' | 119.40 | H28D-C28'-H28E | 109.45 |
| C18'-C19'-H19' | 119.35 | H28D-C28'-H28F | 109.47 |
| C20'-C19'-H19' | 119.54 | H28E-C28'-H28F | 109.57 |
| C19'-C20'-H20' | 119.31 | O36'-C37'-H37D | 110.30 |
| C21'-C20'-H20' | 119.16 | O36'-C37'-H37E | 110.31 |
| C21'-C22'-H22' | 119.70 | C38'-C37'-H37D | 110.26 |
| C38'-C37'-H37E | 110.16 | C37'-C38'-H38F | 109.52 |
| H37D-C37'-H37E | 108.51 | H38D-C38'-H38E | 109.47 |
| C37'-C38'-H38D | 109.41 | H38D-C38'-H38F | 109.47 |
| C37'-C38'-H38E | 109.50 | H38E-C38'-H38F | 109.46 |

**Table A-18.** Anisotropic Displacement Paremeters for **2-3b**.

| Atom | U(1,1) | U(2,2) | U(3,3) | U(2,3) | U(1,3) | U(1,2) |
|---|---|---|---|---|---|---|
| F29 | 0.033(2) | 0.093(4) | 0.105(3) | 0.000(3) | 0.029(2) | -0.002(2) |
| F30 | 0.036(3) | 0.151(5) | 0.090(3) | 0.012(3) | 0.025(2) | 0.010(3) |
| F31 | 0.064(3) | 0.183(6) | 0.101(4) | 0.013(4) | 0.034(3) | 0.067(4) |
| F32 | 0.093(4) | 0.112(5) | 0.092(4) | -0.002(3) | 0.013(3) | 0.062(3) |
| F33 | 0.061(3) | 0.064(3) | 0.076(3) | -0.001(2) | 0.006(2) | 0.016(2) |
| O35 | 0.046(3) | 0.054(3) | 0.097(4) | -0.002(3) | 0.030(3) | -0.008(3) |
| O36 | 0.041(3) | 0.058(3) | 0.062(3) | -0.003(2) | 0.022(2) | 0.002(2) |
| N1 | 0.027(3) | 0.060(4) | 0.049(4) | -0.008(3) | 0.007(3) | -0.001(3) |
| N2 | 0.027(3) | 0.055(4) | 0.040(3) | -0.001(3) | 0.005(2) | 0.003(3) |
| N24 | 0.060(4) | 0.076(5) | 0.044(4) | -0.006(4) | 0.009(3) | 0.004(4) |
| C3 | 0.025(4) | 0.064(5) | 0.028(4) | -0.005(3) | 0.005(3) | -0.007(3) |
| C4 | 0.040(4) | 0.055(5) | 0.052(5) | -0.008(4) | 0.021(3) | -0.006(4) |
| C5 | 0.043(4) | 0.048(5) | 0.046(4) | -0.004(4) | 0.018(3) | -0.012(3) |
| C6 | 0.037(4) | 0.082(6) | 0.026(4) | 0.001(4) | 0.003(3) | 0.013(4) |
| C7 | 0.040(5) | 0.085(7) | 0.043(4) | -0.004(4) | 0.011(3) | 0.014(5) |
| C8 | 0.031(5) | 0.122(8) | 0.046(5) | 0.002(5) | 0.005(4) | 0.016(5) |
| C9 | 0.054(6) | 0.125(10) | 0.055(6) | 0.003(6) | 0.011(5) | 0.035(7) |
| C10 | 0.076(7) | 0.096(8) | 0.047(5) | -0.003(5) | 0.010(5) | 0.045(6) |
| C11 | 0.042(5) | 0.068(6) | 0.047(5) | -0.004(4) | -0.001(4) | 0.015(5) |
| C12 | 0.022(4) | 0.051(5) | 0.041(4) | -0.007(3) | 0.009(3) | -0.004(3) |
| C13 | 0.020(4) | 0.060(5) | 0.055(5) | -0.006(4) | 0.011(3) | -0.006(3) |
| C14 | 0.021(4) | 0.058(5) | 0.052(4) | -0.006(4) | 0.008(3) | -0.010(4) |
| C15 | 0.027(4) | 0.048(5) | 0.036(4) | -0.002(3) | 0.006(3) | -0.002(3) |
| C16 | 0.031(4) | 0.051(5) | 0.041(4) | -0.001(3) | 0.012(3) | -0.007(3) |
| C17 | 0.028(4) | 0.054(5) | 0.036(4) | -0.004(3) | 0.008(3) | -0.013(4) |
| C18 | 0.030(4) | 0.053(5) | 0.047(4) | -0.001(4) | 0.016(3) | -0.003(3) |
| C19 | 0.032(4) | 0.053(5) | 0.044(4) | -0.001(4) | 0.010(3) | -0.004(3) |
| C20 | 0.033(4) | 0.063(5) | 0.051(5) | 0.008(4) | 0.016(3) | 0.003(4) |
| C21 | 0.030(4) | 0.061(5) | 0.045(5) | -0.007(4) | 0.012(3) | 0.002(4) |
| C22 | 0.034(4) | 0.057(5) | 0.048(5) | -0.011(4) | 0.013(3) | -0.001(4) |
| C23 | 0.031(4) | 0.048(5) | 0.064(5) | 0.000(4) | 0.019(3) | -0.001(3) |
| C25 | 0.067(6) | 0.116(8) | 0.068(6) | -0.012(6) | 0.025(5) | 0.008(6) |
| C26 | 0.100(8) | 0.126(9) | 0.114(8) | -0.024(6) | 0.067(7) | -0.025(7) |

**Table A-18.** (continued).

| | | | | | | |
|---|---|---|---|---|---|---|
| C27 | 0.041(5) | 0.123(8) | 0.049(5) | -0.002(6) | 0.009(4) | -0.008(5) |
| C28 | 0.042(5) | 0.109(7) | 0.085(6) | 0.010(5) | 0.004(4) | -0.007(5) |
| C34 | 0.027(4) | 0.059(5) | 0.044(4) | 0.005(4) | 0.008(3) | -0.002(4) |
| C37 | 0.053(5) | 0.055(5) | 0.073(6) | 0.001(4) | 0.025(4) | 0.009(4) |
| C38 | 0.112(8) | 0.103(8) | 0.068(6) | -0.013(5) | 0.023(5) | 0.051(6) |
| F29' | 0.062(3) | 0.058(3) | 0.048(2) | 0.002(2) | 0.018(2) | 0.002(2) |
| F30' | 0.077(3) | 0.055(3) | 0.077(3) | 0.019(2) | 0.033(2) | -0.002(2) |
| F31' | 0.077(3) | 0.044(3) | 0.104(3) | -0.007(2) | 0.038(3) | -0.008(2) |
| F32' | 0.058(3) | 0.074(3) | 0.064(3) | -0.017(2) | 0.023(2) | -0.004(2) |
| F33' | 0.053(2) | 0.066(3) | 0.051(2) | 0.004(2) | 0.0208(19) | 0.013(2) |
| O35' | 0.065(4) | 0.054(4) | 0.097(4) | -0.023(3) | 0.039(3) | -0.006(3) |
| O36' | 0.047(3) | 0.058(3) | 0.060(3) | -0.022(3) | 0.021(3) | 0.000(3) |
| N1' | 0.030(3) | 0.047(4) | 0.052(4) | 0.001(3) | 0.022(3) | 0.003(3) |
| N2' | 0.020(3) | 0.048(4) | 0.046(3) | -0.002(3) | 0.012(2) | 0.004(2) |
| N24' | 0.017(3) | 0.134(6) | 0.062(4) | -0.006(4) | 0.011(3) | 0.018(3) |
| C3' | 0.021(3) | 0.042(5) | 0.054(4) | 0.003(4) | 0.016(3) | 0.004(3) |
| C4' | 0.032(4) | 0.041(4) | 0.067(5) | 0.011(4) | 0.022(4) | 0.008(3) |
| C5' | 0.022(3) | 0.047(4) | 0.049(4) | 0.010(3) | 0.014(3) | 0.004(3) |
| C6' | 0.022(3) | 0.037(4) | 0.048(4) | -0.002(4) | 0.016(3) | -0.001(3) |
| C7' | 0.032(4) | 0.047(5) | 0.042(4) | -0.002(4) | 0.014(3) | 0.001(3) |
| C8' | 0.049(4) | 0.041(5) | 0.063(5) | 0.017(4) | 0.031(4) | 0.002(4) |
| C9' | 0.043(4) | 0.036(5) | 0.069(6) | -0.007(4) | 0.027(4) | -0.007(3) |
| C10' | 0.029(4) | 0.058(5) | 0.048(5) | -0.012(4) | 0.018(3) | -0.009(3) |
| C11' | 0.028(4) | 0.045(5) | 0.049(4) | 0.009(4) | 0.020(3) | 0.006(3) |
| C12' | 0.015(3) | 0.039(4) | 0.050(4) | 0.002(4) | 0.008(3) | 0.004(3) |
| C13' | 0.026(4) | 0.039(5) | 0.054(5) | -0.005(4) | 0.012(3) | -0.002(3) |
| C14' | 0.026(4) | 0.054(5) | 0.047(4) | -0.008(4) | 0.007(3) | 0.002(3) |
| C15' | 0.017(3) | 0.045(5) | 0.051(4) | -0.009(4) | 0.004(3) | 0.009(3) |
| C16' | 0.033(4) | 0.043(5) | 0.068(5) | -0.008(4) | 0.015(4) | 0.002(3) |
| C17' | 0.027(4) | 0.047(5) | 0.057(5) | 0.001(4) | 0.015(3) | 0.004(3) |
| C18' | 0.023(3) | 0.048(4) | 0.041(4) | 0.013(3) | 0.013(3) | 0.005(3) |
| C19' | 0.032(4) | 0.059(5) | 0.051(5) | 0.008(4) | 0.018(3) | 0.006(3) |
| C20' | 0.023(4) | 0.082(6) | 0.042(4) | 0.009(4) | 0.005(3) | 0.013(4) |
| C21' | 0.019(4) | 0.090(6) | 0.045(4) | -0.002(4) | 0.011(3) | 0.007(4) |

**Table A-18.** (continued).

| | | | | | | |
|---|---|---|---|---|---|---|
| C22' | 0.031(4) | 0.090(6) | 0.047(5) | 0.006(4) | 0.018(3) | 0.001(4) |
| C23' | 0.022(4) | 0.073(5) | 0.047(5) | 0.005(4) | 0.009(3) | 0.000(3) |
| C25' | 0.030(4) | 0.161(10) | 0.081(6) | 0.001(7) | 0.017(4) | 0.029(5) |
| C26' | 0.052(6) | 0.214(13) | 0.076(7) | -0.031(8) | 0.023(5) | -0.025(7) |
| C27' | 0.032(5) | 0.148(10) | 0.073(6) | -0.001(6) | 0.027(4) | 0.008(5) |
| C28' | 0.057(6) | 0.176(13) | 0.075(7) | -0.004(7) | 0.029(5) | -0.016(7) |
| C34' | 0.030(4) | 0.051(5) | 0.071(6) | -0.006(5) | 0.012(4) | 0.001(4) |
| C37' | 0.078(6) | 0.081(6) | 0.065(6) | -0.019(5) | 0.032(5) | 0.004(5) |
| C38' | 0.162(10) | 0.093(8) | 0.081(7) | -0.010(6) | 0.077(7) | 0.001(7) |

# APPENDIX B

# COMPUTATIONAL DATA

**Table A-19.** Cartesian Atomic Coordinates for the Geometry Optimized Structure of Pyrazoline **2-1a** (B3LYP/6-31G*).

| atom | x/Å | y/Å | z/Å |
|---|---|---|---|
| N | 2.574107 | 0.614177 | 0.189579 |
| N | 1.369695 | 1.138968 | -0.184483 |
| N | -4.707403 | -1.210556 | 0.310081 |
| C | 2.759301 | -0.533759 | -0.377322 |
| C | 1.611059 | -0.929922 | -1.284336 |
| C | 0.656191 | 0.294815 | -1.178067 |
| C | -0.759413 | -0.064254 | -0.769043 |
| C | -1.078559 | -0.429064 | 0.543871 |
| C | -2.366217 | -0.808165 | 0.903226 |
| C | -3.418608 | -0.835972 | -0.044413 |
| C | -3.089772 | -0.461858 | -1.367889 |
| C | -1.792426 | -0.091034 | -1.709613 |
| C | -5.764364 | -1.355296 | -0.684833 |
| C | -6.521924 | -0.056245 | -0.994152 |
| C | -5.089004 | -1.420842 | 1.703114 |
| C | -4.866329 | -2.854790 | 2.201381 |
| C | 1.108667 | 2.493854 | 0.048966 |
| C | -0.020720 | 3.112857 | -0.516430 |
| C | -0.272962 | 4.462996 | -0.274207 |
| C | 0.579334 | 5.220818 | 0.527546 |
| C | 1.699385 | 4.602601 | 1.091236 |
| C | 1.970006 | 3.258191 | 0.860453 |
| H | 0.376203 | 6.271885 | 0.711955 |
| C | 3.950719 | -1.344163 | -0.125693 |
| C | 4.952033 | -0.906735 | 0.764084 |
| C | 6.083971 | -1.680006 | 0.991149 |
| C | 6.246569 | -2.907888 | 0.339358 |
| C | 5.262033 | -3.352755 | -0.542377 |
| C | 4.124000 | -2.579716 | -0.773589 |
| H | 7.133161 | -3.510106 | 0.519270 |
| H | 1.120014 | -1.845722 | -0.935781 |
| H | 1.941811 | -1.110646 | -2.313418 |

**Table A-19.** (continued).

| | | | |
|---|---|---|---|
| H | 0.621312 | 0.833201 | -2.135605 |
| H | -0.304479 | -0.410039 | 1.307100 |
| H | -2.547896 | -1.093071 | 1.932934 |
| H | -3.852370 | -0.433006 | -2.136907 |
| H | -1.587812 | 0.196480 | -2.739843 |
| H | -6.469543 | -2.106999 | -0.310046 |
| H | -5.341112 | -1.777851 | -1.602656 |
| H | -6.978688 | 0.354277 | -0.086418 |
| H | -7.321598 | -0.241756 | -1.721294 |
| H | -5.853404 | 0.706666 | -1.405863 |
| H | -6.150128 | -1.160401 | 1.797497 |
| H | -4.551343 | -0.708068 | 2.337734 |
| H | -5.449856 | -3.568866 | 1.609356 |
| H | -5.174331 | -2.950639 | 3.249403 |
| H | -3.812480 | -3.141012 | 2.124424 |
| H | -0.710872 | 2.541334 | -1.124908 |
| H | -1.151988 | 4.920872 | -0.721377 |
| H | 2.378184 | 5.175285 | 1.718711 |
| H | 2.843312 | 2.784806 | 1.291325 |
| H | 4.822616 | 0.044693 | 1.269371 |
| H | 6.845884 | -1.326180 | 1.681110 |
| H | 5.377127 | -4.305118 | -1.053632 |
| H | 3.365648 | -2.940154 | -1.463192 |

**Table A-20.** Cartesian Atomic Coordinates for the Geometry Optimized Structure of Pyrazoline **2-1b** (B3LYP/6-31G*).

| atom | x/Å | y/Å | z/Å |
|---|---|---|---|
| N | 1.883452 | 1.277214 | 0.059871 |
| N | 0.667393 | 1.704476 | -0.353184 |
| N | -4.704800 | -1.935988 | 0.380485 |
| N | 8.133652 | -3.084493 | 0.642587 |
| C | 2.233777 | 0.213744 | -0.597114 |
| C | 1.212247 | -0.182571 | -1.645471 |
| C | 0.047611 | 0.813446 | -1.369209 |
| C | -1.223068 | 0.140587 | -0.885320 |
| C | -1.340539 | -0.354642 | 0.418327 |
| C | -2.476049 | -1.035499 | 0.839170 |
| C | -3.569185 | -1.257053 | -0.034185 |
| C | -3.445602 | -0.747550 | -1.348482 |
| C | -2.298538 | -0.071082 | -1.752805 |
| C | -5.758231 | -2.313972 | -0.556186 |
| C | -6.838096 | -1.241219 | -0.752272 |
| C | -4.902915 | -2.321760 | 1.774521 |
| C | -4.303223 | -3.686424 | 2.140031 |
| C | 0.175408 | 2.948092 | 0.056031 |
| C | -1.078801 | 3.398291 | -0.392716 |
| C | -1.553831 | 4.647223 | 0.005848 |
| C | -0.804465 | 5.464241 | 0.851340 |
| C | 0.439747 | 5.011516 | 1.299320 |
| C | 0.933420 | 3.770891 | 0.910600 |
| H | -1.181834 | 6.435549 | 1.157435 |
| C | 3.487342 | -0.478105 | -0.330538 |
| C | 4.371924 | -0.028310 | 0.673688 |
| C | 5.561731 | -0.691153 | 0.921868 |
| C | 5.909279 | -1.832655 | 0.171628 |
| C | 5.038412 | -2.288566 | -0.830830 |
| C | 3.846122 | -1.618174 | -1.075179 |
| C | 7.136466 | -2.522193 | 0.431143 |

**Table A-20.** (continued).

| | | | |
|---|---|---|---|
| H | 0.875831 | -1.218488 | -1.538979 |
| H | 1.621386 | -0.072359 | -2.657768 |
| H | -0.178807 | 1.404932 | -2.264188 |
| H | -0.527161 | -0.203756 | 1.123915 |
| H | -2.501804 | -1.410276 | 1.855373 |
| H | -4.257309 | -0.855594 | -2.057837 |
| H | -2.249759 | 0.306578 | -2.773157 |
| H | -6.220077 | -3.233469 | -0.177791 |
| H | -5.307271 | -2.582505 | -1.517874 |
| H | -7.330769 | -1.004722 | 0.197618 |
| H | -7.605055 | -1.590719 | -1.453947 |
| H | -6.409672 | -0.313526 | -1.145166 |
| H | -5.983133 | -2.335149 | 1.962053 |
| H | -4.498960 | -1.540416 | 2.427192 |
| H | -4.743884 | -4.484044 | 1.531089 |
| H | -4.495018 | -3.920873 | 3.193999 |
| H | -3.220789 | -3.700489 | 1.976789 |
| H | -1.690415 | 2.771481 | -1.030830 |
| H | -2.526540 | 4.977244 | -0.350368 |
| H | 1.040594 | 5.633913 | 1.957828 |
| H | 1.902123 | 3.427566 | 1.251743 |
| H | 4.104014 | 0.848814 | 1.252601 |
| H | 6.234163 | -0.337024 | 1.696986 |
| H | 5.301863 | -3.167311 | -1.410912 |
| H | 3.184730 | -1.986450 | -1.853383 |

**Table A-21.** Cartesian Atomic Coordinates for the Geometry Optimized Structure of Pyrazoline **2-1c** (B3LYP/6-31G*).

| atom | x/Å | y/Å | z/Å |
|---|---|---|---|
| N | 0.537214 | -1.886911 | -0.028138 |
| N | -0.736549 | -2.006288 | 0.420441 |
| N | -5.141280 | 2.726776 | -0.409963 |
| C | 1.143993 | -0.922614 | 0.593454 |
| C | 0.268791 | -0.274285 | 1.649482 |
| C | -1.106608 | -0.964478 | 1.414271 |
| C | -2.188779 | -0.023261 | 0.918204 |
| C | -2.154504 | 0.514142 | -0.373954 |
| C | -3.113152 | 1.418300 | -0.812882 |
| C | -4.177753 | 1.829247 | 0.026728 |
| C | -4.209187 | 1.277399 | 1.328762 |
| C | -3.233576 | 0.380068 | 1.753442 |
| C | -6.173129 | 3.238748 | 0.485552 |
| C | -7.422909 | 2.351951 | 0.572942 |
| C | -5.197969 | 3.176719 | -1.797534 |
| C | -4.339513 | 4.415167 | -2.089236 |
| C | -1.529635 | -3.088032 | 0.030643 |
| C | -2.832763 | -3.235753 | 0.538863 |
| C | -3.612085 | -4.326678 | 0.156144 |
| C | -3.121745 | -5.282666 | -0.732489 |
| C | -1.827412 | -5.131563 | -1.238563 |
| C | -1.032487 | -4.052658 | -0.867225 |
| H | -3.734881 | -6.129244 | -1.027659 |
| C | 2.522744 | -0.557825 | 0.291769 |
| C | 3.244145 | -1.216930 | -0.727093 |
| C | 4.555955 | -0.869940 | -1.001573 |
| C | 5.196423 | 0.146841 | -0.272679 |
| C | 4.489029 | 0.808947 | 0.738896 |
| C | 3.170487 | 0.461193 | 1.015238 |
| C | 6.605642 | 0.470984 | -0.616901 |
| H | 0.192585 | 0.810955 | 1.531003 |
| H | 0.659871 | -0.468458 | 2.656173 |

**Table A-21.** (continued).

| | | | |
|---|---|---|---|
| H | -1.453886 | -1.455974 | 2.330629 |
| H | -1.361554 | 0.217689 | -1.056497 |
| H | -3.024163 | 1.814645 | -1.817213 |
| H | -5.010276 | 1.528532 | 2.013713 |
| H | -3.300765 | -0.022596 | 2.763033 |
| H | -6.457591 | 4.234910 | 0.126143 |
| H | -5.743447 | 3.394514 | 1.481089 |
| H | -7.886433 | 2.234715 | -0.413041 |
| H | -8.165492 | 2.797087 | 1.246044 |
| H | -7.175354 | 1.352989 | 0.945847 |
| H | -6.246430 | 3.396513 | -2.031258 |
| H | -4.914024 | 2.351151 | -2.459200 |
| H | -4.652135 | 5.262275 | -1.468165 |
| H | -4.437168 | 4.711498 | -3.140513 |
| H | -3.281623 | 4.222826 | -1.883619 |
| H | -3.244892 | -2.495401 | 1.213856 |
| H | -4.616915 | -4.421668 | 0.560127 |
| H | -1.425997 | -5.866593 | -1.931982 |
| H | -0.027517 | -3.942895 | -1.255280 |
| H | 2.752898 | -2.000849 | -1.293495 |
| H | 5.113310 | -1.374808 | -1.783950 |
| H | 4.973756 | 1.595432 | 1.306828 |
| H | 2.638910 | 0.986751 | 1.803557 |
| O | 7.244233 | -0.082402 | -1.493058 |
| O | 7.117724 | 1.459369 | 0.155503 |
| C | 8.486063 | 1.825498 | -0.123158 |
| C | 8.874537 | 2.919417 | 0.854010 |
| H | 8.557777 | 2.158931 | -1.163690 |
| H | 9.117932 | 0.937455 | -0.019079 |
| H | 8.792151 | 2.567843 | 1.887624 |
| H | 8.231190 | 3.797541 | 0.736232 |
| H | 9.911189 | 3.225835 | 0.676134 |

**Table A-22.** Cartesian Atomic Coordinates for the Geometry Optimized Structure of Pyrazoline 2-2a (B3LYP/6-31G*).

| atom | x/Å | y/Å | z/Å |
|---|---|---|---|
| N | 2.536082 | 0.268861 | 0.062207 |
| N | 1.384033 | 0.805588 | -0.444271 |
| N | -4.582394 | -1.687315 | 0.383762 |
| N | -0.171485 | 7.317966 | 0.740689 |
| C | 2.738950 | -0.901453 | -0.450834 |
| C | 1.675110 | -1.294200 | -1.457821 |
| C | 0.672085 | -0.107702 | -1.377856 |
| C | -0.713349 | -0.496796 | -0.899745 |
| C | -0.961151 | -0.848272 | 0.432479 |
| C | -2.222540 | -1.244277 | 0.858722 |
| C | -3.319267 | -1.302112 | -0.036937 |
| C | -3.060541 | -0.945538 | -1.381500 |
| C | -1.788515 | -0.557706 | -1.790492 |
| C | -5.685081 | -1.857238 | -0.557758 |
| C | -6.465499 | -0.568249 | -0.850233 |
| C | -4.891271 | -1.902434 | 1.794853 |
| C | -4.624171 | -3.333243 | 2.279351 |
| C | 1.064072 | 2.128362 | -0.196509 |
| C | -0.078944 | 2.712646 | -0.783240 |
| C | -0.390220 | 4.042341 | -0.540646 |
| C | 0.419701 | 4.832408 | 0.292307 |
| C | 1.557628 | 4.246427 | 0.880179 |
| C | 1.878745 | 2.921473 | 0.642640 |
| C | 0.094047 | 6.201777 | 0.539279 |
| C | 3.891282 | -1.725472 | -0.085803 |
| C | 4.820026 | -1.289753 | 0.879820 |
| C | 5.916849 | -2.076851 | 1.209634 |
| C | 6.113807 | -3.314536 | 0.586919 |
| C | 5.200456 | -3.757282 | -0.369372 |
| C | 4.097859 | -2.971070 | -0.703066 |
| H | 6.972634 | -3.926951 | 0.847903 |
| H | 1.191930 | -2.242426 | -1.201367 |

**Table A-22.** (continued).

| | | | |
|---|---|---|---|
| H | 2.102733 | -1.406569 | -2.461464 |
| H | 0.585818 | 0.385961 | -2.353697 |
| H | -0.151363 | -0.808350 | 1.157327 |
| H | -2.350415 | -1.519977 | 1.898814 |
| H | -3.859748 | -0.945669 | -2.113073 |
| H | -1.638512 | -0.284794 | -2.834048 |
| H | -6.364948 | -2.607531 | -0.137037 |
| H | -5.302457 | -2.292152 | -1.487547 |
| H | -6.888507 | -0.151247 | 0.070660 |
| H | -7.291851 | -0.768169 | -1.542662 |
| H | -5.820166 | 0.195098 | -1.296501 |
| H | -5.949908 | -1.657048 | 1.941111 |
| H | -4.334039 | -1.181732 | 2.403072 |
| H | -5.222799 | -4.054867 | 1.712090 |
| H | -4.883561 | -3.435507 | 3.339741 |
| H | -3.570425 | -3.603236 | 2.155129 |
| H | -0.735082 | 2.120899 | -1.409185 |
| H | -1.272820 | 4.478546 | -0.998197 |
| H | 2.192616 | 4.845659 | 1.525579 |
| H | 2.758085 | 2.478485 | 1.091969 |
| H | 4.664983 | -0.329685 | 1.360992 |
| H | 6.624399 | -1.726159 | 1.956458 |
| H | 5.344104 | -4.717007 | -0.858619 |
| H | 3.395225 | -3.328768 | -1.450378 |

**Table A-23.** Cartesian Atomic Coordinates for the Geometry Optimized Structure of Pyrazoline **2-2b** (B3LYP/6-31G*).

| atom | x/Å | y/Å | z/Å |
|---|---|---|---|
| N | 1.875504 | 1.094261 | -0.117947 |
| N | 0.628952 | 1.343105 | -0.599288 |
| N | -4.323742 | -2.769265 | 0.447553 |
| N | -2.630759 | 7.076460 | 1.058072 |
| N | 8.588742 | -2.394384 | 0.927415 |
| C | 2.361840 | 0.029494 | -0.675295 |
| C | 1.424858 | -0.570727 | -1.704825 |
| C | 0.139032 | 0.289295 | -1.531715 |
| C | -1.051344 | -0.480588 | -0.993486 |
| C | -1.090665 | -0.942802 | 0.327653 |
| C | -2.155788 | -1.695074 | 0.804602 |
| C | -3.257616 | -2.022917 | -0.025027 |
| C | -3.212889 | -1.546291 | -1.356989 |
| C | -2.133432 | -0.799800 | -1.818437 |
| C | -5.400857 | -3.212003 | -0.433402 |
| C | -6.539636 | -2.195481 | -0.590050 |
| C | -4.444421 | -3.128787 | 1.858285 |
| C | -3.741441 | -4.440745 | 2.231953 |
| C | -0.038306 | 2.508693 | -0.253565 |
| C | -1.319339 | 2.780889 | -0.775688 |
| C | -1.978612 | 3.954103 | -0.438465 |
| C | -1.386922 | 4.889140 | 0.426748 |
| C | -0.107671 | 4.614905 | 0.947067 |
| C | 0.559166 | 3.448217 | 0.614712 |
| C | -2.072229 | 6.094747 | 0.774315 |
| C | 3.683502 | -0.482946 | -0.330126 |
| C | 4.472164 | 0.147529 | 0.655278 |
| C | 5.728251 | -0.338148 | 0.977420 |
| C | 6.237243 | -1.476624 | 0.321989 |
| C | 5.461184 | -2.112586 | -0.659860 |
| C | 4.201331 | -1.619370 | -0.978218 |
| C | 7.534601 | -1.982713 | 0.655629 |

**Table A-23.** (continued).

| | | | |
|---|---|---|---|
| H | 1.218595 | -1.630042 | -1.524471 |
| H | 1.845682 | -0.483078 | -2.714266 |
| H | -0.138701 | 0.761499 | -2.480752 |
| H | -0.272327 | -0.708265 | 1.004640 |
| H | -2.122625 | -2.038747 | 1.831408 |
| H | -4.034215 | -1.736809 | -2.037301 |
| H | -2.145309 | -0.451140 | -2.850090 |
| H | -5.799267 | -4.146620 | -0.021229 |
| H | -4.982692 | -3.474360 | -1.411172 |
| H | -6.995249 | -1.967824 | 0.380147 |
| H | -7.322495 | -2.593072 | -1.246870 |
| H | -6.177980 | -1.254508 | -1.017093 |
| H | -5.513484 | -3.209434 | 2.086925 |
| H | -4.071263 | -2.304608 | 2.475837 |
| H | -4.148073 | -5.279787 | 1.656210 |
| H | -3.881859 | -4.661049 | 3.296863 |
| H | -2.666511 | -4.387947 | 2.031290 |
| H | -1.807771 | 2.068345 | -1.428216 |
| H | -2.965360 | 4.151287 | -0.845551 |
| H | 0.360985 | 5.330179 | 1.615880 |
| H | 1.545082 | 3.245642 | 1.012717 |
| H | 4.079215 | 1.022500 | 1.161374 |
| H | 6.327815 | 0.153422 | 1.737017 |
| H | 5.850237 | -2.989837 | -1.166754 |
| H | 3.614656 | -2.123452 | -1.740200 |

**Table A-24.** Cartesian Atomic Coordinates for the Geometry Optimized Structure of Pyrazoline **2-2c** (B3LYP/6-31G*).

| atom | x/Å | y/Å | z/Å |
|---|---|---|---|
| N | 0.609997 | -1.627970 | 0.123497 |
| N | -0.670709 | -1.578086 | 0.588225 |
| N | -4.651420 | 3.487906 | -0.495848 |
| N | -5.057367 | -6.565003 | -0.869874 |
| C | 1.312089 | -0.681087 | 0.660755 |
| C | 0.515513 | 0.150818 | 1.646921 |
| C | -0.921554 | -0.427234 | 1.495929 |
| C | -1.930689 | 0.564615 | 0.950106 |
| C | -1.982345 | 0.900753 | -0.407503 |
| C | -2.869628 | 1.856079 | -0.887814 |
| C | -3.762910 | 2.535536 | -0.023145 |
| C | -3.705710 | 2.188173 | 1.347802 |
| C | -2.810895 | 1.228470 | 1.809829 |
| C | -5.462688 | 4.295890 | 0.409936 |
| C | -6.802638 | 3.654186 | 0.793780 |
| C | -4.822164 | 3.738070 | -1.924346 |
| C | -3.842896 | 4.768536 | -2.502696 |
| C | -1.565153 | -2.592318 | 0.286894 |
| C | -2.874054 | -2.572835 | 0.812089 |
| C | -3.763942 | -3.594765 | 0.514299 |
| C | -3.382332 | -4.664034 | -0.313027 |
| C | -2.075229 | -4.680787 | -0.836572 |
| C | -1.179122 | -3.667298 | -0.543529 |
| C | -4.304801 | -5.712069 | -0.619435 |
| C | 2.720440 | -0.479433 | 0.331561 |
| C | 3.368065 | -1.284638 | -0.628433 |
| C | 4.705624 | -1.085187 | -0.928800 |
| C | 5.441098 | -0.077538 | -0.282831 |
| C | 4.807424 | 0.726822 | 0.672062 |
| C | 3.463707 | 0.527870 | 0.973372 |
| C | 6.873620 | 0.089619 | -0.652153 |
| H | 0.540305 | 1.218631 | 1.408621 |

**Table A-24.** (continued).

| | | | |
|---|---|---|---|
| H | 0.902398 | 0.032093 | 2.666403 |
| H | -1.282374 | -0.810855 | 2.457543 |
| H | -1.318421 | 0.403568 | -1.110491 |
| H | -2.855374 | 2.080911 | -1.947502 |
| H | -4.379020 | 2.649220 | 2.060221 |
| H | -2.808282 | 0.989059 | 2.872188 |
| H | -5.646063 | 5.258259 | -0.082444 |
| H | -4.878257 | 4.529829 | 1.306698 |
| H | -7.419596 | 3.475585 | -0.094109 |
| H | -7.363971 | 4.310733 | 1.469284 |
| H | -6.653217 | 2.692083 | 1.294080 |
| H | -5.850206 | 4.086925 | -2.076000 |
| H | -4.748680 | 2.790992 | -2.469724 |
| H | -3.951547 | 5.736556 | -2.000590 |
| H | -4.031398 | 4.918647 | -3.572384 |
| H | -2.805325 | 4.442645 | -2.379323 |
| H | -3.202421 | -1.749146 | 1.433686 |
| H | -4.769330 | -3.566439 | 0.922678 |
| H | -1.767263 | -5.502158 | -1.476188 |
| H | -0.173584 | -3.688457 | -0.943270 |
| H | 2.801926 | -2.062228 | -1.129949 |
| H | 5.208047 | -1.700542 | -1.667989 |
| H | 5.369340 | 1.506163 | 1.174451 |
| H | 2.988991 | 1.161675 | 1.716623 |
| O | 7.451387 | -0.587410 | -1.481426 |
| O | 7.473768 | 1.086651 | 0.038410 |
| C | 8.867521 | 1.313463 | -0.267746 |
| C | 9.357307 | 2.429273 | 0.635895 |
| H | 8.956546 | 1.573288 | -1.327752 |
| H | 9.419665 | 0.381546 | -0.109906 |
| H | 9.263498 | 2.149255 | 1.690133 |
| H | 8.784674 | 3.347646 | 0.470037 |
| H | 10.412223 | 2.638956 | 0.427922 |

**Table A-25.** Cartesian Atomic Coordinates for the Geometry Optimized Structure of Pyrazoline **2-2d** (B3LYP/6-31G*).

| atom | x/Å | y/Å | z/Å |
|---|---|---|---|
| N | 1.692286 | 1.248013 | -0.019008 |
| N | 0.421380 | 1.407948 | -0.511890 |
| N | -4.319714 | -2.959183 | 0.423805 |
| N | -3.146383 | 7.027442 | 0.865573 |
| C | 2.249824 | 0.221442 | -0.576601 |
| C | 1.358762 | -0.443794 | -1.608516 |
| C | 0.022096 | 0.335165 | -1.456249 |
| C | -1.133221 | -0.508732 | -0.948480 |
| C | -1.241654 | -0.874773 | 0.397874 |
| C | -2.277745 | -1.680800 | 0.852970 |
| C | -3.276684 | -2.164780 | -0.027461 |
| C | -3.156821 | -1.794327 | -1.387940 |
| C | -2.109844 | -0.988965 | -1.825515 |
| C | -5.291668 | -3.541920 | -0.495679 |
| C | -6.472228 | -2.619560 | -0.830881 |
| C | -4.539306 | -3.201698 | 1.846882 |
| C | -3.779925 | -4.415859 | 2.398147 |
| C | -0.305794 | 2.545374 | -0.221730 |
| C | -1.591779 | 2.734437 | -0.773618 |
| C | -2.313741 | 3.884447 | -0.492068 |
| C | -1.786714 | 4.880032 | 0.348332 |
| C | -0.506644 | 4.686403 | 0.903414 |
| C | 0.224070 | 3.544230 | 0.626720 |
| C | -2.535233 | 6.062985 | 0.634154 |
| C | 3.599803 | -0.217411 | -0.235630 |
| C | 4.348272 | 0.430105 | 0.772088 |
| C | 5.628362 | 0.014471 | 1.087812 |
| C | 6.213188 | -1.069146 | 0.407337 |
| C | 5.488623 | -1.724242 | -0.593564 |
| C | 4.196022 | -1.296081 | -0.902611 |
| O | 7.475891 | -1.399402 | 0.796855 |
| C | 8.117416 | -2.487984 | 0.149918 |

**Table A-25.** (continued).

| | | | |
|---|---|---|---|
| H | 9.101548 | -2.573561 | 0.613838 |
| H | 8.238026 | -2.303264 | -0.925673 |
| H | 1.220871 | -1.512290 | -1.416159 |
| H | 1.782944 | -0.343086 | -2.615229 |
| H | -0.263351 | 0.793536 | -2.410899 |
| H | -0.504174 | -0.515853 | 1.111690 |
| H | -2.301501 | -1.939724 | 1.904641 |
| H | -3.896958 | -2.113160 | -2.111906 |
| H | -2.064693 | -0.721233 | -2.880111 |
| H | -5.668097 | -4.463987 | -0.036752 |
| H | -4.779531 | -3.855159 | -1.411959 |
| H | -7.018760 | -2.339618 | 0.076769 |
| H | -7.173309 | -3.124134 | -1.506318 |
| H | -6.133371 | -1.697537 | -1.313906 |
| H | -5.616014 | -3.346454 | 1.993870 |
| H | -4.281489 | -2.299793 | 2.412563 |
| H | -4.065538 | -5.329047 | 1.864062 |
| H | -4.004967 | -4.559369 | 3.461733 |
| H | -2.697823 | -4.290541 | 2.290108 |
| H | -2.033733 | 1.971952 | -1.403066 |
| H | -3.301305 | 4.016733 | -0.923168 |
| H | -0.087615 | 5.447408 | 1.554677 |
| H | 1.209925 | 3.402761 | 1.050489 |
| H | 3.901112 | 1.263967 | 1.303106 |
| H | 6.205384 | 0.509195 | 1.862982 |
| H | 5.912795 | -2.560878 | -1.136695 |
| H | 3.650658 | -1.820023 | -1.682676 |
| H | 7.564224 | -3.425270 | 0.295160 |

**Table A-26.** Cartesian Atomic Coordinates for the Geometry Optimized Structure of Pyrazoline **2-3a** (B3LYP/6-31G*).

| atom | x/Å | y/Å | z/Å |
|---|---|---|---|
| F | 1.494199 | -5.180565 | 1.148998 |
| F | 0.011564 | -2.568563 | -2.486596 |
| F | 1.429800 | -4.657585 | -1.538018 |
| F | 0.161759 | -3.528393 | 2.875435 |
| F | -1.158190 | -1.379185 | 1.969791 |
| N | -2.510019 | -0.420852 | -0.184412 |
| N | -1.382571 | -0.853568 | -0.841628 |
| N | 4.066692 | 2.515824 | 0.393966 |
| C | -2.876956 | 0.721388 | -0.666340 |
| C | -1.963239 | 1.213398 | -1.773972 |
| C | -0.778804 | 0.210412 | -1.706219 |
| C | 0.502161 | 0.783640 | -1.136402 |
| C | 0.629153 | 1.110842 | 0.220524 |
| C | 1.791935 | 1.677078 | 0.726949 |
| C | 2.904502 | 1.948714 | -0.107296 |
| C | 2.773154 | 1.605724 | -1.473539 |
| C | 1.600026 | 1.038867 | -1.962685 |
| C | 5.154778 | 2.933996 | -0.483720 |
| C | 6.174137 | 1.827806 | -0.788728 |
| C | 4.256170 | 2.742693 | 1.823348 |
| C | 3.710200 | 4.088049 | 2.320982 |
| C | -0.655877 | -1.913949 | -0.302701 |
| C | 0.045787 | -2.779221 | -1.158375 |
| C | 0.781552 | -3.857404 | -0.681863 |
| C | 0.806745 | -4.130613 | 0.683328 |
| C | 0.116602 | -3.295362 | 1.557058 |
| C | -0.583602 | -2.193099 | 1.073458 |
| C | -4.078543 | 1.411390 | -0.194009 |
| C | -4.861645 | 0.869379 | 0.844150 |
| C | -5.998729 | 1.532680 | 1.289518 |
| C | -6.382590 | 2.748639 | 0.712565 |
| C | -5.615623 | 3.294242 | -0.316299 |

**Table A-26.** (continued).

| | | | |
|---|---|---|---|
| C | -4.473099 | 2.632173 | -0.766427 |
| H | -7.272194 | 3.263996 | 1.064706 |
| H | -1.625602 | 2.243634 | -1.626520 |
| H | -2.477027 | 1.168646 | -2.743012 |
| H | -0.573010 | -0.215387 | -2.690733 |
| H | -0.190992 | 0.906237 | 0.904251 |
| H | 1.826204 | 1.921091 | 1.781935 |
| H | 3.598346 | 1.755872 | -2.159427 |
| H | 1.546981 | 0.781816 | -3.019148 |
| H | 5.663837 | 3.776655 | -0.000852 |
| H | 4.736014 | 3.333255 | -1.414028 |
| H | 6.638331 | 1.459242 | 0.133083 |
| H | 6.970350 | 2.206713 | -1.440816 |
| H | 5.698671 | 0.976344 | -1.286166 |
| H | 5.332374 | 2.685875 | 2.025817 |
| H | 3.805870 | 1.916433 | 2.383816 |
| H | 4.196162 | 4.922192 | 1.802124 |
| H | 3.892847 | 4.204609 | 3.395912 |
| H | 2.632728 | 4.166763 | 2.144579 |
| H | -4.559605 | -0.072520 | 1.290308 |
| H | -6.591827 | 1.101500 | 2.091932 |
| H | -5.904459 | 4.237839 | -0.771762 |
| H | -3.884065 | 3.069204 | -1.567803 |

**Table A-27.** Cartesian Atomic Coordinates for the Geometry Optimized Structure of Pyrazoline **2-3b** (B3LYP/6-31G*).

| atom | x/Å | y/Å | z/Å |
|---|---|---|---|
| F | -4.236298 | -5.172412 | -0.677530 |
| F | -2.666831 | -1.812824 | 2.271258 |
| F | -4.451211 | -3.753112 | 1.665182 |
| F | -2.162076 | -4.621227 | -2.398259 |
| F | -0.335313 | -2.688721 | -1.782790 |
| O | 7.662936 | -0.584430 | -1.356929 |
| O | 7.725394 | 1.092543 | 0.158503 |
| N | 0.757895 | -1.344820 | 0.128008 |
| N | -0.527815 | -1.242108 | 0.569592 |
| N | -4.282378 | 3.975377 | -0.599262 |
| C | 1.487720 | -0.424949 | 0.675143 |
| C | 0.707713 | 0.441482 | 1.644672 |
| C | -0.748419 | -0.079070 | 1.469542 |
| C | -1.707122 | 0.950470 | 0.903067 |
| C | -1.721128 | 1.283763 | -0.456111 |
| C | -2.560744 | 2.272201 | -0.954801 |
| C | -3.441253 | 2.989781 | -0.108139 |
| C | -3.422430 | 2.645101 | 1.264518 |
| C | -2.575138 | 1.651980 | 1.745062 |
| C | -5.076558 | 4.818281 | 0.289656 |
| C | -6.447751 | 4.232056 | 0.651183 |
| C | -4.417492 | 4.227244 | -2.031168 |
| C | -3.387628 | 5.215749 | -2.594751 |
| C | -1.456701 | -2.220760 | 0.255018 |
| C | -2.520739 | -2.508086 | 1.135163 |
| C | -3.444071 | -3.494547 | 0.820052 |
| C | -3.339598 | -4.223236 | -0.376552 |
| C | -2.276770 | -3.933993 | -1.253673 |
| C | -1.349015 | -2.953446 | -0.947379 |
| C | 2.908634 | -0.280954 | 0.370717 |
| C | 3.540414 | -1.114696 | -0.575293 |
| C | 4.890053 | -0.970025 | -0.852229 |

**Table A-27.** (continued).

| | | | |
|---|---|---|---|
| C | 5.653716 | 0.009562 | -0.195898 |
| C | 5.035930 | 0.841894 | 0.745262 |
| C | 3.680177 | 0.697929 | 1.023009 |
| C | 7.098083 | 0.117989 | -0.539963 |
| C | 9.132317 | 1.262295 | -0.123231 |
| C | 9.650293 | 2.360739 | 0.785928 |
| H | 0.779537 | 1.506628 | 1.403957 |
| H | 1.071310 | 0.310853 | 2.671241 |
| H | -1.141395 | -0.444668 | 2.425582 |
| H | -1.065270 | 0.758027 | -1.145772 |
| H | -2.518609 | 2.492660 | -2.014692 |
| H | -4.089314 | 3.135220 | 1.963554 |
| H | -2.600992 | 1.416288 | 2.807962 |
| H | -5.212389 | 5.785550 | -0.208491 |
| H | -4.499223 | 5.031693 | 1.196124 |
| H | -7.055501 | 4.075230 | -0.247094 |
| H | -6.994260 | 4.912808 | 1.314775 |
| H | -6.346003 | 3.266435 | 1.156663 |
| H | -5.427861 | 4.616451 | -2.202215 |
| H | -4.372372 | 3.276133 | -2.572610 |
| H | -3.466253 | 6.189040 | -2.097286 |
| H | -3.550924 | 5.369590 | -3.668060 |
| H | -2.366292 | 4.849017 | -2.451894 |
| H | 2.952581 | -1.870777 | -1.084798 |
| H | 5.380471 | -1.607487 | -1.580615 |
| H | 5.619601 | 1.599870 | 1.255568 |
| H | 3.218079 | 1.352787 | 1.755930 |
| H | 9.250499 | 1.514767 | -1.182181 |
| H | 9.643744 | 0.309645 | 0.046991 |
| H | 9.526589 | 2.088303 | 1.839078 |
| H | 9.117966 | 3.300728 | 0.607404 |
| H | 10.716320 | 2.527302 | 0.596351 |

**Table A-28.** Cartesian Atomic Coordinates for the Geometry Optimized Structure of Pyrazoline **2-4a** (B3LYP/6-31G*).

| atom | x/Å | y/Å | z/Å |
|---|---|---|---|
| N | 1.947118 | 0.803112 | -0.060941 |
| N | 0.685173 | 1.070604 | -0.466576 |
| N | -4.652742 | -2.599435 | 0.455856 |
| C | -0.919082 | 7.136940 | 1.007698 |
| C | 2.360222 | -0.317774 | -0.570396 |
| C | 1.329007 | -0.956236 | -1.479620 |
| C | 0.132445 | 0.037206 | -1.380364 |
| C | -1.148455 | -0.601075 | -0.877145 |
| C | -1.356702 | -0.876961 | 0.478529 |
| C | -2.500558 | -1.529801 | 0.921997 |
| C | -3.510683 | -1.944891 | 0.019274 |
| C | -3.296859 | -1.653296 | -1.348763 |
| C | -2.143818 | -1.000625 | -1.773759 |
| C | -5.627786 | -3.147997 | -0.481088 |
| C | -6.715031 | -2.153718 | -0.910962 |
| C | -4.949461 | -2.761294 | 1.875728 |
| C | -4.335560 | -4.019992 | 2.503509 |
| C | 0.137433 | 2.348016 | -0.264571 |
| C | -1.127426 | 2.676656 | -0.786131 |
| C | -1.665498 | 3.941648 | -0.585757 |
| C | -0.966374 | 4.912073 | 0.141003 |
| C | 0.291354 | 4.590603 | 0.663978 |
| C | 0.836343 | 3.323167 | 0.461666 |
| O | -1.590999 | 6.122805 | 0.282218 |
| C | 3.678011 | -0.859696 | -0.272140 |
| C | 4.562208 | -0.191076 | 0.602658 |
| C | 5.819453 | -0.703439 | 0.872099 |
| C | 6.238505 | -1.909954 | 0.275380 |
| C | 5.367237 | -2.585669 | -0.593996 |
| C | 4.106693 | -2.065554 | -0.860465 |
| C | 7.537640 | -2.441704 | 0.554491 |
| N | 8.593630 | -2.875969 | 0.782118 |

**Table A-28.** (continued).

| | | | |
|---|---|---|---|
| H | -1.584235 | 8.002793 | 1.001559 |
| H | 0.034344 | 7.410287 | 0.535094 |
| H | -0.729013 | 6.834884 | 2.046833 |
| H | 1.037995 | -1.955898 | -1.139359 |
| H | 1.698754 | -1.055818 | -2.507084 |
| H | -0.061521 | 0.500453 | -2.356740 |
| H | -0.610689 | -0.571737 | 1.207949 |
| H | -2.598257 | -1.725626 | 1.983280 |
| H | -4.042334 | -1.913342 | -2.090585 |
| H | -2.025153 | -0.793162 | -2.836165 |
| H | -6.097125 | -4.013985 | 0.001226 |
| H | -5.104157 | -3.544744 | -1.357547 |
| H | -7.269065 | -1.782141 | -0.041614 |
| H | -7.430295 | -2.636467 | -1.587582 |
| H | -6.283834 | -1.289543 | -1.426530 |
| H | -6.040179 | -2.794844 | 1.982754 |
| H | -4.625692 | -1.866001 | 2.417213 |
| H | -4.699247 | -4.923570 | 2.001300 |
| H | -4.603337 | -4.090605 | 3.564472 |
| H | -3.243871 | -4.010607 | 2.424166 |
| H | -1.703666 | 1.940481 | -1.333692 |
| H | -2.641759 | 4.194944 | -0.987355 |
| H | 0.863395 | 5.318307 | 1.228634 |
| H | 1.813143 | 3.083986 | 0.863233 |
| H | 4.239830 | 0.736306 | 1.063253 |
| H | 6.491175 | -0.180287 | 1.545495 |
| H | 5.684349 | -3.515499 | -1.055391 |
| H | 3.446623 | -2.602529 | -1.534890 |

**Table A-29.** Cartesian Atomic Coordinates for the Geometry Optimized Structure of Pyrazoline **2-4b** (B3LYP/6-31G*).

| atom | x/Å | y/Å | z/Å |
|---|---|---|---|
| O | 7.549975 | -0.526868 | -1.412528 |
| O | 7.551513 | 1.169163 | 0.082803 |
| O | -4.144551 | -5.693190 | -0.191936 |
| N | 0.652132 | -1.464525 | 0.039487 |
| N | -0.640569 | -1.380724 | 0.440875 |
| N | -4.744714 | 3.623815 | -0.483746 |
| C | -3.751225 | -6.871332 | -0.871541 |
| C | 1.352451 | -0.507772 | 0.566585 |
| C | 0.530849 | 0.371712 | 1.489949 |
| C | -0.893177 | -0.246640 | 1.366111 |
| C | -1.940319 | 0.727389 | 0.859626 |
| C | -2.042336 | 1.067501 | -0.493789 |
| C | -2.957547 | 2.013282 | -0.940765 |
| C | -3.830350 | 2.676862 | -0.044529 |
| C | -3.726924 | 2.321758 | 1.321096 |
| C | -2.803245 | 1.373065 | 1.749592 |
| C | -5.531425 | 4.419271 | 0.452980 |
| C | -6.853371 | 3.764254 | 0.874984 |
| C | -4.948931 | 3.894088 | -1.903183 |
| C | -3.984634 | 4.934600 | -2.489463 |
| C | -1.501805 | -2.474121 | 0.258549 |
| C | -2.808520 | -2.451560 | 0.780641 |
| C | -3.655007 | -3.539903 | 0.610081 |
| C | -3.231187 | -4.676526 | -0.087474 |
| C | -1.936445 | -4.701615 | -0.617569 |
| C | -1.081902 | -3.613351 | -0.443927 |
| C | 2.768365 | -0.329834 | 0.270666 |
| C | 3.434658 | -1.164068 | -0.653080 |
| C | 4.781742 | -0.987420 | -0.920611 |
| C | 5.513777 | 0.025549 | -0.277215 |
| C | 4.862359 | 0.858825 | 0.641242 |
| C | 3.508703 | 0.683845 | 0.908673 |

**Table A-29.** (continued).

| | | | |
|---|---|---|---|
| C | 6.955097 | 0.168221 | -0.609644 |
| C | 8.953944 | 1.373088 | -0.190218 |
| C | 9.437641 | 2.488833 | 0.717332 |
| H | 0.534789 | 1.420401 | 1.173617 |
| H | 0.906950 | 0.341531 | 2.519636 |
| H | -1.221725 | -0.649508 | 2.333155 |
| H | -1.396089 | 0.578341 | -1.218233 |
| H | -2.980918 | 2.242504 | -1.999513 |
| H | -4.384785 | 2.768256 | 2.057220 |
| H | -2.764002 | 1.127221 | 2.809709 |
| H | -5.737745 | 5.384466 | -0.024699 |
| H | -4.921097 | 4.650210 | 1.333390 |
| H | -7.499993 | 3.593519 | 0.006735 |
| H | -7.395013 | 4.407349 | 1.579098 |
| H | -6.679449 | 2.796278 | 1.355458 |
| H | -5.980845 | 4.243038 | -2.026761 |
| H | -4.885880 | 2.955384 | -2.464308 |
| H | -4.082966 | 5.894848 | -1.970442 |
| H | -4.197390 | 5.100288 | -3.552427 |
| H | -2.944288 | 4.608262 | -2.394125 |
| H | -3.173906 | -1.578525 | 1.308270 |
| H | -4.662398 | -3.523306 | 1.014740 |
| H | -1.574130 | -5.565291 | -1.164095 |
| H | -0.076864 | -3.644712 | -0.845964 |
| H | 2.871859 | -1.945455 | -1.152572 |
| H | 5.295831 | -1.624546 | -1.633011 |
| H | 5.419696 | 1.642948 | 1.141526 |
| H | 3.021082 | 1.341085 | 1.622730 |
| H | 9.074677 | 1.623980 | -1.249445 |
| H | 9.489815 | 0.435280 | -0.011975 |
| H | 9.313348 | 2.217763 | 1.770830 |
| H | 8.881926 | 3.413727 | 0.531433 |
| H | 10.500332 | 2.682722 | 0.534686 |
| H | -4.608047 | -7.546682 | -0.824992 |

**Table A-29.** (continued).

| | | | |
|---|---|---|---|
| H | -2.887603 | -7.349781 | -0.389030 |
| H | -3.506035 | -6.672393 | -1.924240 |

**Table A-30.** Cartesian Atomic Coordinates for the Geometry Optimized Structure of Pyrazoline **2-5** (B3LYP/6-31G*).

| atom | x/Å | y/Å | z/Å |
|---|---|---|---|
| F | -3.821324 | -6.139202 | -0.580905 |
| N | 0.626049 | -1.668882 | -0.015894 |
| N | -0.668517 | -1.687564 | 0.395492 |
| N | -5.039965 | 3.095571 | -0.443171 |
| O | 7.438801 | -0.247614 | -1.439929 |
| O | 7.351045 | 1.378927 | 0.128013 |
| C | 1.262604 | -0.690058 | 0.548297 |
| C | 0.390379 | 0.093889 | 1.509787 |
| C | -0.995311 | -0.598707 | 1.350834 |
| C | -2.090699 | 0.328716 | 0.858328 |
| C | -2.201187 | 0.693789 | -0.487972 |
| C | -3.164368 | 1.597029 | -0.921357 |
| C | -4.078758 | 2.190687 | -0.017493 |
| C | -3.966030 | 1.810307 | 1.340741 |
| C | -2.994869 | 0.904169 | 1.755776 |
| C | -5.861995 | 3.840355 | 0.505117 |
| C | -7.155054 | 3.121939 | 0.913396 |
| C | -5.256309 | 3.377320 | -1.858931 |
| C | -4.347802 | 4.475510 | -2.429054 |
| C | -1.467193 | -2.808554 | 0.143552 |
| C | -2.772488 | -2.885724 | 0.661243 |
| C | -3.563740 | -4.008191 | 0.417483 |
| C | -3.054403 | -5.048465 | -0.345923 |
| C | -1.769125 | -4.993348 | -0.874286 |
| C | -0.975557 | -3.877880 | -0.629718 |
| C | 2.664425 | -0.410168 | 0.258679 |
| C | 3.375234 | -1.158949 | -0.703445 |
| C | 4.707965 | -0.888924 | -0.964983 |
| C | 5.379965 | 0.136302 | -0.277804 |
| C | 4.683544 | 0.886242 | 0.678285 |
| C | 3.343907 | 0.617042 | 0.940046 |
| C | 6.809864 | 0.377516 | -0.606278 |

**Table A-30.** (continued).

| | | | |
|---|---|---|---|
| C | 8.739382 | 1.672149 | -0.138651 |
| C | 9.160466 | 2.783747 | 0.804368 |
| H | 0.333939 | 1.155124 | 1.245740 |
| H | 0.767939 | 0.033396 | 2.537661 |
| H | -1.310303 | -1.048120 | 2.301522 |
| H | -1.523008 | 0.258659 | -1.217715 |
| H | -3.192807 | 1.849839 | -1.974439 |
| H | -4.653551 | 2.202823 | 2.080636 |
| H | -2.950045 | 0.636185 | 2.810296 |
| H | -6.109193 | 4.803965 | 0.043929 |
| H | -5.262650 | 4.081393 | 1.390285 |
| H | -7.792215 | 2.937198 | 0.041040 |
| H | -7.725432 | 3.729638 | 1.626209 |
| H | -6.940648 | 2.154906 | 1.379285 |
| H | -6.304893 | 3.673958 | -1.978188 |
| H | -5.143998 | 2.451377 | -2.433463 |
| H | -4.492574 | 5.420339 | -1.893002 |
| H | -4.573458 | 4.648785 | -3.488095 |
| H | -3.291520 | 4.201529 | -2.343755 |
| H | -3.183659 | -2.066557 | 1.238884 |
| H | -4.571961 | -4.075110 | 0.813595 |
| H | -1.396742 | -5.823306 | -1.466423 |
| H | 0.030951 | -3.824165 | -1.024679 |
| H | 2.859435 | -1.949287 | -1.238351 |
| H | 5.256584 | -1.461678 | -1.705690 |
| H | 5.193657 | 1.679323 | 1.213844 |
| H | 2.821355 | 1.211014 | 1.684468 |
| H | 8.842827 | 1.962906 | -1.189314 |
| H | 9.327958 | 0.761019 | 0.009198 |
| H | 9.051394 | 2.473240 | 1.848595 |
| H | 8.554892 | 3.682199 | 0.646550 |
| H | 10.210817 | 3.041392 | 0.629637 |

**Table A-31.** Cartesian Atomic Coordinates for the Geometry Optimized Structure of Pyrazoline **2-6** (B3LYP/6-31G*).

| atom | x/Å | y/Å | z/Å |
|---|---|---|---|
| O | 6.250218 | -2.045811 | -1.032108 |
| O | 6.740752 | -0.130193 | 0.064499 |
| N | -0.620793 | -0.675290 | 0.121369 |
| N | -1.840800 | -0.150565 | 0.433915 |
| H | -3.982115 | 5.141201 | -1.930852 |
| N | -7.467749 | -3.912957 | -0.218003 |
| C | 0.318000 | 0.133858 | 0.495562 |
| C | -0.219435 | 1.374653 | 1.186340 |
| C | -1.758354 | 1.200021 | 1.039773 |
| C | -2.412223 | 2.280460 | 0.191528 |
| C | -2.319420 | 2.259239 | -1.205571 |
| C | -2.881794 | 3.285051 | -1.964621 |
| C | -3.540674 | 4.345225 | -1.337581 |
| C | -3.636743 | 4.372673 | 0.054098 |
| C | -3.076510 | 3.343898 | 0.812872 |
| C | -2.987975 | -0.919237 | 0.306088 |
| C | -4.242670 | -0.405522 | 0.693446 |
| C | -5.386946 | -1.179964 | 0.562928 |
| C | -5.319037 | -2.482992 | 0.043011 |
| C | -4.064242 | -2.994464 | -0.340105 |
| C | -2.916818 | -2.231300 | -0.210038 |
| C | -6.502541 | -3.272236 | -0.099452 |
| C | 1.731056 | -0.160760 | 0.267810 |
| C | 2.129298 | -1.328492 | -0.415967 |
| C | 3.471847 | -1.596219 | -0.628904 |
| C | 4.459564 | -0.710884 | -0.166664 |
| C | 4.074420 | 0.448909 | 0.516497 |
| C | 2.726031 | 0.719490 | 0.730093 |
| C | 5.885272 | -1.052002 | -0.433346 |
| C | 8.145796 | -0.388276 | -0.157925 |

**Table A-31.** (continued).

| | | | |
|---|---|---|---|
| C | 8.925919 | 0.730037 | 0.507386 |
| H | 0.124987 | 2.298697 | 0.711838 |
| H | 0.092920 | 1.408422 | 2.236852 |
| H | -2.241854 | 1.178559 | 2.023309 |
| H | -1.818004 | 1.430921 | -1.699022 |
| H | -2.810026 | 3.252805 | -3.048339 |
| H | -4.152261 | 5.189362 | 0.551873 |
| H | -3.158945 | 3.367159 | 1.897811 |
| H | -4.329782 | 0.602810 | 1.078948 |
| H | -6.347832 | -0.773673 | 0.862997 |
| H | -3.997087 | -4.001271 | -0.740586 |
| H | -1.953289 | -2.630237 | -0.499175 |
| H | 1.367956 | -2.012693 | -0.774946 |
| H | 3.784619 | -2.490693 | -1.157167 |
| H | 4.832673 | 1.135190 | 0.875832 |
| H | 2.444800 | 1.623771 | 1.261724 |
| H | 8.329012 | -0.432417 | -1.236586 |
| H | 8.394053 | -1.369553 | 0.258765 |
| H | 8.733477 | 0.755253 | 1.584890 |
| H | 8.653807 | 1.702789 | 0.084982 |
| H | 9.999586 | 0.576316 | 0.353198 |

**Table A-32.** Calculated Ground- and Excited State Energies for Pyrazoline **2-1a** (TD-FT, B3LYP/6-31G*//B3LYP/6-31G*). H = HOMO, L = LUMO.

| state | energy [hartree] | multi-plicity | excitation energy [eV] | oscillator strength | transition | | amplitude |
|---|---|---|---|---|---|---|---|
| ground state | -1133.156502 | 1 | 0 | | | | |
| excited state 1 | -1133.067919 | 3 | 2.4105 | 0.0000 | H | –> L | 0.9563 |
| excited state 2 | -1133.025469 | 3 | 3.5656 | 0.0000 | H-1 | –> L | 0.7405 |
| | | | | | H-1 | –> L+1 | -0.6358 |
| excited state 3 | -1133.023700 | 1 | 3.6137 | 0.7569 | H | –> L | 0.9757 |
| excited state 4 | -1133.022209 | 1 | 3.6543 | 0.0085 | H-1 | –> L | 0.9952 |
| excited state 5 | -1133.022208 | 3 | 3.6543 | 0.0000 | H-1 | –> L | 0.4822 |
| | | | | | H-1 | –> L+1 | 0.6622 |
| | | | | | H-1 | –> L+3 | -0.4490 |
| | | | | | H-1 | –> L+4 | -0.2556 |
| excited state 6 | -1133.018455 | 3 | 3.7564 | 0.0000 | H-1 | –> L | 0.4213 |
| | | | | | H-1 | –> L+1 | 0.3149 |
| | | | | | H-1 | –> L+3 | 0.5777 |
| | | | | | H-1 | –> L+4 | 0.4705 |
| excited state 7 | -1133.016828 | 3 | 3.8007 | 0.0000 | H-3 | –> L | 0.4391 |
| | | | | | H-2 | –> L | 0.2545 |
| | | | | | H | –> L+3 | 0.3422 |
| | | | | | H | –> L+4 | -0.2984 |
| | | | | | H | –> L+5 | 0.5090 |
| excited state 8 | -1133.014217 | 3 | 3.8718 | 0.0000 | H | –> L+1 | 0.2725 |
| | | | | | H | –> L+3 | 0.5289 |
| | | | | | H | –> L+4 | -0.5479 |
| | | | | | H | –> L+5 | -0.4045 |
| excited state 9 | -1133.005067 | 1 | 4.1207 | 0.0078 | H | –> L+1 | 0.9946 |
| excited state 10 | -1132.999066 | 1 | 4.2841 | 0.0268 | H-5 | –> L | 0.2943 |
| | | | | | H | –> L+2 | 0.9452 |
| excited state 11 | -1132.993357 | 1 | 4.4394 | 0.0099 | H-2 | –> L | -0.2346 |
| | | | | | H | –> L+3 | 0.9485 |
| excited state 12 | -1132.990486 | 1 | 4.5175 | 0.0330 | H-4 | –> L+3 | 0.2318 |
| | | | | | H-1 | –> L+1 | 0.9352 |

**Table A-33.** Calculated Ground- and Excited State Energies for Pyrazoline **2-1b** (TD-FT, B3LYP/6-31G*//B3LYP/6-31G*). H = HOMO, L = LUMO.

| state | energy [hartree] | multi-plicity | excitation energy [eV] | oscillator strength | transition | | amplitude |
|---|---|---|---|---|---|---|---|
| ground state | -1225.401762 | 1 | 0 | | | | |
| excited state 1 | -1225.325600 | 3 | 2.0725 | 0.0000 | H | –> L | 0.9569 |
| excited state 2 | -1225.291385 | 3 | 3.0035 | 0.0000 | H-1 | –> L | 0.9904 |
| excited state 3 | -1225.290505 | 1 | 3.0274 | 0.0170 | H-1 | –> L | 0.9914 |
| excited state 4 | -1225.283314 | 1 | 3.2231 | 0.9740 | H | –> L | 0.9723 |
| excited state 5 | -1225.269616 | 3 | 3.5959 | 0.0000 | H-4 | –> L | -0.4190 |
| | | | | | H-3 | –> L | -0.6319 |
| | | | | | H-2 | –> L | 0 .2143 |
| | | | | | H | –> L+3 | -0.3050 |
| | | | | | H | –> L+4 | -0.2769 |
| excited state 6 | -1225.269148 | 3 | 3.6086 | 0.0000 | H-1 | –> L+2 | -0.9501 |
| excited state 7 | -1225.265275 | 3 | 3.7140 | 0.0000 | H-1 | –> L+3 | -0.5324 |
| | | | | | H-1 | –> L+5 | 0.7404 |
| excited state 8 | -1225.262882 | 3 | 3.7791 | 0.0000 | H-5 | –> L | -0.2199 |
| | | | | | H | –> L+1 | 0.9351 |
| excited state 9 | -1225.252504 | 1 | 4.0615 | 0.0202 | H-5 | –> L | 0.2752 |
| | | | | | H | –> L+1 | 0.9552 |
| excited state 10 | -1225.245673 | 1 | 4.2474 | 0.0008 | H-5 | –> L | -0.3043 |
| | | | | | H | –> L+1 | 0.9429 |
| excited state 11 | -1225.243068 | 1 | 4.3183 | 0.0070 | H-2 | –> L | 0.8049 |
| | | | | | H | –> L+2 | 0.3108 |
| | | | | | H | –> L+3 | 0.4204 |
| excited state 12 | -1225.238334 | 1 | 4.4471 | 0.0008 | H-1 | –> L+1 | 0.9978 |

**Table A-34.** Calculated Ground- and Excited State Energies for Pyrazoline **2-1c** (TD-FT, B3LYP/6-31G*//B3LYP/6-31G*). H = HOMO, L = LUMO.

| state | energy [hartree] | multi-plicity | excitation energy [eV] | oscillator strength | transition | | amplitude |
|---|---|---|---|---|---|---|---|
| ground state | -1400.356770 | 1 | 0 | | | | |
| excited state 1 | -1400.279016 | 3 | 2.1158 | 0.0000 | H | –> L | 0.9526 |
| excited state 2 | -1400.241366 | 3 | 3.1403 | 0.0000 | H-1 | –> L | 0.9874 |
| excited state 3 | -1400.240419 | 1 | 3.1661 | 0.1059 | H-1 | –> L | 0.9465 |
| | | | | | H | –> L | -0.3125 |
| excited state 4 | -1400.238717 | 1 | 3.2124 | 0.8825 | H-1 | –> L | 0.3138 |
| | | | | | H | –> L | 0.9296 |
| excited state 5 | -1400.223821 | 3 | 3.6177 | 0.0000 | H-1 | –> L+1 | -0.9436 |
| excited state 6 | -1400.223280 | 3 | 3.6325 | 0.0000 | H-3 | –> L | -0.6568 |
| | | | | | H-2 | –> L | -0.2358 |
| | | | | | H | –> L+3 | 0.4629 |
| | | | | | H | –> L+6 | -0.2245 |
| excited state 7 | -1400.219748 | 3 | 3.7286 | 0.0000 | H-4 | –> L+1 | -0.2369 |
| | | | | | H-1 | –> L+1 | -0.2379 |
| | | | | | H-1 | –> L+3 | 0.4862 |
| | | | | | H-1 | –> L+4 | -0.4053 |
| | | | | | H-1 | –> L+5 | -0.6308 |
| excited state 8 | -1400.2148803 | 3 | 3.8610 | 0.0000 | H-3 | –> L | -0.2125 |
| | | | | | H | –> L+3 | -0.5198 |
| | | | | | H | –> L+4 | 0.5258 |
| | | | | | H | –> L+5 | -0.4836 |
| excited state 9 | -1400.203799 | 1 | 4.1626 | 0.0016 | H | –> L+1 | 0.9940 |
| excited state 10 | -1400.201262 | 1 | 4.2316 | 0.0091 | H-5 | –> L | 0.4107 |
| | | | | | H | –> L+2 | 0.9006 |
| excited state 11 | -1400.197248 | 1 | 4.3408 | 0.0079 | H-2 | –> L | 0.6737 |
| | | | | | H | –> L+3 | 0.5917 |
| | | | | | H | –> L+4 | -0.3847 |
| excited state 12 | -1400.191850 | 1 | 4.4877 | 0.0036 | H-2 | –> L | -0.4563 |
| | | | | | H-1 | –> L+1 | 0.4341 |
| | | | | | H | –> L+3 | 0.5269 |
| | | | | | H | –> L+5 | -0.4864 |

**Table A-35.** Calculated Ground- and Excited State Energies for Pyrazoline **2-2a** (TD-FT, B3LYP/6-31G*//B3LYP/6-31G*). H = HOMO, L = LUMO.

| state | energy [hartree] | multi-plicity | excitation energy [eV] | oscillator strength | transition | | amplitude |
|---|---|---|---|---|---|---|---|
| ground state | -1225.405035 | 1 | 0 | | | | |
| excited state 1 | -1225.315628 | 3 | 2.4329 | 0.0000 | H-1 | –> L | 0.2237 |
| | | | | | H | –> L | 0.9319 |
| excited state 2 | -1225.282260 | 3 | 3.3409 | 0.0000 | H-2 | –> L | 0.2997 |
| | | | | | H-1 | –> L | -0.5765 |
| | | | | | H | –> L+1 | 0.6845 |
| excited state 3 | -1225.281034 | 3 | 3.3743 | 0.0000 | H-2 | –> L | 0.2175 |
| | | | | | H-1 | –> L | 0.7498 |
| | | | | | H | –> L | -0.2446 |
| | | | | | H | –> L+1 | 0.4845 |
| excited state 4 | -1225.280069 | 1 | 3.4005 | 0.0283 | H-1 | –> L | 0.9378 |
| | | | | | H | –> L | -0.3412 |
| excited state 5 | -1225.272943 | 1 | 3.5944 | 1.0301 | H-1 | –> L | 0.3371 |
| | | | | | H | –> L | 0.9234 |
| excited state 6 | -1225.272720 | 3 | 3.6005 | 0.0000 | H-1 | –> L+2 | -0.8182 |
| | | | | | H-1 | –> L+4 | -0.4074 |
| | | | | | H | –> L+2 | 0.2868 |
| excited state 7 | -1225.268263 | 3 | 3.7218 | 0.0000 | H-1 | –> L+2 | 0.2694 |
| | | | | | H-1 | –> L+5 | -0.8028 |
| | | | | | H | –> L+5 | 0.2589 |
| excited state 8 | -1225.265962 | 3 | 3.7844 | 0.0000 | H-1 | –> L+4 | -0.2260 |
| | | | | | H | –> L+2 | 0.4154 |
| | | | | | H | –> L+4 | -0.7808 |
| excited state 9 | -1225.246571 | 1 | 4.3120 | 0.0148 | H | –> L+2 | 0.9561 |
| excited state 10 | -1225.243765 | 1 | 4.3884 | 0.0464 | H-1 | –> L+1 | -0.3492 |
| | | | | | H | –> L+1 | 0.4102 |
| | | | | | H | –> L+3 | -.4050 |
| | | | | | H | –> L+4 | -0.6216 |
| excited state 11 | -1225.242997 | 1 | 4.4093 | 0.0196 | H-4 | –> L | 0.2873 |
| | | | | | H | –> L+3 | 0.6779 |
| | | | | | H | –> L+4 | -0.5643 |
| excited state 12 | -1225.241999 | 1 | 4.4365 | 0.0190 | H-1 | –> L+1 | 0.8157 |
| | | | | | H | –> L+1 | -0.2665 |
| | | | | | H | –> L+3 | -0.2909 |
| | | | | | H | –> L+4 | -0.3609 |

**Table A-36.** Calculated Ground- and Excited State Energies for Pyrazoline **2-2b** (TD-FT, B3LYP/6-31G*//B3LYP/6-31G*). H = HOMO, L = LUMO.

| state | energy [hartree] | multi-plicity | excitation energy [eV] | oscillator strength | transition | | amplitude |
|---|---|---|---|---|---|---|---|
| ground state | -1317.648487 | 1 | 0 | | | | |
| excited state 1 | -1317.568962 | 3 | 2.1640 | 0.0000 | H-1 | –> L | 0.8704 |
| | | | | | H | –> L | -0.3990 |
| excited state 2 | -1317.544113 | 3 | 2.8402 | 0.0000 | H-1 | –> L | 0.4105 |
| | | | | | H | –> L | 0.9055 |
| excited state 3 | -1317.543237 | 1 | 2.8640 | 0.0224 | H-1 | –> L | 0.3378 |
| | | | | | H | –> L | 0.9391 |
| excited state 4 | -1317.529163 | 1 | 3.2470 | 1.1235 | H-1 | –> L | 0.9254 |
| | | | | | H | –> L | -0.3329 |
| excited state 5 | -1317.526125 | 3 | 3.3296 | 0.0000 | H-3 | –> L | 0.4166 |
| | | | | | H-2 | –> L | -0.2548 |
| | | | | | H-1 | –> L+1 | 0.7193 |
| | | | | | H-1 | –> L+2 | 0.2362 |
| | | | | | H | –> L+1 | -0.2818 |
| excited state 6 | -1317.516672 | 3 | 3.5869 | 0.0000 | H-1 | –> L+4 | 0.2770 |
| | | | | | H | –> L+3 | 0.4176 |
| | | | | | H | –> L+4 | 0.8168 |
| excited state 7 | -1317.512848 | 3 | 3.6909 | 0.0000 | H-1 | –> L+5 | 0.2660 |
| | | | | | H | –> L+3 | 0.3867 |
| | | | | | H | –> L+5 | 0.7612 |
| | | | | | H | –> L+6 | -0.2774 |
| excited state 8 | -1317.510928 | 3 | 3.7432 | 0.0000 | H-6 | –> L | -0.3456 |
| | | | | | H-3 | –> L | 0.5545 |
| | | | | | H-2 | –> L | -0.3043 |
| | | | | | H-1 | –> L+1 | -0.3189 |
| | | | | | H-1 | –> L+3 | 0.3208 |
| excited state 9 | -1317.494175 | 1 | 4.1990 | 0.0273 | H-5 | –> L | 0.3220 |
| | | | | | H-1 | –> L+1 | -0.2309 |
| | | | | | H-1 | –> L+2 | 0.6744 |
| | | | | | H | –> L+1 | 0.4931 |
| | | | | | H | –> L+2 | -0.3622 |
| excited state 10 | -1317.493157 | | 4.2267 | 0.0010 | H-1 | –> L+1 | 0.3601 |
| | | | | | H-1 | –> L+2 | -0.2203 |
| | | | | | H | –> L+1 | 0.8158 |
| | | | | | H | –> L+2 | 0.3581 |
| excited state 11 | -1317.488140 | | 4.3633 | 0.0115 | H-4 | –> L | -0.4771 |
| | | | | | H-3 | –> L | -0.2125 |
| | | | | | H-1 | –> L+3 | 0.6267 |
| | | | | | H-1 | –> L+4 | -0.2258 |
| | | | | | H | –> L+3 | -0.4395 |
| excited state 12 | -1317.487534 | | 4.3798 | 0.0095 | H-1 | –> L+2 | 0.4570 |
| | | | | | H | –> L+2 | 0.8453 |

**Table A-37.** Calculated Ground- and Excited State Energies for Pyrazoline **2-2c** (TD-FT, B3LYP/6-31G*//B3LYP/6-31G*). H = HOMO, L = LUMO.

| state | energy [hartree] | multi-plicity | excitation energy [eV] | oscillator strength | transition | | amplitude |
|---|---|---|---|---|---|---|---|
| ground state | -1492.604518 | 1 | o | | | | |
| excited state 1 | -1492.522421 | 3 | 2.2340 | 0.0000 | H-1 | –> L | 0.5888 |
| | | | | | H | –> L | 0.7487 |
| excited state 2 | -1492.494956 | 3 | 2.9813 | 0.0000 | H-1 | –> L | 0.7791 |
| | | | | | H | –> L | -0.6160 |
| excited state 3 | -1492.494233 | 1 | 3.0010 | 0.0194 | H-1 | –> L | 0.7346 |
| | | | | | H | –> L | -0.6752 |
| excited state 4 | -1492.484371 | 1 | 3.2694 | 1.1192 | H-1 | –> L | 0.6667 |
| | | | | | H | –> L | 0.7248 |
| excited state 5 | -1492.482417 | 3 | 3.3225 | 0.0000 | H-3 | –> L | 0.2412 |
| | | | | | H-2 | –> L | 0.3499 |
| | | | | | H-1 | –> L+1 | 0.5473 |
| | | | | | H | –> L+1 | 0.6345 |
| excited state 6 | -1492.472261 | 3 | 3.5989 | 0.0000 | H-1 | –> L+2 | -0.5067 |
| | | | | | H-1 | –> L+4 | -0.4907 |
| | | | | | H | –> L+2 | 0.4732 |
| | | | | | H | –> L+4 | 0.4496 |
| excited state 7 | -1492.468590 | 3 | 3.6988 | 0.0000 | H-1 | –> L+5 | -0.5426 |
| | | | | | H-1 | –> L+6 | -0.3535 |
| | | | | | H | –> L+5 | 0.4968 |
| | | | | | H | –> L+6 | 0.3195 |
| excited state 8 | -1492.465619 | 3 | 3.7796 | 0.0000 | H-7 | –> L | 0.2218 |
| | | | | | H-3 | –> L | 0.3099 |
| | | | | | H-2 | –> L | 0.3942 |
| | | | | | H-1 | –> L+2 | 0.3669 |
| | | | | | H-1 | –> L+4 | -0.3172 |
| | | | | | H | –> L+2 | 0.4101 |
| | | | | | H | –> L+4 | -0.3682 |
| excited state 9 | -1492.448417 | 1 | 4.2477 | 0.0051 | H-1 | –> L+1 | -0.6680 |
| | | | | | H | –> L+1 | 0.7313 |
| excited state 10 | -1492.445042 | 1 | 4.3396 | 0.0158 | H-4 | –> L | -0.2692 |
| | | | | | H-1 | –> L+2 | 0.4177 |
| | | | | | H | –> L+1 | 0.2151 |
| | | | | | H | –> L+2 | .7437 |
| excited state 11 | -1492.444522 | 1 | 4.3537 | 0.0388 | H-5 | –> L | -0.4513 |
| | | | | | H-4 | –> L | 0.2980 |
| | | | | | H-1 | –> L+3 | -0.4305 |
| | | | | | H | –> L+3 | -0.6128 |
| excited state 12 | -1492.441825 | 1 | 4.4271 | 0.4046 | H-2 | –> L | -0.4131 |
| | | | | | H-1 | –> L+1 | 0.5453 |
| | | | | | H | –> L+1 | 0.4613 |
| | | | | | H | –> L+2 | -0.2332 |
| | | | | | H | –> L+3 | 0.2544 |
| | | | | | H | –> L+4 | -0.2226 |

**Table A-38.** Calculated Ground- and Excited State Energies for Pyrazoline **2-2d** (TD-FT, B3LYP/6-31G*//B3LYP/6-31G*). H = HOMO, L = LUMO.

| state | energy [hartree] | multi-plicity | excitation energy [eV] | oscillator strength | transition | | amplitude |
|---|---|---|---|---|---|---|---|
| ground state | -1339.928766 | 1 | 0 | | | | |
| excited state 1 | -1339.838596 | 3 | 2.4537 | 0.0000 | H | –> L | 0.9553 |
| excited state 2 | -1339.807040 | 3 | 3.3123 | 0.0000 | H-2 | –> L | -0.3944 |
| | | | | | H | –> L+1 | 0.8198 |
| excited state 3 | -1339.800523 | 3 | 3.4897 | 0.0000 | H-1 | –> L | 0.9256 |
| | | | | | H-1 | –> L+5 | -0.2657 |
| excited state 4 | -1339.798951 | 1 | 3.5325 | 0.1058 | H-1 | –> L | 0.9319 |
| | | | | | H | –> L | -0.3558 |
| excited state 5 | -1339.796099 | 3 | 3.6101 | 0.0000 | H-1 | –> L+2 | -0.7867 |
| | | | | | H-1 | –> L+3 | -0.3481 |
| | | | | | H-1 | –> L+4 | 0.4059 |
| excited state 6 | -1339.795928 | 1 | 3.6147 | 1.1677 | H-1 | –> L | 0.3553 |
| | | | | | H | –> L | 0.9160 |
| excited state 7 | -1339.791918 | 3 | 3.7238 | 0.0000 | H-2 | –> L | -0.2200 |
| | | | | | H-1 | –> L+5 | 0.2619 |
| | | | | | H | –> L+1 | -0.2426 |
| | | | | | H | –> L+2 | 0.4200 |
| | | | | | H | –> L+4 | 0.7315 |
| excited state 8 | -1339.791335 | 3 | 3.7397 | 0.0000 | H-1 | –> L | -0.3008 |
| | | | | | H-1 | –> L+2 | 0.2149 |
| | | | | | H-1 | –> L+4 | 0.2500 |
| | | | | | H-1 | –> L+5 | -0.7644 |
| excited state 9 | -1339.774017 | 1 | 4.2110 | 0.0093 | H | –> L+2 | 0.9001 |
| | | | | | H | –> L+3 | 0.3896 |
| excited state 10 | -1339.771821 | 1 | 4.2707 | 0.0431 | H-5 | –> L | 0.2839 |
| | | | | | H | –> L+1 | 0.3337 |
| | | | | | H | –> L+2 | -0.3076 |
| | | | | | H | –> L+3 | 0.8225 |
| excited state 11 | -1339.769245 | 1 | 4.3408 | 0.0448 | H-4 | –> L | 0.2316 |
| | | | | | H | –> L+1 | -0.2732 |
| | | | | | H | –> L+4 | 0.8820 |
| excited state 12 | -1339.765446 | 1 | 4.4442 | 0.1487 | H-2 | –> L | 0.4709 |
| | | | | | H-1 | –> L+1 | -0.3442 |
| | | | | | H | –> L+1 | 0.6756 |
| | | | | | H | –> L+4 | 0.3201 |

**Table A-39.** Calculated Ground- and Excited State Energies for Pyrazoline **2-3a** (TD-FT, B3LYP/6-31G*//B3LYP/6-31G*). H = HOMO, L = LUMO.

| state | energy [hartree] | multi-plicity | excitation energy [eV] | oscillator strength | transition | | amplitude |
|---|---|---|---|---|---|---|---|
| ground state | -1629.279934 | 1 | 0 | | | | |
| excited state 1 | -1629.183597 | 3 | 2.6214 | 0.0000 | H-1 | –> L | 0.7843 |
| | | | | | H | –> L | 0.5391 |
| excited state 2 | -1629.151875 | 3 | 3.4847 | 0.0000 | H-1 | –> L | -0.4979 |
| | | | | | H | –> L | 0.7354 |
| | | | | | H | –> L+5 | 0.3412 |
| excited state 3 | -1629.149251 | 1 | 3.5561 | 0.0805 | H-1 | –> L | -0.3230 |
| | | | | | H | –> L | 0.9429 |
| excited state 4 | -1629.147958 | 3 | 3.5912 | 0.0000 | H-1 | –> L+1 | 0.2415 |
| | | | | | H-1 | –> L+2 | 0.3835 |
| | | | | | H-1 | –> L+3 | 0.2523 |
| | | | | | H | –> L+1 | 0.6098 |
| | | | | | H | –> L+3 | -0.3106 |
| excited state 5 | -1629.147055 | 3 | 3.6158 | 0.0000 | H-1 | –> L+1 | -0.5084 |
| | | | | | H-1 | –> L+2 | -0.3218 |
| | | | | | H | –> L+1 | 0.2683 |
| | | | | | H | –> L+2 | -0.2619 |
| | | | | | H | –> L+3 | -0.4901 |
| | | | | | H | –> L+4 | 0.2193 |
| excited state 6 | -1629.140620 | 3 | 3.7909 | 0.0000 | H-1 | –> L+5 | -0.2860 |
| | | | | | H | –> L | -0.3211 |
| | | | | | H | –> L+3 | -0.3961 |
| | | | | | H | –> L+5 | 0.6499 |
| excited state 7 | -1629.134227 | 1 | 3.9649 | 0.8668 | H-1 | –> L | 0.9172 |
| | | | | | H | –> L | 0.3074 |
| excited state 8 | -1629.134221 | 3 | 3.9650 | 0.0000 | H-1 | –> L+1 | 0.5652 |
| | | | | | H-1 | –> L+2 | -0.5285 |
| | | | | | H | –> L+1 | 0.3039 |
| | | | | | H | –> L+2 | -0.3737 |
| excited state 9 | -1629.123648 | 1 | 4.2527 | 0.0243 | H-1 | –> L+1 | .3014 |
| | | | | | H-1 | –> L+2 | -0.2252 |
| | | | | | H | –> L+1 | 0.8772 |
| excited state 10 | -1629.119408 | 1 | 4.3681 | 0.0171 | H-1 | –> L+1 | -0.5168 |
| | | | | | H | –> L+1 | 0.3939 |
| | | | | | H | –> L+2 | 0.6880 |
| excited state 11 | -1629.116303 | 1 | 4.4526 | 0.0060 | H-1 | –> L+1 | 0.5735 |
| | | | | | H-1 | –> L+2 | -0.3665 |
| | | | | | H | –> L+2 | 0.6649 |
| excited state 12 | -1629.112902 | 1 | 4.5452 | 0.0108 | H-1 | –> L+1 | 0.2737 |
| | | | | | H-1 | –> L+2 | 0.2879 |
| | | | | | H-1 | –> L+4 | 0.2657 |
| | | | | | H | –> L+3 | -0.6416 |
| | | | | | H | –> L+4 | 0.5054 |

**Table A-40.** Calculated Ground- and Excited State Energies for Pyrazoline **2-3b** (TD-FT, B3LYP/6-31G*//B3LYP/6-31G*). H = HOMO, L = LUMO.

| state | energy [hartree] | multi-plicity | excitation energy [eV] | oscillator strength | transition | | amplitude |
|---|---|---|---|---|---|---|---|
| ground state | -1896.473862 | 1 | 0 | | | | |
| excited state 1 | -1896.388223 | 3 | 2.3304 | 0.0000 | H-1 | –> L | 0.8210 |
| | | | | | H | –> L | -0.4805 |
| excited state 2 | -1896.360978 | 3 | 3.0717 | 0.0000 | H-1 | –> L | 0.4902 |
| | | | | | H | –> L | 0.8622 |
| excited state 3 | -1896.360442 | 3 | 3.0864 | 0.0489 | H-1 | –> L | 0.3224 |
| | | | | | H | –> L | 0.9439 |
| excited state 4 | -1896.346309 | 1 | 3.4709 | 1.0268 | H-1 | –> L | 0.9293 |
| | | | | | H | –> L | -0.3145 |
| excited state 5 | -1896.345208 | 3 | 3.5009 | 0.0000 | H-4 | –> L | -0.3206 |
| | | | | | H-1 | –> L+1 | 0.7243 |
| | | | | | H | –> L+1 | -0.3949 |
| excited state 6 | -1896.340218 | 3 | 3.6367 | 0.0000 | H-1 | –> L+4 | -0.3376 |
| | | | | | H | –> L+4 | -0.8514 |
| excited state 7 | -1896.337070 | 3 | 3.7223 | 0.0000 | H-2 | –> L+4 | 0.2266 |
| | | | | | H-1 | –> L+5 | -0.2917 |
| | | | | | H | –> L+2 | 0.2185 |
| | | | | | H | –> L+4 | -0.2579 |
| | | | | | H | –> L+5 | -0.7156 |
| | | | | | H | –> L+7 | -0.3540 |
| excited state 8 | -1896.331707 | 3 | 3.8683 | 0.0000 | H-4 | –> L | 0.3087 |
| | | | | | H-1 | –> L+2 | -0.7233 |
| | | | | | H | –> L+2 | 0.3887 |
| excited state 9 | -1896.314417 | 1 | 4.3387 | 0.0071 | H-3 | –> L | -0.3884 |
| | | | | | H-1 | –> L+2 | -0.6032 |
| | | | | | H | –> L+2 | 0.6447 |
| excited state 10 | -1896.313075 | 1 | 4.3753 | 0.0155 | H | –> L+1 | 0.9373 |
| excited state 11 | -1896.311639 | 1 | 4.4144 | 0.0030 | H-5 | –> L | -0.4824 |
| | | | | | H-4 | –> L | -0.3278 |
| | | | | | H-1 | –> L+3 | -0.5949 |
| | | | | | H | –> L+3 | 0.4609 |
| excited state 12 | -1896.308580 | 1 | 4.4976 | 0.0122 | H-1 | –> L+2 | 0.4620 |
| | | | | | H | –> L+2 | 0.6021 |
| | | | | | H | –> L+4 | 0.5352 |

**Table A-41.** Calculated Ground- and Excited State Energies for Pyrazoline **2-4a** (TD-FT, B3LYP/6-31G*//B3LYP/6-31G*). H = HOMO, L = LUMO.

| state | energy [hartree] | multi-plicity | excitation energy [eV] | oscillator strength | transition | | amplitude |
|---|---|---|---|---|---|---|---|
| ground state | -1339.922362 | | | | | | |
| excited state 1 | -1339.849625 | 3 | 1.9793 | 0.0000 | H-2 | –> L | 0.2143 |
| | | | | | H | –> L | 0.9524 |
| excited state 2 | -1339.811761 | 1 | 3.0096 | 0.8151 | H | –> L | 0.9587 |
| excited state 3 | -1339.810066 | 3 | 3.0557 | 0.0000 | H-1 | –> L | 0.9928 |
| excited state 4 | -1339.809206 | 1 | 3.0791 | 0.0711 | H-1 | –> L | 0.9765 |
| excited state 5 | -1339.796514 | 3 | 3.4245 | 0.0000 | H-6 | –> L | 0.2489 |
| | | | | | H-2 | –> L | 0.6829 |
| | | | | | H | –> L+2 | -0.2782 |
| | | | | | H | –> L+3 | -0.4996 |
| excited state 6 | -1339.791446 | 3 | 3.5624 | 0.0000 | H-2 | –> L | 0.4736 |
| | | | | | H | –> L+2 | 0.3750 |
| | | | | | H | –> L+3 | 0.6064 |
| | | | | | H | –> L+4 | 0.2443 |
| | | | | | H | –> L+5 | 0.2438 |
| excited state 7 | -1339.789789 | 3 | 3.6075 | 0.0000 | H-1 | –> L+2 | -0.9327 |
| | | | | | H-1 | –> L+3 | 0.3202 |
| excited state 8 | -1339.787806 | 3 | 3.6614 | 0.0000 | H-2 | –> L+1 | 0.2198 |
| | | | | | H | –> L+1 | 0.9472 |
| excited state 9 | -1339.778820 | 1 | 3.9060 | 0.0162 | H | –> L+1 | 0.9716 |
| excited state 10 | -1339.773755 | 1 | 4.0438 | 0.0013 | H | –> L+2 | 0.9823 |
| excited state 11 | -1339.765292 | 1 | 4.2741 | 0.0291 | H-3 | –> L | 0.4072 |
| | | | | | H-2 | –> L | 0.2941 |
| | | | | | H | –> L+3 | 0.8270 |
| excited state 12 | -1339.758933 | 1 | 4.4471 | 0.0119 | H-3 | –> L | 0.3522 |
| | | | | | H | –> L+4 | 0.8928 |

**Table A-42.** Calculated Ground- and Excited State Energies for Pyrazoline **2-4b** (TD-FT, B3LYP/6-31G*//B3LYP/6-31G*). H = HOMO, L = LUMO.

| state | energy [hartree] | multi-plicity | excitation energy [eV] | oscillator strength | transition | | amplitude |
|---|---|---|---|---|---|---|---|
| ground state | -1514.877413 | 1 | 0 | | | | |
| excited state 1 | -1514.802463 | 3 | 2.0395 | 0.0000 | H-2 | –> L | 0.2136 |
| | | | | | H | –> L | 0.9466 |
| excited state 2 | -1514.766655 | 1 | 3.0139 | 0.8471 | H | –> L | 0.9803 |
| excited state 3 | -1514.760584 | 3 | 3.1791 | 0.0000 | H-1 | –> L | 0.9896 |
| excited state 4 | -1514.759763 | 1 | 3.2014 | 0.0212 | H-1 | –> L | 0.9956 |
| excited state 5 | -1514.751036 | 3 | 3.4389 | 0.0000 | H-2 | –> L | -0.4914 |
| | | | | | H | –> L+1 | 0.3530 |
| | | | | | H | –> L+3 | 0.6554 |
| excited state 6 | -1514.745925 | 3 | 3.5780 | 0.0000 | H-7 | –> L | -0.2472 |
| | | | | | H-2 | –> L | 0.6547 |
| | | | | | H | –> L+1 | 0.2577 |
| | | | | | H | –> L+3 | 0.3596 |
| | | | | | H | –> L+4 | -0.3988 |
| excited state 7 | -1514.744374 | 3 | 3.6202 | 0.0000 | H-1 | –> L+1 | -0.9361 |
| | | | | | H-1 | –> L+3 | 0.2957 |
| excited state 8 | -1514.740534 | 3 | 3.7247 | 0.0000 | H-4 | –> L+1 | 0.2460 |
| | | | | | H-1 | –> L+3 | 0.3693 |
| | | | | | H-1 | –> L+5 | -0.8389 |
| excited state 9 | -1514.731031 | 1 | 3.9833 | 0.0005 | H | –> L+1 | 0.9847 |
| excited state 10 | -1514.726363 | 1 | 4.1103 | 0.0073 | H-5 | –> L | 0.3134 |
| | | | | | H | –> L+2 | 0.9416 |
| excited state 11 | -1514.721244 | 1 | 4.2496 | 0.0321 | H-3 | –> L | 0.2741 |
| | | | | | H-2 | –> L | 0.2198 |
| | | | | | H | –> L+3 | 0.8661 |
| | | | | | H | –> L+5 | -0.2360 |
| excited state 12 | -1514.715389 | 1 | 4.4089 | 0.0058 | H-3 | –> L | -0.3104 |
| | | | | | H | –> L+4 | 0.3564 |
| | | | | | H | –> L+5 | -0.8524 |

**Table A-43.** Calculated Ground- and Excited State Energies for Pyrazoline **2-5** (TD-FT, B3LYP/6-31G*//B3LYP/6-31G*). H = HOMO, L = LUMO.

| state | energy [hartree] | multi-plicity | excitation energy [eV] | oscillator strength | transition | | amplitude |
|---|---|---|---|---|---|---|---|
| ground state | -1499.589257 | 1 | 0 | | | | |
| excited state 1 | -1499.510743 | 3 | 2.1365 | 0.0000 | H | –> L | 0.9504 |
| excited state 2 | -1499.473618 | 3 | 3.1467 | 0.0000 | H-1 | –> L | 0.9916 |
| excited state 3 | -1499.472879 | 1 | 3.1668 | 0.0122 | H-1 | –> L | 0.9962 |
| excited state 4 | -1499.471661 | 1 | 3.2000 | 0.9799 | H | –> L | 0.9175 |
| excited state 5 | -1499.458628 | 3 | 3.5546 | 0.0000 | H-2 | –> L | -0.3593 |
| | | | | | H | –> L+1 | 0.5670 |
| | | | | | H | –> L+3 | .6515 |
| excited state 6 | -1499.456476 | 3 | 3.6132 | 0.0000 | H-1 | –> L+1 | 0.8391 |
| | | | | | H-1 | –> L+3 | -0.5018 |
| excited state 7 | -1499.454546 | 3 | 3.6657 | 0.0000 | H-7 | –> L | -0.2282 |
| | | | | | H-2 | –> L | 0.6546 |
| | | | | | H | –> L+1 | 0.2408 |
| | | | | | H | –> L+4 | 0.4789 |
| | | | | | H | –> L+6 | 0.2282 |
| excited state 8 | -1499.452662 | 3 | 3.7170 | 0.0000 | H-1 | –> L+3 | 0.2493 |
| | | | | | H-1 | –> L+5 | -0.8514 |
| excited state 9 | -1499.436771 | 1 | 4.1494 | 0.0023 | H | –> L+1 | 0.9619 |
| | | | | | H | –> L+3 | -0.2272 |
| excited state 10 | -1499.433371 | 1 | 4.2419 | 0.0081 | H-5 | –> L | 0.4110 |
| | | | | | H | –> L+2 | 0.9006 |
| excited state 11 | -1499.430368 | 1 | 4.3236 | 0.0191 | H-3 | –> L | 0.2190 |
| | | | | | H | –> L+3 | 0.8990 |
| excited state 12 | -1499.424517 | 1 | 4.4828 | 0.0334 | H-1 | –> L+1 | 0.9197 |

**Table A-44.** Calculated Ground- and Excited State Energies for Pyrazoline **2-6** (TD-FT, B3LYP/6-31G*//B3LYP/6-31G*). H = HOMO, L = LUMO.

| state | energy [hartree] | multi-plicity | excitation energy [eV] | oscillator strength | transition | | amplitude |
|---|---|---|---|---|---|---|---|
| ground state | -1280.005249 | 1 | 0 | | | | |
| excited state 1 | -1279.921999 | 3 | 2.2654 | 0.0000 | H | –> L | 0.9511 |
| excited state 2 | -1279.883960 | 1 | 3.3005 | 1.1022 | H | –> L | 0.9847 |
| excited state 3 | -1279.882639 | 3 | 3.3364 | 0.0000 | H-2 | –> L | -0.2767 |
| | | | | | H-1 | –> L | -0.3354 |
| | | | | | H | –> L+1 | 0.8267 |
| excited state 4 | -1279.866218 | 3 | 3.7833 | 0.0000 | H-7 | –> L | -0.2709 |
| | | | | | H-2 | –> L | -0.3569 |
| | | | | | H-1 | –> L | -0.3545 |
| | | | | | H | –> L+2 | 0.4717 |
| | | | | | H | –> L+5 | 0.5115 |
| excited state 5 | -1279.862907 | 3 | 3.8734 | 0.0000 | H-4 | –> L | -0.5514 |
| | | | | | H-2 | –> L | 0.2711 |
| | | | | | H-1 | –> L | 0.3014 |
| | | | | | H | –> L+1 | 0.2262 |
| | | | | | H | –> L+2 | 0.2900 |
| | | | | | H | –> L+5 | 0.3930 |
| excited state 6 | -1279.862197 | 3 | 3.8927 | 0.0000 | H-4 | –> L | 0.7148 |
| | | | | | H-1 | –> L | 0.2540 |
| | | | | | H | –> L+5 | 0.2743 |
| excited state 7 | -1279.854658 | 3 | 4.0978 | 0.0000 | H-5 | –> L+3 | -0.2173 |
| | | | | | H-3 | –> L+3 | 0.4889 |
| | | | | | H-2 | –> L+2 | 0.3946 |
| | | | | | H-1 | –> L+2 | -0.4552 |
| | | | | | H | –> L+2 | 0.2149 |
| excited state 8 | -1279.850515 | 1 | 4.2105 | 0.0106 | H | –> L+2 | 0.9725 |
| excited state 9 | -1279.846693 | 1 | 4.3146 | 0.0011 | H | –> L+3 | 0.9592 |
| excited state 10 | -1279.844245 | 1 | 4.3812 | 0.0570 | H-4 | –> L | -0.5466 |
| | | | | | H | –> L+1 | 0.2936 |
| | | | | | H | –> L+4 | -0.7076 |
| excited state 11 | -1279.842148 | 1 | 4.4382 | 0.3866 | H-1 | –> L | 0.6365 |
| | | | | | H | –> L+1 | 0.6511 |
| | | | | | H | –> L+4 | 0.2713 |
| excited state 12 | -1279.841115 | 1 | 4.4663 | 0.0601 | H-2 | –> L | 0.4199 |
| | | | | | H | –> L+1 | 0.2434 |
| | | | | | H | –> L+3 | -0.2136 |
| | | | | | H | –> L+5 | 0.7363 |

# VITA

Liuchun Yang was born in Guangxi, China on March 23, 1974. She graduated from Liuzhou high school in 1991. She attended Peking University, Beijing, China and graduated in 1996 with bachelor's degree in chemistry. Then she studied in bioinorganic chemistry in Peking University and received master's degree in June, 2000. She then entered graduate school at Georgia Institute of Technology in August, 2000 and conducted research under the direction of Dr. Christoph J. Fahrni.